Modelling Permeation Passive Sampling

by

Faten Salim

A thesis
presented to the University of Waterloo
in fulfillment of the
thesis requirement for the degree of
Doctor of Philosophy
in
Chemistry

Waterloo, Ontario, Canada, 2019

© Faten Salim 2019

EXAMINING COMMITTEE MEMBERS

The following served on the Examining Committee for this thesis. The decision of the Examining Committee is by majority vote.

External Examiner	Tom Harner Senior Research Scientist Environment and Climate Change Canada
Supervisor(s)	Tadeusz Górecki Professor Department of Chemistry University of Waterloo
Internal Member	Janusz Pawliszyn Professor Department of Chemistry University of Waterloo
Internal Member	Wojciech Gabryelski Associate Professor Department of Chemistry University of Guelph
Internal-external Member	André Unger Associate Professor Department of Earth and Environmental Sciences University of Waterloo
Other Member(s)	Marios Ioannidis Professor Department of Chemical Engineering University of Waterloo

AUTHOR DECLARATION

This thesis consists of material all of which I authored or co-authored: see Statement of Contributions included in the thesis. This is a true copy of the thesis, including any required final revisions, as accepted by my examiners.

I understand that my thesis may be made electronically available to the public.

STATEMENT OF CONTRIBUTIONS

The introduction and the literature review presented in the first Chapter were searched, organized, and written by the author of this thesis. Planning and performing experimental work presented in Chapter 2, as well as data analysis, interpretation of the results, and writing were also performed by the author of the thesis.

The third chapter of this thesis was published as the following article: F. Salim, M. Ioannidis and T. Górecki, "Experimentally validated mathematical model of analyte uptake by permeation passive samplers", *Environ. Sci.: Processes Impacts*, 2017, 19, 1363. The work was supervised by Professor Tadeusz Górecki. Professor Marios Ioannidis introduced me to modelling and provided his guidance during the development of the model equations and their solutions. Application of the model, finding the model solutions, writing the MATLAB code, planning and performing experimental work, data analysis, interpretation of the results, and writing were performed by the author of the thesis.

The fourth chapter was published as the following article: F. Salim, M. Ioannidis and T. Górecki, "New applications of the mathematical model of a permeation passive sampler: prediction of the effective uptake rate and storage stability", *Environ. Sci.: Processes Impacts*, 2019, 21, 113. This work was coauthored by the supervisor Professor Tadeusz Górecki and Professor Marios Ioannidis, who also supervised the development of the model equations. In this work, the model application and the development of its extension, the MATLAB code, planning and performing experimental work, data analysis, interpretation of the results, and writing were all performed by the author of the thesis. Parts of the experimental procedures in the laboratory were performed by undergraduate students, Hashthana Puvanendran and Ruiyi Zhao.

The fifth chapter of the thesis was published as the following article: F. Salim, M. Ioannidis, A. Penlidis and T. Górecki, "Modelling permeation passive sampling: intraparticle resistance to mass transfer and comprehensive sensitivity analysis", *Environ. Sci.: Processes Impacts*, 2019, 21, 469. The coauthors of this work were Prof. Górecki, Prof. Ioannidis and Prof. Penlidis. Development of the model equations was performed by the author under the guidance of Prof. Ioannidis. Sensitivity analysis was also performed by the author under the guidance of Prof. Penlidis. Solving and application of the model extension, writing the MATLAB code, planning and performing experimental work, data analysis, interpretation of the results, and writing were all performed by the author of the thesis.

The extension and application of the model presented in Chapter 6, as well as interpretation of the results, and writing were performed by the author of this thesis under the guidance of Prof. Ioannidis and supervision of Prof. Górecki.

ABSTRACT

Understanding the theory behind passive sampling, as well as factors influencing its accuracy, is crucial for proper planning and application of passive sampling methods. The Waterloo Membrane Sampler (WMS) is a permeation air passive sampler that is used for determining the Time Weighted Average (TWA) concentrations of Volatile Organic Compounds (VOCs) in air and soil gas. Determination of the TWA concentrations has been based on the zero-sink assumption, according to which the adsorbent of the sampler efficiently removes analytes permeating through the membrane leaving negligible concentrations at the barrier-sorbent interface. In this thesis, a dynamic model is presented to simulate the sampling process in the WMS. The model equations were solved numerically using MATLAB. The calculated uptake rates were successfully compared to the experimental data. The model predicted that resistance to mass transfer within the sorbent bed may develop during sampling. This resistance needs to be taken into consideration when significant. Therefore, the applicability of the zero-sink assumption depends on the significance of this resistance and, hence, on the properties of the analyte-adsorbent pair, as well as the concentration level and the sampling time. The model presented in this thesis provides the tool to evaluate this effect in a given sampling scenario, allowing optimization of the sampling method. Alternatively, the TWA concentration of the sampled analyte can be calculated using a method that accounts for this effect, as demonstrated in the thesis. An extension of the model that evaluates the post-sampling/storage period of analytes in the WMS is also presented. It was proven both theoretically and experimentally that the amounts of analytes retained in the PDMS membrane are negligible after sampling; therefore, analyzing the sorbent is sufficient to quantitatively determine the sampled amounts. The experimental evaluation also showed that the amounts of analytes found in the sorbent were

stable over up to three-weeks of storage at room temperature. Additionally, the effect of intraparticle resistance to mass transfer within the sorbent bed was evaluated. The aim of this evaluation was to extend the applicability of the model to include the case of adsorbents with porous particles. This evaluation is followed by comprehensive sensitivity analysis using two types of adsorbents with different properties and adsorption strengths. The purpose of this analysis was to detect the influential parameters that have major control over the model output, the uptake rate, and to optimize the model parameters. Finally, the effect of air face velocity on the uptake rate of the WMS was added to the model, so that the resistance to mass transfer in the air boundary layer is taken into consideration. The work presented in this thesis provides better understanding of the sampling process in permeation passive samplers similar to the WMS. This understanding permits correct application of the sampler in environmental analysis.

ACKNOWLEDGEMENTS

First, I would like to extend my gratitude to my supervisor, Professor Tadeusz Górecki for giving me the opportunity to work in his group. I have been fortunate to work under his supervision, gaining knowledge and experience, receiving guidance and support, and having a good example of a scientist, a researcher, and a humanist in his personality. I also sincerely appreciate the guidance provided by Professor Marios Ioannidis. I am very grateful for the time he spent discussing with me issues arising during my work on the model and its applications. I wish to thank my advisory committee member Professor Janusz Pawliszyn for directing me towards modelling of the sampling process in the WMS and providing his critical feedback on my work. I also greatly appreciate the valuable reviews and encouragement provided by my committee member Professor Wojciech Gabryelski. I wish also to express my appreciation to Professor Alexander Penlidis for providing his guidance during the performance of the sensitivity analysis.

I would like to thank the staff of the Department of Chemistry, especially Cathy Van Esch for her continuous and kind support. My sincere thanks are expressed to Jacek Szubra for providing his technical support with analytical instruments. I would like to express my gratitude to Professor Eric Prouzet and Dr. Andrew Kacheff for performing the characterization of the Anasorb 747 adsorbent. I would like to express my appreciation to my colleagues and friends, Oana Goli, Humam El-Mugammar, Alshymaa Aly, John Chow, and Haleigh Boswell for their continuous support and timely help.

No words can express my gratitude to my parents, brothers and sisters for their love and support. My deep appreciation and thanks are expressed to my husband, Ziad Halabi for his

support and encouragement from the time I applied for the graduate studies and throughout my way to the completion of this work.

This work was funded by the Natural Sciences and Engineering Research Council (NSERC), and partially by Queen Elizabeth II Graduate Scholarship in Science & Technology (QEII-GSST), the University of Waterloo President's Graduate Scholarship, and MAX Jabir Ibn Hayyan Scholarship.

DEDICATION

This thesis is dedicated to my children, Tarek, Ahmad, Ali, Amer, and Abdurrahman Halabi.

TABLE OF CONTENTS

LIST OF FIGURES

LIST OF TABLES

LIST OF ABBREVIATIONS

DC - Depuration Compound

GAPS - Global Atmospheric Passive Sampling

GC - Gas Chromatography

LDPE - Low-Density Polyethylene

LTPRI - Linear Temperature Programmed Retention Index

MS - Mass Spectrometry

OVM - Organic Vapor Monitor

PCE - Tetrachloroethylene

PAHs – Polyaromatic hydrocarbons

PCBs – Polychlorinated biphenyls

PDB - Polyethylene Diffusion Bag

PDMS – Polydimethylsiloxane

PES - Polyethersulfone

PFCs - polyfluoroalkyl compounds

POCIS - Polar Organic Chemical Integrative Sampler

POM - Polyoxymethylene

POPs – Persistent Organic Pollutants

pp-LFER - Polyparameter Linear Free Energy Relationships

PRC - Performance Reference Compounds

PTFE - Polytetrafluoroethylene

PUF - Polyurethane Foam

QSPR - Quantitative Structure-Property Relationship

SIP - Sorbent-Impregnated Polyurethane foam

SPMD - Semipermeable Membrane Device

SPME- Solid-Phase Microextraction

SVOC – Semi Volatile Organic Compounds

TCE – Trichloroethylene

TD – Thermal Desorption

TWA – Time-Weighted Average Concentration

VOC - Volatile Organic Compound

WMS - Waterloo Membrane Sampler

CHAPTER 1.

INTRODUCTION, LITERATURE REVIEW AND SCOPE OF THE THESIS

1.1 Passive Sampling

Monitoring the presence of man-made chemicals in the different compartments of the environment, including outdoor and indoor air, groundwater surface water and soil, became a necessity due to their often detrimental effects on the environment and on humans' health. Successful selection and application of the sampling method in any environmental monitoring task is crucial to ensure representativeness of the samples that reflect the composition of the evaluated medium. Sampling tools vary depending on the environmental matrix, the level of contamination, and the physicochemical properties of the contaminants. Also, different sampling methods produce results that could reflect certain points in time and space or provide integrative information over a period of time in the monitored location;[1] therefore, the stability of the contaminant concentration and the purpose of the monitoring task are important factors that need to be taken into consideration when comparing sampling methods. Additionally, the design and properties of the sampling tool affect the accuracy and precision of the results.[2] For all these reasons, the knowledge of the available sampling techniques, the theory behind them, the data they reflect, and their susceptibility to the effects of the sampling tool design and environmental factors are vital to the decision-making process.

Two types of sampling approaches are commonly employed in environmental monitoring: active sampling (also known as discrete or grab sampling), and passive sampling. In

active sampling, samples from the evaluated medium are collected at specific points in time to be extracted and analyzed later. This method, in most cases, involves pumping of the samples into or through an appropriate collecting medium. Passive sampling relies on spontaneous migration of analyte molecules from the evaluated medium to the collecting medium owing to the difference in the chemical potentials of the analyte between these media.[3] This approach provides several advantages compared to active sampling methods. First, with the low cost of the passive samplers and their simple deployment without the need for a pumping device or a power source, they are easier to operate in remote areas and for long monitoring periods, in which cases a large number of active samples would be needed.[1,4] Second, several sample preparation goals can typically be achieved simultaneously during passive sampling, including analyte isolation and preconcentration from the sampled matrix.[5] Also, solvent use is usually significantly reduced in this method as it reduces the number of steps required for sample preparation before the analysis.[3] An important advantage of passive sampling is that it can be used to measure the time weighted average (TWA) concentrations, which are the average concentrations over the time of exposure.[5] Nonetheless, some limitations are associated with passive sampling including the need for calibration and the sensitivity to meteorological factors, such as temperature and convection conditions around the sampler.[6]

Applications of passive sampling date back to 1873, when passive methods were used to determine atmospheric ozone presence.[7,8] Passive sampling was later used to determine the presence of carbon monoxide in 1927.[9] The first truly quantitative passive samplers, though, were introduced in 1973 as a diffusive passive sampler[10] and a permeation passive sampler[11] for sulfur dioxide in air. Since then, an enormous number of studies have been devoted to develop passive samplers and expand their applications. Passive samplers are commonly categorized

based on the kinetic region of operation they belong to, the types of matrix they are used to evaluate, or their designs.

Commonly, passive samplers operate either in the so-called kinetic/linear region, or in the equilibrium region. In the linear region, analyte molecules migrate continuously from the sampled medium to the collecting medium until the process is terminated by the operator. In this case, analyte amount collected by the sampler is assumed to be proportional to the product of the sampling time and analyte concentration in the evaluated medium. In the equilibrium region, analyte uptake continues until the sampler reaches equilibrium with the surrounding concentration. The concentration measured in this case is similar to that measured using grab sampling methods, while the concentration measured using the kinetic passive samplers is the TWA concentration. More extensive description of these two types of passive samplers is provided in the theoretical section of this chapter.

A passive sampler can be designed with a single phase (a single-phase passive sampler) or with two phases (a two-phase passive sampler). A single-phase passive sampler consists of a single sorption medium that is directly exposed the evaluated matrix. Examples of this type of samplers include low density polyethylene (LDPE/PE) strips,[12,13] polyoxymethylene (POM) samplers,[14] polydimethylsiloxane (PDMS) thin films[15] and rods,[16] and XAD-Pockets passive sampler.[17] A two-phase passive sampler, on the other hand, consists of an uptake-limiting barrier and a receiving phase. The barrier can be a semipermeable membrane (a permeation passive sampler) or a diffusion region consisting of a static section of the evaluated medium (a diffusive passive sampler). Various passive samplers have the two-phase design including the semipermeable membrane devices (SPMDs),[18] and polar organic chemical integrative samplers (POCIS)[19] as permeation passive samplers; whereas the tube-type passive samplers[20] and 3M™

Organic Vapor Monitor (OVM) 3500 samplers[21] are examples of diffusive passive samplers. The focus of this introduction is on the theory of passive sampling and different approaches used in passive sampling modelling. Only a brief description of several passive samplers is provided below. These samplers were selected to represent the types of samplers widely used in different environmental matrices, especially those that will frequently appear in the theoretical section.

1.1.1 Air Passive Samplers

1.1.1.1 Polyurethane foam (PUF) passive air sampler

PUF discs are used for both active[22] and passive air sampling.[23] They are cheap, easy to handle and have high capacity, which makes them suitable for long-term monitoring purposes. These advantages make the PUF passive sampler attractive for applications in passive air sampling.[24] The PUF disks used in passive sampling are typically of 14 cm diameter and 1.35 cm thickness.[24] They are protected inside a sheltering chamber consisting of two steel bowls (flying saucer design),[25] presented in Figure 1-1, arranged in a way that still allows air circulation inside the chamber.[24] The purpose of this chamber is to protect the sampler from the effects of wind

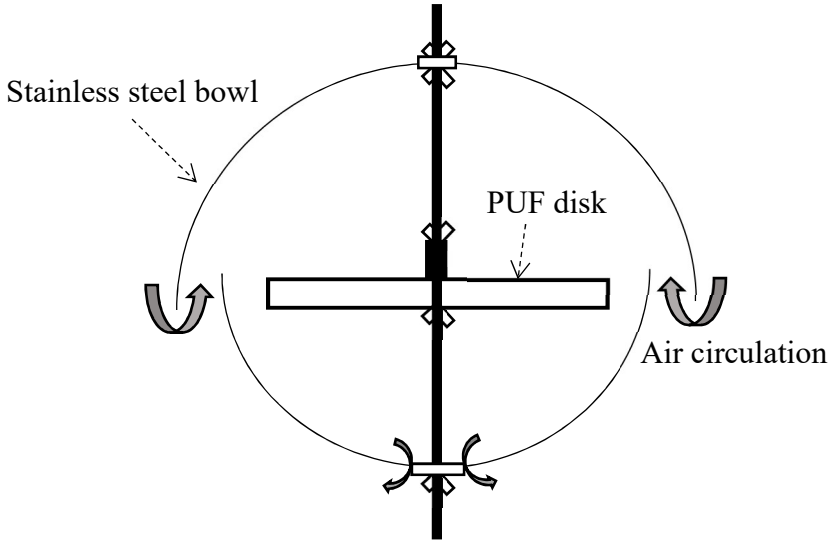

Figure 1-1: Schematic of the PUF passive sampler (based on ref. [25])

speeds and sunlight radiation, and prevent undesired wet or dry deposition on the disk.[24] The sampler has been widely adopted as a reliable sampling tool for sampling semi volatile organic compounds (SVOCs) and persistent organic pollutants (POPs) such as polyaromatic hydrocarbons (PAHs) and polychlorinated biphenyls (PCBs).[4] It has been applied in regional and international environmental investigations. For instance, PUF passive samplers have been widely deployed in the Global Atmospheric Passive Sampling (GAPS) network to monitor persistent organic pollutants (POPs) in ambient air.[26,27] Sorbent-impregnated polyurethane foam (SIP) disk passive air samplers are PUF disks impregnated with finely ground XAD-4 resin (styrene-divinylbenzene copolymer).[28] The SIP passive sampler was shown to have a significantly higher sorptive capacity than the PUF sampler for more volatile and polar compounds such as neutral polyfluoroalkyl compounds (PFCs),and ionic PFCs, which extended the linear-range of sampling for these compounds.[29]

1.1.1.2 Tube-type passive sampler

Tube-type passive samplers are often known as the Perkin Elmer samplers because these samplers were first produced and commercialized by this company.[20] A Perkin Elmer passive sampler, presented in Figure 1-2, typically, consists of a 90-mm-long stainless steel tube of 6.3 mm O.D. and 5.0 mm I.D., packed with an adsorbent that can be selected from a wide variety of

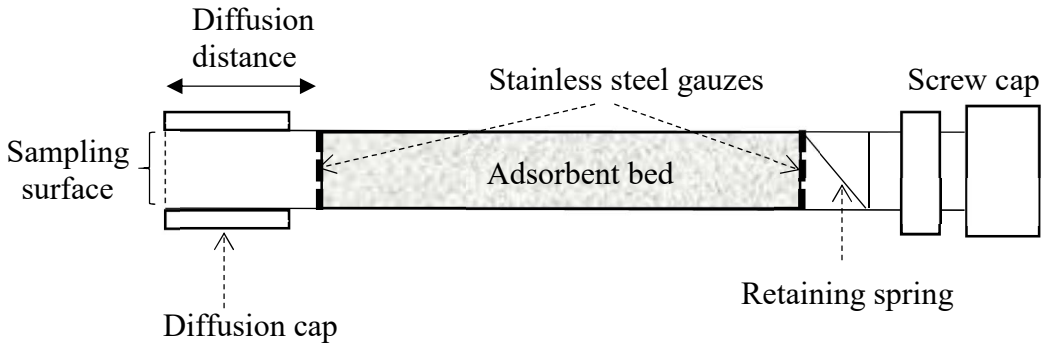

Figure 1-2: Tube-type diffusive passive sampler (based on ref. [20])

available materials.[20] The adsorbent is retained in place by means of stainless steel gauzes at both ends. Analyte molecules diffuse through the sampling end, which is equipped with a diffusion cap containing a gauze disk, for a diffusion distance, that is typically 15 mm,[20] before they are trapped in the adsorbent. These samplers are reusable after desorption. They are also directly analyzed using a thermal desorption (TD) instrument coupled with gas chromatography, without the need for additional pre-treatment.[20]

1.1.1.3 XAD-resin based passive air sampler

Wania et al. introduced a passive sampler that utilizes XAD-2 resin, a styrene-divinylbenzene copolymer, for sampling persistent organic pollutants (POPs) from the atmosphere.[30] The sampler was developed to exploit the efficient adsorption properties of the XAD resin in order to obtain a wider linear sampling range compared to that provided by the SPMDs. The sampler consists of an XAD-resin-filled cylindrical container. The wall of the container is made of a fine stainless-steel mesh and the sorbent is held in place using caps at both ends. The container is protected inside a shelter equipped with an opening at the bottom. The

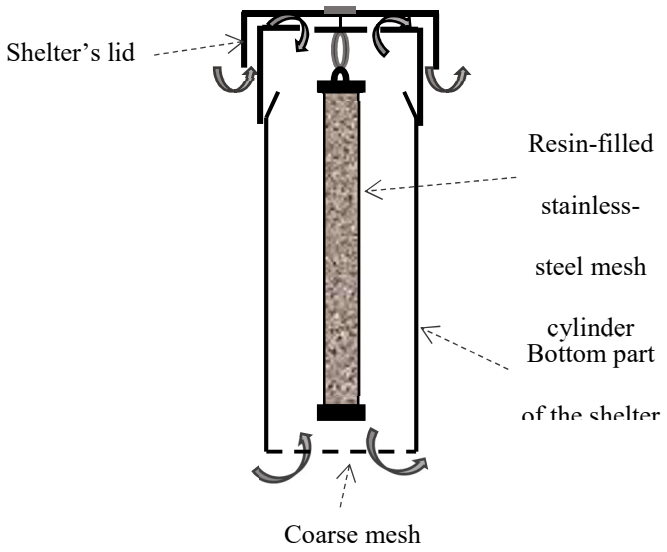

Figure 1-3: XAD-resin based passive air sampler (based on ref.[30])

bottom part of the shelter and its lid are made of stainless steel, and they fit snugly into each other. The design of the sampler is presented in Figure 1-3.

1.1.1.4 The Waterloo Membrane Sampler (WMS)

The Waterloo Membrane Sampler (WMS), presented in Figure 1-4, is a permeation passive sampler developed by Seethapathy and Górecki at the University of Waterloo.[31,32] The permeation barrier in this sampler is a PDMS membrane, and the receiving phase is an adsorbent material. The WMS has a very simple design and is fabricated using off-the-shelf materials, including a small glass chromatographic vial and a small amount (~ 250 mg) of an adsorbent material. The mouth of the vial is covered with a thin PDMS membrane, typically of a 100 μm thickness. This membrane, cut into a circular shape, is held in place by means of an aluminum crimp cap and a PTFE washer to provide a good sealing along the membrane edge to the vial's mouth. Several types of adsorbents are used in the sampler including Anasorb 747 (activated carbon), Carbopack B (graphitized carbon black) and Carboxen-1016 (carbon molecular sieve). The WMS has been successfully utilized for sampling volatile organic compounds (VOCs) from

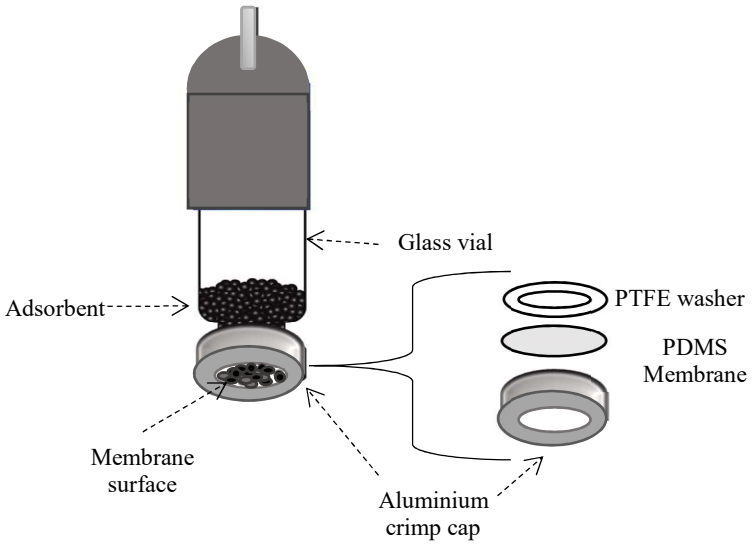

Figure 1-4: The Waterloo Membrane Sampler (WMS)

air and soil gas.[33,34,35,36] The sampler has also been applied for preconcentration of organic compounds from soil gas before compound-specific isotope analysis (CSIA).[37]

1.1.2 Water Passive Samplers

1.1.2.1 Chemcatcher passive sampling devices

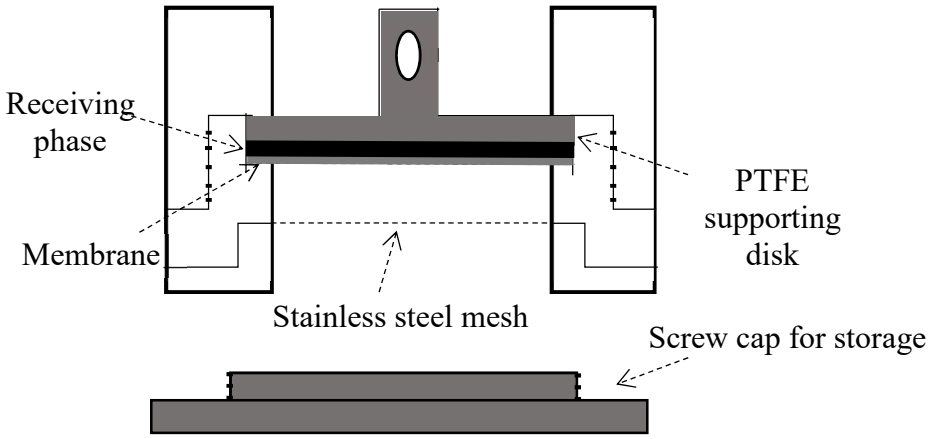

Figure 1-5: Schematic of the Chemcatcher device (based on ref.[39])

Chemcatcher was first developed by Kingston et al. to sample organic contaminants from aquatic environments.[38] The receiving phase of the Chemcatcher consists of a solid adsorbent immobilized in the form of a disk using an inert polymeric matrix.[39] This system can incorporate different types of adsorbents and membranes, which permits optimisation of the sampling device for a broad range of analytes with various properties.[38] C_{18} Empore™ disk is a typical receiving phase used with a nonporous low-density polyethylene membrane to sample hydrophobic organic compounds with log $K_{ow} > 3$, whereas the same disk used with a microporous polysulfone membrane allows sampling hydrophilic organic compounds with log $K_{ow} < 3$.[39] Chemcatcher can also be configured in a manner that allows the sampling of other classes of pollutants including metals, mercury and organotin compounds.[39] The design of the sampler is presented in Figure 1-5.

1.1.2.2 Polar organic chemical integrative sampler (POCIS)

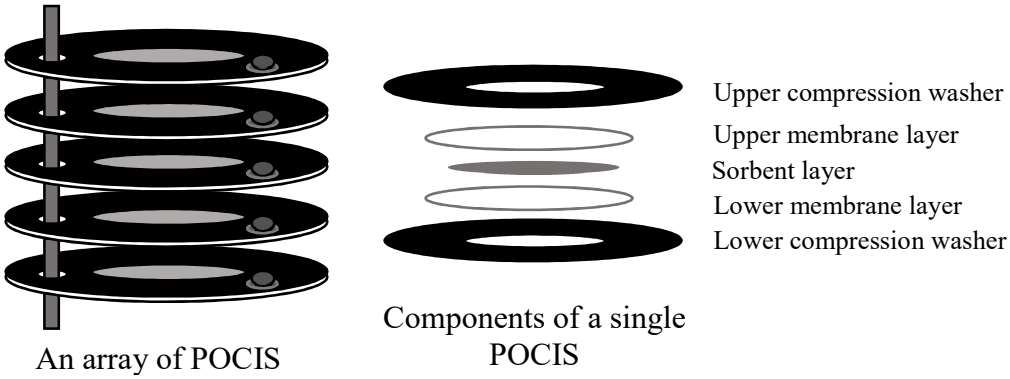

Figure 1-6: The Polar Organic Chemical Integrative Sampler (POCIS) (based on ref. [40])

POCIS was developed to address the need for integrative sampling of hydrophilic organic contaminants such as pharmaceuticals, pesticides, personal care products, and other industrial, household, and agricultural chemicals in aquatic environments.[19] As presented in the previous section, log K_{ow} is commonly used as a means for distinguishing hydrophilic and hydrophobic organic compounds, and a value of 3.0 is usually selected as a cut-off point for log K_{ow} of hydrophilic compounds sampled by POCIS.[5,40] Nonetheless, there is no such sharp discontinuity of the properties at that value.[40] The POCIS is a disk-like sampler consisting of two layers of microporous polyethersulfone (PES) membrane with a layer of a solid-phase sorbent or a sorbent mixture sandwiched in between the membrane layers. Two rigid washers, made of a material that does not interfere with the sampling process, are used to provide mechanical compression sealing of the membrane layers, leaving a sampling area of approximately 41 cm^2 for a typical field study, as presented in Figure 1-6.[19,40] POCIS is often deployed in arrays of samplers mounted on a support rod.[5]

1.1.3 Mixed Use Passive Samplers

1.1.3.1 ***Semipermeable membrane devices (SPMDs)***

An SPMD consists of a low-density polyethylene lay-flat tube filled with triolein and sealed at both ends. SPMDs were first introduced by Huckins et al. in 1990 to sample nonpolar contaminants in aquatic environments and to predict their bioavailability for organisms.[41] Since then, SPMDs have been extensively used for the monitoring of hydrophobic organic contaminants in water.[18,42,43,44] In 1993, Petty et al. introduced the application of SPMDs in passive air sampling,[45] which was followed by many studies that used SPMDs for monitoring nonpolar atmospheric contaminants such as POPs.[24,46-49] The sampler is available in different versions, with varying sampling surfaces and protection cages.[5] These devices are widely used in environmental applications due to many advantages they provide, including accuracy, easy deployment and standardization, and high capacity with long equilibration time.[50] The last advantage allows using the SPMDs to measure the TWA concentrations of contaminants, as will be explained in the theoretical part of this chapter. However, the procedure required to extract the sampled analytes from the SPMDs for analysis is complex and consumes large amounts of solvents, which is the main disadvantage of this sampler.[50] The low-density polyethylene (LDPE) membrane is also used as an extraction phase on its own without the additional receiving phase, in what is called the LDPE (or simply PE) strip sampler.[13]

1.1.3.2 Solid-phase microextraction (SPME)

An SPME device consists of a thin stationary phase (7-100 μm thick) coated on a fused silica fiber protected inside a stainless-steel needle. For common extraction purposes, the fiber coating is exposed directly to the sample or to the headspace of the sample. The sampler can be easily used as a passive sampler in the equilibrium mode (grab sampling).[51,52] It can also be used

for the measurement of the TWA concentrations by retracting the fiber into the needle, leaving a diffusion distance inside the needle,[53] as presented in Figure 1-7. The diffusion barrier created in this manner is not sensitive to the air velocity across the opening of the needle due to its

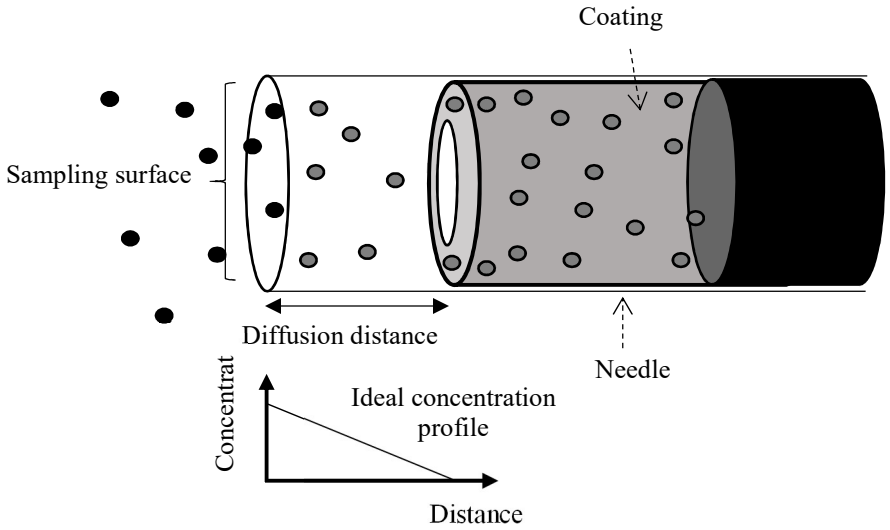

Figure 1-7: TWA sampling using SPME with retracted fiber (based on ref. [3])

extremely small inner diameter.[54] The length of the diffusion distance, and, hence, the sampling rate, are adjustable through controlling the retraction length into the needle.[3] The device has been used for TWA passive air sampling as well as water passive sampling. More details about these applications are provided by Ouyanga and Pawliszyn.[50] The most popular coating in SPME is the PDMS coating, the applications of which are limited to analytes with coating-air partition coefficients greater than 1,000 to ensure efficient trapping of the sampled analytes; however, other types of available coatings with a higher affinity to the target analyte can be selected (e.g. porous polymer coatings).[3] On-fiber derivatization is a technique used to convert the sampled analyte into a stable product, with a high affinity towards the coating, immediately as it reaches this coating.[55] This technique can be used to maintain a negligible concentration in the gas phase immediately above the coating.[3]

1.1.3.3 Bare PDMS passive samplers

Due to its high sorption and unique stability properties,[56] PDMS has been used in many forms of passive samplers that rely solely on the PDMS phase. Silicon Rod (SR) is a passive sampling device that consists of a simple PDMS rod (several cm long and 1-2 mm diameter).[16,57] It is used for sampling various types of contaminants including polyaromatic hydrocarbons (PAH), chlorinated organic compounds, and semivolatile organic compounds (SVOCs) from both water and air matrices.[57] The device can be used to measure the TWA concentrations[57] due to its high capacity. PDMS has been also used as a thin film passive sampler. Bragg et al. used a PDMS thin film of a house shape (5 cm^2 surface area of one side and 0.0635 cm^3 total volume) for sampling PAH from water. PDMS films have also been used as personal passive air samplers to monitor exposure of individuals to SVOCs in air. The PDMS samplers used for this purpose had various shapes such as PDMS brooches[58] or hand bands.[59]

1.2 Passive Sampling Theory and Modelling

1.2.1 Passive Sampling Modelling Based on the Two-Film Theory

In the first approach of passive sampling modelling, represented in Figure 1-8, the passive sampler is considered as a single uniform phase in contact with the evaluated medium. Mass transfer of a solute from the sampled medium to the passive sampler is defined by both the mass transfer across the boundary layer at the evaluated medium's side, and the mass transfer across the boundary layer at the sampler's side. This approach was based on the two-film theory by Whitman,[60] in which two boundary regions exist at the interface between the matrix and the sampler. Conditions outside of the matrix boundary are the same as the bulk conditions, while the conditions beyond the sampler's boundary inside the sampler are the same as those of the

bulk sampling phase. Analyte molecules migrate from the sampled matrix to the sampling phase and experience resistance to mass transfer through these two boundaries.[60] Moreover, net accumulation of a solute in the passive sampler is the result of two processes: the uptake into and the loss from the sampler, which are defined by the uptake rate constant, k_u, (time^{-1}) and the loss rate constant, k_l, (time^{-1}), respectively.[61] The ratio between these two constants is equal to the sampler/medium partition coefficient, K_{SM}, which is the ratio between the concentration in the passive sampler and the concentration in the evaluated medium at equilibrium (dimensionless), as follows:

$$K_{SM} = \frac{k_u}{k_l} \tag{1.1}$$

The accumulation rate into the passive sampler can then be expressed as follows:[61]

$$\frac{dC_s}{dt} = k_u C_M - k_l C_s \tag{1.2}$$

where C_s is the concentration of the solute in the passive sampler (amount of the solute per unit volume of the passive sampler), t is time and C_M is the solute's concentration in the evaluated medium (amount of the solute per unit volume of the evaluated medium). The total resistance to mass transfer into the passive sampler is equal to the sum of resistances in the medium's boundary layer and in the sampler's boundary layer as described in the following equation:[23,62]

$$\frac{1}{k_o} = \frac{1}{k_m} + \frac{1}{k_s K_{SM}} \tag{1.3}$$

in which k_o is the total mass transfer coefficient from the evaluated medium to the passive sampler (length · time^{-1}), while k_m and k_s are the mass transfer coefficients in the boundary layers

on the sampled medium's side and the passive sampler's side, respectively (length · time^{-1}). It is commonly assumed, though, that mass transfer is controlled by resistance in only one of these

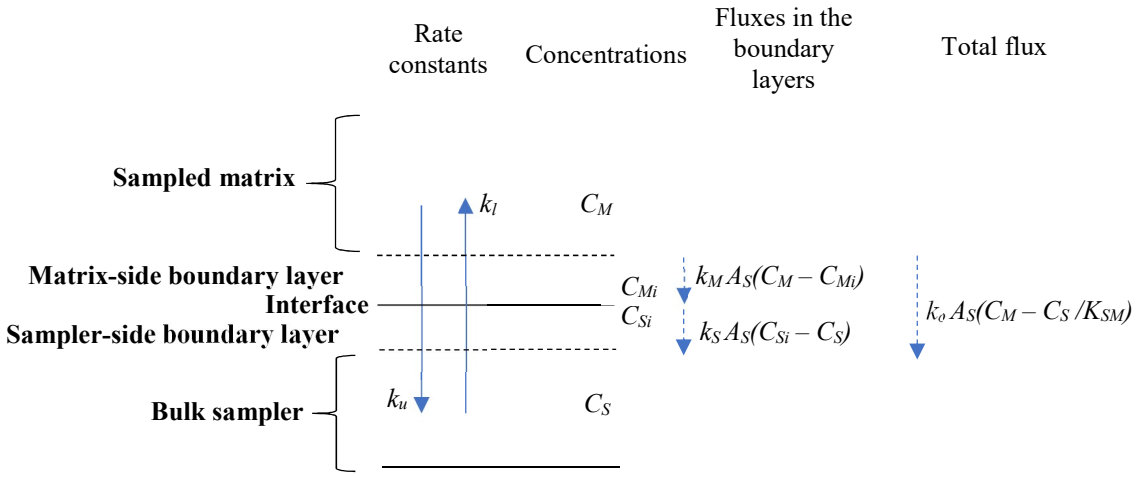

Figure 1-8: Schematic of rate constants and mass fluxes between the sampled medium and the passive sampler, where C_{Mi} and C_{Si} are the analyte concentrations at the interface on the matrix's side and the sampler's side, respectively (based on ref.[60,66]).

boundary layers. In the case of the medium's side control, $k_o = k_m$; whereas $k_o = k_s K_{SM}$ when resistance to mass transfer in the sampler's side boundary layer dominates.

This approach was adopted in many models that described passive sampling in both single phase and two-phase passive samplers. Only examples of these applications are presented here. Johnson used this method to evaluate sampling of organic contaminants from water using hexane-filled dialysis bags.[61] Huckins et al. based his model for semipermeable membrane devices (SPMDs) on this approach, considering that the polyethylene membrane thickness defines the region of resistance to mass transfer inside the sampler.[18] Müller et.al. used this approach to model the sampling of semivolatile organic compounds (SVOCs) from air into tristearin-coated fibreglass sheets.[63] Similarly, Shoeib and Harner modeled passive air sampling of persistent organic pollutants (POPs) using this approach in a comparison of three passive samplers: semipermeable membrane devices (SPMDs), polyurethane foam (PUF) disks, and soil

as a passive sampling medium.[23] Harner et al. also used this model to describe the sampling of POPs into a polymer-coated glass passive air sampler.[62] Bayen et al. modeled the accumulation process of hydrophobic organic chemicals in organisms and passive samplers using this method as well.[64] Resistance in the biofilm at the SPMDs surface in water is commonly added to the total resistance expressed in eqn. (1-1).[42,65] Bartkow et al. added the resistance to mass transfer in the protective chamber of passive samplers used for sampling SVOCs from air.[66]

The mass transfer coefficient in each region, i, can be expressed as a function of the diffusivity, D_i (area · time^{-1}), in that region and the region's thickness, δ_i (length), as presented in eqn. (1.4):[66]

$$k_i = \frac{D_i}{\delta_i} \tag{1.4}$$

Therefore, eqn. (1.3) can be generalized to account for resistances in sequential regions as follows:[67]

$$\frac{1}{k_o} = \sum \frac{\delta_i}{D_i K_{iM}} \tag{1.5}$$

where K_{iM} is the equilibrium partition coefficient between the region i and the evaluated medium.

In consideration of the analyte amount accumulated in the polyethylene membrane vs. the triolein (the lipid) inside the SPMD, Huckins et al. assumed that the membrane is a lipid-equivalent volume; hence, the SPMD-water partition coefficient, K_{SM}, was expressed as follows:[43,67]

$$K_{SM} = \frac{K_{LW}V_L + K_{mW}V_{memb}}{V_{SPMD}} \tag{1.6}$$

In this equation, K_{LW} and K_{mW} are the lipid/water partition coefficient and the membrane/water partition coefficient respectively, V_L and V_{memb} are the volumes of the lipid phase and the membrane respectively, and V_{SPMD} is the total volume of the SPMD (both phases: the membrane and the lipid). Eqn. (1.6) can also be generalized as follows:[67]

$$K_{SM} = \frac{\sum V_i K_{iM}}{\sum V_i} \tag{1.7}$$

where V_i is the volume of the region i of the passive sampler.

Bartkow et al. provided a comprehensive explanation of this approach to passive sampling modelling.[66] Based on the flux into the passive sampler, accumulation of the solute in the sampler can be described as in eqn. (1.8):

$$V_s \frac{dC_s}{dt} = k_o A_s \left(C_M - \frac{C_s}{K_{SM}} \right) \tag{1.8}$$

In this equation, V_s is the volume of the passive sampler, while A_s is the sampling area. Comparing eqns. (1.2) and (1.8), one can describe the relationships between the rate constants and mass transfer coefficients as follows:

$$k_u = k_o \frac{A_s}{V_s}$$
$$k_l = k_o \frac{A_s}{V_s K_{SM}} \tag{1.9}$$

Integration of eqn. (1.8) yields the following expression of the solute's concentration in the passive sampler:

$$C_s = K_{SM} C_M \left(1 - \exp\left(-\left(\frac{k_o A_s}{V_s K_{SM}}\right) t\right)\right) \quad (1.10)$$

This exponential approach to equilibrium gives the general description of the entire passive sampling process; nonetheless, it is based on the linear exchange kinetic assumption, as described in eqn. (1.1). This condition, in reality, applies to passive samplers with absorption-based receiving phase, while it only applies during the initial stages of sampling using passive samplers with adsorption-based receiving phases. Additionally, this model relies on assumed linear concentration gradients in all regions of resistance to mass transfer with a local equilibrium at all interfaces.[67]

1.2.1.1 Passive sampling regimes

The process of passive sampling, described in eqn. (1.10), can be divided into three sampling regions: linear uptake, curvilinear uptake, and equilibrium regions, as described in Figure 1-9. Initially, the concentration of the sampled analyte is negligible in the passive sampler; therefore, the second term within the brackets in the right-hand side of eqn. (1.8) is approximately zero. Consequently, integration of this equation, assuming a constant concentration in the evaluated medium, produces the following expression:

$$C_s = \frac{k_o A_s}{V_s} C_M t = k_u C_M t \quad (1.11)$$

In eqn. (1.11), the concentration in the passive sampler is linearly proportional to the sampling time. Samplers that operate in this uptake region are known as kinetic passive samplers.

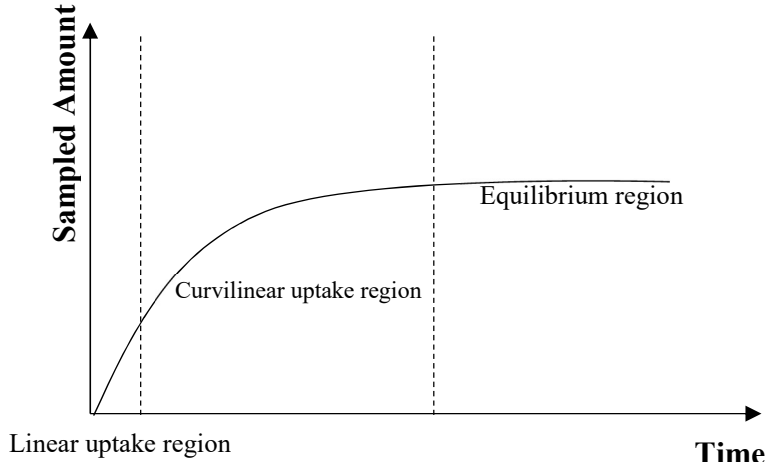

Figure 1-9: Theoretical uptake curve in passive samplers (based on ref. 66)

The amount of analyte, N_s, collected by the passive sampler can be calculated using eqn. (1.12):

$$N_s = k_u V_s C_M t \tag{1.12}$$

The product $k_u V_s = k_o A_s$, known as the sampling rate or the uptake rate, R_s (volume · time^{-1}), represents the equivalent sampled volume of the evaluated medium per unit of time. Therefore, eqn. (1.12) can be written as follows:

$$N_s = R_s C_M t \tag{1.13}$$

Based on the expression of the mass transfer coefficient presented in eqn. (1.4), if mass transfer is controlled by the boundary layer in the evaluated air or water, the sampling rate can be written as follows:

$$R_s = \frac{D_m A_s}{\delta_m} \tag{1.14}$$

On the other hand, if mass transfer is sampler-side controlled, the sampling rate is written as follows:

$$R_s = \frac{D_s K_{SM} A_s}{\delta_s} \tag{1.15}$$

In eqns. (1.14) and (1.15), the subscripts *m* and *s* represent the boundary layers in the evaluated matrix and in the sampler, respectively. Assuming matrix boundary layer control, estimation of sampling rates using correlations established in the chemical engineering literature, namely the Sherwoods correlation, was shown to be applicable in some cases.[68]

As the analyte's concentration in the passive sampler increases, the loss rate becomes increasingly significant and cannot be ignored. The sampler, in this case, enters the curvilinear region of operation. If sampling continues for long enough, eqn. (1.10) is reduced to the form:

$$C_s = K_{SM} C_M \tag{1.16}$$

In this case, the sampler is said to have reached equilibrium. Usually, the equilibration time is defined as the time needed to reach 95 % [23] or 99 % [66] of the true equilibrium. The equilibrium time can be estimated as follows:[66]

$$t_{eq}(99\ \%) = \frac{4.605\ V_s}{A_s k_m} K_{SM} \tag{1.17}$$

Samplers that are operated in the equilibrium region are characterized by a rapid achievement of equilibrium between the sampled medium and the sampler.[69] Application of these samplers for measuring an analyte's concentration relies on the knowledge of the partition coefficient, K_{SM}, value, as shown in eqn. (1.16). Concentrations measured using this type of

sampler are comparable with those measured using grab sampling.[69] Nonetheless, this depends on the equilibration time of the sampler: the shorter the equilibration time is, the closer the measured concentration will be to the grab sampling results.[2] On the other hand, concentrations measured using kinetic passive samplers reflect the TWA concentrations over the period of sampling. It is assumed, for this type of samplers, that the sampling rate remains constant throughout the sampling period (linear uptake).[69] In reality, the sampling rate is reduced as soon as sampling begins due to the accumulation of the sampled analyte at the collecting surface.[30] However, a linear range can be approximated up to the time needed to achieve ~25 % of the true equilibrium.[23] Therefore, in many applications, the knowledge of K_{SM} value is needed to approximate the linear range.

Passively sampled amount is often described using the equivalent sampled volume, V_{eq}, which is the volume of the evaluated medium that contains the same amount of the analyte as the amount collected by the sampler. Based on eqn. (1.10), one can write the following equation:[70]

$$V_{eq} = K_{SM} V_s \left(1 - \exp\left(-\left(\frac{k_o A_s}{V_s K_{MS}}\right) t\right)\right) \tag{1.18}$$

The partition coefficient, K_{SM}, can, therefore, be interpreted as the volume of the sampled medium that contains the same amount of analyte as one unit volume of the passive sampling medium at equilibrium.[70] This coefficient can be determined or estimated using several methods, including experimental calibration.[23,71] Direct calibration, however, is not practical for those chemicals that require long time to equilibrate with the sampler. Other methods of determining or estimating partition coefficients were evaluated in the literature.[70,72-76]

1.2.1.2 Determination of the sampling rate

The sampling rates of kinetic passive samplers can be determined using one of several methods.[4,77] The sampling rate can be calculated using eqns. (1.14) or (1.15) if all parameters are known. This approach, however, is not common in passive sampling studies and applications. The sampling rate is usually calibrated experimentally by deployment of the passive sampler in a similar matrix contaminated with the target analyte either under controlled conditions in laboratory settings, or in the field, while using a reference grab sampling method to measure the concentration during the exposure.[42,78] The sampling rate is then derived using eqn. (1.13), after the collected amount in each experiment is determined. In many cases, the sampling rate is determined from the slope of the linear regression plot of the equivalent air volume against the exposure time, as in eqn. (1.19):[17,23,58]

$$V_{eq} = \frac{N_s}{C_M} = R_s t \qquad (1.19)$$

To account for temporal variation of the sampling rate, measurements can be performed as successive events with a certain interval.[77] The sampling rate during each interval is calculated from the increase in the amount of the analyte collected during that interval. Alternatively, the sampling rate can be measured using calibration compounds, namely Performance Reference Compounds (PRCs) or Depuration Compounds (DCs). PRCs are compounds that are not present in the evaluated medium (commonly deuterated analogues). Those compounds are spiked into the passive sampler before deployment. The sampling rate of the target analyte is related to the elimination rate of these compounds based on the assumption that they are controlled by the same mechanisms .[65] Assuming that isotropic exchange kinetic applies to the uptake into and dissipation from the passive sampler, the elimination (loss) rate and the uptake rate constants, for

both the analyte and the PRC, are correlated. Therefore, if the PRCs have similar physico-chemical properties as the target analyte (e.g. using isotopic labeling), they can be assumed to have similar rate constants.[4,18,79]

When the initial concentration in the passive sampler is not zero, the general solution of eqn. (1.8) takes the following form:[67]

$$C_s = K_{SM} C_M \left(1 - \exp\left(-\left(\frac{k_o A_s}{V_s K_{SM}}\right) t\right)\right) + C_o \exp\left(-\left(\frac{k_o A_s}{V_s K_{SM}}\right) t\right) \qquad (1.20)$$

in which C_o is the initial concentration of the analyte in the sampler. The first term represents the uptake process into the sampler, while the second term represents the offload process of the initial amount present in the sampler. Both processes are characterized by the same rate constant in the exponent, which is the constant k_l presented in eqn. (1.9). This principle is the basis of the use of PRCs in measuring the sampling rate.[67] The dissipation of the PRCs is described by an exponential model derived from eqn. (1.20) when the PRC is not present in the environment, $C_{M\,(PRC)} = 0$, as presented in eqn. (1.21).[65,79]

$$C_{PRC} = C_{0PRC} \exp(-k_{lPRC} t) \qquad (1.21)$$

In this equation, C_{PRC}, is the concentration of the PRC after time t of deployment, C_{0PRC} is the initial concentration of the PRC in the passive sampler, and k_{lPRC} is the loss rate constant of the PRC. If the PRC's concentration is determined before and after the deployment, the following expression can be used:[4,65]

$$k_{lPRC} = \ln\left(\frac{C_{oPRC}}{C_{PRC}}\right)/t \qquad (1.22)$$

To correct for various sources of variability such as losses during spiking, cleanup or matrix effects, C_{PRC} value can be divided by the recovered fraction of a stable PRC that does not dissipate during deployment.[80] Once the loss rate constant, k_{lPRC}, is determined, the uptake rate constant of the PRC, k_{uPRC}, can be calculated using eqn. (1-1), given that the partition coefficient of the PRC into the passive sampler, K_{SM}, is predetermined. Assuming that the sampling rate of the target analyte equals the sampling rate of the PRC, one can calculate the sampling rate, R_s, as in the following equation:[4]

$$R_s = \ln\left(\frac{C_{oPRC}}{C_{PRC}}\right) K_{SM} V_s / t \tag{1.23}$$

This method permits the calculation of site-specific sampling rates for analytes, taking into account the influence of environmental parameters such as temperature and convection conditions on the sampling rate.[4] It is important that the loss of the PRC during deployment is large enough (20 % – 80 %) to ensure it can be distinguished from analytical uncertainty.[80] Moeckel et al. provided important recommendations when using PRCs to measure sampling rates of passive air samplers.[80] PRCs are also used to correct for the influence of environmental factors in the field (e.g. meteorological factors or biofouling in aqueous environment) by assuming that the effects of these factors on the elimination rate of the PRC is similar to their effects on the sampling rate of the target analyte as in eqn. (1.24):[2,78,81]

$$R_{s-f} = \left(\frac{R_{s-cal}}{k_{l-cal}}\right) k_{l-f} \tag{1.24}$$

in which $R_{s\text{-}cal}$ and $k_{l\text{-}cal}$ are the sampling rate of the analyte and the loss rate of the PRC produced in calibration studies, while $R_{s\text{-}f}$ and $k_{l\text{-}f}$ are those in field sampling. Huckins et al. described the calculation of an exposure adjustment factor (EAF) for the above-described purpose.[65]

Ai developed an exponential model to describe the process of sampling into the SPME device.[82] His model has an exponential form similar to that in eqn. (1-6) and is presented in eqn. (1.25) as follows:

$$n = n_e[1 - \exp(-at)] \tag{1.25}$$

where n and n_e are the amounts sorbed into the coating at time t and at equilibrium, respectively, and α is a constant that defines how fast sampling can reach equilibrium. Based on that, Chen et al. presented a kinetic approach to SPME calibration based on the isotropic exchange into the SPME extraction phase.[83,84] The model describing the dissipation of pre-loaded standards is given in eqn. (1.26):[84]

$$Q = q_0 - q = q_0 \exp(-at) \tag{1.26}$$

in which Q is the amount of standard remaining on the fiber coating after time t of deployment, q is the desorbed amount of the standard during that time, q_0 is the amount of the standard pre-loaded on the fiber, and α is the rate constant. Assuming that the rate constant α in equations (1-25) and (1-26) has the same value, one can write,[83,84]

$$\frac{n}{n_e} + \frac{Q}{q_0} = 1 \tag{1.27}$$

The amount of the analyte extracted by the fiber coating at equilibrium can be described as follows:[16]

$$n_e = K_{SM} V_s C_M \tag{1.28}$$

Considering eqns. (1.27) and (1.28), the concentration in the evaluated medium can be calculated from the amount extracted at any point of the sampling time using the fraction of the standard remaining on the extraction phase as follows:[16]

$$C_M = \frac{n}{K_{SM} V_s \left(1 - \left(\frac{Q}{q_0}\right)\right)} \tag{1.29}$$

This method, so called "on-fiber standardization technique", was also applied in the cases of sampling using a PDMS rod[16] and using a PDMS thin film.[15]

A similar approach was followed by Adams et al. using the PRCs in polyethylene devices to correct for non-equilibrium extraction conditions and calculate the concentrations of hydrophobic organic compounds in aquatic matrices.[85] This method was also used to correct for nonachievement of equilibrium conditions in sediment porewater[86] and in water;[13] however, those researchers did not use the exponential model for the dissipation of the PRCs. They used, instead, dynamic models, as will be explained later.

The use of PRCs allows calibration of the passive sampler for the entire sampling region regardless of the equilibration time. If the sampler does not reach equilibrium during the sampling time, the measured concentration reflects the TWA concentration; otherwise, the measured concentration is the concentration at the time of retrieval[50] (or around it if the equilibration time is long). The use of PRC, nonetheless, requires laboratory calibration of the required parameters such as K_{SM}, and, in many cases, the ideal loss and uptake rate constants.[2,65] Additionally, it becomes impractical when screening for a wide range of compounds, where analogues for all of the compounds of interest are needed for accurate determination of the sampling rates.[2] Also, the application of this method requires that the loss of the PRCs during the

exposure time be significant, so that accurate quantitation can be achieved.[80,87] This requirement in addition to the requirement of linear relationship between the uptake rate and the elimination rate constant rules out the use of this technique with adsorption-based passive samplers.[5]

Ouyang et al. proposed a standard-free method of calibration for on-site measurement using SPME.[88] This approach relies on only two sampling events, which are sufficient to calibrate for all the target analytes. The amounts of an analyte extracted over two different times of sampling can be calculated using eqn. (1.25) as follows:

$$\frac{n_1}{n_e} = 1 - \exp(-\alpha t_1) \tag{1.30}$$

$$\frac{n_2}{n_e} = 1 - \exp(-\alpha t_2) \tag{1.31}$$

In eqns. (1.30) and (1.31), n_1 and n_2 are the amounts of the analyte sampled for the times t_1 and t_2 respectively. Combining these two equations, one can write,

$$\frac{t_2}{t_1} \ln\left(1 - \frac{n_1}{n_e}\right) = \ln\left(1 - \frac{n_2}{n_e}\right) \tag{1.32}$$

Two methods, described in the original work, are followed to solve eqn. (1.32) and obtain the value of the sampled amount of the analyte at equilibrium, n_e. This calculated amount, in turn, is used in eqn. (1.28) to find the concentration in the evaluated medium.[88]

1.2.2 Two-Phase Sampler Design Modelling

A common approach in modelling passive samplers is based on a two-phase design. The barrier in these samplers is of a well-defined length, through which transport of analyte molecules occurs by molecular diffusion while convection is avoided.[5] Most of these samplers

operate in the linear (kinetic) region of sampling. Models of these samplers usually assume linear concentration gradient within the sampler's barrier; therefore, using Fick's first low of diffusion, the flux of analyte into the sampler can be calculated using eqn. (1.33).[41]

$$F = \frac{DA_s}{L}(K_{MB}C_M - K_{BR}C_R) \tag{1.33}$$

In this equation, D is the diffusion coefficient in the barrier, A_s is the sampling area, L is the length of the barrier, K_{MB} is the partition coefficient between the evaluated medium and the barrier, K_{BR} is the partition coefficient between the barrier and the receiving phase, C_M is the concentration in the evaluated medium assuming that it equals the concentration at the inlet of the passive sampler, while C_R is the concentration in the receiving phase assuming it is a well-mixed phase. In passive air samplers, it is also often assumed that the analyte concentration at the barrier-receiving phase interface is zero due to efficient sorption in the receiving phase (zero-sink assumption).[3,5,89] This is achieved by using an adsorption-based receiving phase. In such cases, eqn. (1.33) takes the forms shown in eqns. (1.34) and (1.35) for permeation and diffusive passive air samplers, respectively.[3,5,89]

For diffusive passive samplers $$\frac{N_s}{t} = \frac{DA_sC_M}{L} \tag{1.34}$$

For permeation passive samplers $$\frac{N_s}{t} = \frac{DA_sK_{MB}}{L}C_M \tag{1.35}$$

The sampling rate, R_s, is defined as follows:

For diffusive passive samplers $$R_s = \frac{DA_s}{L} \tag{1.36}$$

For permeation passive samplers $$R_s = \frac{DA_sK_{MB}}{L} \tag{1.37}$$

Substituting eqns. (1.36) and (1.37) in eqns. (1.34) and (1.35), respectively, produces the linear relationship between the analyte amount collected by the passive sampler and the product of the concentration and the sampling time (exposure dose) similar to that presented earlier in eqn. (1.13). The assumption of a constant sampling rate that is independent from the exposure dose forms the basis of measuring the TWA concentrations using these samplers. This assumption, in turn, is related to the zero-sink assumption as explained above, which maintains the concentration gradient across the barrier during sampling. The concentration profile in this ideal behavior is presented in Figure 1-10.

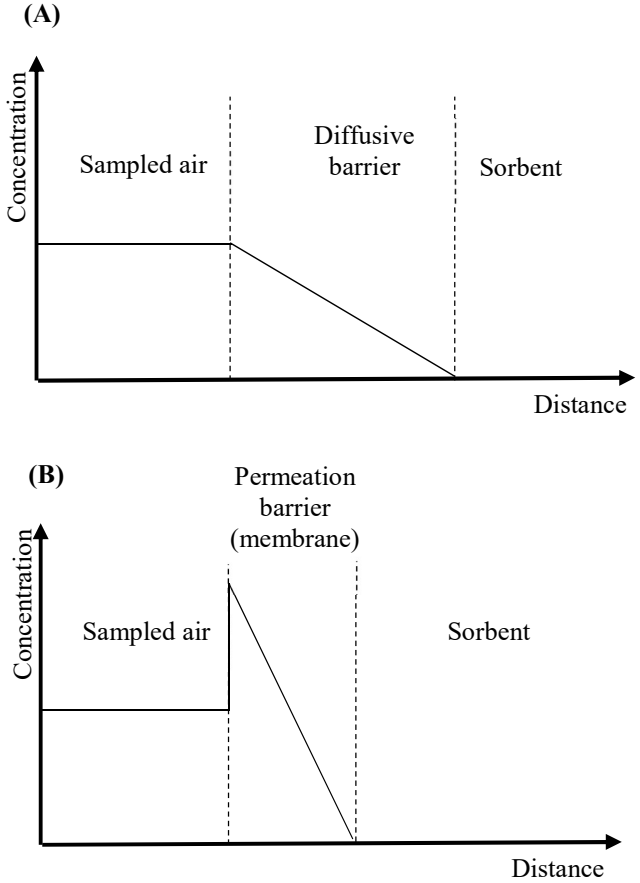

Figure 1-10: Ideal concentration profile for diffusive passive samplers (A), and permeation passive samplers (B) (based on ref. [5]).

Passive water samplers usually include receiving phases that trap analytes by partitioning.[5] This type of receiving phases does not behave as a zero sink except at the initial stage of sampling, during which the concentration of the sampled analyte in the receiving phase is negligible. Additionally, regardless of the convection conditions, a stationary layer, known as the boundary layer, exists at the interface between the barrier and the evaluated medium.[90,91] Mass transport within the boundary layer is mainly by diffusion; therefore, additional resistance to mass transfer occurs in this boundary layer. The contribution of this resistance to the total resistance depends, to a large extent, on the convection conditions.[89,90,92] The higher is the flow velocity across the sampler surface, the thinner the boundary layer becomes and the smaller influence it has on the total sampling rate of the passive sampler. The concentration profile for permeation passive samplers in water sampling is presented in Figure 1-11. Resistance to mass transport in the matrix boundary layer and the receiving phase boundary layer are usually

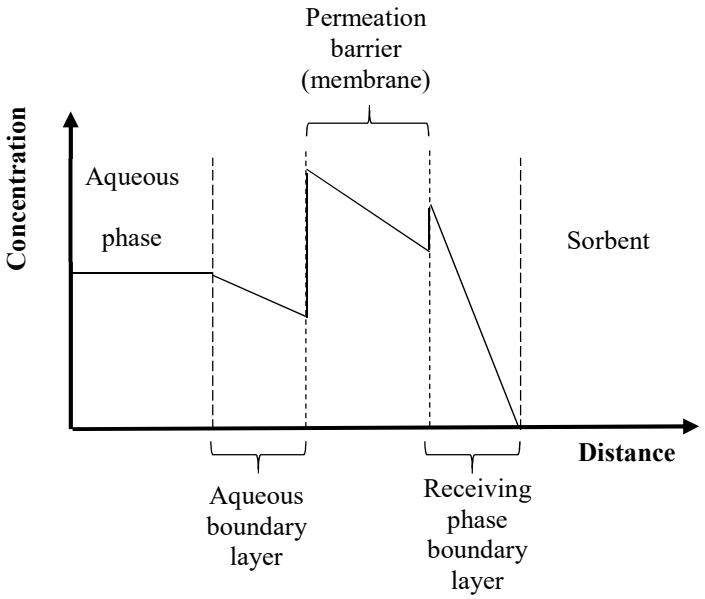

Figure 1-11: Concentration profile for permeation passive samplers in water sampling (based on ref.[5])

accounted for using equations similar to that presented in eqn. (1.3) for the resistance to mass transfer, and eqn. (1.10) for the concentration in the passive sampler, as explained earlier.

1.2.3 Corrections for the Non-Ideal Behaviour in Air Passive Sampling

The zero-sink assumption applied to kinetic passive air samplers has proven to be invalid in various scenarios, and efforts have been made to correct/account for this behaviour as it leads to a narrower linear range than predicted. Weak adsorbents are desired for some applications, in which thermal desorption of the sorbent material is preferred for sensitivity or environmental reasons. In such scenarios, analyte concentration in the gas phase at the barrier-sorbent interphase increases considerably during sampling, leading to a decreasing concentration gradient across the barrier (C_R increases during the exposure).[93,94] This consequence has been also attributed to non-uniform distribution of the sampled analyte within the sampler.[95] Zhang et al. concluded from their experiments on sampling SVOCs using XAD and PUF-based passive samplers that a kinetic resistance to chemical transfer within the passive sampler medium exists, as the sorbed analyte was not uniformly distributed inside the receiving phase, but accumulated near the sampling surface.[95]

Posner and Moore described the deviation from the linear uptake region using a model they developed based on the following relationships: 1) Fick's first low of diffusion, 2) mass balance expression, and 3) an equilibrium relationship between the adsorbed concentration and the concentration in the vapor phase in the adsorbent (assuming that the linear portion of the Langmuir isotherm applies).[96] Their model, however, considered the reversible nature of the adsorption process but not the non-uniform distribution of the analyte inside the adsorption phase, which is only valid in the case of a thin adsorption layer. Their model presented an

exponential decrease of the flux into the passive sampler, and a non-linear increase in the analyte's mass inside the sampler.[96]

Van Den Hoed and Van Asselen developed a computer model to calculate the effective uptake rates of tube-type passive samplers, taking into account the change in the concentration gradient as explained above.[93] In this model, Fick's first law was applied on a sequence of steady-state processes. The length of the absorbent bed, *L*, was divided into thin segments of length *dx*, as illustrated in Figure 1-12. During a short time-element, *dt*, of the exposure time, it was assumed that steady state exists within each segment of the adsorbent bed; hence, the mass of the analyte collected during this short time in each slice can be approximated as follows:[93]

$$dM_1 = \frac{D_a A_s}{L}(C_0 - C_1)dt \tag{1.38}$$

$$dM_n = \frac{D_e A_s}{dx}(C_{n-1} - C_n)dt \tag{1.39}$$

In these equations, dM_1 is the analyte mass within the diffusive barrier (stagnant air), dM_n is the analyte mass adsorbed in the bed slice, n = 1,2,3,…, N during the period dt, D_a is the diffusion coefficient of the analyte in air, D_e is the effective diffusivity in the sorbent bed (calculated by considering the effect of the bed porosity and tortuosity on the total diffusivity), C_0 is the analyte concentration in the ambient air, and C_1, C_2, …, C_n are the concentrations in the gas phase within the pores of segments 1, 2, …, n. The analyte's free concentration, C_n, in any segment of the sorbent bed is related to the sorbed concentration in that segment, M_n, using an experimentally determined isotherm of the Freundlich, Langmuir, or other type. After the amount adsorbed during each time element was determined, numerical integration of eqns. (1.38) and (1.39) was applied to calculate the mass accumulated in each slice, followed by the determination of the

new concentrations C_1, C_2, …, C_n based on the isotherm.[93] The model allowed the calculation of the effective mass uptake rate [ng/(ppmv.min)], equivalent to what is called above the sampling rate, over the exposure time taking into account the deviation from the zero-sink assumption for the non-ideal analyte-sorbent pair. The model was applied in an iterative procedure to assess the effective uptake rates of the tube-type diffusive passive samplers in the field at unknown concentrations in the evaluated air.[93] Nordstrand and Kristensson extended Hoed and Asselen's model to develop a computer program that estimates the effective uptake rate, calculates the atmospheric concentrations based on Dubinin-Radushkevich isotherm, and predicts the effects of back diffusion when a significant decrease in the atmospheric concentration occurs.[97] Tolnai et al. also used this approach to evaluate the effective uptake rate in the same type of passive samplers using the linear range of Langmuir isotherm to approximate the phase equilibrium in the sorbent bed.[98]

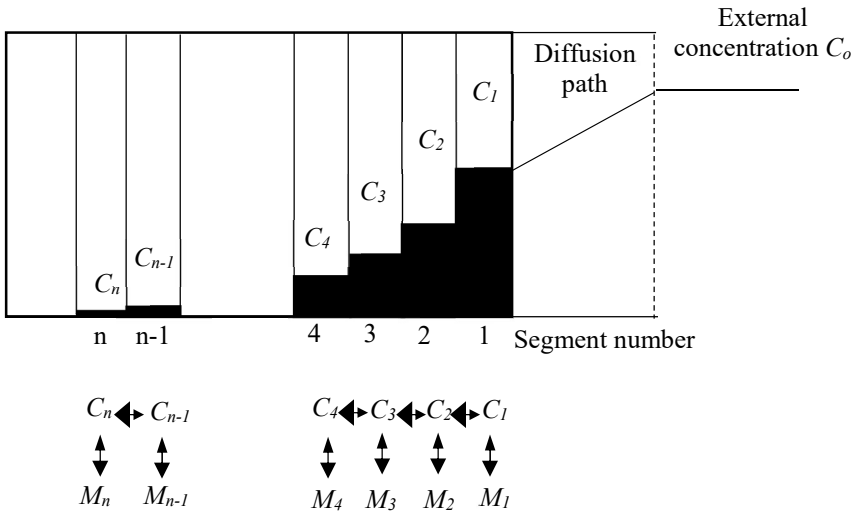

Figure 1-12: Schematic of the concentration profile and mass exchange between hypothetical segments of the sorbent bed in tube-type passive samplers (based on ref. [93,98])

Armitage et al. modeled the passive sampling process using the mass transfer coefficient and the fugacity approaches.[99] The model considered mass transport through the air-side

boundary layer and the sampler-side boundary layer, as well as mass exchange in successive hypothetical segments inside the passive sampler. The model utilized the fugacity approach to predict the fate of neutral organic chemicals when exchanged between air and the XAD passive sampler. Diffusivities in the different phases involved in the mass transport process were used to calculate mass transfer coefficients as described in eqn. (1.4). Those coefficients characterized transport in the air-side boundary layer, in the gas phase inside the pores of the sampler, and in the solid phase of the sampler. The mass transfer coefficients were used to calculate the transport-*D* values that were used according to the fugacity approach. The transport-*D* value ($mol \cdot Pa^{-1} \cdot h^{-1}$) for a specific process is the product of the corresponding mass transfer coefficient ($m \cdot h^{-1}$), the area of exchange (m^2) and the sorption capacity of the phase ($mol \cdot m^{-3} \cdot Pa^{-1}$). The calculated transport-*D* value was multiplied by the corresponding fugacity (Pa) of that process to obtain the mass exchange rate ($mol.h^{-1}$) at each time step. These exchange rates were used to determine the uptake and elimination of the chemical in each layer of the sampler over the time of simulation following the appropriate mass balance description in that layer. In this model, only the fraction of analyte in the gas phase of the pores is available for transport within the sampler, hence, the resistance to mas transport inside the sampler is a function of K_{SA}.[99] This model was shown to be capable of accounting for the non-uniform distribution of analytes within the passive sampler due to the segmentation of the porous medium into thin layers, from which the fugacity of the outer layer determines the uptake and elimination on the passive sampler without assuming uniform distribution inside it.[99] The model evaluated the sampling rate under variable wind and temperature conditions. The effect of wind was incorporated into the model by multiplying the transport-*D* value across the boundary layer by a scaling factor calculated based on the wind speed, whereas the effect of temperature appeared in the calculation of the

diffusivities in air, the sampler-air partition coefficient, and the aerosol-air partition coefficient at the measured temperature.[99]

1.2.4 Dynamic Models

Most previous modelling approaches, describing the passive sampling process, are based on the establishment of linear concentration profiles in the regions of resistance to mass transfer. Several researchers used dynamic models instead, to describe mass accumulation in the passive sampler and its transient response, and to assess its response to fluctuation in the environmental concentrations.[100] These models assume one-dimensional mass transfer, in the direction perpendicular to the sampling surface. This approach was used to model mass transfer of analytes between water and polyethylene passive samplers.[13,101] In such a single-phase passive sampler that collects analytes via partitioning, mass transport consists of two processes that can be represented by Fick's second law: diffusion through the matrix boundary layer, described in eqn. (1.40), and diffusion through the sampling phase, as presented in eqn. (1.41):

$$\frac{\partial C_{BL}}{\partial t} = D_w \frac{\partial^2 C_{BL}}{\partial x^2} \tag{1.40}$$

$$\frac{\partial C_{PS}}{\partial t} = D_{PS} \frac{\partial^2 C_{PS}}{\partial x^2} \tag{1.41}$$

In eqns. (1.40 and (1.41), C_{BL} and C_{PS} are the concentrations in the matrix boundary layer and in the passive sampler, respectively, (mass/volume), while D is the diffusion coefficient (area/time). A similar model was used to describe mass transport between sediment porewater and polyethylene passive sampler, considering mass transport within the pores of infinite sediment bed and in the passive sampler.[86] On the other hand, mass transport through a multi-phase passive sampler involves mass balance equations in all involved phases. To our knowledge,

dynamic models for multi-phase passive samplers have only been applied to diffusive types of passive samplers.

Effective diffusion coefficients, D_{eff}, in porous regions were calculated by taking into consideration the effect of the solid phase and the tortuous path on diffusivity as follows:

$$D_{eff} = \frac{D\varepsilon}{\tau} \tag{1.42}$$

In this equation, D is the diffusion coefficient in the free phase (usually air or water), ε is the porosity of the porous region, and τ is its tortuosity. In many cases, the effective diffusivity was approximated as follows:[102] $D_{eff} = D\varepsilon^{3/2}$; whereas in some other cases, it was calculated using the following expression: $D_{eff} = D\varepsilon^{4/3}$.[103]

When modelling mass transport through the barrier, many researchers considered this process as a pseudo-steady-state process, because changes in concentrations within the barrier are much faster than changes in the sorbent bed. Thus, a linear concentration gradient was assumed in the barrier, and equations similar to eqn. (11.38) were used with diffusivities that were reduced according to the barrier porosity .[102,104] In other models, transient mass transport through the barrier and the matrix boundary layer was evaluated using Fick's second law similar to eqns. (1.40) and (1.41).[103,105,106] Within the sorbent phase, the mass balance equation included a diffusion term of the free chemical molecules within the pores and a sink term accounting for reversible adsorption. In their model, Countant et al. described mass transport through the adsorbent bed as follows.[104]

$$\varepsilon_s \frac{\partial C}{\partial t} = D_{eff}\left(\frac{\partial^2 C}{\partial x^2}\right) - \rho\left(\frac{\partial q_s}{\partial t}\right) \tag{1.43}$$

where C is the concentration in the gas phase in the pores of the sorbent bed (mass/volume), D_{eff} is the diffusivity in the gas phase of the pores, ρ is the bed density (mass/volume), ε_s is the bed porosity, and q_s is the adsorbed analyte concentration (mass of adsorbate/mass of adsorbent). In this model, the authors related the free and the sorbed concentrations using a linear relationship that uses the retention volume (V_b) of the sorbate/sorbent pair:

$$q_s = V_b C \tag{1.44}$$

Therefore, and taking into account the definition of the bed density, eqn. (1.43) was written as follows:[104]

$$\frac{\partial C}{\partial t} = D\left(\frac{\partial^2 C}{\partial x^2}\right) - \frac{WV_b}{\varepsilon_s lA}\left(\frac{\partial C}{\partial t}\right) \tag{1.45}$$

In this equation, W is the mass of the adsorbent bed, l is the length of the adsorbent bed, x is the length variable along the passive sampler, t is the time variable, and A is the cross-section area of the adsorbent bed. Eqn. (1.45) can be rewritten as follows:

$$\frac{\partial C}{\partial t} = \frac{D}{\left(1 + \frac{WV_b}{\varepsilon_s lA}\right)}\left(\frac{\partial^2 C}{\partial x^2}\right) \tag{1.46}$$

Eqn. (1.46) can by rewritten in the following form, considering $D_{eq} = \frac{D}{1+\frac{WV_b}{\varepsilon_s lA}}$:

$$\frac{\partial C}{\partial t} = D_{eq}\left(\frac{\partial^2 C}{\partial x^2}\right) \tag{1.47}$$

This equation has the form of Fick's second low of diffusion, but with an equivalent diffusivity that is significantly reduced by sorption compared to that in the diffusive barrier.[104]

Patel et al. modelled mass transport of toxic vapor through the adsorbent bed of tube-type samplers using a similar approach; however, they presented scenarios in which the sorption rate term was calculated differently.[105] Their general model had the following form:

$$\varepsilon_s \frac{\partial C}{\partial t} = D_{eff} \frac{\partial^2 C}{\partial x^2} - \bar{R} \tag{1.48}$$

In these equations, C is the concentration in the vapor phase in the diffusive barrier and in the sorbent bed, D_{eff} is the effective bed diffusivity, ε_s is the bed porosity (void fraction of the total volume (dimensionless), and $\bar{R}$ is the average rate of adsorption [amount analyte/(volume . time)]. The authors considered five scenarios that define the average rate of adsorption.[105] In the first scenario, adsorption into the solid surfaces is the dominant mechanism that controls the transfer inside the sorbent bed, whereas the resistances to mass transfer from the bulk gas phase to the surface of the particle and due to the intraparticle diffusion are negligible. In this case, the vapor concentration is uniform throughout the particle and equal to the bulk concentration. The adsorbed concentration, in this scenario, is related to the bulk vapor-phase concentration through the equilibrium isotherm such as Langmuir, or a linear isotherm at low concentrations. In the second scenario, mass transfer from the bulk gas phase to the surface of the particle is the controlling mechanism while the effects of the other mechanisms are not important; therefore, the following equation describes the average rate of adsorption:

$$\bar{R} = \frac{3h_D}{R}\left(C - C_p\big|_{r=R}\right) \tag{1.49}$$

in which, r is the radius variable in the spherical particles, R is the particle radius, h_D is the mass transfer coefficient (length/time), and C_p is the intraparticle vapor concentration (amount/volume).

Intraparticle resistance to mass transfer is the rate-limiting process in the third scenario; thus, the gas concentration is not uniform throughout the particle, and the average sorption rate is calculated using eqn. (1.50):

$$\bar{R} = \frac{3}{R} D_p \left. \frac{\partial C_p}{\partial r} \right|_{r=R} \tag{1.50}$$

where D_p is the effective intraparticle diffusivity. When adsorption into the interior surfaces of the particles controls the overall adsorption rate, the overall adsorption rate is described using eqn. (1.51):

$$\bar{R} = \frac{k_a}{q_m} \left[C_p (q_m - q) - \frac{q}{b} \right] \tag{1.51}$$

where k_a is an empirical rate constant for adsorption, C_p is equal to C when intraparticle resistance is negligible, q is concentration of the analyte adsorbed to the particles (amount of analyte/mass of adsorbent), whereas q_m and b are constants from Langmuir expression: $q = \frac{q_m b C}{1 + bC}$, in which q_m is the monolayer capacity of the surface.

Last, the adsorption rate is described to be proportional to the difference between the equilibrium adsorbed concentration and the actual adsorbed concentration as in eqn. (1.52):

$$\bar{R} = k_q (q^* - q) \tag{1.52}$$

in which k_q is the kinetic constant [mass/(volume · time)], and q^* is the adsorbed concentration in equilibrium with the vapour concentration in the evaluated matrix according to Langmuir isotherm. Whenever the influence of the intraparticle diffusion is significant to the overall uptake, the intraparticle concentration, C_p, is not uniform throughout the particle and should be

differentiated from the interparticle concentration, C. Patel et al. described the concentration profile inside the particle as in eqn. (1.53):[106]

$$\varepsilon_p \frac{\partial C_p}{\partial t} + \rho_p \frac{\partial q}{\partial t} = D_p \frac{1}{r^2} \frac{\partial}{\partial r}\left(r^2 \frac{\partial C_p}{\partial r}\right) + D_s \rho_p \frac{1}{r^2} \frac{\partial}{\partial r}\left(r^2 \frac{\partial q}{\partial r}\right) \tag{1.53}$$

where ε_p is the intraparticle porosity, ρ_p is the particle density (mass/volume), and D_s is the surface diffusivity. The second term in the right-hand side of this equation is usually neglected as surface diffusion has much smaller influence than the other types of diffusion.

Semenov et al. modeled the sampling process into the thin adsorbent layer of SPME using a similar approach.[106] In this approach, mass transport through the thin porous adsorbent layer was described using a simplification of the Langmuir type of isotherm: $C_s = \frac{QKC}{Q+KC}$, in which C and C_s are the concentrations of the free and the bound analyte molecules, respectively, K is the sorbent partition constant, and Q is the maximum concentration of the bound analyte. A simplification was made by considering an approximate linear region and a saturation region as explained in eqn. (1.54):[106]

$$\begin{aligned} C_s &= KC \; when \; C \leq \frac{Q}{K} \\ C_s &= Q \; when \; C > \frac{Q}{K} \end{aligned} \tag{1.54}$$

A time-dependent, moving boundary between the two regions exists with a coordinate x_o on the axis x along the flow direction of the analyte into the sampling phase as follows:

$$C(x_o, t) = \frac{Q}{K} \tag{1.55}$$

Therefore, within the non-saturated region, mass balance equation was expressed as in eqn. (1.56):

$$\frac{\partial C}{\partial t} = D_i \left(\frac{\partial^2 C}{\partial x^2}\right) - \frac{\partial C_s}{\partial t} \tag{1.56}$$

in which D_i is the diffusion coefficient of the free analyte within the pores of the sorbent bed. Since a linear model correlates C and C_s in this region according to eqn. (1.54), eqn. (1.56) can be rewritten in the form of Fick's second law as follows:[106]

$$\frac{\partial C}{\partial t} = \frac{D_i}{1 + K}\left(\frac{\partial^2 C}{\partial x^2}\right) \tag{1.57}$$

where $\frac{D_i}{1+K}$ represents the diffusivity in the bed retarded by adsorption. This is similar to the form presented earlier in eqn. (1.46), with equivalent diffusivity $D_{eq} = \frac{D_i}{1+K}$. It should be noted that the left-hand side in eqn. (1.56) was not multiplied by the porosity of the adsorbent, indicating that the concentration was calculated relative to the entire bulk volume of the adsorbent unlike the case of eqns. (1.43) and (1.48), where the concentration of the free analyte within the pores was calculated in the gas phase volume inside the pores. Also, the sink (rate of adsorption) term in eqn. (1.56) did not include the density of the adsorbent, meaning that the unit of the adsorbed analyte's concentration was the same as that of the concentration of the free analyte (amount/volume). In the saturation region, the bound analyte fully occupies the available adsorption sites and the mass balance equation includes only a diffusion term as presented in eqn. (1.58):[106]

$$\frac{\partial C}{\partial t} = D_i \left(\frac{\partial^2 C}{\partial x^2}\right) \tag{1.58}$$

For samplers with cylindrical geometry, similar models were applied but in the cylindrical coordinate system, in which mass transfer was assumed to occur along the radial

axis.[102,103] Dynamic representation of the transport process through the barrier or the matrix boundary layer is given in this case by eqn. (1.53):[103]

$$\frac{\partial C}{\partial t} = D\frac{\partial^2 C}{\partial r^2} + D\frac{1}{r}\frac{\partial C}{\partial r} \tag{1.59}$$

where C is the concentration in the air-boundary layer (amount/volume), and r is the length in the radial coordinate of the cylindrical sampler.

Transport within the pores of the sorbent of the sampler is described as in eqn. (1.60):[103]

$$\frac{\partial C}{\partial t} = D_{eff}\frac{\partial^2 C}{\partial r^2} + D_{eff}\frac{1}{r}\frac{\partial C}{\partial r} - \rho\frac{\partial q_s}{\partial t} \tag{1.60}$$

where, C is the concentration in the gas-phase of the porous structure (mass/bulk volume), D_{eff} is the effective diffusivity in the bed, ρ is the density of the bulk sorbent (mass/volume), and q_s is the sorbed analyte concentration (mass analyte/mass adsorbent). This equation can also be expressed as follows:[102]

$$\frac{\partial C}{\partial t} = D_{eq}\left(\frac{\partial^2 C}{\partial r^2} + \frac{1}{r}\frac{\partial C}{\partial r}\right) \tag{1.61}$$

Zhang and Wania described the chemical exchange between the gas phase in the macropores and the XAD pellets as in eqn. (1.62). The intraparticle diffusion was considered to be of lower importance than macropore diffusion, thus it was imbedded within the chemical exchange process described in eqn.(1.62):[103]

$$\frac{\partial q_s}{\partial t} = \frac{k_{sorb}C}{\rho} - k_{des}q_s \tag{1.62}$$

where k_{sorb} and k_{des} are sorption and desorption rate constants (time^{-1}), the ratio of which is equal to the air/sorbent partition coefficient similar to that in eqn. (1.1).

Boundary conditions used to solve models of this type include case-dependent conditions, the most common of which are:

1) Continuity in concentration is assumed at an interface (e.g. between the matrix and a diffusive barrier), hence, the concentration is equal on both sides of the interface.[100,105,106]

2) Local equilibrium is assumed at the interface between the matrix and a single-phase passive sampler.[13,86,101] This condition has been used at the boundary between the permeation barrier and the evaluated matrix in the first modelling approach based on the two-film model.

$$C_{PS} = KC_M \text{ at the interface} \tag{1.63}$$

where C_{PS} is the concentration in the in the passive sampler at the interface with the medium, K is the partition coefficient between the passive sampler and the matrix, and C_M is the concentration in the evaluated medium at the interface.

3) Continuity in flux at the interfaces: matrix-passive sampler interface for single phase samplers,[13,86,101] matrix -barrier and barrier-sorbent interfaces as presented in eqns.(1.64) and (1.65):

$$D_M \frac{\partial C_M}{\partial x} = D_B \frac{\partial C_B}{\partial x} \text{ at the medium-barrier interface} \tag{1.64}$$

$$D_B \frac{\partial C_B}{\partial x} = D_S \frac{\partial C_S}{\partial x} \text{ at the barrier-sorbent interface} \tag{1.65}$$

In these equations, D_M, D_B, and D_S are the diffusivities in the evaluated medium, the barrier, and the sorbent, respectively, whereas C_M, C_B, and C_S are the concentrations in these phases. The flux into the passive sampler can be described using mass transfer coefficients. Cao et al. described

the boundary condition at the interface between the barrier and the sorbent using the following equation:

$$D_{eq}\left.\frac{\partial C}{\partial r}\right|_{r=R} = h_{m,e}\left(C_a - \frac{C}{K}\right) \tag{1.66}$$

where R is the radius of the cylindrical sampler, C_a is the concentration in the evaluated air, C is the concentration in the sorbent, K is the equilibrium partition coefficient between the sorbent and air, and $h_{m,e}$ is the mass transfer coefficient. This coefficient constituted convective mass transfer coefficient at the external surface of the barrier, h_m, and the equivalent mass transfer coefficient for diffusion through the barrier, h_m', as in eqn. (1.67):

$$\frac{1}{h_{m,e}} = \frac{1}{h_m} + \frac{1}{h'_m} \tag{1.67}$$

4) Concentration gradient is zero at the dead end of a passive sampler (e.g. tube-type passive samplers),[104,105] at the centre of a flat passive sampler with sampling surfaces on both sides,[13,86,101] and at the centre of a cylindrical passive sampler.[102,103,106] This condition can be described as follows:

$$\frac{\partial C}{\partial x(r)} = 0 \text{ at the end (center) of the sorbent} \tag{1.68}$$

Initial conditions usually are stated as zero concentration inside the sampler, unless the samplers start with a preloaded amount of the analyte (e.g. depuration compounds), in which case the analyte is assumed to be in equilibrium between all phases inside the sampler.[103]

This type of dynamic passive sampling models can be solved numerically using finite difference approximation,[13,102,103,105] or analytically, commonly using Laplace

transformation.[86,101,106] Analytical solutions, however, are only achievable in the case of linear partial differential equations, when linear type of equilibrium isotherm is used.[107]

1.2.5 Empirically Calibrated Models

Several approaches have been presented in the literature attempting to simplify the process of sampling rate determination. Some of these models focused on the prediction of the sampling rate under various meteorological conditions, whereas others predicted the sampling rate based on the molecular structure or physicochemical properties of the analytes. Several studies addressed the effects of meteorological factors on the sampling rate of the PUF passive sampler, for instance. Computational fluid dynamic was a method used to model the effect of the air flow surrounding the PUF sampler housing.[108,109] Petrich et al. presented a method for modelling hourly sampling rates using hourly meteorology.[110] Their model was empirically calibrated using a data set obtained from depuration experiments. This approach aimed at simulating the effects of meteorology including temperature, wind speed, humidity and pressure on sampling rates and analyte concentrations. This approach was further improved later by Herkert et al. by adding hourly temperature correction of the sampler-air partition coefficient and calculation of the effective sampling volume.[111] Recently, Herkert et al. presented a mathematical model capable of determining the sampling rates and the effective sampling volumes for chemicals sampled by the PUF passive air sampler.[27] This model was also empirically calibrated using a set of sampling rates derived from depuration compounds in samples deployed by the Global Atmospheric Passive Sampling (GAPS) network in 24 locations around the world under more diverse meteorological conditions than those used in previous studies presented above.[27]

The quantitative structure–property relationship (QSPR) method is a tool to predict physicochemical properties of chemicals based on molecular structural information.[112] This method was applied to estimate the sampling rates of polycyclic aromatic hydrocarbons (PAHs)[112] and organochlorine pesticides[113] from air into SPMDs. Millar et al. also presented the application of this method in developing a model capable of estimation of sampling rates for Polar Organic Chemical Integrative Samplers (POCIS).[114] QSPR was also used to develop a model that predicts the diffusivity of chemicals in PDMS, which is an important parameter needed for passive samplers that utilize PDMS.[115] Lin et al. also applied this approach to model the pre-equilibrium passive sampling rates of hydrophobic organic compounds (HOCs) from environmental samples.[116]

Furthermore, based on a theoretically established correlation between the PDMS-air partition coefficient of VOCs and their retention on a PDMS stationary phase, Seethapathy and Górecki presented empirical models that simplified the prediction of the sampling rates of VOCs into the WMS from linear temperature programmed retention indices (LTPRI) in GC column with pure PDMS stationary phase.[31] Additionally, many other empirical models presented the sampling rate as a function of log K_{OW}[117,118,119] or simply the molecular size.[117,119] To simplify the correction of the free concentrations determined by PE passive samplers under non-equilibrium conditions, Lao et al. determined the values of the uptake rate constant, the elimination rate constant and the partition coefficient into the PE passive sampler experimentally, and developed correlative relationships with K_{OW} to calculate these parameters.[120] They then linked these parameters to field measurements and generated a generic non-equilibrium correction equation applicable in the case of water boundary layer-controlled sampling using the PE passive sampler.[120] Jia and Fue modeled the sampling rate into the ATD

sorptive tube passive samplers empirically as well.[121] In this work, they presented the sampling rate as a function of the boiling point of the chemical for both short term (8 hours) and long term (7 days) exposures separately, and as a function of the retention volume of the chemical for the short-term exposure.

1.3 Summary

Passive samplers' designs and applications in the various environmental compartments have been broadened significantly since their introduction. Several approaches have been presented to describe the theory behind the process of passive sampling. A common approach originated from Whitman's two-film theory, and is based on the assumption of a uniform passive sampling phase, in which collected analytes are trapped. The process of passive sampling in this manner involves mass transfer through successive resistance regions between the sampled medium and the passive sampler. Linear concentration gradients are assumed in these regions with local equilibrium at the interfaces. This approach also assumes linear exchange kinetics between the sampled medium and the passive sampler. The resulting exponential model describes the entire process of passive sampling. Passive samplers, however, are commonly operated in the linear region or the equilibrium region. In the former region, the concentration in the passive sampler is negligible during the initial stages of sampling, therefore, the amount of analyte collected by the passive sampler is proportional to the product of the sampling time and the concentration (the exposure dose) in the evaluated medium. The sampling rate in this case is assumed to be constant and independent of both the time and the analyte concentration. Therefore, the measured concentrations reflect the TWA concentrations. In the latter region, the passive sampler achieves equilibrium within the time of exposure. The concentration can then be calculated using the equilibrium relation (the partition coefficient) between the sampled medium

and the collecting medium; thus, the calculated concentration reflects a discrete concentration that is in equilibrium with the concentration in the passive sampler.

The sampling rate is commonly calibrated experimentally in the laboratory under controlled conditions or in the field. Another method relies on using performance reference compounds (PRC) preloaded on the passive sampler. These PRCs are used to determine site-specific sampling rates through the isotropic relationship between the offload rate constant of the PRC and the uptake rate constant of the target analyte. PRCs are also used to correct for the effect of the field-specific conditions on the sampling rate, as well as to correct for non-achievement of equilibrium conditions. The last advantage is made possible because the entire sampling process, including all sampling regimes, is included in this calibration method. However, this technique can only be applied in the case of absorption-based receiving phases in the passive sampler.

A common design of a passive sampler consists of a diffusion or permeation barrier and a receiving phase. The receiving phase in the case of sampling from air is usually an adsorbent, the strength of which is assumed to be sufficient to consider this phase as a zero sink. Therefore, these samplers are usually operated in the linear region, assuming a constant sampling rate. Nonetheless, studies showed that, in many cases, this assumption becomes invalid due to both the reversible nature of the adsorption and the non-uniform distribution of the collected analyte in the adsorbent layer of the passive sampler. Several models have been presented in attempts to address the deviation from linearity in such types of samplers. The scope of those models covered diffusive passive samplers, such as tube-type passive samplers, as well as PUF and XAD-based passive samplers. One approach to modelling attempts to simulate the sampling process by an approximate temporal-steady state in hypothetical segments in the adsorption

phase. Another approach used dynamic models to determine accumulation of analytes in passive samplers.

Dynamic models use mass balance equations in all phases involved in the mass transfer process. These models have been applied to both single phase and multi-phase passive samplers. When modelling mass transport through a diffusive passive sampler, mass transfer across the barrier was considered either as a pseudo-steady-state process, or as a transient state process. On the other hand, the mass balance equation within the sorbent phase included a diffusion term of the free analyte molecules within the pores, and a sink term describing reversible adsorption. Some researchers chose to use linear adsorption isotherms as an approximation at low concentrations, hence were able to solve the resulting model equations analytically. Others applied non-linear adsorption isotherms and solved the model equations numerically. In most cases, adsorption to the solid surfaces was considered to be the controlling process of the sink term. Nonetheless, researchers also distinguished other processes that could take control of this term, including mass transfer from the bulk gas phase inside the sorbent bed to the outer particle surface, and diffusion within the porous particles (intraparticle diffusion).

Finally, several empirical models have been presented to simplify the process of sampling rate determination. Some of these models addressed the influence of various meteorological conditions on the sampling rate, while others described the sampling rate as a function of the molecular structure or physicochemical properties of the sampled analytes. The effect of meteorological factors on the sampling rates of the PUF passive sampler was addressed in several studies, which used data on sampling rates obtained using PRCs. The quantitative structure–property relationship (QSPR) method was used as a tool to predict sampling rates of many passive samplers based on the structure of the analyte molecules. Other models used

physicochemical properties of analytes such as K_{OW}, chromatographic retention properties, or boiling points to predict passive sampling rates.

1.4 Scope of the Thesis

The WMS is a PDMS-based permeation passive sampler that utilizes an adsorbent as a receiving phase, as explained earlier. The sampler has been operated in the linear region of passive sampling assuming a zero sink in the adsorbent. Therefore, the sampling rate/uptake rate was previously considered constant and determined using eqn. (1.37). The scope of the present thesis includes:

1. Evaluation of the distribution of sampled analytes inside the adsorption phase of the WMS and the linearity of the uptake rate over periods within commonly applied sampling times.
2. Development of a dynamic model that can explain the decline in the uptake rate occurring earlier than predicted based on the adsorbent capacity, in permeation adsorption-based passive samplers, in general, and in the WMS specifically. The purpose of this model is to develop a better understanding of the sampling process in these samplers, and to provide a tool for optimizing the sampler geometry and design as well as the sampling time, so that the zero-sink approximation can be safely applied.
3. Introduction and evaluation of a method of estimating the effective uptake rate of the WMS. The purpose of this method is to account for potential deviations of the WMS uptake rate from linearity by using the developed dynamic model. This method permits accurate determination of the TWA concentration of the sampled analyte over the sampling time.

4. Extension of the model to describe the storage period after sampling using the WMS. The objectives of this work are to assess the stability of the sampled analytes in the WMS during storage, to evaluate the propagation of the sampled analyte distribution within different sampler's compartments during the storage time, and to validate the efficiency of the current analysis method that excludes the PDMS membrane from analysis.
5. Extension of the model to take into account intraparticle resistance to mass transfer in porous adsorbent particles and its influence on the net uptake rate.
6. Conducting a comprehensive sensitivity analysis of the model. The purpose of this analysis includes the determination of the influence of uncertainty in different input parameters on the uptake rate calculated by the model, identification of the influential input parameters that require accurate determination, and development of practical implications of the sensitivity analysis results in identifying temperature effect on the uptake rate and optimizing the membrane thickness.
7. Describing the effects of the convection conditions in the evaluated medium on the uptake rate of the WMS using a modification of the boundary conditions at the interface between the sampled medium and the PDMS membrane in the developed dynamic model.

CHAPTER 2.

PRELIMINARY EXPERIMENTS

2.1 Introduction

In the initial experiments, the applicability of the WMS in sampling VOCs from water was put into further investigation (details about this application and the setup used in these experiments are available in the author's Master's thesis[122]). For this purpose, a modification of the sampler's design, in a way that would allow deployment of the sampler in any orientation, was needed. The first proposed design, presented in Figure 2-1 (b), consisted of the regular 2-mL chromatographic vial, used with the standard WMS, equipped with a 100-μL glass insert that was filled with the adsorbent. The PDMS membrane, of the regular thickness of 100 μm, was then sealed against the mouth of the insert by means of the crimp cap and a PTFE washer. However, this design failed in providing reproducible results compared to the original design of the sampler when exposed to a water matrix (see ref.[122]). It was hypothesised that increasing the membrane thickness and removing the washer, so that the PDMS membrane would be directly sealed against the glass vial's mouth, would reduce the chances of water leak into the adsorbent.

One important observation in the experiments with the insert-included design of the WMS led to a new scope of investigation, the results of which are included throughout the remaining chapters of this thesis. It was observed that when one of the samplers was decrimped for analysis, a very small portion of the adsorbent inside the insert was lost. Although this was thought to have a negligible effect on the measured amounts of analytes, the analysis of the remaining amount of the adsorbent returned an identical result to those produced by blank samples. This raised the question about the efficiency of distribution of the analyte within the

sorbent bed. Therefore, the next step was to evaluate the distribution of the sampled analytes within the adsorbent bed of the WMS starting with sampling from air. For this purpose, another design was proposed consisting of a 300-µL vial filled with the adsorbent, and a PDMS membrane crimped to the mouth of the vial as illustrated in Figure 2-1 (c).

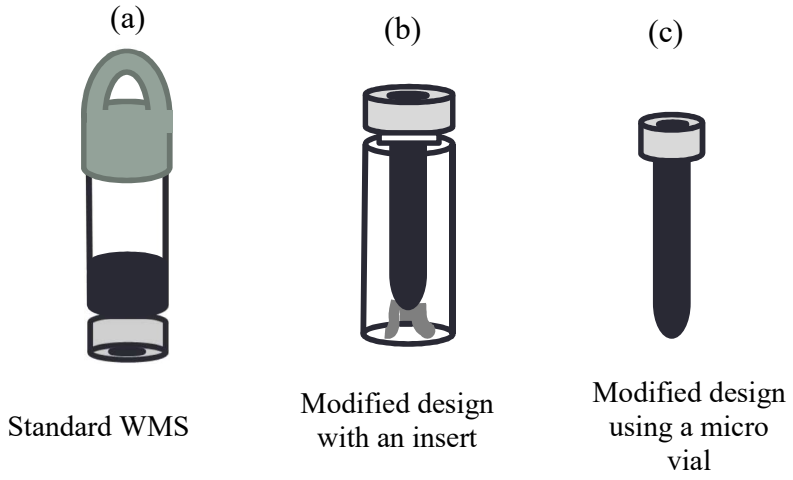

Figure 2-1: Standard design of the WMS (a), and two modified designs: one equipped with an insert inside the vial (b), and another based on a micro-vial (c), both filled with the adsorbent material.

The aim of the work presented in this chapter was to evaluate the effects of potential design modifications on the sampler's performance, and most importantly, to assess the distribution of the sampled analytes within the adsorbent bed of the WMS and the stability of its uptake rates towards analytes in a mixture.

2.2 Experimental

2.2.1 Waterloo Membrane Sampler (WMS)

Three versions of the WMS were included in this evaluation: the standard WMS with a 2-mL vial (C223682C, Chromatographic Specialties INC., Brockville, ON, Canada), the WMS with a 1-mL vial (C223706, Chromatographic specialties), and the modified version consisting

of a round bottom microvial of 300 µL capacity (C2211051, Chromatographic Specialties INC). Anasorb 747, purchased from SKC INC., Eighty Four, PA, USA, was used as the adsorbent. Approximately 200 mg of the adsorbent were added to the 2-mL WMS vial, while about 100 mg was used in the 1-mL WMS. The microvial was filled completely with the adsorbent (~ 160 mg). Each type of the sampler was covered with a PDMS membrane, cut into a circular shape matching the size of the vial mouth and fixed in place by an aluminum crimp cap. Both the 1-mL vial and the microvial have the same size of the top part (the vial's mouth) and both use the same size of the crimp cap. The standard design of the WMS included a polytetrafluoroethylene (PTFE) washer between the vial's opening and the PDMS membrane to provide sufficient sealing. the PTFE washers used in the 2-mL WMS were of the dimensions 0.040" × 0.440" × 0.216" (thickness × OD × ID), whereas the dimensions of the washers used in the 1-mL WMS and the microvial WMS were 0.040" × 0.281" × 0.188" " (thickness × OD × ID). The PTFE washers were purchased from Penn Fibre Plastics (Bensalem, PA, US). The thickness of the membrane used in these experiment (only in this chapter) was 300 µm, which is three times bigger than the standard membrane's thickness of 100 µm. Weighing the membrane was the method of controlling the thickness, as the membranes were cut using dies of fixed diameters. The target weight in the case of the membrane in the 2-mL WMS was 24.0 ± 0.5 mg, while the target weight of the PDMS membrane was 10.8 ± 0.2 mg for the other two versions of the sampler.

2.2.1.1 Fabrication of the PDMS membrane

This procedure was described in the author's Master's thesis,[122] and repeated here with the modification made to produce thicker membranes. Silicone elastomer base was mixed with silicone elastomer curing agent in a ratio of 10:1. These components are available as

SYLGARD® 184 SILICONE ELASTOMER KIT from Dow Corning, USA. Mixing continued for half an hour, after which the mixture was lightly covered with an aluminium foil and placed under vacuum inside a closed vacuum manifold for another half an hour. Air was released intermittently into the manifold to remove bubbles. The mixture was, afterwards, coated on the surfaces of polished crystalline silicon wafers of 19.95 cm diameter (part no. 6TPP1051, from MEMC KOREA COMPANY). An aliquot of approximately 10 g of the mixture was placed on the center of the wafer and processed in a precision spin coating machine (Cee® model 200X, available from Brewer Science, Inc). In the coating method, designed for the regular membrane thickness (~ 100 μm), the wafers were processed for 60 s at the velocity of 625 RPM with a 500 RPM/s ramp. To increase the membrane thickness, approximately 10 g of the mixture was placed on a wafer of a smaller diameter (100 mm) (Montco Silicon, Spring City, PA, USA). The coating method was the same as above except for the spinning velocity, which was reduced to 208 RPM for a membrane of ~ 300 μm thickness, and 315 RPM for a membrane of ~ 200 μm thickness. The coated wafers were then placed inside an oven at 60 °C for two hours. After they were cooled to room temperature, the membranes were coated with fumed silica powder (Catalogue no. S5505, Sigma-Aldrich, Canada, available in 100 g quantities) to prevent the sorbent material inside the WMS from sticking to the membrane. The membranes were then peeled off and used.

2.2.2 Experimental Setup

The Waterloo Membrane sampler, WMS, was exposed to an atmosphere of nitrogen with vapors of 52 VOCs using the setup presented in Figure 2-2. In this setup, the standard gas mixture in nitrogen was delivered from a pressurized custom-made cylinder at a flow rate of 10 mL/min and diluted with a nitrogen flow of 500 mL/min. The flow of the standard gas mixture and the diluting nitrogen were controlled using mass flow

controllers (MKS, Andover, MA, 0-100 mL/min and 0-5000 mL/min respectively) connected to an MKS 4-channel readout system (Andover, MA, Type 247). The diluted standard gas mixture then entered the exposure chamber. This chamber consisted of a cylindrical glass jar of about 10-liter volume, equipped with a circulation fan inserted through the lid. The samplers were inserted through holes drilled in the lid and kept closed during the exposure. The glass jar was wrapped with an insulated jacket connected to a water circulation thermostat (TOMSON, NESLAB Instrument, Inc.). The concentrations inside the chamber were evaluated using active sampling method by pumping the exposure mixture from the chamber through sorption tubes packed with Anasorb 747 at flow rates ranging from 24 to 26 mL/min for times ranging from one to two hours.

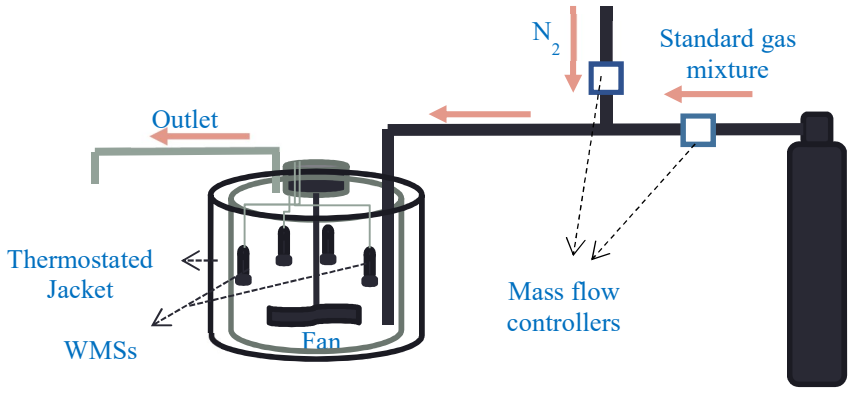

Figure 2-2: Experimental setup used in the initial evaluation of the different designs of the WMS

2.2.3 Desorption of Analytes

Anasorb 747® used both in the sorption tubes and in the WMSs was transferred after sampling into 4 ml glass vials with PTFE/SIL screw caps. To each sample, one ml of CS_2 (purchased from Sigma-Aldrich, Canada) was added. The vials were subsequently sealed and left

at ambient temperature for 40 min with intermittent shaking. For analysis, aliquots of the extract were drawn and transferred into 2 ml crimp top chromatographic vials with 100 µl glass inserts (C731100S, available from Chromatographic Specialties Inc.).

2.2.4 GC-MS Instrument

Agilent 6890 GC- 5973 MS system was used for the analysis. The system was equipped with a 7683 Agilent autosampler with a tray of a 100-sample capacity and a Hewlett Packard (hp) 3683 autoinjector. An Rxi®-624Sil MS capillary column (60 m × 0.32 mm ID × 1.8 µm film thickness) was used with helium as the carrier gas. Chemstation software (Enhanced ChemStation G1701CA, Version C.00.00 21-Dec-1999, Agilent Technologies) was used for data acquisition.

2.2.5 GC-MS Method

The injection was performed in split mode at 2:1 split ratio and 250 °C inlet temperatures. The injection volume was 1 µl. The carrier gas flow rate was set at 2 ml/min. The oven temperature program was set as follows: 35 °C for 5 min, a ramp of 4 °C/min up to 220 °C, which was held for 3 min. External standards were used for multipoint calibration. Selected Ion Monitoring (SIM) mode was used with 2-3 ions for each compound. The list of analytes and target ions are presented in Table 2-1.

Table 2-1: List of analytes and their ions used in the analysis

Analyte	Ions	Analyte	Ions
1,1-Dichloroethylene	96, 61	p-Xylene + m-Xylene	91, 106
Dichloromethane	49, 84	*o*-Xylene	91, 106
trans-1,2-Dichloroethylene	61, 96	Styrene	104, 103, 78
1,1-Dichloroethane	63, 65	Bromoform	173, 171
cis-1,2-Dichloroethylene	61, 96	Isopropylbenzene	105, 120
2,2-Dichloropropane	77, 41	Bromobenzene	77, 156
Bromochloromethane	49, 130	1,1,2,2-Tetrachloroethane	83, 85
Chloroform	83, 85, 47	1,2,3-Trichloropropane	75,77
1,1,1-Trichloroethane	97, 99	Propylbenzene	91, 120
1,1-Dichloro-1-propene	75	2-Chlorotoluene	91, 126
Carbon tetrachloride	117, 119	4-Chlorotoluene	91, 126
Benzene	78, 77	1,2,4-Trimethylbenzene	105, 120
1,2-Dichloroethane	62, 64	tert-Butylbenzene	119, 91, 134
Trichloroethylene	95, 130	1,3,5-Trimethylbenzene	105, 120
1,2-Dichloropropane	63, 62, 41	sec-Butylbenzene	105,134, 91
Dibromomethane	93, 174	p-Isopropyltoluene	119,134,91
Bromodichloromethane	83, 85	1,2-Dichlorobenzene	146, 148
Toluene	91, 92	1,4-Dichlorobenzene	146, 148
1,1,2-Trichloroethane	97, 83	1,3-Dichlorobenzene	146, 148
Tetrachloroethylene	166,164	Butylbenzene	91, 92, 134
1,3-Dichloropropane	76, 41	1,2-Dibromo-3-chloropropane	157, 75
Dibromochloromethane	129, 127	1,2,4-Trichlorobenzene	180, 182
1,2-Dibromoethane	109, 107	Hexachloro-1,3-butadiene	225, 227, 223
Chlorobenzene	112, 77	Naphthalene	128, 127, 129
Ethylbenzene	91, 106	1,2,3-Trichlorobenzene	180,182
1,1,1,2-Tetrachloroethane	133, 131		

2.3 Results and Discussion

2.3.1 Testing the Influence of the Exposure Position in the Chamber

The exposure chamber was designed with eight holes, of the same diameter as the 2-mL WMS, drilled through the top plate to insert the WMSs. Only eight samplers can be exposed simultaneously through these holes. Since the plan was to include a larger number of samplers simultaneously, any additional samplers had to be exposed inside the chamber by attaching them to strings and inserting them through a bigger hole into the chamber. The hole was tightly sealed by a plug wrapped by a layer of aluminum foil and a layer of PTFE tape, and was only open during the insertion of the samplers into the chamber. It was important, though, to evaluate the influence of the exposure position, through the top plate or inside the chamber, on the amounts of analytes sampled by the WMSs. For this purpose, six samplers of the standard-2mL size were prepared with the membrane held in place using a PTFE washer. The samplers were exposed simultaneously. Three of them were inserted through the top plate, while the other three were exposed inside the chamber. The remaining holes in the top plate were sealed. The samplers were removed after one day of exposure and analyzed within the same day.

The results are presented in Figure 2-3, showing that the analyte amounts collected by the samplers inserted through the top plate were lower than those collected by the samplers exposed inside the chamber. This effect becomes clearer when moving from the left side of the graph to the right side, in which direction the boiling point of the analytes increases. This observation can be attributed to the higher face velocity experienced by the samplers inside the chamber as they are closer to the circulation fan. This effect becomes more significant as the partition coefficient of an analyte between PDMS and air increases and as the diffusivity in air decreases, which is the case when the size of the molecule increases. T-test confirmed these results with *t-statistical* = 7.316

much higher than *t-critical* (one tail) = 1.676; therefore, the exposure position has a significant effect on the sampled amounts of analytes. For all experiments performed in this thesis, the samplers were exposed inside the exposure chamber.

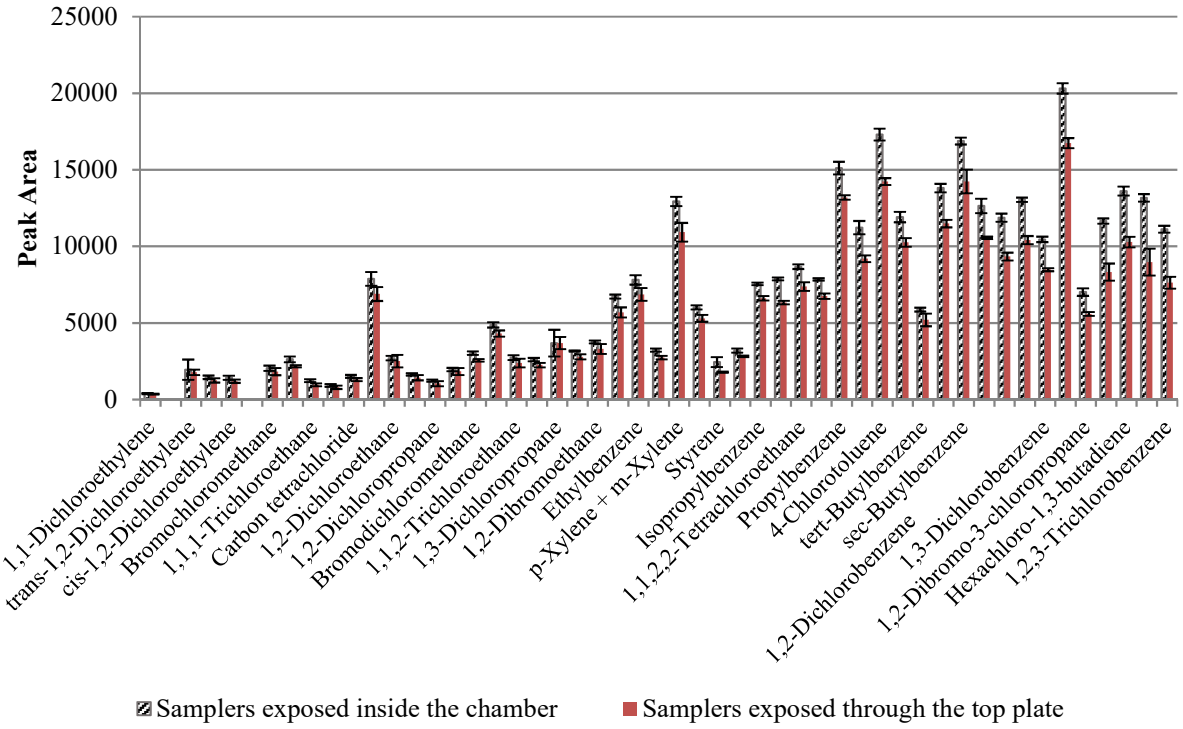

Figure 2-3: Evaluation of the influence of the exposure position in the chamber

2.3.2 Evaluating the Effect of Excluding the Washer from the Sampler's Configuration

To evaluate the sampler's performance if the membrane was directly sealed against the vial's opening by the crimp cap without the support of the PTFE washer, WMSs were prepared using the three sizes of the vials described earlier but without the use of the washers in the 1-mL WMS and the microvial WMS. The performance of these samplers was compared to their performance in the case of washer-supported sealing of the membrane. When the WMSs were

prepared without the use of washers, the edges of the aluminium cap had to be shortened by 1- 2 mm to provide sufficient sealing. Two exposures for each configuration of the 1mL and microvial WMSs (with or without washers) were performed for two different exposure periods, two and seven days. In each exposure, a total of nine samplers were exposed, three of each size (the 2 mL WMS, the 1 mL WMS and the microvial WMS). The 2 mL sampler was prepared with a washer-supported sealing in all exposures. The sampling area in the case of the 2 mL WMS (~ 34 mm^2) is approximately two times the sampling area in either the 1-mL sampler and the microvial sampler (~ 18 mm^2); therefore, it was expected that the amount of analyte collected by the 2-mL sampler would be two times higher than the amount collected by each of the other two versions.

The results of the analysis of the WMSs with the two smaller sizes prepared without washers are presented in Figure 2-4, whereas the results obtained from the analysis of the WMSs prepared with washers are presented in Figure 2-5. It should be noted that the concentrations of analytes in the standard gas were not accurately determined in the former case, and they might have been different than those in the latter case. Nonetheless, it can be seen that the results obtained from the WMSs prepared with washers (Figure 2-5) can be described to be approximately reflecting the predicted ratio explained above. One the other hand, the amounts of analytes in the left side of Figure 2-4 (A) do not reflect this relative ratio. As we move to the right side of the chart, the volatility of the analytes decreases, and the relative intensities representing analytes in different versions of the WMS become more reasonable. This trend becomes more obvious after one week of exposure. The amounts of analytes in the left half of the chart are very similar in the three versions of the sampler, while the amounts of analytes detected in the 2-mL WMS become approximately twice as high as the amounts found in either

of the other two types in the right side of the chart. These observations can be explained by a non-sufficient sealing of the membrane to the sampler's vial without the support of the washer, which led to undesired diffusion of the more volatile components of the gas mixture into the sorbent without permeating through the membrane. This effect became less significant for analytes with higher partition coefficients between the PDMS membrane and air since they have higher tendency to permeate through the membrane.

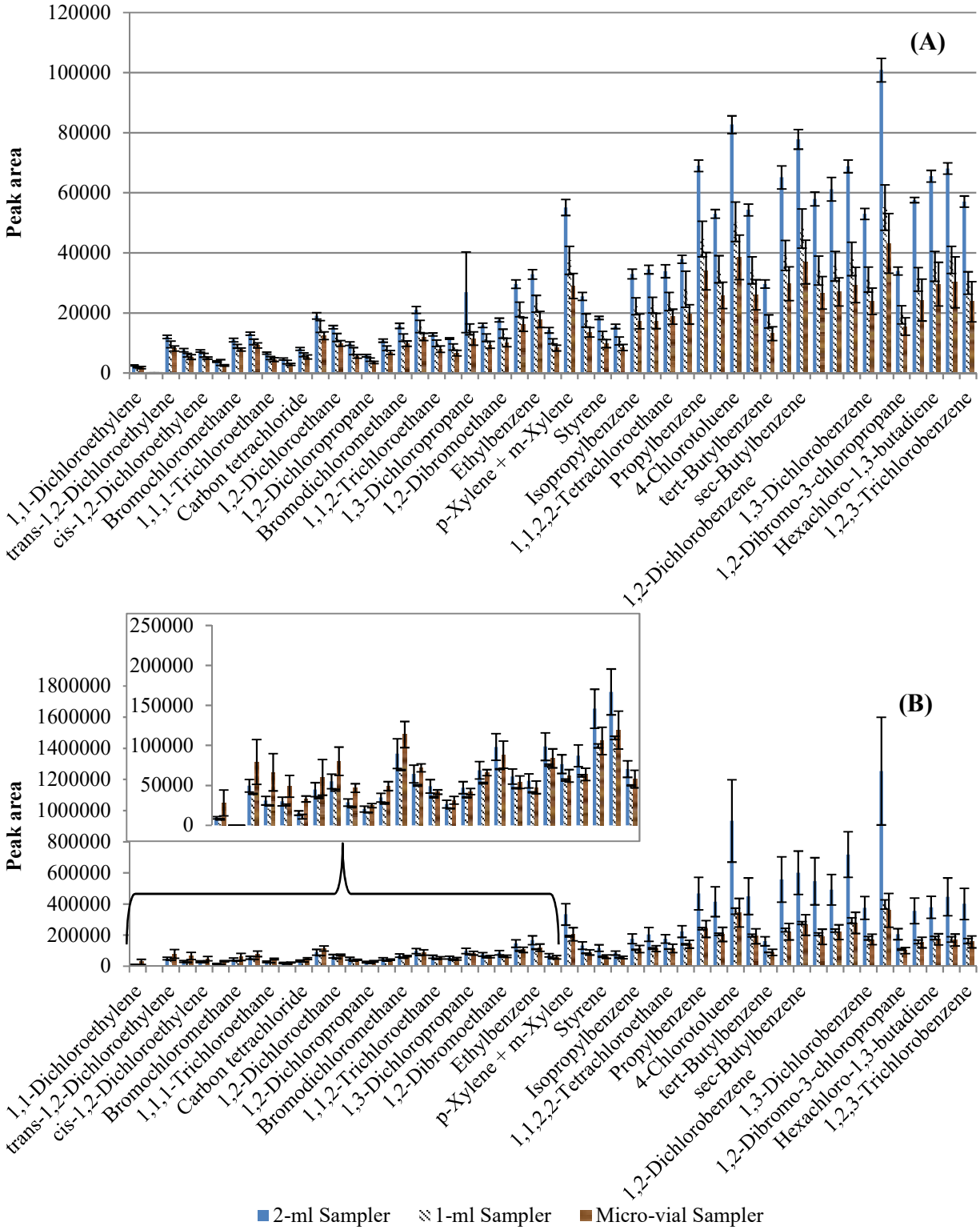

Figure 2-4: Peak areas obtained from the analysis of the three versions of the WMS exposed for two days (A), and for one week (B). The 1 mL WMS and the microvial WMS were prepared without washers.

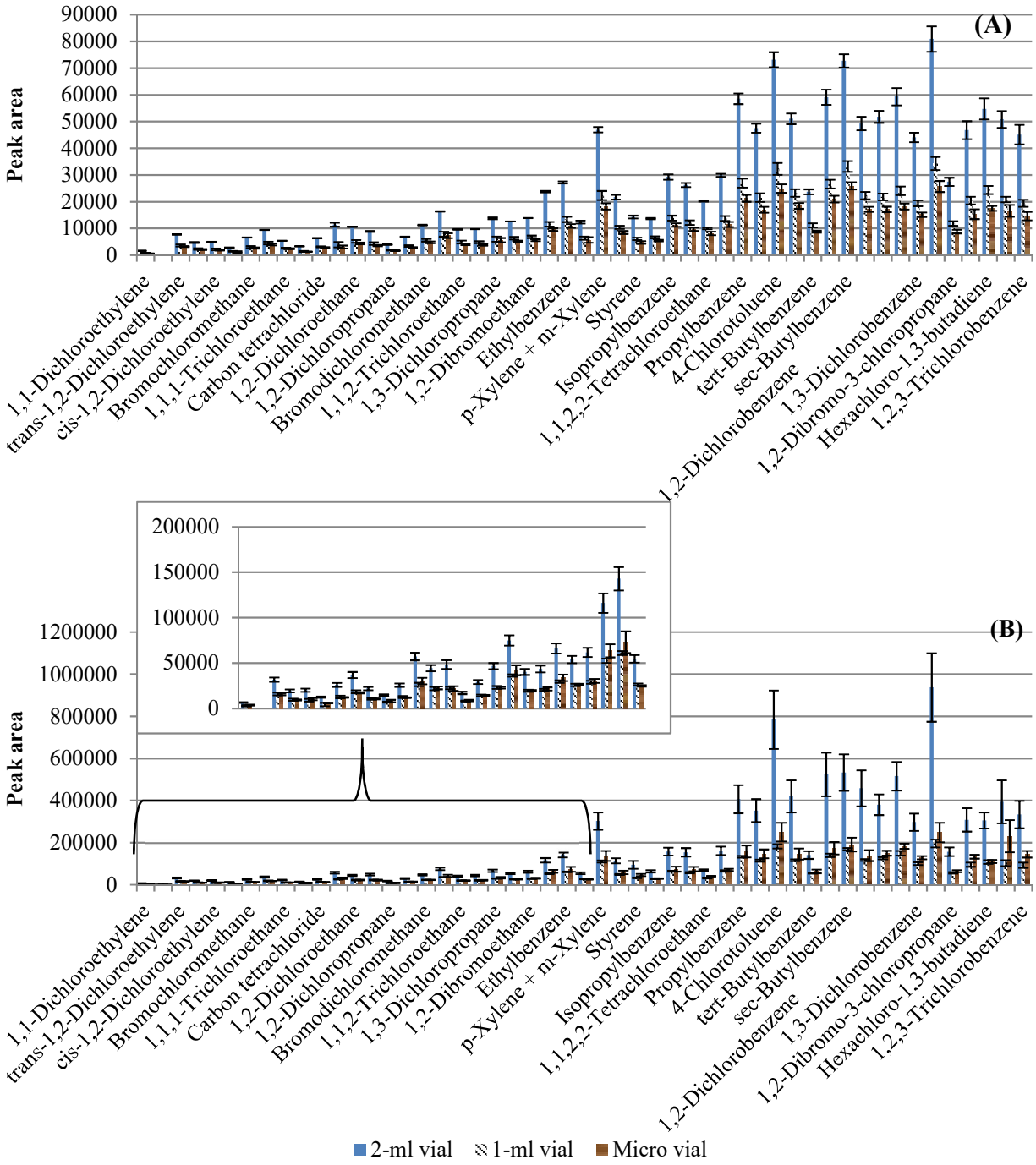

Figure 2-5: Peak areas obtained from the analysis of the three versions of the WMS with washers and exposed for two days (A), and for one week (B).

2.3.3 Evaluation of the Efficiency of Mass Transfer Inside the Sorbent of the WMS and the Linearity of the Analyte Uptake

In this evaluation, the three versions of the WMS (all prepared with PTFE washers) were simultaneously exposed to the standard gas mixture. Three samplers from each size were deployed. In some exposures, three additional microvial WMS (a total of six microvial samplers) were added. After each exposure, the sorbent from each of the three additional microvial samplers was divided into two portions: portion 1 included the layer of the sorbent in contact with the membrane (~ 45±5 mg) and Portion 2 included the rest of the sorbent deeper in the vial. Portion 2 was divided into two other portions for the initial experiments; however, it was found that two portions were sufficient to achieve the purpose of these experiments. The portions were analysed separately. The uptake/sampling rate, U (mL/min), was calculated using the following equation:

$$U = \frac{M}{Ct} \tag{2.1}$$

where M is the amount of an analyte collected by the sampler (μm), C is the concentration in the standard gas inside the chamber (μg/cm^3), which was measured using the parallel active sampling method, and t is the exposure time (min).

2.1.1.1 Results

The results, presented in Figure 2-6, demonstrate accumulation of the analytes in the sorbent portion near the membrane surface, while the rest of the sorbent was found to be practically analyte-free. In some cases, small amounts of the analyte were found in the second portion, but this could be attributed to imprecise separation of the second portion from the first portion of the sorbent. The average concentrations in the chamber were in the range of 3×10^{-5} –

1×10^{-4} g/m^3. The uptake rates measured for the 2-mL WMS, the 1-mL WMS and the microvial WMS are presented in Table 2-2, Table 2-3, and Table 2-4, respectively, for two, three, five, and seven days of exposure. In all three tables, the uptake rates for individual analytes were relatively stable for up to the five-day exposure. For the seven-day exposure, the results seem to reflect a general trend of a decrease in the uptake rates. Although the significance of this decrease differed from one analyte to another, and it could not be observed for some analytes, especially in the case of the microvial sampler, it was a behaviour that needed to be further explored both theoretically and experimentally.

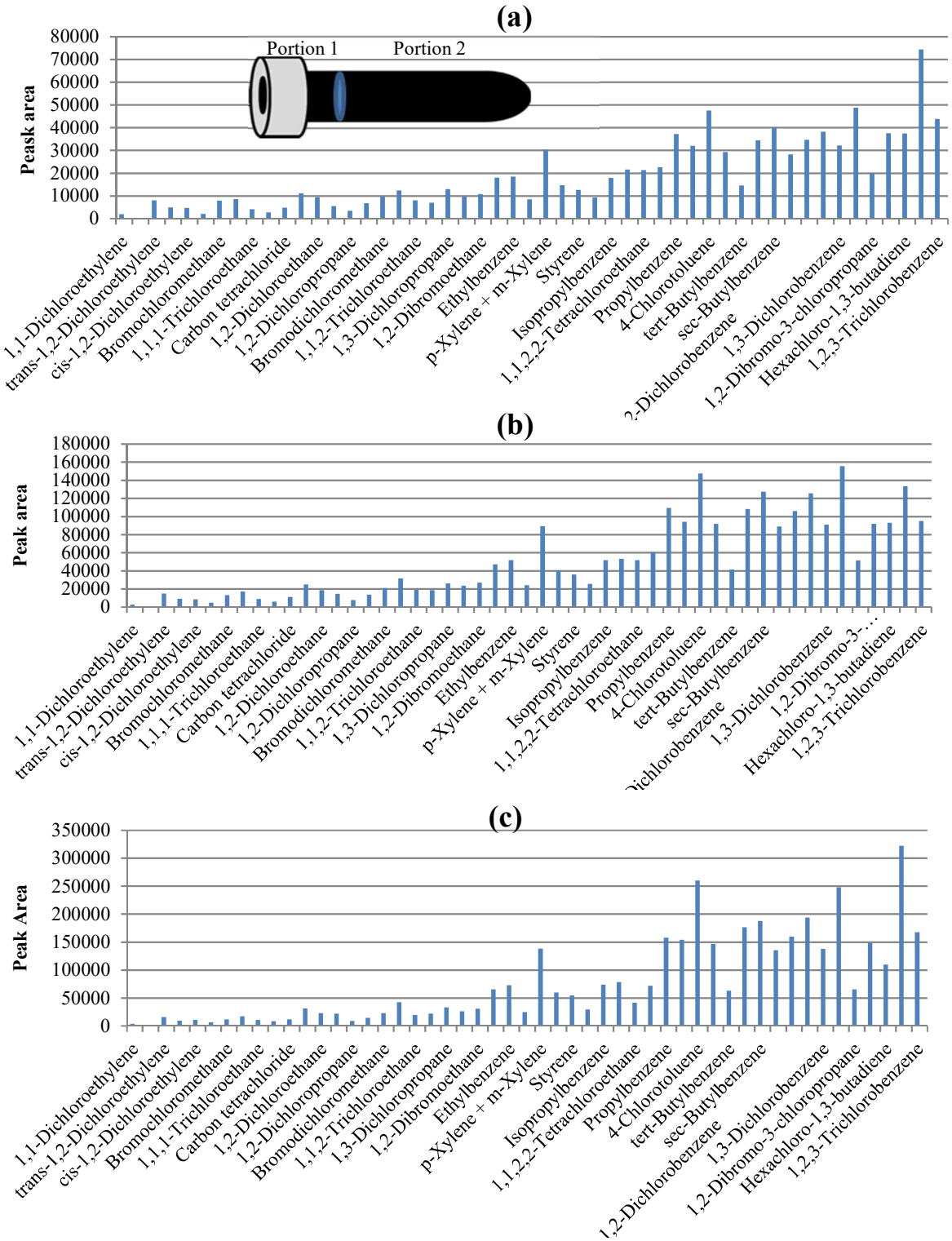

Figure 2-6: Distribution of analytes between the top portion (Portion 1) near the membrane surface, represented by the blue bars, and in Portion 2 deeper inside the vial, represented with red lines (which do not appear clearly in the Figure due to the very negligible amounts found in this portion). The samplers were exposed for two days (a), five days (b) and seven days (c).

Table 2-2: The uptake rate values obtained for the 2-mL WMS

Exposure time (min)	**2673**			**4651**			**6969**			**10130**		
Compound	U (mL/min)	n	RSD %	U (mL/min)	n	RSD %	U (mL/min)	n	RSD %	U (mL/min)	n	RSD %
1,1-Dichloroethylene	0.29	2	1.1	0.23	2	6.1	0.22	3	6.1	0.12	3	7.0
trans-1,2-Dichloroethylene	0.46	2	0.02	0.45	2	5.9	0.48	3	7.4	0.36	3	7.1
1,1-Dichloroethane	0.30	2	2.6	0.26	2	7.2	0.28	3	7.6	0.23	3	8.0
cis-1,2-Dichloroethylene	0.50	2	1.5	0.48	2	7.3	0.52	3	5.5	0.30	3	8.3
2,2-Dichloropropane	0.20	2	2.9	0.23	2	9.2	0.21	3	10.0	0.16	3	5.6
Bromochloromethane	0.64	2	0.8	0.65	2	4.1	0.66	3	7.1	0.57	3	8.1
Chloroform	0.45	2	0.6	0.42	2	4.1	0.45	3	6.5	0.40	3	9.2
1,1,1-Trichloroethane	0.29	2	0.4	0.29	2	1.0	0.30	3	6.6	0.26	3	7.8
1,1-Dichloro-1-propene	0.55	2	0.2	0.56	2	4.4	0.61	3	7.0	0.28	3	7.0
Carbon tetrachloride	0.34	2	1.2	0.35	2	0.0	0.36	3	6.2	0.33	3	7.6
Benzene	0.47	2	6.1	0.53	2	0.8	0.60	3	5.2	0.34	3	7.3
1,2-Dichloroethane	0.68	2	0.7	0.67	2	4.4	0.71	3	5.4	0.55	3	7.7
Trichloroethylene	1.36	2	2.1	1.37	2	3.5	1.40	3	7.3	1.05	3	9.6
1,2-Dichloropropane	0.57	2	0.2	0.60	2	0.9	0.63	3	6.5	0.40	3	7.6
Dibromomethane	1.04	2	0.6	1.08	2	0.8	1.15	3	4.2	0.88	3	7.4
Bromodichloromethane	0.75	2	1.2	0.80	2	0.2	0.82	3	4.7	0.69	3	7.1
Toluene	1.19	2	0.6	1.26	2	0.9	1.33	3	7.8	0.61	3	7.1
1,1,2-Trichloroethane	1.15	2	1.8	1.21	2	0.7	1.25	3	3.0	0.96	3	8.1
Tetrachloroethylene	1.47	2	0.5	1.62	2	1.0	1.72	3	2.9	1.03	3	8.2
1,3-Dichloropropane	1.41	2	2.2	1.61	2	0.8	1.71	3	3.3	0.96	3	8.0
Dibromochloromethane	1.34	2	0.3	1.47	2	1.7	1.50	3	2.6	1.16	3	7.3
1,2-Dibromoethane	1.91	2	0.2	2.09	2	0.9	2.15	3	2.3	1.42	3	7.7
Chlorobenzene	2.26	2	1.2	2.45	2	1.6	2.61	3	1.6	1.33	3	8.8
Ethylbenzene	2.13	2	1.5	2.34	2	0.8	2.51	3	1.6	1.18	3	8.5
1,1,1,2-Tetrachloroethane	1.28	2	4.4	1.43	2	2.0	1.50	3	3.5	1.20	3	7.4
p-Xylene + m-Xylene	2.50	2	2.1	2.76	2	0.4	3.15	3	1.3	1.66	3	12.7
o-Xylene	2.50	2	4.0	2.69	2	1.3	2.91	3	1.6	1.26	3	10.2
Styrene	3.32	2	3.5	3.40	2	3.7	3.99	3	2.5	2.60	3	18.0
Bromoform	2.35	2	1.8	2.56	2	2.4	2.68	3	1.0	2.01	3	8.2
Isopropylbenzene	2.59	2	3.4	2.82	2	1.7	3.01	3	0.7	1.53	3	11.3
Bromobenzene	3.84	2	2.9	4.16	2	2.5	4.75	3	1.5	2.53	3	12.4
1,1,2,2-Tetrachloroethane	1.67	2	1.2	1.93	2	3.9	2.20	3	1.0	1.15	3	5.4
1,2,3-Trichloropropane	2.64	2	1.8	2.90	2	2.7	3.22	3	1.0	2.26	3	11.6
Propylbenzene	3.93	2	3.3	4.52	2	1.5	5.39	3	0.9	3.08	3	14.9
2-Chlorotoluene	3.77	2	3.4	4.36	2	2.4	5.46	3	1.0	2.96	3	14.2
4-Chlorotoluene	4.97	2	3.7	6.12	2	2.7	8.90	3	3.4	5.75	3	16.1

Exposure time (min)	2673			4651			6969			10130		
Compound	U (mL/min)	n	RSD %	U (mL/min)	n	RSD %	U (mL/min)	n	RSD %	U (mL/min)	n	RSD %
1,2,4-Trimethylbenzene	4.13	2	3.8	4.66	2	1.6	6.00	3	1.8	3.73	3	16.5
tert-Butylbenzene	3.13	2	3.9	3.57	2	2.1	4.00	3	1.6	2.11	3	12.2
1,3,5-Trimethylbenzene	5.07	2	4.7	6.03	2	1.8	7.84	3	2.8	5.05	3	17.8
sec-Butylbenzene	4.04	2	3.3	4.60	2	1.8	5.78	3	2.7	3.41	3	14.9
p-Isopropyltoluene	5.51	2	5.0	6.64	2	0.5	9.03	3	4.4	6.23	3	16.9
1,2-Dichlorobenzene	6.17	2	4.2	7.49	2	2.5	9.53	3	4.1	5.73	3	12.0
1,4-Dichlorobenzene	7.72	2	5.3	9.82	2	2.0	14.14	3	5.7	8.41	3	12.2
1,3-Dichlorobenzene	6.54	2	3.9	7.38	2	2.3	9.17	3	3.3	5.37	3	12.8
Butylbenzene	8.14	2	5.8	9.76	2	2.7	15.75	3	7.0	10.96	3	15.8
1,2-Dibromo-3-chloropropane	7.29	2	5.6	7.58	2	3.3	8.68	3	2.9	5.77	3	12.2
1,2,4-Trichlorobenzene	15.40	2	7.1	15.46	2	1.8	19.97	3	7.7	11.55	3	16.6
Hexachloro-1,3-butadiene	11.57	2	7.2	11.33	2	1.4	13.90	3	7.0	9.35	3	11.6
Naphthalene	14.04	2	6.0	13.26	2	3.0	17.91	3	11.1	12.10	3	23.1
1,2,3-Trichlorobenzene	15.13	2	8.1	15.27	2	2.0	21.26	3	10.3	13.19	3	17.8

Table 2-3: The uptake rate values obtained for the 1 mL WMS

Exposure time (min)	2673			4651			6969			10130		
Compound	U (mL/min)	n	RSD %	U (mL/min)	n	RSD %	U (mL/min)	n	RSD %	U (mL/min)	n	RSD %
1,1-Dichloroethylene	0.19	3	5.0	0.13	2	6.2	0.12	3	8.5	0.06	2	15.6
trans-1,2-Dichloroethylene	0.24	3	8.9	0.23	2	2.0	0.24	3	3.8	0.18	2	13.9
1,1-Dichloroethane	0.17	3	7.8	0.13	2	1.8	0.13	3	4.7	0.12	2	16.2
cis-1,2-Dichloroethylene	0.25	3	12.6	0.24	2	3.1	0.23	3	4.0	0.13	2	19.5
2,2-Dichloropropane	0.11	3	8.4	0.11	2	17.0	0.11	3	9.0	0.07	2	13.4
Bromochloromethane	0.32	3	9.8	0.33	2	1.5	0.32	3	2.7	0.28	2	13.2
Chloroform	0.24	3	8.5	0.21	2	0.7	0.21	3	4.2	0.20	2	11.2
1,1,1-Trichloroethane	0.17	3	6.2	0.14	2	2.5	0.14	3	5.2	0.13	2	9.6
1,1-Dichloro-1-propene	0.25	3	13.2	0.30	2	2.3	0.29	3	3.1	0.13	2	12.1
Carbon tetrachloride	0.19	3	5.5	0.17	2	1.4	0.17	3	4.9	0.16	2	11.2
Benzene	0.18	3	19.7	0.27	2	7.0	0.27	3	5.0	0.15	2	11.3
1,2-Dichloroethane	0.37	3	7.5	0.35	2	0.8	0.34	3	3.9	0.27	2	11.7
Trichloroethylene	0.67	3	10.3	0.74	2	0.6	0.68	3	7.1	0.48	2	7.9
1,2-Dichloropropane	0.30	3	5.4	0.32	2	0.6	0.30	3	4.6	0.19	2	9.6
Dibromomethane	0.54	3	8.5	0.57	2	0.5	0.56	3	2.5	0.43	2	9.4
Bromodichloromethane	0.39	3	7.7	0.41	2	0.9	0.40	3	3.8	0.34	2	10.0

Exposure time (min)	2673			4651			6969			10130		
Compound	U (mL/min)	n	RSD %	U (mL/min)	n	RSD %	U (mL/min)	n	RSD %	U (mL/min)	n	RSD %
Toluene	0.58	3	10.7	0.67	2	0.7	0.63	3	3.3	0.29	2	5.6
1,1,2-Trichloroethane	0.59	3	10.2	0.64	2	0.1	0.62	3	3.0	0.46	2	8.2
Tetrachloroethylene	0.73	3	7.3	0.85	2	2.4	0.83	3	3.4	0.48	2	6.8
1,3-Dichloropropane	0.65	3	13.9	0.84	2	3.0	0.80	3	3.2	0.44	2	4.7
Dibromochloromethane	0.69	3	7.4	0.77	2	1.5	0.74	3	3.2	0.56	2	6.3
1,2-Dibromoethane	0.96	3	6.2	1.09	2	3.1	1.05	3	2.5	0.66	2	6.3
Chlorobenzene	1.11	3	6.7	1.28	2	0.6	1.26	3	2.7	0.61	2	3.9
Ethylbenzene	1.08	3	6.7	1.22	2	1.0	1.18	3	3.0	0.51	2	3.8
1,1,1,2-Tetrachloroethane	0.68	3	8.7	0.75	2	2.4	0.73	3	2.8	0.58	2	5.9
p-Xylene + m-Xylene	1.25	3	6.7	1.39	2	0.5	1.37	3	2.6	0.61	2	4.3
o-Xylene	1.23	3	5.6	1.39	2	0.7	1.32	3	1.6	0.54	2	5.2
Styrene	1.50	3	6.4	1.66	2	0.8	1.63	3	1.4	0.95	2	3.3
Bromoform	1.18	3	5.2	1.32	2	1.7	1.29	3	2.0	0.91	2	4.5
Isopropylbenzene	1.27	3	6.1	1.42	2	2.8	1.38	3	2.6	0.63	2	2.7
Bromobenzene	1.84	3	6.4	2.11	2	5.5	2.08	3	5.3	0.98	2	0.7
1,1,2,2-Tetrachloroethane	0.89	3	2.8	0.95	2	2.8	1.03	3	2.3	0.55	2	7.8
1,2,3-Trichloropropane	1.29	3	5.9	1.44	2	2.6	1.46	3	2.1	0.93	2	4.6
Propylbenzene	1.87	3	5.7	2.14	2	1.6	2.18	3	4.5	1.03	2	1.8
2-Chlorotoluene	1.80	3	6.4	2.03	2	1.8	2.13	3	4.7	0.98	2	3.1
4-Chlorotoluene	2.31	3	6.0	2.60	2	0.1	2.88	3	7.6	1.43	2	0.4
1,2,4-Trimethylbenzene	1.94	3	5.6	2.17	2	0.3	2.27	3	4.8	1.08	2	0.3
tert-Butylbenzene	1.51	3	6.2	1.73	2	0.9	1.76	3	1.2	0.82	2	1.8
1,3,5-Trimethylbenzene	2.35	3	5.5	2.68	2	1.6	2.87	3	5.3	1.39	2	3.2
sec-Butylbenzene	1.91	3	5.6	2.12	2	1.3	2.24	3	4.3	1.11	2	1.3
p-Isopropyltoluene	2.56	3	5.7	2.91	2	0.1	3.11	3	7.0	1.66	2	0.9
1,2-Dichlorobenzene	2.72	3	5.1	3.15	2	0.4	3.51	3	9.5	1.99	2	0.6
1,4-Dichlorobenzene	3.29	3	5.9	3.80	2	1.4	4.46	3	10.8	2.58	2	2.67
1,3-Dichlorobenzene	2.98	3	5.2	3.30	2	1.7	3.59	3	8.1	1.91	2	2.5
Butylbenzene	3.51	3	6.6	3.87	2	2.9	4.45	3	11.6	2.43	2	3.6
1,2-Dibromo-3-chloropropane	3.22	3	6.6	3.35	2	1.0	3.61	3	8.6	2.12	2	4.8
1,2,4-Trichlorobenzene	6.79	3	6.7	6.81	2	7.1	7.89	3	20.2	3.64	2	8.7
Hexachloro-1,3-butadiene	5.18	3	6.0	5.02	2	5.8	5.72	3	17.2	3.36	2	7.1
Naphthalene	5.91	3	4.8	5.85	2	7.6	6.58	3	19.0	3.26	2	10.5
1,2,3-Trichlorobenzene	6.57	3	6.5	6.56	2	8.1	7.82	3	22.7	3.83	2	9.3

Table 2-4: The uptake rate values obtained for the microvial WMS

Exposure time (min)	**2673**			**4651**			**6969**			**10130**		
Compound	U (mL/min)	n	RSD %	U (mL/min)	n	RSD %	U (mL/min)	n	RSD %	U (mL/min)	n	RSD %
1,1-Dichloroethylene	0.18	3	0.7	0.12	3	1.5	0.13	3	25.3	0.08	2	3.9
trans-1,2-Dichloroethylene	0.20	3	3.9	0.22	3	2.1	0.24	3	23.6	0.19	2	1.8
1,1-Dichloroethane	0.15	3	3.3	0.12	3	5.1	0.14	3	32.1	0.12	2	3.3
cis-1,2-Dichloroethylene	0.21	3	6.2	0.23	3	1.4	0.26	3	31.2	0.17	2	2.6
2,2-Dichloropropane	0.11	3	21.7	0.11	3	2.3	0.12	3	33.7	0.08	2	3.6
Bromochloromethane	0.27	3	1.9	0.30	3	3.1	0.33	3	23.9	0.28	2	1.9
Chloroform	0.20	3	5.8	0.20	3	4.8	0.23	3	27.1	0.20	2	1.0
1,1,1-Trichloroethane	0.15	3	4.8	0.13	3	6.7	0.15	3	26.4	0.13	2	1.0
1,1-Dichloro-1-propene	0.24	3	8.4	0.28	3	3.0	0.30	3	21.6	0.19	2	0.6
Carbon tetrachloride	0.16	3	7.8	0.15	3	7.6	0.18	3	24.5	0.16	2	1.6
Benzene	0.12	3	11.4	0.24	3	1.5	0.29	3	26.2	0.20	2	2.0
1,2-Dichloroethane	0.31	3	5.9	0.32	3	2.9	0.35	3	23.8	0.30	2	0.8
Trichloroethylene	0.49	3	6.7	0.57	3	2.3	0.68	3	24.5	0.53	2	0.7
1,2-Dichloropropane	0.27	3	6.1	0.29	3	2.3	0.31	3	19.9	0.23	2	0.4
Dibromomethane	0.43	3	6.7	0.52	3	2.5	0.56	3	20.5	0.45	2	0.1
Bromodichloromethane	0.32	3	6.1	0.37	3	4.3	0.41	3	20.4	0.35	2	0.2
Toluene	0.47	3	17.5	0.59	3	5.3	0.72	3	30.9	0.39	2	0.6
1,1,2-Trichloroethane	0.45	3	5.5	0.55	3	3.1	0.62	3	19.9	0.47	2	2.3
Tetrachloroethylene	0.53	3	5.3	0.72	3	5.0	0.84	3	20.4	0.54	2	2.7
1,3-Dichloropropane	0.59	3	17.2	0.71	3	5.1	0.82	3	20.7	0.54	2	1.1
Dibromochloromethane	0.54	3	3.8	0.67	3	4.2	0.75	3	18.6	0.58	2	1.9
1,2-Dibromoethane	0.72	3	5.0	0.92	3	4.4	1.05	3	20.1	0.75	2	3.0
Chlorobenzene	0.87	3	2.9	1.09	3	4.9	1.25	3	19.9	0.80	2	1.6
Ethylbenzene	0.84	3	2.2	1.01	3	4.6	1.19	3	20.8	0.70	2	0.02
1,1,1,2-Tetrachloroethane	0.51	3	6.2	0.67	3	2.5	0.72	3	19.9	0.56	2	4.0
p-Xylene + m-Xylene	0.99	3	2.2	1.15	3	5.0	1.38	3	22.3	0.88	2	0.2
o-Xylene	0.96	3	3.5	1.15	3	6.4	1.34	3	20.5	0.74	2	0.1
Styrene	1.12	3	2.3	1.36	3	5.0	1.67	3	22.7	1.19	2	0.4
Bromoform	0.94	3	3.1	1.11	3	5.3	1.29	3	19.6	0.95	2	3.1
Isopropylbenzene	0.99	3	2.7	1.17	3	5.9	1.38	3	20.9	0.84	2	0.2
Bromobenzene	1.40	3	2.3	1.70	3	8.4	2.08	3	22.7	1.38	2	1.9
1,1,2,2-Tetrachloroethane	0.71	3	1.9	0.94	3	8.3	1.03	3	18.5	0.68	2	7.4

Exposure time (min)	2673			4651			6969			10130		
Compound	U (mL/min)	n	RSD %	U (mL/min)	n	RSD %	U (mL/min)	n	RSD %	U (mL/min)	n	RSD %
1,2,3-Trichloropropane	1.02	3	10.3	1.19	3	6.1	1.43	3	21.2	1.06	2	3.8
Propylbenzene	1.45	3	1.2	1.70	3	6.9	2.15	3	22.8	1.42	2	1.3
2-Chlorotoluene	1.37	3	3.3	1.65	3	8.1	2.12	3	24.2	1.40	2	1.6
4-Chlorotoluene	1.77	3	0.3	2.07	3	9.4	2.84	3	27.5	2.15	2	1.7
1,2,4-Trimethylbenzene	1.51	3	0.9	1.73	3	8.0	2.26	3	24.3	1.53	2	1.7
tert-Butylbenzene	1.17	3	2.3	1.38	3	5.8	1.70	3	23.9	1.08	2	1.9
1,3,5-Trimethylbenzene	1.82	3	1.2	2.11	3	6.3	2.88	3	27.3	1.96	2	1.4
sec-Butylbenzene	1.47	3	1.7	1.70	3	5.1	2.27	3	26.5	1.44	2	1.3
p-Isopropyltoluene	1.95	3	0.8	2.24	3	6.1	3.17	3	27.2	2.25	2	1.9
1,2-Dichlorobenzene	2.15	3	2.3	2.48	3	7.6	3.50	3	29.0	2.37	2	4.4
1,4-Dichlorobenzene	2.50	3	2.1	2.89	3	7.9	4.51	3	32.1	3.12	2	4.4
1,3-Dichlorobenzene	2.28	3	2.7	2.62	3	8.8	3.56	3	26.6	2.39	2	3.5
Butylbenzene	2.56	3	2.5	2.89	3	9.8	4.45	3	29.7	3.45	2	2.9
1,2-Dibromo-3-chloropropane	2.30	3	3.2	2.69	3	10.2	3.45	3	27.1	2.56	2	4.3
1,2,4-Trichlorobenzene	4.91	3	6.7	5.23	3	11.8	7.48	3	22.9	4.91	2	1.9
Hexachloro-1,3-butadiene	3.72	3	5.4	3.88	3	11.6	5.41	3	25.7	3.60	2	4.3
Naphthalene	4.71	3	6.0	4.54	3	11.8	6.27	3	23.0	4.65	2	3.5
1,2,3-Trichlorobenzene	5.02	3	7.1	5.10	3	13.9	7.34	3	23.8	5.21	2	2.9

The above results raised the question about the efficiency of the mass transfer within the adsorbent bed of the WMS (Figure 2-6), which could challenge the validity of the zero-sink assumption. Accumulation of collected analytes near the membrane increases the concentration in the gas phase within the pores of the sorbent bed at its interface with the membrane, which potentially decreases the concentration gradient across the membrane and decreases the flux into the adsorbent. Although the change in the uptake rate with time needed further verification with more experimental data, the non-uniform distribution of the analytes in the sorbent bed directed the research towards developing a better understanding of the sampling process using the WMS and the effects of resistance to mass transfer in the sorbent bed on the uptake rate.

2.1.2 Challenge Exposure of the WMS

To further confirm the observation of non-uniform distribution of the analytes in the adsorbent bed, and to ensure that this observation was not only due to the small concentration of the analytes inside the sampler, the following experiments were conducted in which microvial WMSs were exposed to the headspace of pure trichloroethylene (TCE). In these experiments, each sampler was inserted through a small hole in the lid of a 250-mL glass jar containing pure TCE. The sampler was wrapped with a Teflon tape to provide sufficient sealing with the lid. The adsorbent was divided immediately after retrieval into three portions: the top portion, which was in contact with the membrane (45 ± 5 mg of the adsorbent), the middle portion deeper inside the vial (50 ± 5 mg), and the deepest portion (50 ± 5 mg). These portions were analyzed separately. The procedure was also repeated following the same steps but with a one-day storage period after retrieval of the samplers. The microvial WMSs were in this case placed after retrieval inside a 20-mL glass vial sealed with a plastic screw-cap with an aluminium liner. The threads of the 20-mL vial were wrapped with Teflon tape to provide sufficient sealing. The samplers inside the storage vials were then left at ambient temperature for one day. For the analysis, the desorption method and the instruments were the same as those described in sections 2.2.3 and 2.2.4 respectively. The injection volume was 2 µL. The inlet temperature was 250 °C with a split ratio of 100:1 for the analysis of the top portion of the adsorbent, and 5:1 for the other two portions. The flow rate through the column was 2 mL/min, with a temperature program that started at 35 °C with a ramp of 30 °C/min up to 200 °C which was held for one min. SIM mode was used to detect the TCE ions with m/z of 95 and 130. The detector was turned off for the first five min of the run as a solvent delay time.

2.1.2.1 Results

Details about the amounts found in each fraction and the exposure times are presented in Table 2-5.

Table 2-5: Amounts detected in each portion of the adsorbent after exposures to the headspace of pure TCE.

			Amount of TCE (µg)		
			Top portion	**Second portion**	**Third portion**
No storage	**1 h &12 min exposure**	Sampler 1	22000	0.15	0.04
		Sampler 2	19000	0.15	0.02
		Sampler 3	19000	1.6	0.06
	2 h exposure	Sampler 1	25000	610	0.06
		Sampler 2	21000	80	0.03
		Sampler 3	21000	8.3	0.02
Analysis after one day of storage	**2 h exposure**	Sampler 1	20000	7400	240
		Sampler 2	16000	7500	0.17

To confirm the huge amounts of the analyte collected by the sampler, the same experiment was repeated by exposing three microvial WMSs to the headspace of TCE for two hours and measuring the collected amounts of analyte by weighing the samplers before and directly after the exposure. The results, presented in Table 2-6, show that an amount of 25 mg of TCE was collected, which confirms the results presented earlier in Table 2-5.

Table 2-6: Evaluation of the amount of analyte collected by the WMS by weighing the sampler.

Sampler	Weight Before exposure (g)	Weight after 2h of exposure (g)	Increase (g)
1	1.374437	1.400043	0.025606
2	1.388185	1.41336	0.025175
3	1.393012	1.41845	0.025438

It can be concluded from these results that resistance to mass transfer exists within the adsorbent bed. Significant analyte amounts were detected in the very top portion of the samplers in all cases, while the amounts detected in the other portions were negligible when the adsorbent was analyzed immediately after retrieval. Storage for a certain time, however, allowed diffusion of a small amount of the analyte deeper inside the bed. Despite the fact that vapor concentration at this level does not represent most real-life sampling scenarios, and that in an actual sampling process the analyte flux into the adsorbent bed through the membrane is much smaller, the results reflect a mechanism of sampling involving three processes: permeation through the membrane, reversible adsorption onto the sorbent, and diffusion inside the sorbent bed. The first process can be considered rate determining while the other two are significantly faster. The evaluation of these processes was conducted through the development of a mathematical model that describes the sampling process in the WMS, which represents the main theme of this thesis.

CHAPTER 3.

EXPERIMENTALLY VALIDATED MATHEMATICAL MODEL OF ANALYTE UPTAKE BY PERMEATION PASSIVE SAMPLERS*

3.1 Introduction

Passive sampling is a sampling technique in which analyte molecules are collected passively via transport driven by the chemical potential difference between the sampled medium and the collecting medium.[3] The approach is employed increasingly often for sampling from different environmental compartments due to its many advantages, including the relatively low cost of the samplers and the simplicity of the deployment procedures that do not involve pumping and do not require attendance during operation.[69] In addition, several sample preparation goals can be achieved simultaneously when using passive samplers, including isolation of the analytes from the matrix, pre-concentration of the analytes to improve the analytical sensitivity, and, in some cases, modification of the matrix for instrumental compatibility. Consequently, passive sampling is an effective tool for saving the analysis time and costs, in addition to the often-significant reduction in solvent use.[5]

---

* This chapter was published as the following article: F. Salim, M. Ioannidis and T. Górecki, Experimentally validated mathematical model of analyte uptake by permeation passive samplers, *Environ. Sci.: Processes Impacts*, 2017, 19, 1363.

Passive samplers commonly consist of a mass transfer-defining barrier and a receiving phase. The barrier can be either a permeable (or semipermeable) membrane in permeation passive samplers, or a static layer of the matrix in diffusive passive samplers.[5] The barrier is assumed to control the rate at which analyte molecules migrate into the receiving phase, which can be a solid adsorbent or a liquid solvent. In so-called kinetic passive samplers, analytes are collected continuously during the exposure at rates that are dependent on their concentrations in the sampled medium, the design of the sampler, the temperature, and the properties of the analytes. In equilibrium passive samplers, sampling continues until equilibrium between the receiving phase and the sampled medium is achieved. The concentrations determined with the latter type of samplers reflect analyte concentrations around the time of sampler retrieval, whereas they reflect time-weighted average (TWA) concentrations in the case of kinetic passive samplers. TWA concentration determination constitutes an important advantage of kinetic passive samplers as compared to other sampling tools that provide snapshot information about the measured concentrations. This work was motivated by the desire to improve TWA concentration determination in kinetic permeation passive samplers.

When kinetic passive samplers are used for sampling from air, the receiving phase, which is an adsorbent in most cases, is assumed to behave as a "zero sink", meaning that molecules permeating or diffusing through the barrier are completely removed at the barrier interface with the receiving phase. In this idealized behavior, all resistance to mass transfer is in the membrane (the barrier), and the concentration profile is similar to that presented in Figure 3-S1 in the Supporting Information section (Appendix A). Assuming that the air around the sampler is well-mixed, so that the bulk concentration in the sampled air, C_0 (amount of analyte / unit volume),

approximately equals the concentration near the sampler's surface, this concentration can then be calculated as follows:[5]

$$C_0 = \frac{M}{Ut} \tag{3.1}$$

where M is the amount of analyte collected by the sampler in time t, and U (volume / time) is the uptake rate of the sampler towards the analyte, which is a conventional term used to define the sampling rate. This uptake rate is defined as the flow rate that would yield the same mass collected by the passive sampler if drawn through a sorptive medium within the same sampling time.

Under the zero-sink assumption, the uptake rate of permeation passive samplers is expressed as follows:[5]

$$U = \frac{DKA}{L_m} \tag{3.2}$$

in which D (m^2/sec) is the diffusion coefficient of the analyte in the membrane material, K (unitless) is the partition coefficient of the analyte between air and the membrane, A (m^2) is the sampling area and L_m (m) is the thickness of the membrane. In this idealized sampling process, the uptake rate of the sampler is assumed to remain constant until the adsorbent approaches saturation. This assumption is consistent with the idea that mass transfer of the analyte within the sorbent bed is sufficiently rapid so that the sorption capacity of the entire sorbent bed is available for maintaining the zero sink conditions during the sampling time.

Other models have been developed for different types of passive samplers, such as tube-type diffusive samplers,[97,98,105] polyurethane foam (PUF) and XAD passive samplers,[103] and

diffusion gradients in thin films (DGT) passive sampler.[123,124] Cao et al. developed an inverse optimization method for a diffusive passive sampler.[102] In this work, we develop a mathematical model to more accurately describe the sampling process in a permeation passive sampler with an adsorbent as a receiving phase, aiming to elucidate the limitations of eqn. (3.2). The model was numerically solved using the method of lines in MATLAB. The permeation passive sampler used in this evaluation was the Waterloo Membrane Sampler (WMS) described next. The model, however, can be tailored to suit different types of permeation passive samplers, including samplers employing porous adsorbent phases. The novelty of the developed model is the description of the sampling process in adsorbent-based passive samplers equipped with a permeation barrier, used mainly for sampling VOCs from air (although the model can be modified to suit other applications of permeation passive samplers). This study develops a better understanding of the sampling process in an adsorption-based permeation passive sampler by considering resistance to mass transfer within the sorbent bed and its effect on the uptake rates during sampling.

The Waterloo Membrane Sampler (WMS), shown schematically in Figure 3-1, is a permeation passive sampler developed at the University of Waterloo.[31,32] This sampler utilizes a polydimethylsiloxane (PDMS) membrane as the permeation barrier, and an adsorbent material as the receiving phase (see the Experimental section for a detailed description). Several types of granular adsorbents have been used in the WMS, including Anasorb 747 (activated carbon), Carbopack B (graphitized carbon black) and Carboxen-1016 (carbon molecular sieve). Carbopack B, which is a non-porous adsorbent, was used in this study. The WMS has been successfully employed in sampling of volatile organic

compounds (VOCs) from air and soil gas.[34-36] The performance of the sampler has also been evaluated in comparison with three other passive samplers.[125]

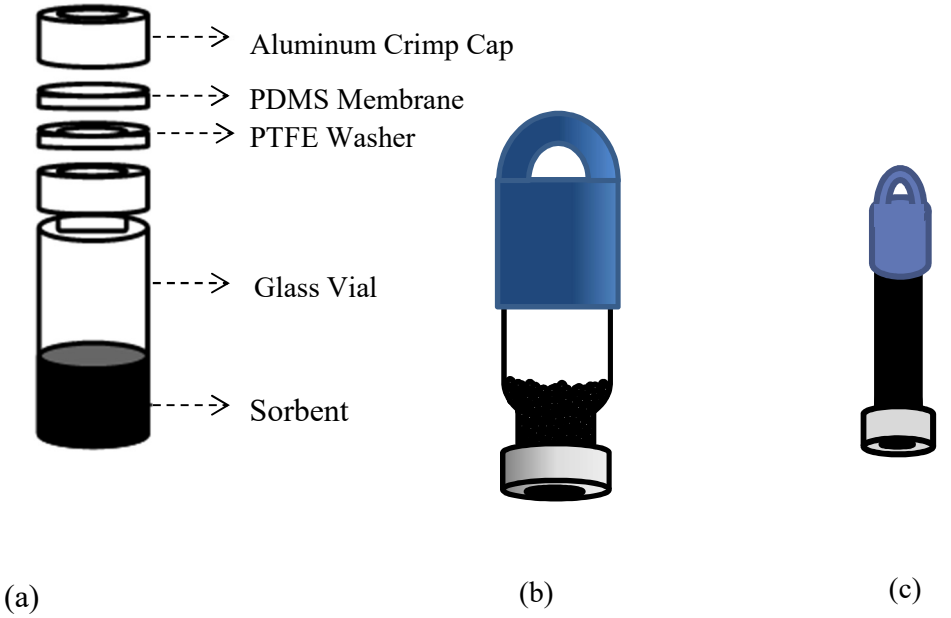

Figure 3-1: The Waterloo Membrane Sampler (WMS): fabrication (a), regular WMS (b), modified microvial WMS (c).

On several separate occasions (unpublished data), it has been observed that the uptake rates of the sampler decreased with long exposure times, an observation previously attributed to sorbent saturation. However, experiments using a modified, microvial version of the WMS, showed that during exposure to high analyte concentrations, analytes accumulated almost exclusively within a few-millimeter thick sorbent layer near the membrane, whereas the rest of the sorbent was practically analyte-free (see Supplementary Information for details).[1] This means that resistance to mass transfer within the sorbent bed was created during sampling, rendering the zero sink assumption

[1] These details were moved to Chapter 2 in this thesis

progressively less valid. Uptake rate decrease with time was also reported for diffusive passive samplers.[98,126,127] Recall that accurate determination of environmental concentrations relies on accurate knowledge of the uptake rate (see eqn. (3.1)). The current work provides a model that can explain uptake rate declines in permeation passive samplers. Most importantly, this work provides a tool for optimizing the sampler geometry and the sampling time, and for matching the target analyte with the proper adsorbent so that the zero-sink approximation can be applied for the assigned exposure time. Otherwise, the model can predict the significance of changes in the uptake rate and the appropriate correction that is needed when this change is important. This is essential when investigating environmental problems, such as vapor intrusion investigations, in which accurate determination of the contamination level is required.

3.2 Theory

In the presented model, mass transfer is assumed to occur in one dimension, as shown in Figure 3-2. In this figure, which conceptually illustrates sampling using the WMS, the membrane thickness is L_m (m) and the sorbent bed thickness is L_b (m):

$$0 \le x \le L_m : \text{ membrane}$$

$$L_m \le x \le (L_m + L_b) : \text{sorbent bed}$$

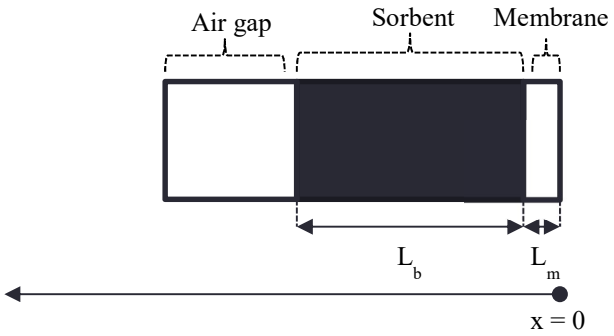

Figure 3-2: Conceptual model of the sampler evaluated in the study.

Transient diffusion of analyte in the membrane is described by the following equation:

$$\frac{\partial C_m}{\partial t} = D_m \frac{\partial^2 C_m}{\partial x^2} \tag{3.3}$$

where C_m is the concentration of the analyte in the membrane (mol/m^3), t is the time (s), D_m is the diffusion coefficient of the analyte in the membrane material (m^2/s), and x is the distance (m). Mass balance of the analyte in the void phase within the sorbent bed, on the other hand, may be stated as follows:[128]

$$\varepsilon \frac{\partial C_b}{\partial t} = D_{eff} \frac{\partial^2 C_b}{\partial x^2} - (1 - \varepsilon) \frac{\partial q}{\partial t} \tag{3.4}$$

In eqn. (3.4), ε is the interparticle porosity of the sorbent bed (the ratio of void volume to the total bed volume), C_b is the concentration of the free analyte molecules in the gas phase within the void space of the sorbent bed (mol/m^3), q is the abundance of the solute associated with the solid phase expressed as moles of solute adsorbed per unit volume of the solid particles (mol/m^3), and D_{eff} is the effective diffusion coefficient of the free molecules in the gas phase within the sorbent bed. The effective diffusion coefficient is calculated as follows:

$$D_{eff} = \frac{D_a \cdot \varepsilon}{\tau} \tag{3.5}$$

where D_a is the diffusion coefficient of the analyte in air (m^2/s) and τ is the tortuosity of the sorbent bed, which represents the ratio of the tortuous path length of diffusion to the straight path length ($\tau > 1$).

Material balance for the analyte in the solid phase within the bed leads to the following equation:

$$(1-\varepsilon)\frac{\partial q}{\partial t} = (k_c \alpha)(C_b - C^*) \tag{3.6}$$

in which k_c is the mass transfer coefficient (m/s), which expresses the kinetics of analyte mass transfer between the void and solid phases within the bed; α is the specific surface area (1/m), that is the surface area available for adsorption per unit bulk volume of the sorbent bed; and C^* is the concentration of the free analyte that is in equilibrium with the adsorbed analyte concentration. This concentration is expressed as a function of the adsorbed concentration using the adsorption isotherm, as presented later in the paper.

The air gap at the other end of the sorbent bed (see Figure 3-2) is assumed well-mixed, such that material balance for the analyte in this space yields:

$$V_a \frac{\partial C_a}{\partial t} = -AD_{eff} \left.\frac{\partial C_b}{\partial x}\right|_{x=L_b} \tag{3.7}$$

In this equation, C_a is the concentration of the analyte in the air gap (mol/m^3), V_a is the volume of the air gap at the back of the sampler (m^3), and A is the surface area of the sorbent bed-air gap interface (m^2). When the vial is completely filled with sorbent, the volume of the air gap is zero ($V_a = 0$), and eqn. (3.7) can be written as follows:

$$\left.\frac{\partial C_b}{\partial x}\right|_{x=L_b} = 0 \tag{3.8}$$

Initially, no analyte is present inside the sampler (including the membrane, the sorbent bed and the air gap). Therefore, one can write the initial conditions:

$$\begin{aligned} &C_m = 0 \ ; \quad 0 < x \leq L_m \ and \ t = 0 \\ &C_b = 0; L_m < x \leq L_m + \ L_b \ and \ t = 0 \\ &q = 0; L_m < x \leq L_m + L_b \ and \ t = 0 \\ &C_a = 0; x \geq L_m + L_b \ and \ t = 0 \end{aligned} \tag{3.9}$$

The boundary conditions are given as follows:

At the interface between the sampled air and the membrane ($x = 0$), local equilibrium is assumed at all times:

$$C_m = KC_0 \tag{3.10}$$

where K is the partition coefficient of the analyte between air and the PDMS membrane (unitless), and C_0 is its concentration in the air near the membrane surface (mol/m^3).

At the interface between the membrane and the sorbent bed ($x = L_m$), local equilibrium is also assumed at all times:

$$C_m = KC_b \tag{3.11}$$

Additionally, due to continuity in flux across the interface, one can write:

$$-D_m \left.\frac{\partial C_m}{\partial x}\right|_{x=L_m} = -D_{eff} \left.\frac{\partial C_b}{\partial x}\right|_{x=L_m} \tag{3.12}$$

Differential equations (3.3), (3.4) and (3.7) subject to the initial and boundary conditions stated above were solved numerically using the method of lines.[129] This method relies on replacing the spatial derivatives in the partial differential equations with algebraic approximations using the finite difference approximation. As shown next, this results in a system of coupled ordinary differential equations that are integrated in time.

In the membrane, distance in the *x* direction along the thickness of the membrane is discretized into *M+1* points with a spacing of Δx_m:

$$\Delta x_m = \frac{L_m}{M} \tag{3.13}$$

The position of each point $j = 1, \ldots, M+1$ in the *x* direction is given as follows:

$$x_j = (j-1) \cdot \Delta x_m \tag{3.14}$$

Using the centered finite difference approximation of the second spatial derivative, the following relationship is obtained:

$$\left.\frac{\partial^2 C_m}{\partial x^2}\right|_{x=x_j} \approx \frac{C_{m(j+1)} - 2C_{m(j)} + C_{m(j-1)}}{(\Delta x_m)^2} \tag{3.15}$$

where $C_{m(j)}$ is short for $C_m(x_j, t)$. Eqn. (3.3) at each point j = 1,…, *M*+1 can then be written as follows:

$$\frac{dC_{m(j)}}{dt} = D_m \frac{C_{m(j+1)} - 2C_{m(j)} + C_{m(j-1)}}{(\Delta x_m)^2} \tag{3.16}$$

Similarly, a grid of *N+1* points is used to discretize the sorbent bed, with a spacing of Δx_b:

$$\Delta x_b = \frac{L_b}{N} \tag{3.17}$$

In this grid, the position of each point $i = 1, \ldots, N+1$ is given as x_i:

$$x_i = (i-1) \cdot \Delta x_b \tag{3.18}$$

Eqn. (3.4) can then be written for each point i in the grid as follows:

$$\frac{dC_{b(i)}}{dt} = \left(\frac{D_{eff}}{\varepsilon}\right) \cdot \left(\frac{C_{b(i+1)} - 2C_{b(i)} + C_{b(i-1)}}{(\Delta x_b)^2}\right) - \left(\frac{1-\varepsilon}{\varepsilon}\right) \cdot \left(\frac{dq_i}{dt}\right) \tag{3.19}$$

Additionally, eqn. (3.6) at each point in the sorbent bed takes the form:

$$\frac{dq_i}{dt} = \frac{k_c \alpha}{(1-\varepsilon)} [C_{b(i)} - C^*(q_i)] \tag{3.20}$$

The concentration in the membrane at the air-membrane interface can be obtained from eqn. (3.10), assuming constant concentration in the air in contact with the sampler:

$$\frac{dC_{m(1)}}{dt} = 0 \tag{3.21}$$

At the point of contact of the membrane with the sorbent bed ($x = L_m$), the condition of equilibrium is expressed by eqn. (3.11) as follows:

$$\frac{dC_{m(M+1)}}{dt} = K \frac{dC_{b(1)}}{dt} \tag{3.22}$$

The concentration of the free analyte in the sorbent bed at $x = L_m$ can be expressed using Eqn. (3.19) as follows:

$$\frac{dC_{b(1)}}{dt} = \left(\frac{D_{eff}}{\varepsilon}\right) \cdot \left(\frac{C_{b(2)} - 2C_{b(1)} + C_{b(0)}}{(\Delta x_b)^2}\right) - \left(\frac{1-\varepsilon}{\varepsilon}\right) \cdot \left(\frac{dq_1}{dt}\right) \tag{3.23}$$

Eqn. (3.23) includes the concentration, $C_{b(0)}$, at a fictitious point, $i = 0$. This fictitious concentration can be eliminated by considering the boundary condition given in eqn. (3.12), which is rewritten using finite difference approximations as follows:

$$D_{eff}\frac{C_{b(0)}-C_{b(2)}}{2\Delta x_b}=D_m\frac{C_{m(M)}-C_{m(M+1)}}{\Delta x_m} \tag{3.24}$$

Accordingly, $C_{b(i=0)}$ is calculated from the following equation:

$$C_{b(0)}=C_{b(2)}+\left(2\cdot\frac{D_m}{D_{eff}}\cdot\frac{\Delta x_b}{\Delta x_m}\right)\cdot\left(C_{m(M)}-C_{m(M+1)}\right) \tag{3.25}$$

Additionally, eqn. (3.7) can be rewritten using the centered finite difference approximation:

$$\frac{dC_a}{dt}=-\frac{A}{V_a}D_{eff}\frac{C_a-C_{b(N)}}{2dx_b} \tag{3.26}$$

The concentration C_a calculated in this equation is used to formulate eqn. (3.19) at point $i = N+1$, which is the deepest point within the sorbent bed:

$$\frac{dC_{b(N+1)}}{dt}=\left(\frac{D_{eff}}{\varepsilon}\right)\left(\frac{C_a-2C_{b(N+1)}+C_{b(N)}}{(\Delta x_b)^2}\right)-\left(\frac{1-\varepsilon}{\varepsilon}\right)\left(\frac{dq_{N+1}}{dt}\right) \tag{3.27}$$

When the vial is completely filled with sorbent and no air gap is present, eqn. (3.8) can be approximated as follows:

$$\frac{\partial C_{b(N+1)}}{\partial x}\approx\frac{C_{b(N+2)}-C_{b(N)}}{2\Delta x_b}=0 \tag{3.28}$$

which means that $C_{b(N+2)}=C_{b(N)}$. This equation can be used to rewrite eqn. (3.19) for $i = N+1$ when the vial is completely filled with sorbent:

$$\frac{dC_{b(N+1)}}{dt}=\left(\frac{D_{eff}}{\varepsilon}\right)\left(\frac{2C_{b(N)}-2C_{b(N+1)}}{(\Delta x_b)^2}\right)-\left(\frac{1-\varepsilon}{\varepsilon}\right)\left(\frac{dq_{N+1}}{dt}\right) \tag{3.29}$$

A MATLAB (R2015a, MathWorks, USA) code was written to solve the ODEs presented above using an ODE solver appropriate for stiff problems, *ODE15s*. The mesh sizes were as follows: M =19, N = 200. These sizes produced stable concentration and

uptake profiles. Changing these sizes did not show significant effect on the simulation results. The code calculates the concentrations at different points within the membrane and within the sorbent bed (both free and adsorbed concentrations) at a series of time steps throughout the exposure time. Subsequently, the code calculates the total number of moles present in the sorbent bed both as adsorbed analyte and as free analyte at the end of each time step. The total amount present in the membrane at each time step is also calculated. Finally, the code uses the total adsorbed amount at each point in time to calculate the integrated uptake rate over the exposure time up to that point using the equation:

$$U(t_n) = \frac{M(t_n)}{C_0 \cdot t_n} \tag{3.30}$$

in which $U(t_n)$ (m^3/s^{-1}) is the uptake rate calculated at time t_n (s). The time t_n ranges from $t_0 = 0$ at the beginning of sampling, and $t = t_f$, the time of sampler retrieval (end of sampling), with n time steps. $M(t_n)$ is the amount (number of moles) adsorbed at time t_n. The code is available upon request from the authors.

3.3 Experimental

3.3.1 Waterloo Membrane Sampler (WMS)

The PDMS membrane in the WMS covers the mouth of a glass chromatographic vial (usually 1 or 2 mL volume) in which the adsorbent material is contained, as shown in Figure 3-1. The design presented in Figure 3-1 (c) is a modified design of the sampler, in which a microvial of 300 µL volume is filled with the sorbent before crimping the cap with the membrane. In this way, the sampler can be operated in any orientation unlike the original design, which has to be deployed with the membrane facing downward to maintain it in contact with the sorbent. The

modified design was first used in the work presented in this paper. This design would also be more suitable for the application of the sampler in sampling from groundwater, where less control of the sampler orientation is possible, especially that the regular design sampler tends to float at the water surface. The application of the WMS in groundwater sampling is still under investigation. Both the regular WMS and the modified microvial WMS were used in this work. The regular WMS was prepared using a 2 mL chromatographic crimp-top vial with approximately 250 mg of Carbopack^{TM} adsorbent enclosed. Carbopack^{TM} is a graphitized carbon black available from Supelco, Sigma-Aldrich (Oakville, Ontario, Canada). The PDMS membrane was fabricated following a process described elsewhere.[122] The membrane was cut into circular pieces of the size of the vial mouth opening using a die, and crimped in place in between the aluminum cap and a polytetrafluoroethylene (PTFE) washer. The thickness of the membrane was approximately 100 μm. Weighing the membrane was employed as a method of controlling its thickness, as the diameters of the cut membranes were always the same. The target weight of the membrane in the 2 mL WMS was 8.0 ± 0.5 mg, and the PTFE washers were of the dimensions 0.040" × 0.440" × 0.216" (thickness × OD × ID). These washers were made of virgin PTFE, and purchased from Penn Fibre Plastics (Bensalem, PA, US). The microvial WMS was prepared in the same manner using a glass, round bottom microvial of 300 μL capacity (C2211051, Chromatographic Specialties INC, Brockville, ON, Canada) with 93 mg of Carbopack^{TM} adsorbent enclosed. The target weight of the PDMS membrane was 3.7 ± 0.2 mg for this version of the sampler. The PTFE washers of the dimensions 0.040" × 0.281" × 0.188" (thickness × OD × ID) were purchased from the same vendor.

3.3.2. Chemicals

Anhydrous toluene (99.8 %) used in this evaluation was purchased from Sigma-Aldrich (Oakville, Ontario, Canada). All standards were prepared in methanol, HPLC grade (≥ 99.9%), also purchased from Sigma-Aldrich, Canada.

3.3.3. Experimental Setup

The experimental evaluation was conducted using the setup illustrated in Figure 3-S2 (Appendix A). In this setup, nitrogen gas was obtained from a high-pressure cylinder and passed through an activated charcoal purifier before it entered a mass flow controller (MKS, Andover, MA, 0-100 mL/min). The flow rate was monitored and set using an MKS 4-channel readout system (Andover, MA, Type 247) connected to the mass flow controller in series. The purified nitrogen gas, flowing at a rate of 100 mL/min, was passed through an analyte vapor generator. This generator consisted of a flow-through vessel with a vapor source enclosed. The vessel was placed inside a GC oven to control the temperature as a method of controlling the vapor concentration. Toluene vapor was produced inside the vessel using a diffusion source or a PTFE permeation source for lower concentrations. The diffusion source consisted of a 4 mL glass vial with neat liquid toluene enclosed. The vial was sealed with an open top screw cap and Teflon/Silicon septum (purchased from Fisher Scientific, Ottawa, ON, Canada). A 60 mm long fused silica capillary (Restek guard column) of 0.25 mm ID was inserted through the cap septum as a diffusion path. Details about the PTFE permeation source are available elsewhere.[1] Equilibration of the standard gas temperature to room temperature was achieved by passing the gas through an approximately 4 m long copper tube of a 1/8” OD before entering the exposure cell. This cell consisted of a 1 L, 3-neck, round-bottom flask with the standard gas entering through one side neck and flowing through the flask to the other

side neck, which was connected to a fume hood with a flexible tube. The samplers were inserted into the exposure cell through the top neck kept closed at all times except during sampler insertion and removal. A three-way valve was connected before the exposure cell to allow collecting active samples for concentration determination. Active sampling was conducted by switching the flow to pass through a sorption tube with the other end connected to a bubble flow meter to accurately measure the flow. The active sampling time ranged from 40 s to 5 min, depending on the concentration. For two sets of experiments (1, 2, 3, and 4-day exposures at a concentration of 1.6_1 mg/m^3 and the experiment at the concentration of 5.3 mg/m^3 for up to 26 days), the flow rate of the purified nitrogen entering the standard gas generator was increased to 896 ml/min to lower the concentration. In these experiments, with longer exposure times planned and more control of the temperature required, a thermostated chamber was used instead of the exposure cell. This chamber consisted of a cylindrical glass jar of about 10-liter volume, equipped with a circulation fan inserted through the lid. The samplers were inserted through a hole drilled in the lid and kept closed during the exposure. The glass jar was wrapped with a Tygon tube and an insulated jacket. The tube was connected to a water circulation thermostat (TOMSON, NESLAB Instrument, Inc.). The concentration in this case was measured either by drawing 1 ml of the standard gas entering the chamber using a gas-tight syringe and injecting it directly to the GC in splitless mode, or by drawing 10 ml of the standard gas (using a gas tight syringe) through a sorption tube packed with Carbopack B, which was analyzed using the same method used to analyze the sorbent of the passive sampler (WMS).

3.3.4. Analysis

All passive samples obtained using the WMS were analyzed by transferring the sorbent into thermal desorption tubes, described in the next section. The sorbent was sandwiched between two layers of glass wool (Fisher Scientific, Ottawa, ON, Canada) of approximately 1.5 cm thickness for each layer. The tube with the glass wool was thermally cleaned at approximately 350 °C before using it to analyze the sorbent. The tube with the sorbent inside was then transferred to a thermal desorption unit for analysis. Active samples were taken using the same desorption tubes and analyzed directly after sampling. Multipoint calibration was achieved using external standards prepared in methanol. A 1 µL aliquot of each standard was spiked using a 10 µL syringe into a cleaned desorption tube packed with a clean sorbent in between two layers of glass wool as explained above.

3.3.5. Instruments

A Dynatherm thermal desorption (TD) unit (model 9300 ACEM, CDS Analytical , Oxford, PA, USA) equipped with a single glass sorbent tube, 8 mm OD × 6 mm ID × 4.5" long, with a glass frit, was used for desorbing the analytes from the sorbent. The TD unit was connected to an Agilent 6890 GC-5973 MS system through a heated transfer line inserted into the injector of the GC. The GC instrument was equipped with an Rxi®-624Sil MS capillary column (60 m × 0.32 mm ID × 1.8 µm film thickness, Restek, Bellefonte, PA) with helium as the carrier gas. Chemstation software was employed for data acquisition and processing and for calibration and quantification.

Perkin Elmer thermal desorption unit (ATD 400) was used in two sets of experiments (1, 2, 3, and 4-day exposures at a concentration of 1.75×10^{-5} mol/m^3 (1.61 mg/m^3) and the

exposures at the concentration of 5.3 mg m-3 for up to 26 days). This TD unit was equipped with stainless steel tubes, 6.35 mm OD × 90 mm long, with two PTFE caps. The transfer line of the TD unit was connected directly to the GC column with a press-tight universal connector (Restek, Bellefonte, PA, U.S.).

3.3.6. TD-GC-MS Method

When Dynatherm TD unit was used, the sorption tube was heated to 330 °C for 7 min during desorption with the focusing trap held at ambient temperature. Desorption was then followed by tube cooling for 1 min before the focusing trap was heated to 300 °C for 5 min. When tubes with the standards were analyzed, a solvent drying time of 1 min was added before desorption. The GC inlet was set to 250 °C with a split ratio of 1:150 and a carrier gas flow rate at 1 mL/min. The temperature program of the oven was set to 90 °C for 5 min, followed by a ramp of 50 °C/min up to 300 °C. Selected Ion Monitoring (SIM) mode was used, with the two ions for toluene being m/z 65 and 91.

When the Perkin Elmer TD unit was used, shorter desorption times were found to be sufficient. The tube was heated to 330 °C for 5 min during desorption. The focusing trap was held at -23 °C during primary desorption, which was followed by the trap heating to 300 °C for 3 min. Inlet pressure that controls the column flow was set at 116 KPa to obtain a flow of approximately 2 ml/min, and the desorption flow was 16 ml/min. Inlet split was off, while outlet split was utilized with a split flow of 20 ml/min. The temperature program of the oven was set to 90 °C for 2 min, followed by a ramp of 30 °C/min to 300 °C, held for 3 min. Because of small fluctuations in the column flow from run to run and with the presence of components other than toluene in the standards, the mass spectrometer was operated using scan mode and the m/z = 91 ion was quantified.

When standard gas was injected directly to the GC, the temperature program was started at 40 °C for 2 min, followed by a ramp of 20 °C/min to 200 °C. Ions of m/z = 91 and 92 were monitored in this case using SIM mode.

3.3.7. Parameter Determination

The numerical model was tested using Carbopack B (60/80 mesh) as a test adsorbent, and toluene as a test analyte. This selection of the test sorbent and analyte was based on the availability of literature data related to the parameters used in the model, in addition to the prediction that with a weak sorbent like Carbopack B, the model results could be easily evaluated within the experimental time frame. It is important to emphasize here that the rate at which the uptake rate changes with time and the resultant predictions of the validity of the zero sink assumption depend on the particular sorbent-analyte combination. Model results with this regard depend on the unique parameters for every analyte and every sorbent. Other sorbent-analyte combinations will be evaluated in future work.

The sorption isotherm of toluene on Carbopack B is of Freundlich type in the range $(0 < C^* < 100)$ ppmv:[93]

$$q = 28.875 \cdot \left(\frac{C^*}{1500}\right)^{\frac{1}{1.566}} \tag{3.31}$$

with q in mg/cm^3 and C in ppmv. Equilibrium between free and adsorbed analyte within the sorbent bed at equilibrium can then be expressed as follows:

$$C^* = (7.666 \times 10^{-6}) \cdot q^{1.566} \tag{3.32}$$

in which the adsorbed concentration, q, and the free concentration (C*) at equilibrium with the adsorbed concentration are expressed in mol/m^3. The value used for the partition coefficient of toluene between air and PDMS, K = 840 ± 30, was an average value of measured, calculated and estimated values found in the literature.[72,130] The value of the toluene diffusion coefficient in air used in the evaluation was 8.50×10^{-6} m^2/sec,[131] while an average value of $(1.1 \pm 0.5)\times10^{-10}$ m^2/sec for the toluene diffusion coefficient in PDMS was calculated based on values found in the literature.[132-136]

The porosity ε used in this evaluation was the bed interparticle porosity, as the sorbent, Carbopack B, consists of non-porous granular particles. The porosity of randomly packed particles is expected to be in the range of 0.43 for loose packing to 0.37 for close packing.[137] In this study, an average value of 0.40 was used. The tortuosity value for a granular porous bed is reported to be in the range 1.1-1.7.[138] The value of 1.61 was used here and it was verified that changing tortuosity within the above-mentioned range did not affect the model results. In the absence of convection inside the sampler, as is appropriate for passive sampling, the mass transfer coefficient, k_c, was estimated from the following relationship:[139]

$$Sh = \frac{k_c \cdot d}{D_{eff}} = 2 \qquad (3.33)$$

where Sh is Sherwood number, and d is the diameter of the particle, which has an average value of 213.5 µm.

The value of the specific surface area, α, was obtained by multiplying the surface area provided by the manufacturer (as the surface area per unit of the bulk sorbent mass) by the bulk density. The specific surface area of Carbopack B reported by the manufacturer is 100

m^2/g of the bulk sorbent. The bulk density (ρ_b) was calculated from the porosity as follows:

$$\varepsilon = 1 - \frac{\rho_b}{\rho_s} \tag{3.34}$$

The particle density, ρ_s, was measured using a pycnometer, yielding the value of 1.9 ± 0.2 g/cm^3. The calculated bulk density value was 1.12 g/cm^3.

The sampling areas, A, in the 2 mL and the microvial samplers were 34 ± 3 mm^2 and 18 ± 2 mm^2 respectively. The thickness of the membrane was initially measured using a micrometer, producing a value of 100 μm. This value was verified using optical comparator measurement (Mitutoyo PH-14LS). The value obtained from four measurements was 101.6 μm with a standard deviation of 10.37. Therefore, the value of 100 μm was accepted in this evaluation. The thickness of the sorbent bed, L_b, in the regular WMS is approximately 14 mm, leaving an air gap at the back of approximately 1.36 cm^3 in volume, whereas the thickness of the sorbent bed in the microvial WMS was ~26 mm with a small air gap observed at the end of the sampler of approximately 50 mm^3 in volume. A summary of the parameters and their values used in this work can be found in Table 3-S1(see Appendix A).

3.4 Results and Discussion

Figure 3-3 demonstrates the predicted changes in the concentration profiles within the membrane and the sorbent bed in a 2 mL WMS after exposure times of 1 day, 1 week, and 1 month at a constant toluene concentration of 4.7×10^{-2} mg/m^3 (0.01 ppmv) in the air. As seen in Figure 3-3 (a), the concentration gradient in the membrane decreases as the exposure time is extended for the combination of a weak Carbopack B sorbent and

toluene. This gradient becomes significantly smaller after 1 month of exposure leading to a significant decrease in the toluene diffusion flux into the sorbent. Figure 3-S3 in the Supporting Information (Appendix A) shows that the concentration profile within the membrane under these conditions propagates rapidly and becomes linear within one minute of exposure. This indicates fast dynamics in the membrane, which may be assumed to be at quasi-steady state. The concentration gradient within the membrane then diminishes slowly as the concentration at the membrane-sorbent interface increases. The changes in the concentration gradient can be attributed to the increase in the concentration of the analyte within the sorbent bed near the membrane surface. Figure 3-3 shows changes in the concentration profiles of the adsorbed analyte (Figure 3-3 (b)) and the analyte in the air within the sorbent bed (Figure 3-3 (c)); note the vastly different concentration scales) for different exposure times. The concentration gradient within the sorbent bed diminishes over time, leading to a decrease in the driving force for diffusion inside the bed. As a result, the assumption that the sorbent bed acts as a "zero-sink" for toluene/Carbopack B combination is valid only during early stages of the sampling process.

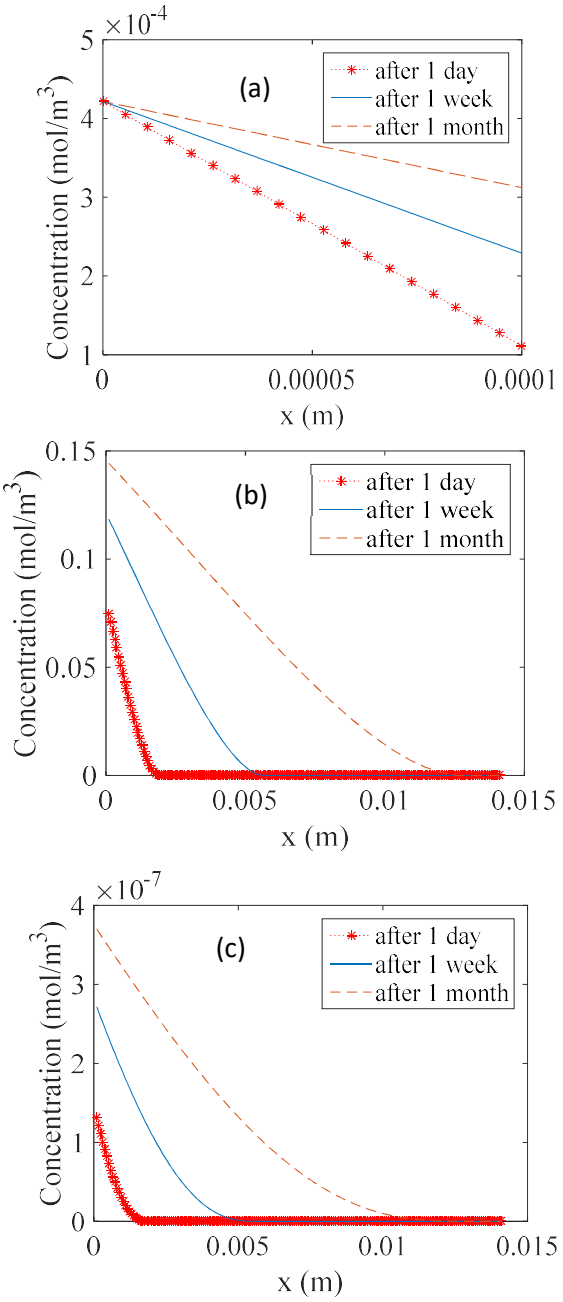

Figure 3-3: Model results presented as concentration profiles of the analyte in the membrane (a), in the sorbent bed as adsorbed analyte (b), and in the air phase within the sorbent bed (c) at different times of sampling at a concentration of 4.7×10^{-2} mg/m^3. Note the different scales in all three panels.

Resistance to mass transfer within the sorbent bed results in the development of analyte concentration gradients in the air inside the bed. As the amount of adsorbed analyte at the beginning of the sorbent bed increases with time, so does the concentration

of analyte in the air at equilibrium with it. Consequently, the concentration gradient within the membrane, hence also the analyte flux through the membrane, gradually decrease. The latter is directly related to the uptake rate.

The resultant uptake rate time profiles are presented in Figure 3-4 (A and B) for different toluene concentration levels for both versions of the sampler packed with Carbopack B. This figure also shows a comparison of these profiles with the ideal uptake rate profile, calculated using eqn. (3.2). The ideal uptake rate profile suggests independence of the uptake rate from the concentration level in the ambient air and from the time of exposure. On the other hand, according to the developed model and at a concentration of 2.3×10^{-3} mg/m^3 of toluene in the sampled air, the uptake rate of both samplers decreases by 25-26% after one week of exposure and by 34% after two weeks. This means that for Carbopack B and this concentration level of toluene, the zero sink assumption would be applicable for ~1-week exposures with an error not exceeding the 30% uncertainty as assigned by US-EPA Method TO-15. However, at higher concentrations, the decrease in the uptake rate becomes more significant. The decline in the uptake rate in the microvial sampler is very similar to that in the regular sampler, as presented in this figure. When increasing the thickness of the membrane by a factor of two, not only does the uptake rate decrease by the same factor, but the rate at which the uptake rate changes with time also decreases. This effect is shown in Figure 3-4 (C) and in Table 3-1. These results demonstrate the importance of optimizing the dimensions of the

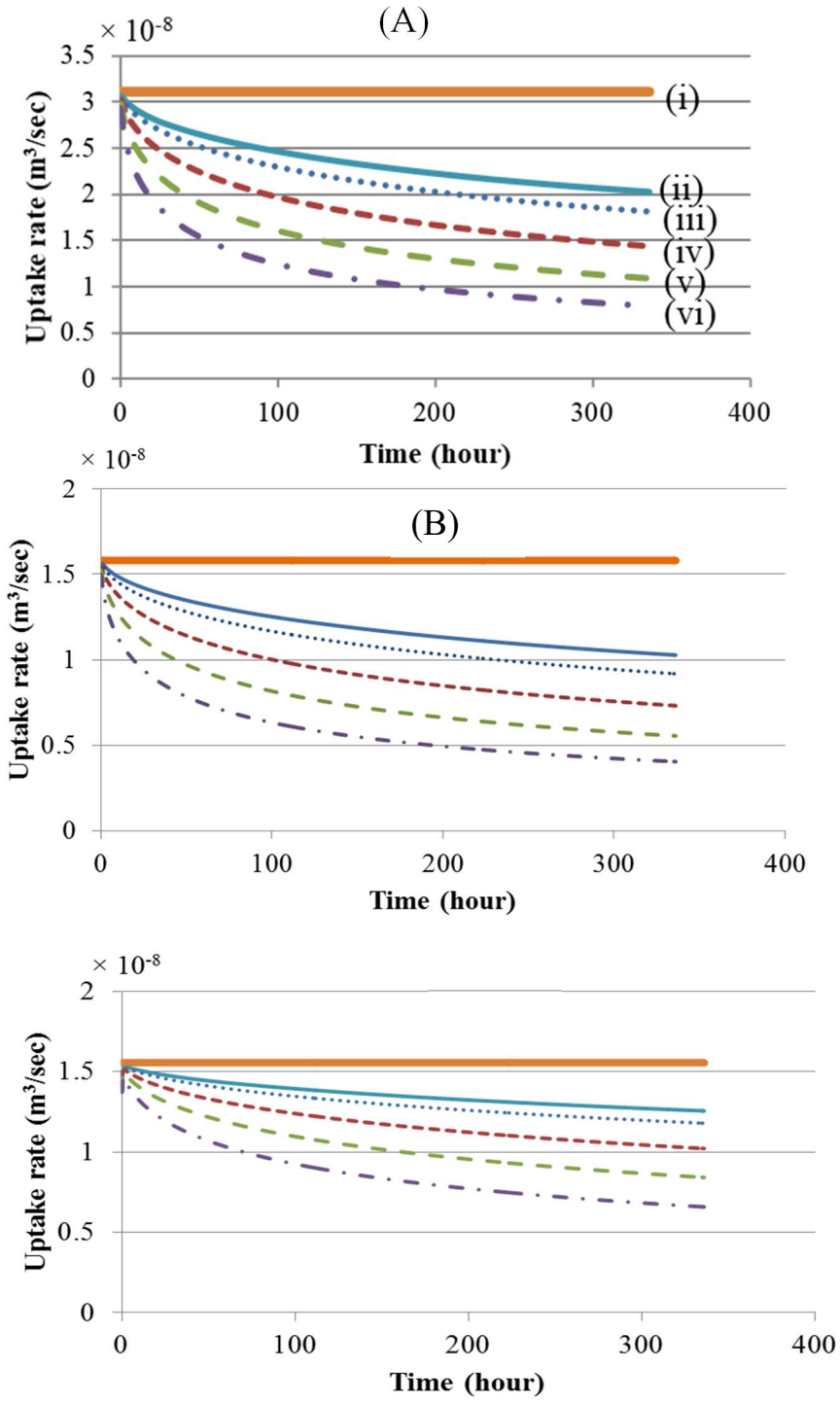

Figure 3-4: Model results presented as uptake rate time profiles of the 2 mL WMS with a 100-µm thick membrane (A), microvial WMS with a 100-µm thick membrane (B), and the 2 mL WMS with a thicker membrane (200 µm) (C) based on the ideal, zero sink, behavior (i), and the developed model at toluene concentration levels of 2.3×10^{-3} mg/m^3 (ii), 9.2×10^{-3} mg/m^3 (iii), 9.2×10^{-2} mg/m^3 (iv), 9.2×10^{-1} mg/m^3 (v), 9.2 mg/m^3 (vi) for total exposure time of 2 weeks.

sampler to suit the purpose of the sampling process. For monitoring requiring long exposure times, a thicker membrane would help minimize the change in the uptake rate with time, leading to more accurate estimation of the TWA concentrations. Experiments to verify this are currently under way and will be the subject of a future contribution.

Table 3-1: Predicted percent change in the uptake rate of toluene on Carbopack B after one and two weeks of exposure at different concentrations in the evaluated air.

	Concentration in air, C_0 (mg/m^3)	**2.3×10^{-3}**	**9.2×10^{-3}**	**9.2×10^{-2}**	**9.2×10^{-1}**	**9.2**
After 1 week of exposure	2 mL WMS with 100-µm thick membrane	-25%	-31%	-42%	-54%	-65%
	2 mL WMS with 200-µm thick membrane	-12%	-16%	-23%	-33%	-45%
After 2 weeks of exposure	2 mL WMS with 100-µm thick membrane	-34%	-41%	-52%	-63%	-73%
	2 mL WMS with 200-µm thick membrane	-18%	-22%	-32%	-43%	-55%

When using Carbopack B, the current version of the WMS with a 100-µm thick membrane is best suited for ppbv range concentration levels of toluene (or analytes with similar sorption isotherms) and exposure times up to approximately ten days. Outside of this range, a correction to the uptake rate values should be applied, which is possible using the model developed in this work.

To validate the applicability of the model, four sets of experiments were conducted by exposing the WMS to a standard gas containing toluene at four different concentrations: 1.6, 9.2, 26.8, and 43.0 mg/m^3. The uptake rates of both versions of the WMS were determined for different exposure times and compared with the uptake rate

values calculated using the model. The uncertainty in the model results was estimated from the model parameter uncertainties using eqn. (3.2) as a guide for error propagation. The relative uncertainty based on the parameter uncertainty was estimated to be ~48 % of the uptake rate value calculated using the model. Additional uncertainty was contributed by the sorption isotherm parameters used in the model. A close agreement between the theoretical uptake rate and the experimental values was observed, as illustrated in Figure 3-5 for the 2 mL WMS and in Figure 3-S4 (see Appendix A) for the microvial WMS. In Figure 3-5, the experimental data points of the uptake rate are presented along with the

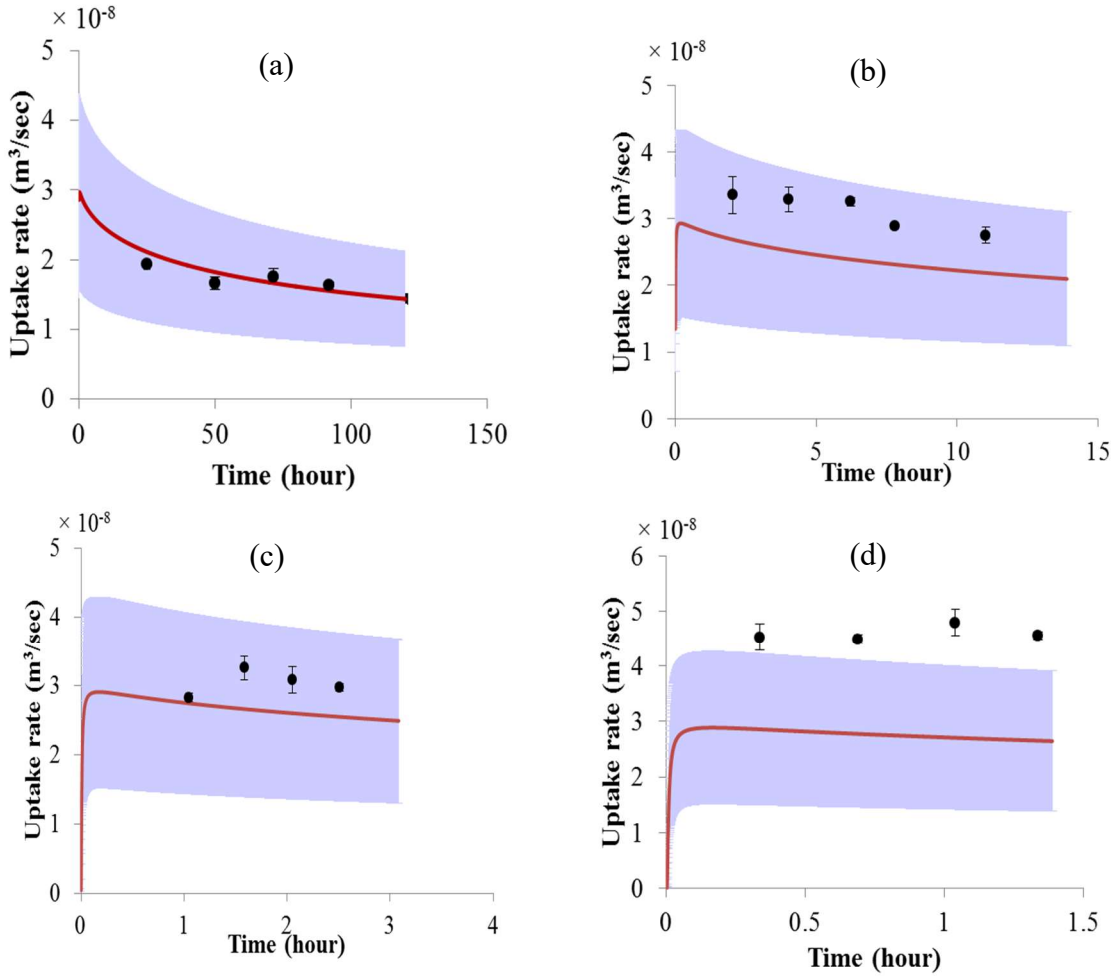

Figure 3-5: Experimental uptake rate profiles of the 2 mL WMS, at the concentrations of: 1.6 mg/m^3 (a), 9.2 mg/m^3 (b) , 26.8 mg/m^3 (c), and 43.0 mg/m^3 (d), compared to the model results, which are presented with an estimated uncertainty band based on the uncertainty in the parameter values. (• Experimental data, - Model results). Note the different time scales in panels (a) – (d).

uptake rate profiles calculated based on the model. The uncertainty bands on both sides of these profiles are based on the uncertainties in the parameter values as explained above. This uncertainty was calculated by applying the propagation of error rules using eqn. (3.2), since the influence of the uncertainties of the parameters in this equation on the results of the model would be similar to that in the ideal uptake rate behavior (based on the zero sink assumptions). In panel (a) of this figure, the model predicted a decrease in the uptake rate with respect to the ideal uptake rate (corresponding to the highest value in the curve as explained earlier) of approximately 52% after 5 days of exposure at 1.6 mg/m^3. Panel (b) shows a 28% decrease after 14 hrs of exposure at a concentration of 9.2 mg/m^3 (note that for the lower concentration shown in panel (a), the decrease after 14 hrs would be only ~22%). Experimental data points in panel (a) are in a very close agreement with the theoretical uptake rate profile, while in panel (b) they fall within the uncertainty band of the predicted values with a slight decrease in the uptake rate over time. For higher concentrations/shorter exposure times presented in Figure 3-5 (c) and (d), the predicted uptake rates were essentially constant, which agreed with the experimental observations.

The experimental data points in Figure 3-5 (c) were close to the theoretical uptake rate profile, whereas the data points in Figure 3-5 (d) were slightly above the border of the uncertainty band of the theoretical uptake rate profile. The latter can be attributed to higher uncertainty in the experimentally determined concentration due to the very short active sampling time (40 sec). This time could not be exceeded at this extremely high concentration level (43 mg/m^3) due to the limitation on the amount of analyte that can be introduced to the analytical instrument without saturating the detector.

In Figure 3-6, the experimental results collected over a longer exposure period along with the model prediction of the uptake rate profile are presented. In this figure, the model results demonstrate a ~78 % decrease in the uptake rate after 26 days of exposure to 5.3 mg/m^3 of toluene in the air. The experimental data points also demonstrated a clear decrease in the uptake rate over the time of exposure. For all experiments presented above, deviation from theoretical values may also be attributed to unknown uncertainty in the isotherm parameters used in the model.

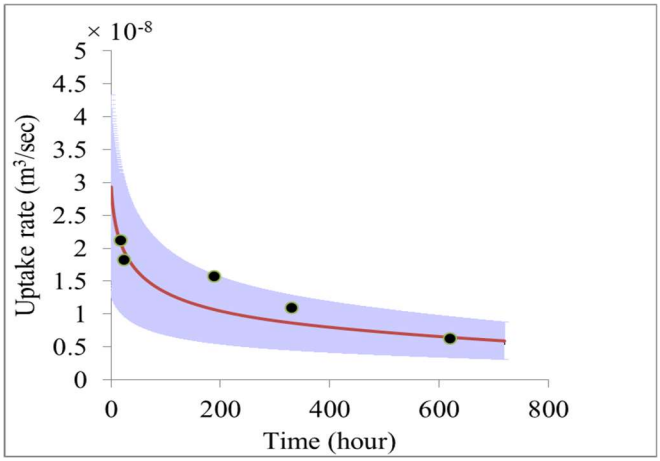

Figure 3-6: Experimental uptake rate profile of the 2 mL WMS for a one-month exposure at the concentration of 5.3 mg/m^3 compared to the model results, which are presented with an estimated uncertainty band (• Experimental data, - Model results).

3.5. Conclusions

The model developed in this paper explains the dynamic process of sampling using permeation passive samplers that utilize adsorbents as receiving phases. The application of the model to the Waterloo Membrane Sampler (WMS) was evaluated in this work. The results demonstrate a decrease in the uptake rate during sampling at a rate dependent on the measured concentration level and the strength of the sorbent, which is explained by considering mass transfer resistance in the sorbent bed. The performance of the sampler

can be optimized by matching the analyte with an appropriate sorbent, and/or by adjusting the geometry of the sampler. A correction to the uptake rate value can otherwise be applied based on the model results. In the field, information about the expected concentration levels is usually drawn from previous experiments or using online detection methods. When analyzing passive samplers exposed for a certain time, concentrations calculated using uptake rate values based on laboratory calibration or estimation can be used to determine whether a significant reduction in the uptake rate within the exposure timeframe can be expected. If that is the case, the model can be used in an iterative manner to estimate the error and apply appropriate correction factor(s). This will be the topic of future work, the results of which will be published in a separate paper.

The results of this work are significant for the design of WMS-like samplers and the sampling strategies. Most importantly, the model is significant for the correct interpretation of the sampling results obtained using such devices and calculating the analyte concentration in the evaluated air or soil gas. Applying the ideal zero-sink theory resulting in the uptake rate that is independent of analyte concentration and the exposure time for weak sorbents/weakly sorbed analytes could result in underestimation of the actual concentrations. It is important to point out that not only is a similar behavior expected of diffusive samplers with an adsorbent bed, since the same mass transport mechanism within the adsorbent phase applies, but that the change in the uptake rate is expected to be more significant for diffusive samplers as they have generally higher uptake rates. An example of such diffusive passive samplers is the sorption tubes when used in the passive sampling mode.

CHAPTER 4.

NEW APPLICATIONS OF THE MATHEMATICAL MODEL OF A PERMEATION PASSIVE SAMPLER: PREDICTION OF THE EFFECTIVE UPTAKE RATE AND STORAGE STABILITY*

4.1. Introduction

Passive sampling is an approach that offers many advantages, including simplicity and low cost relative to conventional active grab sampling method. In the latter approach, samples from the evaluated medium are collected at given times to be analysed online, or, in most cases, transferred to the laboratory for analysis. Unlike this method, the passive sampling approach does not require pumping or attendance during operation.[69] Instead, analyte molecules are driven into the sampling medium by the chemical potential difference between the sampled and the collecting media.[3] This method allows integration of several sample preparation goals, such as analyte isolation and pre-concentration, into the sampling process, and therefore, reduction of sample preparation time and cost and reduction of solvent use.[3]

Passive sampling can operate in the kinetic or equilibrium regions. In the former case, analyte molecules continuously migrate through a rate-determining barrier before they are

---

* This chapter was published as the following article: F. Salim, M. Ioannidis and T. Górecki, New applications of the mathematical model of a permeation passive sampler: prediction of the effective uptake rate and storage stability, *Environ. Sci.: Processes Impacts*, 2019, 21, 113.

trapped in a receiving phase until the sampling process is stopped by the user. The rate-determining barrier can be a membrane or a diffusive region, whereas the receiving phase can be an adsorbent material or a solvent. The amounts of analytes collected by these types of samplers reflect their average concentrations over the time of exposure, so-called time-weighted average (TWA) concentrations. When passive sampling is conducted in the equilibrium region, the flow of analytes between the sampled medium and the receiving medium continues until equilibrium is reached between the two. In this case, the amounts of analytes collected by the sampler reflect the analyte concentrations around the time the sampler was collected. In both cases, the integrity of the collected samples is important to assure accurate determination of the concentrations. This involves sufficient preservation of the sampled analytes during storage and shipment of the samples, as well as a well-controlled and optimized analytical methods in which the analytes collected are introduced quantitatively to the analytical process.

The measurement of the TWA concentrations using the kinetic passive samplers is based on the assumption that the uptake rates of the sampler remain constant during the exposure and are independent of the analyte concentration and sampling time. The uptake rate of a passive sampler is a conventional expression of the sampling rate and can be defined as "the flow rate that would yield the same mass collected by the passive sampler if drawn through a sorptive medium within the same sampling time".[140] TWA concentration can then be calculated using eqn. (4.1) as follows:[5]

$$C = \frac{M}{Ut} \tag{4.1}$$

in which M is the analyte amount collected by the sampler over the time t, and U is the uptake rate of the sampler towards the target analyte. Ideally, in permeation passive samplers, the uptake rate is defined as follows:[5]

$$U = \frac{DKA}{L_m} \tag{4.2}$$

In this equation, D (m^2/sec) is the diffusion coefficient of the analyte in the membrane material, K (dimensionless) is the partition coefficient of the analyte between air and the membrane material, A (m^2) is the sampling area and L_m (m) is the thickness of the membrane. These equations result from the assumption that the receiving phase (the sorbent) acts as a zero sink, meaning that analyte molecules permeating through the membrane into the sorbent are removed completely by sorption leaving negligible concentration of the analyte at the membrane-sorbent interface.[32]

Determination of the uptake rate is achieved using one of three methods:[4] 1) theoretical determination based on the knowledge of measured or estimated values of the parameters presented in eqn. (4.2) (D and K in the case of permeation passive samplers) and the dimensions of the sampler; 2) experimental evaluation of the uptake rate by exposing the passive samplers to an atmosphere of the analyte vapor with known concentration (from a parallel reference method); 3) Performance Reference Compounds (PRCs) or Depuration Compounds (DCs), which are usually deuterated compounds that are not present in the evaluated medium and are spiked into the receiving phase of the passive sampler before deployment. This method is based on the assumption that the loss rate of the PRC is controlled by the same mechanisms as the uptake of the target analyte.[65] Although the last approach simplifies the calibration process and permits determination of site-specific sampling rates for individual analytes,[4] its application is

limited to linear sorption isotherms, as this method is based on the assumption that both the uptake and the release process are of first order kinetics and have the same rate constant (isotropic exchange),[141] which mainly applies to absorption processes. The drawback of all of these approaches is that they produce a single value of the uptake rate towards each analyte, whereas variabilities associated with exposure time, concentrations, or site-specific conditions should be taken into consideration.

The Waterloo Membrane Sampler (WMS), shown in Figure 4-S1 (a) in the Supplementary Information section (Appendix B), is a permeation passive sampler developed at the University of Waterloo.[32,31] In this sampler, a polydimethylsiloxane (PDMS) membrane is used as the permeation barrier, while an adsorbent material is used as the receiving phase. Details about the sampler components and preparation are provided in the Experimental section of the Electronic Supplementary Information. The WMS has been utilized for sampling volatile organic compounds (VOCs) from air and soil gas.[34-35] The sampler is exposed to the evaluated air for a certain time. During this time, analyte molecules permeate through the PDMS membrane and are trapped by the sorbent. The sampler is retrieved at the end of the assigned exposure period, repacked and sealed, to be transferred to the laboratory for analysis.

In a previous work,[140] a mathematical model was developed to describe the sampling process in a permeation passive sampler, to assess the sampler performance during sampling, and to identify the most important factors that affect this performance. Numerical solutions of this model were evaluated experimentally using the WMS. The model predicts the distribution of the collected analyte within the different compartments of the sampler as a function of the sampling time. It then uses this information to calculate the uptake rate of the sampler at any point in time to assess its stability. The purpose of the presented study is to demonstrate practical applications

to exploit the model results. The scope of these applications is twofold. In the first part, a new method of estimating the effective uptake rate of the passive sampler, based on the model, is proposed. This method takes into account potential changes in the uptake rate as a result of the sampling process itself. In the second part, the model is extended to describe the post-sampling period using the WMS.

Many sources of variation of the passive sampler uptake rates are reported and evaluated in the literature. They include the effects of sampler configuration[142] and housing,[143] and the influence of meteorological parameters such as temperature, humidity and wind speed.[25,30,99,144] Furthermore, other factors related to the sampling process itself were also found to be influential on the stability of the uptake rate of passive samplers. These factors are related to analyte accumulation in a non-uniform manner within the receiving phase of the passive sampler[95]. This non-uniform distribution of analyte within the passive sampler challenges the zero-sink assumption and causes an increase in the analyte concentration in the primary air layer (just above the sorbent bed next to the sampler barrier).[94] This, in turn, reduces the driving force for sampling, which is the concentration gradient across the sampler barrier.[94] In such cases, using the ideal zero-sink assumption leads to quantitation errors as a result of the overestimation of the sampler linear range.[94,95] Another source of error, also associated with non-uniform distribution of the analyte, is back-diffusion of the analyte into the evaluated medium when the concentration in this medium drops below the concentration in the primary air layer.[94] Tolnai et. al. developed a theoretical approach to describe the changes in the uptake rate of tube-type diffusive samplers,[98] while Zhang and Wania proposed a mathematical model to describe analyte transfer through diffusive passive samplers, namely XAD resin-based passive air sampler, and polyurethane foam passive air sampler.[103]

Similar conclusions were drawn from the model developed previously for permeation passive samplers[140]: the uptake rate of the sampler was found to be affected by non-uniform distribution of the analyte at the interface of the sorbent bed with the membrane to a degree that depends on the concentration level, the sampling time and the selection of the analyte/sorbent pair. When this effect becomes significant, the sampler does not operate in the linear range anymore as a result of the increase in the analyte concentration in the primary air layer. Using the zero-sink assumption in such scenarios leads to overestimation of the overall uptake rate of the sampler over the sampling time, and, consequently, underestimation of the TWA concentration. In the first part of this paper, a new method of estimating the effective uptake rate of the passive sampler is presented. The purpose of this method is to account for any potential decrease in the uptake rate of the WMS using the model developed previously and, therefore, to more accurately predict the TWA concentration of the target analyte over the evaluation time. This method accounts for changes in the concentration gradient across the barrier as a result of the non-uniform distribution of the sampled analyte in the receiving phase. The method, afterwards, calculates the TWA concentration in a given sampling scenario. Back diffusion is not an issue when the concentration outside the sampler is steady as in the scenarios presented in this work. The influence of other factors, including temperature, humidity, and air velocity around the sampler, was evaluated previously.[32,145]

In the second part of this paper, the model is extended to describe the post-sampling storage period for the WMS. The objectives of this work were, first, to assess the stability of the collected analytes in the sampler during storage, and second, to evaluate the efficiency of the current analysis method in which the sorbent is the only component of the sampler that is analyzed. PDMS has important sorption properties that form the basis of many extraction

techniques, such as solid phase microextraction (SPME), thin film extraction, stir bar sorptive extraction (SBSE), PDMS rod extraction, etc.[56] It is crucial, therefore, to evaluate the significance of the potential sorption competition between the membrane and the sorbent, which could lead to losses of analytes that remain absorbed in the membrane if only the sorbent is analyzed.

4.2 Theory

The work is based on a previously developed model, which is briefly summarized below.[140]

4.2.1 Sampling Period (Previous Work)

As shown in Figure 4-S1(b), the model is based on the assumption that mass transfer within the WMS occurs in one dimension. In the membrane, diffusion of analytes is described by eqn. (4.3):

$$\frac{\partial C_m}{\partial t} = D_m \frac{\partial^2 C_m}{\partial x^2} \tag{4.3}$$

in which C_m is the analyte concentration in the membrane (mol/m^3), t is the time (s), D_m is the diffusion coefficient of the analyte in the membrane (m^2/s), and x is the distance (m). On the other hand, mass balance equations for the free analyte molecules within the void spaces of the sorbent bed, and for the molecules sorbed to the solid particles, are presented in eqn. (4.4) and (4.5), respectively:

$$\varepsilon \frac{\partial C_b}{\partial t} = D_{eff} \frac{\partial^2 C_b}{\partial x^2} - (1-\varepsilon) \frac{\partial q}{\partial t} \tag{4.4}$$

$$(1-\varepsilon)\frac{\partial q}{\partial t} = (k_c \alpha)(C_b - C^*) \tag{4.5}$$

where ε is the porosity of the sorbent bed, defined as the ratio of the void volume to the total bed volume, C_b is the free analyte molecules concentration within the void volume of the sorbent bed (mol/m^3), q is the concentration of the analyte sorbed to the solid phase (mole per m^3 of the solid phase of the particles), D_{eff} is the effective diffusivity of the molecules within the void spaces of the sorbent bed (m^2/s), k_c is the mass transfer coefficient from the free phase to the sorbed phase (m/s), α is the specific surface area, defined as the available surface area for adsorption per unit bulk bed volume (1/m) ; and C^* is the free analyte concentration that is in equilibrium with the adsorbed concentration based on the sorbent-analyte adsorption isotherm. Eqn. (4.6) represents the mass balance equation of the analyte in the air gap at the back of the sampler:

$$V_a \frac{\partial C_a}{\partial t} = - AD_{eff} \left.\frac{\partial C_b}{\partial x}\right|_{x=L_m+L_b} \tag{4.6}$$

in this equation, V_a is the volume of the air gap (m^3), C_a is the analyte concentration in the air gap (mol/m^3), A is the surface area of the interface of the sorbent bed with the air gap (m^2), and L_b is the thickness of the sorbent bed. The effective diffusivity in the sorbent bed is calculated using eqn. (4.7) as follows:

$$D_{eff} = \frac{\varepsilon D_{air}}{\tau} \tag{4.7}$$

where D_{air} is the diffusion coefficient of the analyte in air (m^2/s) and τ is the tortuosity of the sorbent bed. When the volume of the air gap is zero (Va = 0), that is, the sorbent completely fills the sampler, eqn. (4.6) becomes:

$$\left.\frac{\partial C_b}{\partial x}\right|_{x=L_b} = 0 \tag{4.8}$$

The sampler is assumed to be initially free of analytes; therefore, the initial concentration is zero within all the sampler compartments:

$$\text{At } t = 0 \quad \begin{cases} C_m = 0 \ ; \quad 0 < x \leq L_m \\ C_b = 0; L_m < x \leq L_m + L_b \\ q = 0; \ L_m < x \leq L_m + L_b \\ C_a = 0; \ x \geq L_m + L_b \end{cases} \tag{4.9}$$

Local equilibrium is assumed at the membrane's interface with the air outside the sampler and at the membrane's interface with the sorbent bed, as shown in eqns. (4.10) and (4.11):

$$\text{At } x = 0 \qquad C_m = KC_0 \tag{4.10}$$

$$\text{At } x = L_m \qquad C_m = KC_b \tag{4.11}$$

in which K is the partition coefficient of the analyte between air and PDMS, and C_0 is the concentration in the evaluated air at the membrane surface (mol/m^3). The flux out of the membrane at its interface with the sorbent bed equals the flux into the sorbent bed, which gives the boundary condition expressed in eqn. (4.12) as follows:

$$-D_m \left.\frac{\partial C_m}{\partial x}\right|_{x=L_m} = -D_{eff} \left.\frac{\partial C_b}{\partial x}\right|_{x=L_m} \tag{4.12}$$

The partial differential eqns. (4.3) to (4.6), subject to the initial and boundary conditions described above, were solved numerically using the method of lines in MATLAB (R2015a, MathWorks, USA). The reader is referred to previous work for details.[140] The values of different parameters needed for the model, such as the diffusion coefficient in the membrane, the partition coefficient between air and the membrane material, the diffusion coefficient in air, and the

isotherm parameters at a given sampling temperature need to be obtained from the literature, measured experimentally, or estimated using a validated method. The solutions provide the concentrations at a number of discrete points within the membrane and within the sorbent bed in both phases: "free" in the pores and "sorbed" onto the solid particles. These concentrations are calculated at a series of time steps during the course of sampling. The total number of moles in each compartment and in each phase is calculated afterwards at each time step t_n by integration. The total number of moles of the adsorbed analyte, $M(t_n)$, is used to calculate the average uptake rate $U(t_n)$ (m^3/s) over time t_n (s) based on eqn. (4.13):

$$U(t_n) = \frac{M(t_n)}{C_0 \cdot t_n} \tag{4.13}$$

4.2.2 Calculating the Effective Uptake Rate and the TWA Concentration

In the proposed method, summarized in Figure 4-1, the ideal uptake rate value calculated in eqn. (4.2) is used to evaluate the concentration of the target analyte using eqn. (4.1), following the determination of the amount of analyte collected by the sampler over the specified exposure time. The calculated concentration is then used as the input to the model (Equations (4.3) to (4.13)) to recalculate the effective uptake rate, accounting for its predicted decrease over the given time of exposure. The resulting uptake rate value is then entered again into eqn. (4.1), and the concentration is re-calculated based on this uptake rate value. The procedure is repeated iteratively until the values of uptake rate and concentration converge. The method was automated by writing a code in MATLAB (R2015a) (available upon request from the authors) that was based on the original code used to solve the model equations.[140] The values of different parameters used in this evaluation are presented in Table 4-S1(see Appendix B).

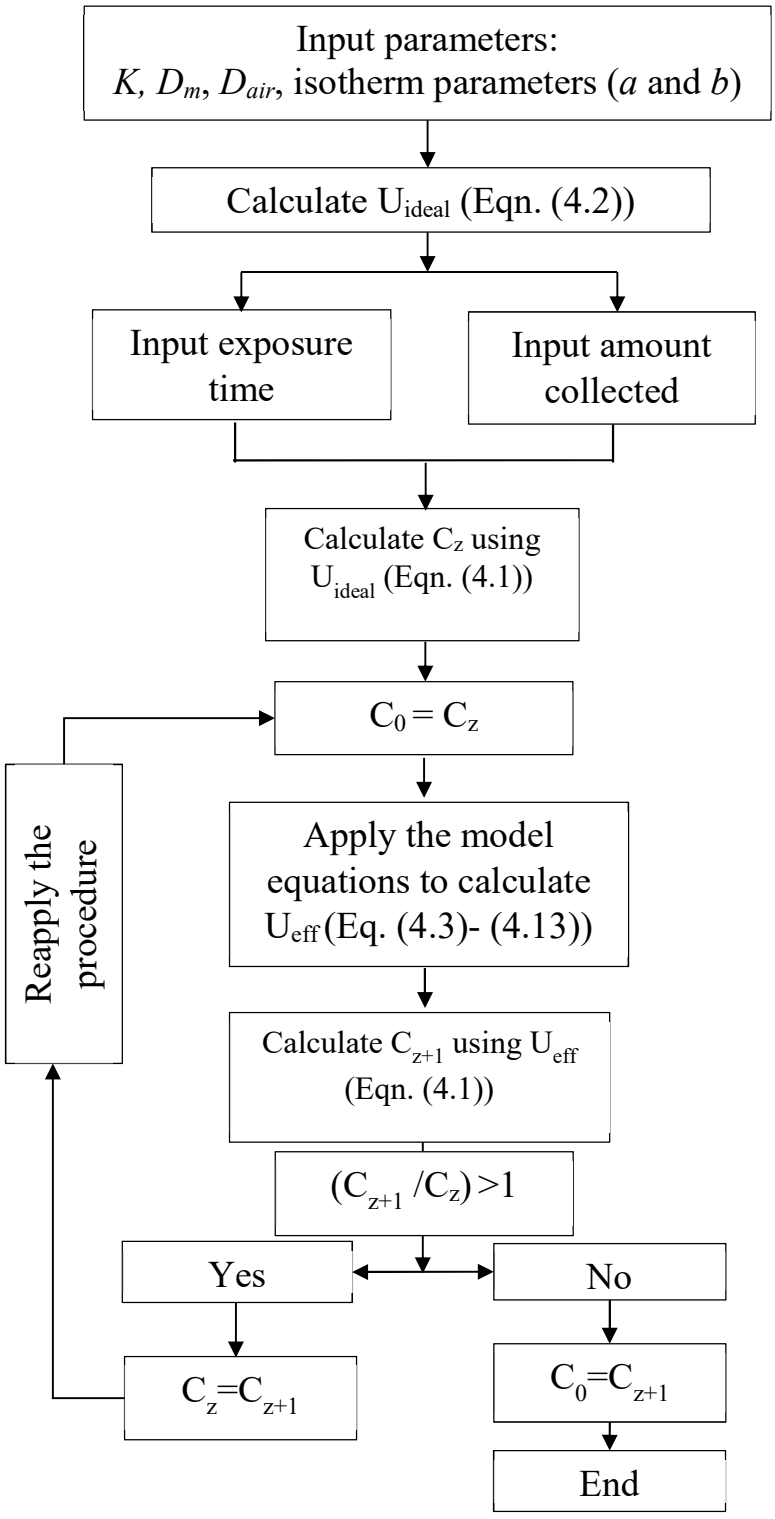

Figure 4-1: Algorithm of the new method of estimating uptake rates and TWA concentrations.

4.2.3 Storage (Post-Sampling) Period

After retrieval, the sampler is placed in a bigger, well-sealed vial, as shown in Figure 4-2a. This bigger vial is in turn placed in a sealed aluminized plastic bag containing a charcoal sorbent packet to remove any trace contamination that might be present in the air inside the bag. For analysis, the sampler is removed from the packaging and from the storage vial. The sampler is then de-crimped and the sorbent is analyzed. To describe the analyte fate during the storage time, another component is added to the model, which is the air inside the storage vial (see Figure 4-2b).

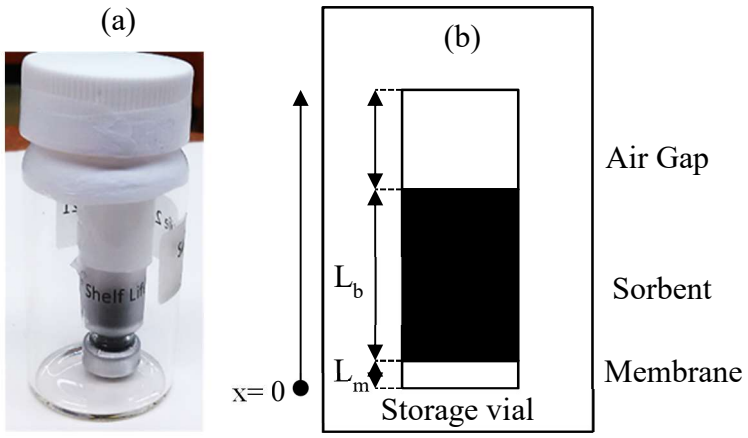

Figure 4-2: An image of the WMS in the storage vial (a) and a conceptual representation of it (b).

Equations (4.3) to (4.8) are also applicable during the post-sampling period. In addition to those equations, assuming that the air in the outside vial is well-mixed, mass balance of the analyte in the air of the storage vial can be expressed as follows:

$$V_o \frac{\partial C_v}{\partial t} = -A_m D_m \frac{\partial C_m}{\partial x}\Big|_{x=0} \tag{4.14}$$

In this equation, V_o is the volume of air in the storage vial containing the sampler, and C_v is the concentration of the analyte within the storage vial.

The boundary conditions stated in Equations (4.10), (4.11), and (4.12) are still valid; however, the equilibrium equation in eqn. (4.10) becomes an equation that relates the concentration in the membrane at its interface with the air outside the sampler to the concentration in the storage vial, C_v as shown in the following equation:

$$C_m = KC_v \tag{4.15}$$

Therefore, the concentration in the membrane at $x = 0$ changes in response to changes in the concentration in the outside vial, as expressed in eqn. (4.16):

$$\left.\frac{dC_m}{dt}\right|_{x=0} = K\frac{dC_v}{dt} \tag{4.16}$$

Furthermore, the initial analyte concentrations in the various sampler compartments are equal to the final concentrations at the end of the sampling time, therefore one can write:

$$\begin{aligned} &At\ t = 0 \\ &\qquad C_m = C_{m\,(n)}\ ;\quad 0 < x \le L_m \\ &\qquad C_b = C_{b\,(n)}; L_m < x \le L_m + L_b \\ &\qquad q = q_{(n)}; L_m < x \le L_m + L_b \\ &\qquad C_a = C_{a\,(n)}; x \ge L_m + L_b \end{aligned} \tag{4.17}$$

where the subscript n denotes the concentrations at the end of the exposure time (i.e. at the end of the sampling period), and $C_{m(n)}$, $C_{b(n)}$, $q_{(n)}$, $C_{a(n)}$ are the concentrations in the membrane, the free phase within the sorbent bed, the solid phase of the particles, and the back air gap of the sampler, respectively. The concentration in the air inside the storage vial is initially assumed to be zero, which also defines the initial concentration in the membrane at $x = 0$ according to eqn. (4.18). In reality, the initial concentration at $x = 0$ is related to the analyte concentration in the membrane at the end of sampling, but this has negligible effect on the outcome of the model. Therefore, one can write:

$$At\ t = 0 \qquad C_v = 0$$
$$C_m = 0\ at\ x = 0 \tag{4.18}$$

Equations (4. 3) to (4.6) and (4.14), subject to the initial and boundary conditions listed in Equations (4.11), (4.12), and (4.15) to (4.18), were solved numerically using the same method used to evaluate the sampling process.

4.3 Experimental

Experimental details are included in the Electronic Supplementary Information section (Appendix B). Only a summary of the experimental procedures is included here.

4.3.1 Calculating the Effective Uptake Rate and the TWA Concentration

The proposed method was tested using experimental data on toluene sampling using the WMS,[140] in addition to results from an experimental evaluation of trichloroethylene (TCE) sampling. Passive sampling data were used to calculate analyte concentrations using the iterative uptake rate prediction method, and then compare them with those obtained from active sampling. In these experiments, the amounts of the target analyte sampled by the WMS after different periods of exposures at known concentrations were determined. The amount collected after each exposure was then entered into the uptake rate prediction program along with the exposure time and the specific parameters related to the sampler and the sampled analyte (including diffusivity in the membrane, partition coefficient into the membrane, and isotherm parameters of the analyte sorption onto the sorbent). The output of the MATLAB program represented the predicted concentration. This concentration was compared with the concentration obtained from the reference active sampling method.

The experiments were conducted by exposing the WMS to an atmosphere of nitrogen mixed with the target analyte vapour for different periods and at different concentrations. The standard gas mixture was generated by passing purified nitrogen gas through a flow-through vessel containing a permeation source of the target analyte. The vapor source was placed inside a GC oven to control the temperature and, therefore, the analyte vapor concentration. The standard gas then entered the exposure chamber in which the samplers were exposed. The chamber was kept at a temperature of 21°C using a thermostated jacket. The concentration in the chamber was evaluated and monitored during the exposure of the samplers by analyzing samples of the standard gas directly through injection of gas samples into the GC-MS system, or by passing known volumes of the standard gas through sorption tubes packed with a sorbent and analyzing them later using the same system.

4.3.2 Evaluation of the Post-Sampling Period

To evaluate the fate and the distribution of the sampled analytes after sampling and during storage, the WMS was exposed for certain periods to known concentrations of the analytes. The sampler was then retrieved, repacked and sealed inside the storage vial. The sorbent and the membrane were analyzed separately after a certain storage period to evaluate the percentage of the analyte amount left in the membrane. The procedure was repeated for different storage periods to monitor the changes in the measured amounts over storage time.

The experiments were conducted by exposing the WMS with a membrane of 100 μm thickness to an atmosphere of a single analyte or a mixture of analytes for a certain time. Three samplers were exposed simultaneously, but stored for different times. After each assigned storage time, the sampler was de-crimped, the membrane was removed and immediately placed in a sorption tube in between two layers of approximately 80 mg of Carbopack B^{TM}, held in

place using three 1-cm-thick layers of glass wool, as demonstrated in Figure 4-S2. The purpose of these sorbent layers was to preserve the analyte that was present in the membrane at the time of sorbent retrieval. By placing the membrane between two sorbent layers, any analyte that could be lost during handling of the tube and purging in the thermal desorption unit was preserved. The packed tubes with all components except for the membranes were thermally pre-cleaned and analyzed as blanks prior to membrane insertion for analysis. The sorbent of the WMS was transferred to a separate sorption tube and packed in between two 1-cm-thick layers of glass wool. For storage, the WMS was sealed in a 20-ml glass vial immediately after the end of the exposure. The vial was closed with a plastic cap equipped with an aluminium liner and a Teflon tape was used to improve the seal around the cap. The samplers inside the storage vials were left at room temperature in a ventilated area.

4.4 Results and Discussion

4.4.1 Model Results

4.4.1.1 Calculating the effective uptake rate and the TWA concentration

To demonstrate the validity of the approach, the amount of analyte collected after 21 days of exposure to toluene vapour was used to recalculate toluene concentration following the steps described above. Figure 4-3a shows the progress of the calculated uptake rate with each iteration. The uptake rate in this figure starts at a value corresponding to the ideal uptake rate. The uptake rate value calculated based on the model equations in the first iteration is smaller than the initial value, and it converges after the second iteration. Similarly, the calculated analyte concentration starts at a value based on the ideal uptake rate and is an underestimation of the actual concentration, represented with a dashed line in Figure 4-3b. The analyte concentration quickly

evolves towards higher values and stabilizes after the second iteration, converging on the actual (experimental) concentration as demonstrated in this figure.

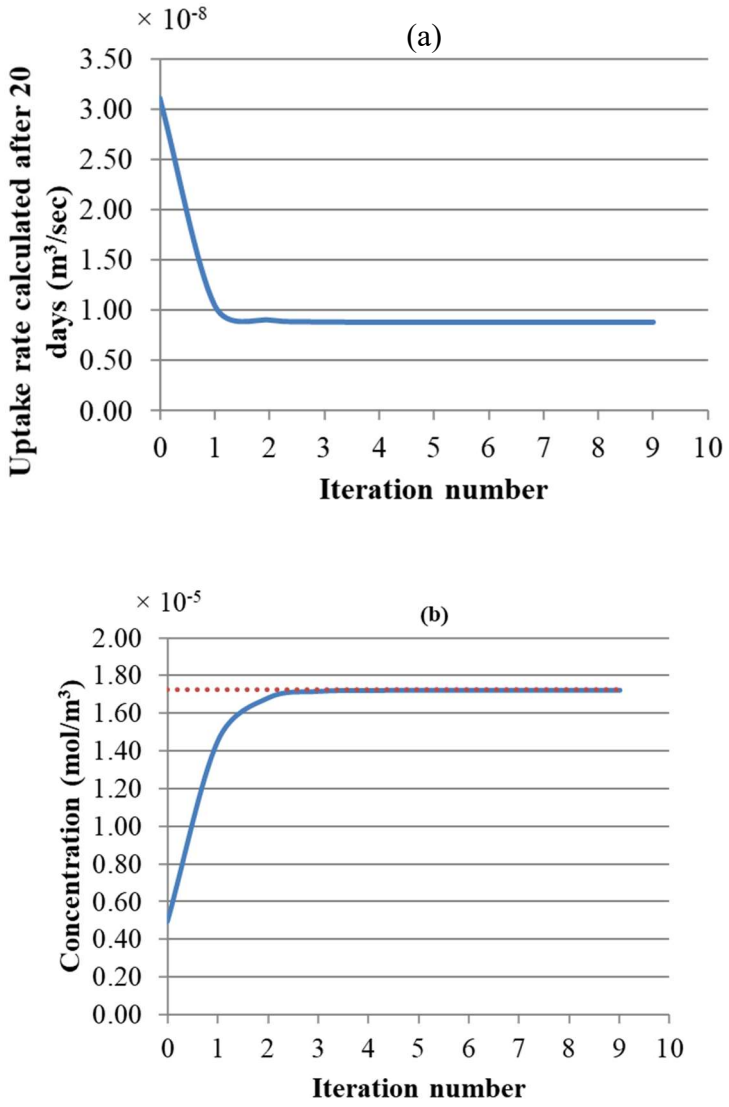

Figure 4-3: Progress of the iterative method for the uptake rate value (a), and the concentration in the evaluated air (b) (Calculated concentration is represented with a solid line, and the actual concentration is represented with a dashed line).

4.4.1.2 Evaluation of the post-sampling period

The model results were obtained for toluene and Carbopack B as the test analyte and sorbent, respectively, using the parameter values presented in the previous work.[140] The reason

for choosing this analyte/sorbent pair was the availability of parameter values needed in the model. Additionally, results obtained using such a relatively weak sorbent would represent the worst-case scenario. The simulation was performed assuming sampling for one day from an atmosphere with toluene vapor at a concentration of 9.2 mg/m^3. The results were obtained as concentrations within the storage vial and in finite volumes of the different components of the WMS (membrane, gas phase within the sorbent bed, sorbed phase in the sorbent bed, and the air gap at the back end of the sampler) at various times during the storage. The amounts of analyte in each compartment were also calculated by integration over the entire volume of the sampler component.

Figure 4-4 illustrates the changes in the analyte concentration profiles in the membrane over one hour (a) and one week (b) of storage, and in the free analyte concentration in the sorbent bed over one week of storage (c). Figure 4-4a shows that the concentration gradient is immediately reversed after sampler placement in the storage vial (within the first minute), as the concentration of the analyte in the air outside the sampler is initially zero. As a result, a small fraction of the analyte amount present in the membrane and in the gas phase of the sorbent bed at the interface with the membrane at the end of the sampling period diffuses into the storage vial. Nonetheless, within one hour of storage this concentration gradient becomes zero, as presented in this figure. Afterwards, analyte concentration in the membrane decreases with increasing storage time as demonstrated in Figure 4-4b. Examining the concentration profiles within the sorbent bed, as presented in Figure 4-4c, helps elucidate these observations. Within the first hour after the end of the sampling period, the entire amount of the sorbed analyte is accumulated within the first three millimeters of the sorbent bed near the interface with the membrane. As a result, the concentration of the analyte in the gas phase at this interface is significantly higher

relative to the rest of the sorbent bed. This concentration at the sorbent/membrane interface defines the concentrations in the membrane, and consequently in the storage vial according to the equilibrium relationships presented in eqn. (4.11) and eqn. (4.15). The concentration profile in the sorbent bed changes, however, over the storage time, as shown in Figure 4-4c. Analyte molecules present in the sorbent bed diffuse deeper inside the sampler to occupy larger volume of the sorbent bed, which, in turn, decreases the analyte concentration at the sorbent bed interface with the membrane, leading to a decrease in the equilibrium concentrations in the membrane and the in the storage vial. It is critical to point out here that this description represents the worst-case scenario for the standard 2 mL sampler, as it assumes that the sorbent bed remains undisturbed after sampler retrieval. In real life, the sampler would be moved many times during repackaging, sealing and shipping, leading to mixing of sorbent particles. This, in turn, means that the analyte present in the sorbent bed would be more uniformly distributed immediately after sampling, and low concentrations in the membrane and in the storage vial would be established much faster than the calculations described above suggest.

Figure 4-5a shows the results of the amounts sorbed to the solid particles over seven days of storage. It can be seen in this figure that this amount remains constant over time. Additionally, Figure 4-5b presents the percent amounts present in all other sampler compartments during the same storage period relative to the sorbed amount in the sorbent bed. All fractions present in those compartments remain negligible (less than 1 % in the storage vial, less than 0.1 % in the membrane, and less than 0.001 % in the gas phase of the sorbent bed) despite the initial increase in analyte fraction in the membrane and in the storage vial.

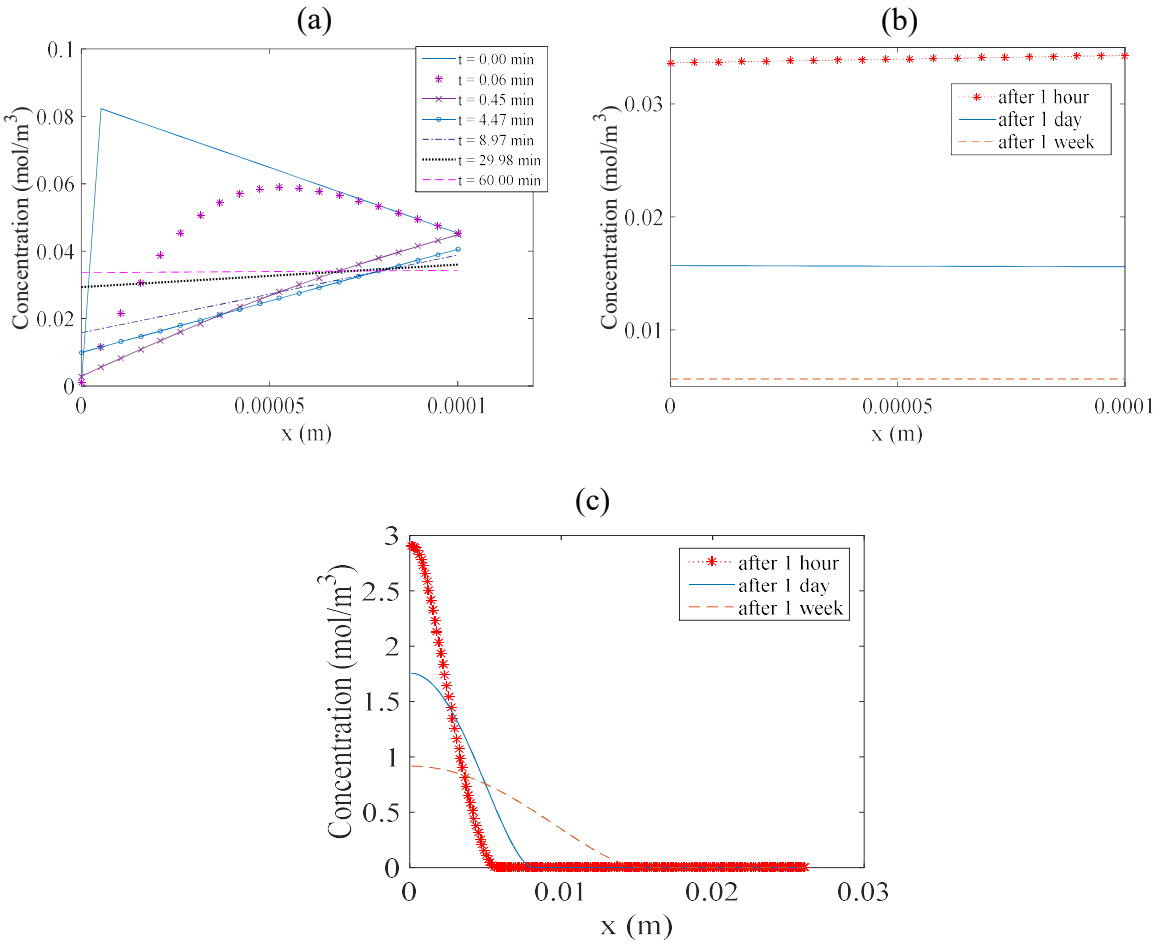

Figure 4-4: Propagation of the concentration profile during storage in the membrane over one hour (a) and one week (b), and the concentration profile for the free analyte molecules in the sorbent bed (c).

The above results support the hypothesis that the sorbent particles are by far the major sink for the analytes collected by the WMS, and that analysing these particles is sufficient to measure the amount of analyte collected by the sampler. Another conclusion drawn based on these results is that the collected analyte is preserved in the sorbent once the sampler is sealed inside the storage vial, and the length of the storage period does not affect the amount of the trapped analyte if no chemical degradation occurs.

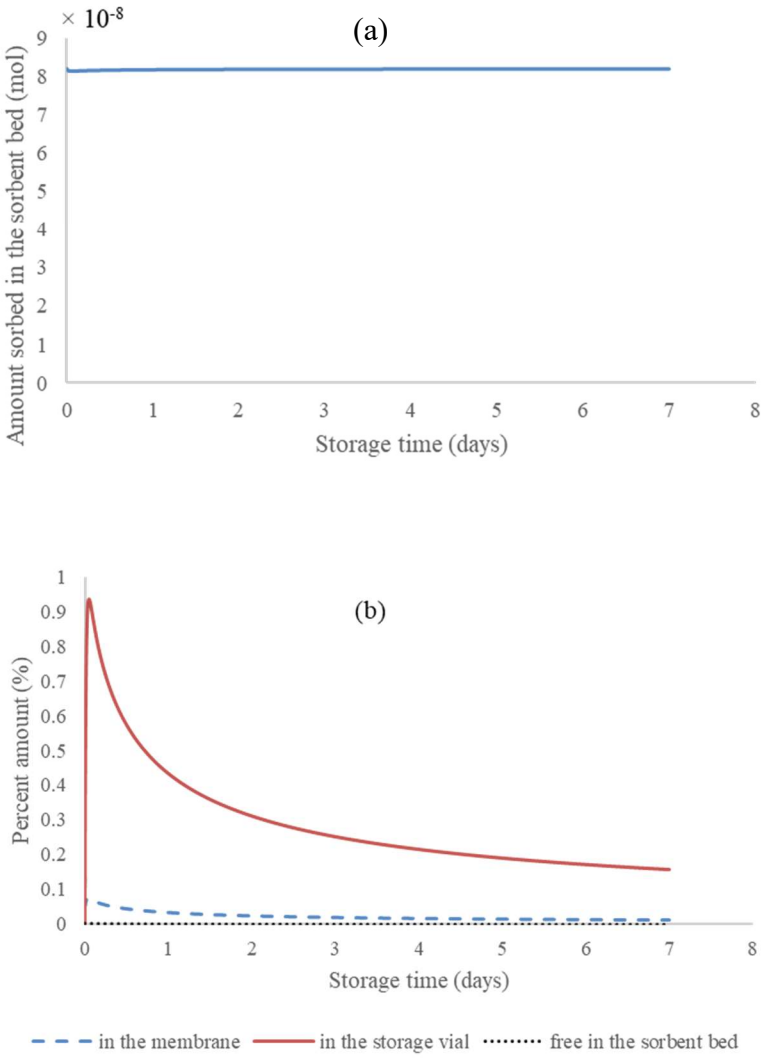

Figure 4-5: Changes over time of the amount sorbed to the solid particles (a), and the percent amounts present in the different compartments of the stored WMS relative to that sorbed to the particles (b).

4.4.2 Experimental Verifications

4.4.2.1 Calculating the effective uptake rate and the TWA concentration

The new method of calculating the effective uptake rate was tested using experimental data collected previously in addition to experimental results obtained for sampling TCE vapour using the WMS as explained in the Experimental section. The amount of analyte collected in each experiment and the exposure time were used as inputs into the code built based on the

method, and the calculated concentration was compared to the concentration measured using active sampling. The results are presented in Figure 4-6, in which the concentrations based on the ideal uptake rate values are compared with those calculated based on the new method. and with the average concentration measured in parallel using active samplers. In this figure, Exposures 1 and 2 were conducted within the same experiment in which WMS with PDMS membranes of the regular thickness (100 μm) were exposed to toluene vapor for 330.42 hours and 617.97 hours, respectively. Similarly, Exposures 3 and 4 were conducted within the same experiment of sampling toluene vapor using the regular thickness of the WMS but for different times (92.17 hours and 71.57 hours respectively). TCE vapor was sampled in one experiment shown as exposures 5 to 8. The PDMS membrane used in the WMS in this experiment had the thickness of 100 μm in Exposures 5 and 6, while it had the thickness of 200 μm in Exposures 7 and 8. These exposures were conducted simultaneously, with exposures 5 and 7 conducted for 264.78 hours, and exposures 6 and 8 conducted for 432.52 hours. In all of the above exposures, average concentrations and standard deviations were obtained from three samplers exposed concurrently.

The comparison between the concentrations produced by the proposed method and the concentrations calculated based on the ideal value of the uptake rate revealed a considerable increase in the TWA concentration when the new method was applied. The values obtained using the proposed method closely approached the values obtained from active sampling with overlapping uncertainty ranges. These values were in significantly better agreement with the active sampling measurements than the concentrations determined based on the ideal uptake rate values. The only exception was one measurement of TCE concentration in Exposure 5 due to the uncharacteristically wide scatter between the amounts collected by the three samplers used in

this measurement. Student's t-test (paired two sample for means) at 95 % probability level revealed that the differences between the calculated concentrations using the proposed method and the results of the active sampling were statistically insignificant with $|t_{calc}|$= 1.74 smaller than $t_{critical}$ = 1.89 (one-tail) and $t_{critical}$ = 2.36 (two-tail). On the other hand, the same test demonstrated significant differences between the calculated values based on the ideal behaviour and the measured concentrations using active sampling with $|t_{calc}|$ = 4.78, higher than both $t_{critical}$ (one-tail) and $t_{critical}$ (two-tail).

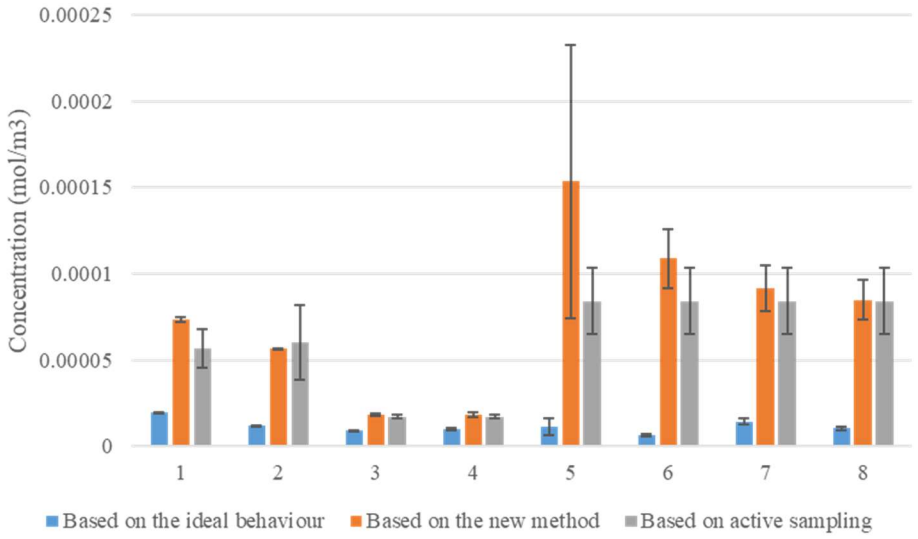

Figure 4-6: Demonstration of the performance of the proposed method in determining the TWA concentration using experimental data (uncertainties represent one standard deviation). In exposures 1 - 4, a WMS with a 100-µm-thick membrane was used to sample toluene vapor. A sampler with the same thickness membrane (100 µm) was used to sample TCE vapor in exposures 5 and 6, while a WMS with a 200-µm-thick membrane was used for TCE in exposures 7 and 8.

4.4.2.2 Storage time evaluation

In the initial experiments, a modified version of the WMS with a micro vial (as explained in the experimental section of the Supplementary Information) was exposed to atmospheres of nitrogen containing toluene, *o*-xylene, and 1,2,4-trichlorobenzene separately. Table 4-S5 (in Appendix B) shows that the amounts detected in the sorbent after different times of storage were

found to be statistically constant over the storage periods (uncertainty is represented in this case by confidence interval at the 95% confidence level). The fraction of the analyte found in the membrane was negligible relative to that measured in the sorbent, as presented also in Table 4-S5. The average percent amount found in the membrane did not exceed 1% for all analytes after the listed storage times except for the fraction of 1,2,4-trichlorobenzene detected in the membrane when it was analyzed immediately after the exposures. Nonetheless, this average fraction did not exceed 5 %, which is still insignificant. Additionally, this fraction decreased shortly after that to less than 1 % after two hours of storage, which is still shorter than the minimum period of time usually taken between sampling and analysis.

It is important to add here that the analytes detected "in" the membrane may have been, at least in part, adsorbed to fine sorbent particles still attached to the membrane after sampling (easily detected visually), which might also explain the high uncertainty in the measured fractions. Figure 4-S4 (in Appendix B) shows the difference in the appearance of the membrane before and after sampling. It can be seen in this figure that fine sorbent particles adhered to the membrane after sampling and could not be easily removed. Nevertheless, even with this contribution, the overall analyte loss to the membrane was insignificant in all the experiments presented in this paper.

In the next two sets of experiments, the WMS was exposed to mixtures of VOCs. Figure 4-7 shows the amounts of seven VOCs found in the sorbent after up to three-weeks of storage time. The samplers were exposed for one hour to a mixture of seven compounds with the concentrations presented in Table 4-1. The results presented in Figure 4-7 demonstrate the stability of the amounts detected in the sorbent over the evaluated storage time. Table 4-1 also shows that the average fractions of each analyte detected in the membranes did not exceed 5 %

of the amount found in the sorbent. The variation of these fractions, however, did not affect the results of the analyte amount determination in the sorbent.

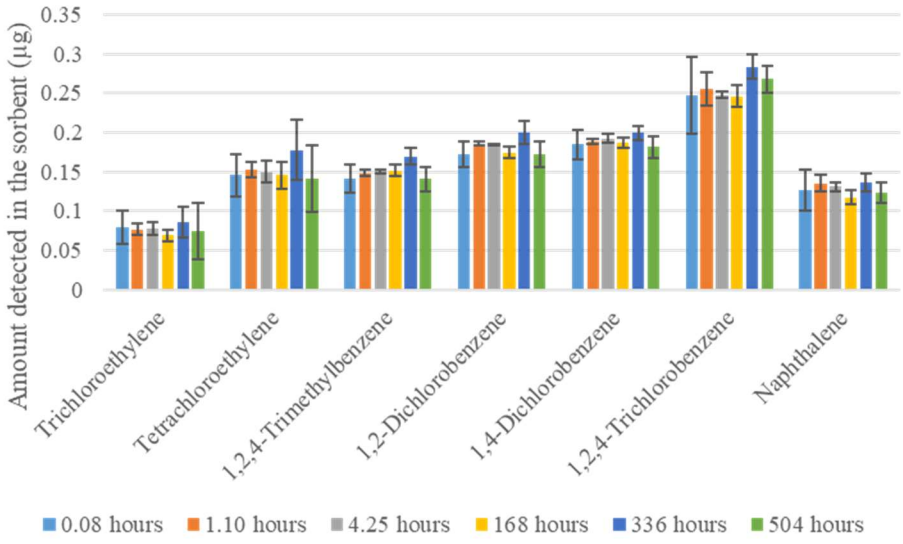

Figure 4-7: Amounts of analytes measured in the sorbent at different points of storage time (error bars represent one standard deviation).

In the next experiment, the WMS were exposed to an atmosphere of nitrogen containing a mixture of 29 VOCs at concentrations presented in Table 4-2 for three hours. The average fractions of sampled analytes detected in the membrane did not exceed 2 % of each analyte when the sampler was analyzed immediately after sampling. These fractions diminished to zero or close to zero after the one-week and two-week storage periods.

Table 4-1: Percent amounts detected in the membrane relative to those detected in the adsorbent after sampling from a standard gas containing a mixture of seven VOCs (uncertainties represent 95% confidence intervals)

Compound	Exposure concentration (mg/m^3)	Storage time (hours)					
		0.083	1.1	4.25	168	336	504
		Average (Membrane/Sorbent) (%)					
Trichloroethylene	1.42	0.0 ± 0.0	0.0 ± 0.0	2.0 ± 6.6	0.7 ± 1.9	2.3 ± 5.0	5 ± 16
Tetrachloroethylene	1.79	0.50 ± 0.28	0.22 ± 0.48	0.12 ± 0.53	0.40 ± 0.49	0.4 ± 1.9	0.25 ± 0.37
1,2,4-Trimethylbenzene	0.75	1.3 ± 1.0	0.29 ± 0.65	1.8 ± 3.6	0.29 ± 0.53	0.14 ± 0.15	0.3 ± 1.1
1,2-Dichlorobenzene	0.83	0.008 ± 0.035	0.0 ± 0.0	0.0 ± 0.0	0.0 ± 0.0	0.0 ± 0.0	0.0 ± 0.0
1,4-Dichlorobenzene	0.71	0.013 ± 0.054	0.5 ± 2.2	0.0 ± 0.0	0.52 ± 0.00	0.0 ± 0.0	0.5 ± 3.1
1,2,4-Trichlorobenzene	0.72	3 ± 10	0.8 ± 3.5	2.7 ± 12	4.9 ± 6.9	0.1 ± 1.9	4 ± 11
Naphthalene	0.48	3 ± 13	1.3 ± 3.8	3.7 ± 16	3.7 ± 8.1	0.4 ± 5.2	4 ± 15

Table 4-2: Percent amounts detected in the membrane relative to those detected in the adsorbent after sampling from a standard gas containing a mixture of 29 VOCs (uncertainties represent 95% confidence intervals)

Compound	Average Exposure Concentrations (mg/m^3)	Average (Membrane/Sorbent) (%)		
		Immediately analyzed	1 week storage	2 week storage
1,1-Dichloroethane	1.56	0.0 ± 0.0	0.0 ± 0.0	0.0 ± 0.0
cis-1,2-Dichloroethylene	1.48	0.0 ± 0.0	0.0 ± 0.0	0.0 ± 0.0
Chloroform	1.71	0.5 ± 2.2	0.0 ± 0.0	0.0 ± 0.0
1,1,1-Trichloroethane	2.48	0.0 ± 0.0	0.0 ± 0.0	0.0 ± 0.0
Benzene	1.89	0.38 ± 0.55	0.0 ± 0.0	0.0 ± 0.0
1,2-Dichloroethane	1.63	0.0 ± 0.0	0.0 ± 0.0	0.0 ± 0.0
Trichloroethylene	1.75	0.77 ± 0.66	0.0 ± 0.0	0.0 ± 0.0
1,2-Dichloropropane	1.95	1.4 ± 5.9	0.0 ± 0.0	0.0 ± 0.0
Toluene	1.73	0.13 ± 0.48	0.3 ± 1.2	0.0 ± 0.0
1,1,2-Trichloroethane	1.65	0.8 ± 2.1	0.7 ± 1.5	0.6 ± 1.4
Tetrachloroethylene	1.79	0.03 ± 0.15	0.5 ± 2.0	0.0 ± 0.0
Dibromochloromethane	1.45	1.7 ± 4.0	1.6 ± 7.0	0.0 ± 0.0
1,2-Dibromoethane	1.55	0.7 ± 2.8	0.0 ± 0.0	0.0 ± 0.0
Chlorobenzene	1.59	0.26 ± 0.44	0.0 ± 0.0	0.0 ± 0.0
Ethylbenzene	1.75	0.25 ± 0.31	0.0 ± 0.0	0.0 ± 0.0
p-Xylene	1.76	0.25 ± 0.28	0.0 ± 0.0	0.0 ± 0.0
o-Xylene	2.10	0.20 ± 0.43	0.0 ± 0.0	0.0 ± 0.0
Isopropylbenzene	1.73	0.30 ± 0.29	0.08 ± 0.34	0.06 ± 0.15
1,1,2,2-Tetrachloroethane	1.35	0.7 ± 3.2	0.0 ± 0.0	0.0 ± 0.0
1,2,3-Trichloropropane	1.54	0.11 ± 0.45	0.0 ± 0.0	0.0 ± 0.0
Propylbenzene	1.54	0.08 ± 0.34	0.0 ± 0.0	0.0 ± 0.0
tert-Butylbenzene	1.22	0.79 ± 0.89	0.0 ± 0.0	0.0 ± 0.0
1,2,4-Trimethylbenzene	1.72	0.50 ± 0.27	0.0 ± 0.0	0.0 ± 0.0
sec-Butylbenzene	1.37	0.70 ± 0.41	0.0 ± 0.0	0.0 ± 0.0
1,2-Dichlorobenzene	1.32	0.57 ± 0.46	0.0 ± 0.0	0.0 ± 0.0
1,4-Dichlorobenzene	1.44	0.58 ± 0.49	0.0 ± 0.0	0.0 ± 0.0
1,3-Dichlorobenzene	1.43	0.64 ± 0.54	0.0 ± 0.0	0.0 ± 0.0
1,2,4-Trichlorobenzene	1.11	1.4 ± 2.2	0.0 ± 0.0	0.0 ± 0.0
1,2,3-Trichlorobenzene	0.80	1.8 ± 2.2	0.0 ± 0.0	0.0 ± 0.0

4.5 Conclusions

Two applications were derived in this work as extensions of the mathematical model developed previously.[140] The uptake rate prediction method allows calculation of the effective uptake rate of the WMS at the end of the sampling period. It provides a valuable tool for more accurate measurement of the TWA concentrations. The determination of these concentrations relies on the accuracy of the uptake rates values towards the target analytes. Changes in these values during sampling result in underestimation of the measured concentrations if an appropriate correction is not applied. This deviation from linearity is not unique to the WMS, but common for all passive samplers with an adsorbing receiving phase. The proposed method was implemented in a MATLAB program allowing the corrected concentration to be calculated once the amount of analyte collected by the sampler was determined. Experimental evaluation of the proposed method using actual amounts of analytes collected by the WMS over different exposure times showed excellent performance, with calculated concentrations that did not differ statistically significantly from the concentrations measured using a parallel active sampling method. The method presented in this work can also be applied to different types of passive samplers (e.g. diffusive ones) after adjusting the mathematical model to reflect the sampler of interest. More research is on the way to provide values of parameters needed in the model for a wide range of analytes of interest and sorbents in use. The method could be developed to be more practical by adding a library of the needed parameters of a wide range of common analytes at different temperatures, so that the user would only need to enter the target analyte, the sampling time and temperature, and the amount detected in the sampler to calculate the concentration in the evaluated medium.

In the second part, the model was extended to describe the post-sampling storage of a permeation passive sampler (WMS). The developed model predicts the distribution of analytes within different compartments of the sampler and its storage container, in addition to the changes of this distribution during the storage time. The model revealed that negligible amounts of the analyte remain in the membrane and the storage container shortly after placing the sampler in storage, as analyte molecules diffuse deeper into the sorbent bed. As a result, the amounts of analyte collected by the sampler are expected to be preserved inside the sorbent throughout the storage period. Additionally, analyzing the sorbent is sufficient to correctly measure the collected amounts of the analytes, with only negligible analyte fractions lost to the membrane and distributed in the air inside the storage vial. These conclusions were verified and confirmed by the experimental results obtained through the analysis of both the sorbent and the membrane (separately) at different points of the storage time. The results of this work are important in verifying the efficiency of the current storage and analysis methods in accurately reflecting the actual sampled amounts of VOCs, which, in turn, have a significant contribution to the accuracy of the concentrations determined in the evaluated medium. These results also address the concerns of some users about a potentially significant loss of analytes sorbed into the PDMS membrane, which is commonly excluded from the analysis. The results demonstrate unequivocally that the membrane serves only as the uptake rate-defining barrier, as intended, and does not compete in any significant way with the sorbent inside the sampler. Finally, based on the results of this study, it is recommended to mix the sorbent immediately after retrieval of the WMS after sampling to minimize the amount of the sampled analyte diffusing into the storage vial.

CHAPTER 5.

MODELLING PERMEATION PASSIVE SAMPLING: INTRA-PARTICLE RESISTANCE TO MASS TRANSFER AND COMPREHENSIVE SENSITIVITY ANALYSIS*

5.1 Introduction

Passive sampling is "any sampling technique based on free flow of analyte molecules from the sampled medium to a collecting medium, as a result of a difference in chemical potentials of the analyte between the two media"[3]. Passive samplers can be classified based on the operating regime into equilibrium and non-equilibrium ones.[69] In the former type, sampling continues until equilibrium between the sampled medium and the passive sampler is achieved, whereas in the latter type, sampling is terminated before equilibrium is reached.[69] In this case, if the mass transfer rate is linearly proportional to the chemical potential difference between the passive sampler and the evaluated phase, the sampler is considered a linear uptake passive sampler.[69] The concentration measured using this type of passive samplers reflects the average concentration over the sampling time, known as the Time Weighted Average (TWA) concentration.

---

* This chapter was published as the following article: F. Salim, M. Ioannidis, A. Penlidis and T. Górecki, Modelling permeation passive sampling: intraparticle resistance to mass transfer and comprehensive sensitivity analysis, *Environ. Sci.: Processes Impacts*, 2019, 21, 469.

Most passive samplers consist of two main components: an uptake rate-determining barrier and a receiving phase.[5] The barrier, in general, is either a static layer of the evaluated medium, or a polymeric membrane.[5] In the former case, the samplers are called diffusive passive samplers, whereas samplers with the second type of barrier are known as permeation passive samplers. The Waterloo Membrane Sampler (WMS) is a permeation passive sampler that utilizes a polydimethylsiloxane (PDMS) membrane as a barrier, and an adsorbent material as a receiving phase. The sampler has been used for sampling volatile organic compounds (VOCs) from air and soil gas since its development in 2009.[31,32,34-36] The performance of the WMS in sampling common indoor air contaminants was evaluated along with three other types of passive samplers.[125] An important feature of the sampler is its simple design consisting of a small chromatographic vial in which the adsorbent is enclosed. The PDMS membrane covers the mouth of the vial and is fixed in place using an open-top aluminum crimp cap equipped with a PTFE washer. The sampler is exposed to the evaluated air with the membrane surface facing down, so that the adsorbent is in direct contact with the membrane.

In a previous work, a mathematical model that describes the sampling process in permeation passive samplers was developed and evaluated using the WMS.[140] A schematic of the WMS with a summary of the model equations is presented in Figure 5-1. All symbols included in the equations are explained in Table 5-1. The model accounts for resistance to mass transfer within the receiving phase, in addition to that in the permeation barrier (the membrane). Consequently, the model enables prediction of any potential deviations from linearity as a result of significant resistance to mass transfer within the receiving phase. These results were similar to those described earlier for diffusive passive samplers.[98,103,126,127]

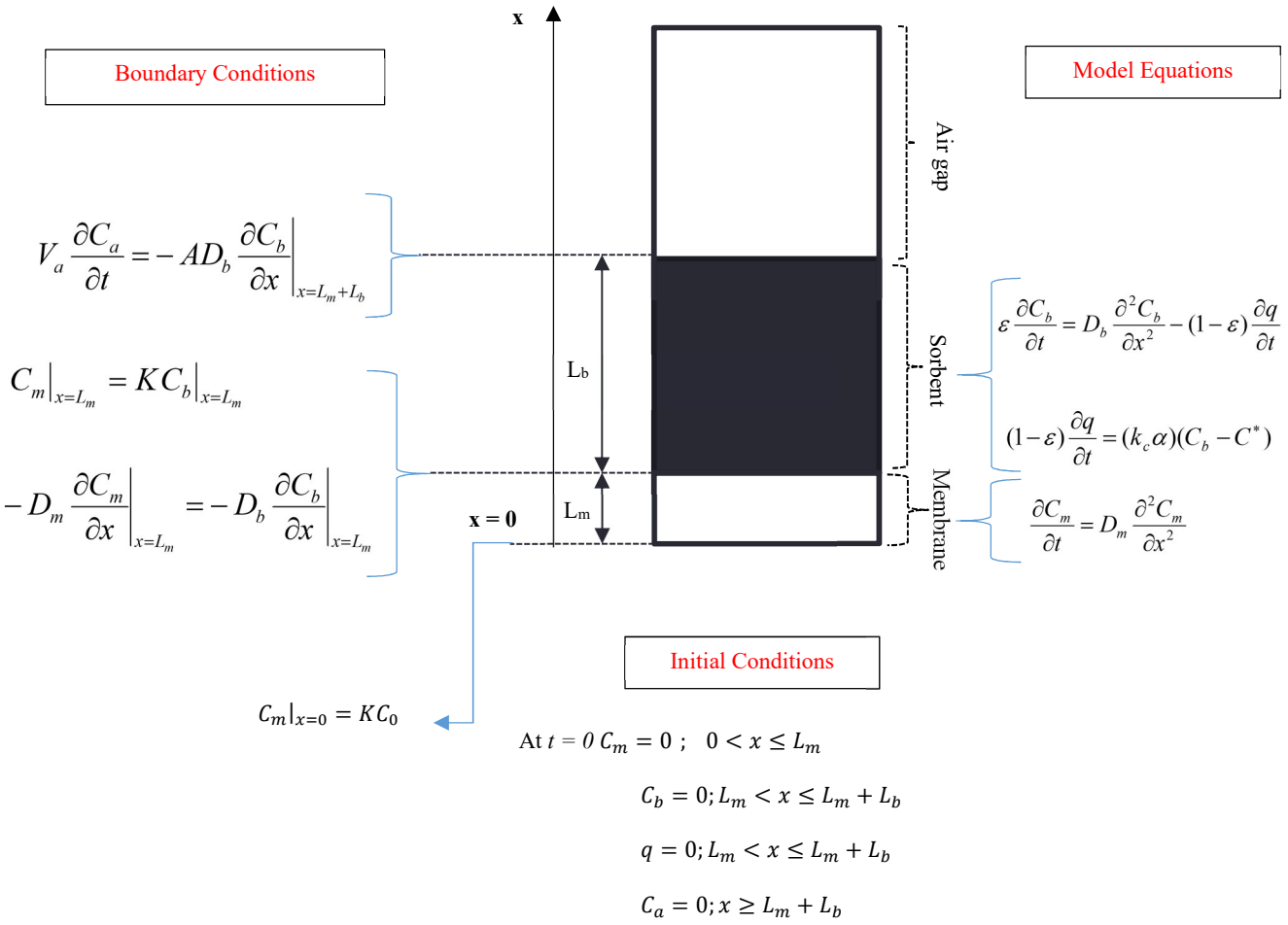

Figure 5-1: Schematic of the WMS with a summary of the model equations (based on ref. [140]).

Table 5-1: Description of symbols used in the model of Figure 5-1.

Symbol	Description	Unit
C_m	Concentration in the membrane	mol/m^3
t	Sampling time	sec
D_m	Diffusion coefficient in the membrane	m^2/s
x	Distance	m
ε	Porosity of the sorbent bed	dimensionless
C_b	Free analyte molecules concentration within the void volume of the sorbent bed	mol/m^3
q	Concentration of the analyte sorbed to the solid phase	mol/m^3
τ	Tortuosity of the sorbent bed	dimensionless
D_b	Effective diffusivity of the molecules within the void spaces of the sorbent bed	m^2/s
k_c	Mass transfer coefficient from the free phase to the sorbed phase	m/s
α	Specific surface area (available surface area for adsorption per unit bulk bed volume)	1/m
C^*	Free analyte concentration in equilibrium with the adsorbed concentration based on the sorbent-analyte adsorption isotherm ($C^* = aq^b$), in which a and b are empirical isotherm parameters.	mol/m^3
V_a	Volume of the air gap	m^3
C_a	Analyte concentration in the air gap	mol/m^3
A	Surface area of the interface of the sorbent bed with the air gap	m^2
K	Partition coefficient of the analyte between air and PDMS	dimensionless
C_0	Concentration in the evaluated air at the membrane surface	mol/m^3
U	Average uptake rate over the exposure time	m^3/sec
M	Total number of moles of the adsorbed analyte	moles
D_a	Diffusion coefficient of the analyte in the air	m^2/s
d	Particle diameter	m

The previous evaluation and validation of the model were applicable to the WMS containing a non-porous adsorbent; therefore, intra-particle resistance to mass transfer was not a factor influencing the net mass transfer inside the sorbent bed. The purpose of that choice was to evaluate the effect of resistance to mass transfer within the bed using a simple scenario, in which the bed consists of solid, non-porous particles with macropores in between these particles. A modification is required, however, for the model to be applicable to porous particles. Most

adsorbents used with WMS are composed of porous particles, therefore, additional processes need to be taken into consideration. In the work presented in this paper, a modification is proposed, so that intra-particle resistance to mass transfer can be taken into account. Anasorb 747 is an activated carbon-based sorbent made of "a synthetic carbon with low ash content", as described by the manufacturer (SKC Inc., Eighty Four, PA, USA). This adsorbent consists of highly porous particles, and is the most widely used in the WMS due to its strong adsorptivity toward VOCs and high capacity. Such properties are required in many applications, especially ones involving long-term monitoring. In these cases, efficient sorption and significant capacity are desired not only to maintain a linear uptake throughout the sampling time, but also to avoid the risk of back diffusion when concentrations in the evaluated medium drop significantly. Anasorb 747 was used in this work to evaluate the applicability of the model to the case of an adsorbent with porous particles.

Furthermore, a comprehensive sensitivity analysis was conducted to evaluate the influence of uncertainty in different input parameters on the main model output, the uptake rate of the passive sampler, and to identify the input parameters that require accurate determination and those that have insignificant effect on the model results. This evaluation was also aimed at understanding the output behavior in response to changes in input parameter values. The uptake rate, as defined previously,[140] is the hypothetical flow rate that would be required to collect the same mass of the analyte with the evaluated air being pumped through a sorptive medium over the same sampling time. The sensitivity analysis included both types of adsorbents: Carbopack B, which was the adsorbent used in the previous evaluation,[140] and Anasorb 747, which was used in this work as the test sorbent with porous particles.

5.2 Theory

The model, developed in a previous work,[140] is summarized in Figure 5-1. All symbols are described in Table 5-1. The model was evaluated using Carbopack B adsorbent, which consists of nonporous particles. In this case, the effective diffusivity in the bed, D_b, was calculated as:

$$D_b = \frac{D_a \cdot \varepsilon}{\tau} \tag{5.1}$$

The mass transfer coefficient, k_c, for this type of adsorbent was calculated from the Sherwood number, *Sh*, which in the case of mass transfer by diffusion to/from a sphere is given by:

$$Sh = \frac{k_c \cdot d}{D_b} = 2 \tag{5.2}$$

For the model to be applicable to a sorbent with microporous particles, the effective diffusivity and mass transfer coefficient (D_b and k_c) need to be estimated in a manner that accounts for additional resistance to diffusion within, and mass transfer towards porous particles.

5.2.1 Determination of Diffusivity in the Sorbent Bed

Diffusion in porous media may involve ordinary, Knudsen, and surface diffusion.[146] Ordinary diffusion occurs in pores with large diameter with respect to the mean free path of the gas molecules. It applies to diffusion in an adsorbent bed with non-porous particles, and diffusion in the macropores between the microporous particles. On the other hand, Knudsen diffusion is dominant when the pores are small compared to the mean free path. In this case, collisions of molecules with the pore walls occur more often than collisions with other molecules, resulting in increased resistance to molecule transport inside the pores. Knudsen diffusivity in straight, round pores is calculated using equation (5.3):[146]

$$D_K = 97.0\, r_p \left(\frac{T}{M_A}\right)^{1/2} \tag{5.3}$$

in which r_p is the pore radius (m), T is the temperature (K), and M_A is the molecular weight of the adsorbate, A. Finally, in surface diffusion, molecules adsorbed to the surface of the solid are transported from one adsorption site to another on the surface in the direction of decreasing concentration.[146] The contribution of this type of diffusion to the overall diffusivity is assumed negligible, and, therefore, often ignored.[146]

Systems with two different pore sizes, micropores within particles and macropores between particles, are known as bidisperse porous systems. Several models have been developed to describe diffusion in such systems. The applications of these models are extensive in the fields of catalysis, sorption and ion exchange. Turner modelled the flow structure in a packed bed as channels with uniform cross sections connected to pockets with dead ends distributed uniformly along the main channels.[147] A similar model was used by Tartarelli et. al. to study diffusion and reaction during catalysis in a bidisperse porous system.[148] In this system, the macropores are cylindrical, from which micropores of a smaller radius branch uniformly at right angles with respect to the macropore and provide the adsorption capacity. Knudsen diffusion is considered dominant in the micropores, while molecular diffusion dominates in the macropores.[148] Petersen adapted Turner's pore structure to study adsorption in a bidisperse-pore system.[149] Silva and Rodrigues also used Turner's structure to evaluate the transient state of adsorption using several types of equilibrium isotherms.[150] On the other hand, Ruckenstein et al. considered a spherical macroporous particle/pellet consisting of small spherical microporous uniform particles.[151] Sorbate diffusion and sorption occurred in both the micropores and the macropores. The model, therefore, evaluated the competing effects of diffusion resistances in the macropores and the

micropores. This model has been used extensively since its development in a number of applications and forms the backbone of the current model development.[152-160]

In many applications, using a single effective diffusivity in the porous medium is desirable. In such cases, the relationship between the structure of the porous medium and the transport process within the void spaces needs to be taken into consideration.[161] The effective diffusivity accounts for the fact that the area available for the diffusion of molecules is reduced by the solid phase of the porous material, in which the pore cross sections may vary. It also accounts for the tortuosity of the diffusion paths.[161] Hence, models are used to predict the effective diffusivity based on the molecular diffusivity and the structure of the porous system. The effective diffusivity, D_b, presented in eqn. (5.1), results from a parallel-pore model, which applies to mono-disperse pore-size distribution.[162] In this model, Wheeler (as cited in Ref.[162]) imagined the complex structure of a porous pellet as an assembly of cylindrical pores with a radius equal to the mean pore radius. On the other hand, the value of D_b for sorbents with a bidisperse pore system can be estimated using the random-pore model.[162] In this model, pores are modeled by an assembly of void regions in between and around individual particles. The basis of the model is the nature of the interconnection between macro and micro voids, and diffusion is assumed to take place through the macro and micro regions. According to this model, D_b is calculated as follows:[162]

$$D_b = D_M \varepsilon_M^2 + \frac{\varepsilon_\mu^2 (1 + 3\varepsilon_M)}{1 - \varepsilon_M} D_\mu \tag{5.4}$$

In eqn. (5.4), ε_M is the bulk porosity describing the void fraction resulting from the macropores between particles, while ε_μ is the porosity of the microporous particles. D_M and D_μ are the diffusivities in the macropores and the micropores, respectively. Diffusion in the

macropores is dominated by ordinary diffusion, whereas it is dominated by Knudsen diffusion in the micropores.

The literature is rich with approaches and applications of modelling mass transfer in porous systems, details of which can be found elsewhere.[161,163-165] Nonetheless, due to the complexity of mass transport mechanisms in porous adsorbents with multiple pore sizes, these models are mostly approximations. In order to maintain the simplicity of the model used for the permeation passive sampler as explained in the Introduction while extending its applicability to adsorbents consisting of microporous particles, the use of a single effective diffusion coefficient in the sorbent bed, D_b, estimated using eqn. (5.4), was adopted in this work.

5.2.2 Determination of Mass Transfer Coefficient

The next step is to predict the appropriate value of the mass transfer coefficient, k_c, presented in the equations shown in Figure 5-1. This coefficient represents resistance to analyte transport from the free phase to the sorbed phase in the sorbent bed. In the case of microporous particles, resistance to mass transfer to the sorbed phase is dominated by resistance within the particles, since the majority of the sorption sites are inside these particles. In order to evaluate this resistance, mass transfer inside an individual particle was evaluated. A mass balance inside the spherical particle yields the equation:

$$\varepsilon_\mu \frac{\partial C_p}{\partial t} = D_{p,eff} \frac{1}{r^2} \frac{\partial}{\partial r}\left(r^2 \frac{\partial C_p}{\partial r}\right) - (1-\varepsilon_\mu)\frac{\partial q_p}{\partial t} \qquad (5.5)$$

in which ε_μ is the void fraction inside the particle, C_p is the concentration in the micro-void region within the particle (mol/m^3), r is the distance from the center of the particle (m) ($0 \leq r \leq R$, the radius of the particle), q_p is the concentration of the analyte sorbed to the solid material

(mole per m^3 of the solid matter), and $D_{p,eff}$, is the effective diffusivity inside the micropores of the particles, calculated as follows:

$$D_{p,eff} = \frac{\varepsilon_\mu D_k}{\tau_\mu} \tag{5.6}$$

where D_k is the Knudsen diffusion coefficient in the micropores calculated using eqn. (5.3), and τ_μ is the tortuosity of the microporous medium inside the particle. It is helpful here to approximate the tortuosity, τ_μ, as $\varepsilon_\mu^{(-1/2)}$.[102]

The sorbed analyte is assumed to be in equilibrium with the free concentration at all points within the particle according to the equilibrium isotherm, which is assumed to be of the Freundlich type:

$$q_p = \text{ƙ}C_p^{\frac{1}{n}} \tag{5.7}$$

in which ƙ and n are empirical isotherm parameters.

Bulk concentration C_b is assumed at the surface of the particle; therefore, the first boundary condition is given as follows:

$$C_p = C_b \; at \; r = R \tag{5.8}$$

The boundary condition at the center of the particle is given by:

$$\left.\frac{\partial C_p}{\partial r}\right|_{r=0} = 0 \tag{5.9}$$

Initially, it is assumed that the concentration everywhere inside the particle is at equilibrium at a concentration $C_{p\,(in)}$:

$$C_p = C_{p(in)}\ when\ t = 0\ and\ 0 \le r < R \tag{5.10}$$

The partial differential equation (*PDE*) presented in Equation (5.5), subject to the boundary and initial conditions described in eqns. (5.8) – (5.10), was solved numerically using the Method of Lines.[129] Details about the approximations used to achieve the numerical solution are provided in the Supplementary Information section (Appendix C). The solutions were found using MATLAB software (R2015a, MathWorks, USA). The results were calculated as concentrations of the free analyte within the pores at different points inside the particle.

The mass transfer coefficient, k_c, can then be calculated from the flux boundary condition presented in eqn. (5.11):

$$-D_{p,eff}\left.\frac{dC_p}{dr}\right|_{r=R} = k_c(C_{bulk} - C_{p(ave)}) \tag{5.11}$$

In this equation, $C_{p(ave)}$ is the average free concentration inside the particle and $\left.\frac{dC_p}{dr}\right|_{r=R}$ is the concentration gradient inside the particle near the surface. Details about calculating these two terms can also be found in the Supplementary Information section.

5.3 Experimental

The model was evaluated by comparing uptake rates of the WMS obtained based on the model for porous particles with those measured experimentally. Equilibrium isotherms were

determined using the method described in the Supplementary Material (Appendix C). Anasorb 747 was characterized to determine the pore size and the particle porosity. The characterization method and its results are presented in Supplementary Material (also in Appendix C). The experiments for uptake rate measurement were conducted by exposing the WMS to the vapor of a VOC for various periods while monitoring the concentration using an active sampling method in parallel. The VOCs included in these experiments were trichloroethylene (TCE) and toluene. After determining the amount of the sampled analyte, M (moles), the uptake rate, U (m^3/s), was calculated using the following equation:

$$U = \frac{M}{C_0 t} \tag{5.12}$$

where C_0 is the concentration of the analyte in the sampled air (mol/m^3), and t is the sampling time (s).

5.3.1 Waterloo Membrane Sampler (WMS)

The WMS was fabricated by filling a 2-ml chromatographic glass vial with approximately 200 mg of the Anasorb 747 adsorbent (SKC Inc.). The PDMS membrane was cut into the size of the vial opening before it was crimped in place, covering the mouth of the vial, between the aluminum cap and a polytetrafluoroethylene (PTFE) washer of the dimensions 0.040" × 0.440" × 0.216" (thickness × OD × ID) (virgin PTFE, purchased from Penn Fibre Plastics, Bensalem, PA, US). The process of the PDMS membrane preparation has been explained elsewhere.[122] In these experiments, the thickness of the membrane was controlled by weight, since the membranes were always cut using the same die providing a reproducible surface area. The target weight of the membrane was 8.0 ± 0.5 mg for a 100-µm thick membrane, and 16.0 ± 0.5 mg for a 200-µm thick membrane.

5.3.2 Experimental Setup

The setup was similar to that used previously.[140] In this setup, purified nitrogen gas flowed at a rate of 896 mL/min, controlled by a mass flow controller. The nitrogen flow swept analyte vapor produced continuously using a vapor generator. This generator consisted of a flow-through vessel containing a permeation vapor source. The permeation source contained a neat liquid analyte. Two analytes were separately used in this evaluation: toluene and trichloroethylene (TCE). Analyte concentration was controlled by adjusting the temperature of the vapor source placed inside a GC oven. The resultant standard gas was then directed towards a 10-liter cylindrical glass jar used as an exposure chamber. Through the center of the top cover of this chamber was inserted a circulation fan. Samplers were inserted through holes drilled in the top cover, which were opened only during the insertion. The temperature inside the exposure chamber was kept constant at 21 °C by using an insulating jacket around the chamber and a water circulation thermostat (TOMSON, NESLAB Instrument Inc.) connected to the chamber by means of a Tygon tube wrapped around the glass jar. The concentration was measured actively by drawing the standard gas through a sorption tube packed with an adsorbent using a gas-tight syringe or an AirCheck® sampling pump (XR5000, from SKC Inc., Eighty Four, PA, USA). Details about temperatures and concentration measurements using active sampling are presented in Table 5-S1(Appendix C). The adsorbent used for active sampling was Carbopack B™, purchased from Supelco, Sigma-Aldrich (Oakville, Ontario, Canada) or Anasorb 747, as presented in Table 5-S1.

5.3.3 Analysis

After each exposure, the sorbent from the WMS (Anasorb 747) was transferred to a 4 mL glass vial with an open-top screw cap and a PTFE/silicone septum (purchased from Fisher

Scientific, Ottawa, Ontario). A 1 mL aliquot of carbon disulfide (purchased from Sigma-Aldrich) was added to each of those vials for desorption while they were placed in an ice bath. The vials were then sealed and left for 40 min at ambient temperature with sporadic shaking. Two aliquots of the extract were then transferred to 2 mL crimp top chromatographic vials with 100 µL glass inserts (purchased from Chromatographic Specialties Inc. Brockville, ON, Canada) for GC-MS analysis. Anasorb 747 used in the active samples was analyzed similarly to that used in the WMS, while Carbopack B^{TM}, used for this purpose, was analyzed by transferring the sorption tube to a thermal desorption unit (Perkin Elmer - ATD 400) connected to a GC-MS system.

5.3.4 Instruments and Methods

An Agilent 6890 GC- 5973 MS system was used for the analysis. Carbon disulfide extract aliquots were injected directly using a 7683 Agilent autosampler with a tray of a 100-sample capacity and a Hewlett Packard (*HP*) 3683 injector. An Rxi®-624Sil MS capillary column was used in the GC (60 m × 0.32 mm ID × 1.8 µm film thickness) obtained from Restek (Bellefonte, PA). Helium was used as the carrier gas. ChemStation software (Enhanced ChemStation G1701CA, Version C.00.00, Agilent Technologies) was used for data acquisition and processing. Calibration and quantification, using multi-point calibration curves, were also performed using ChemStation software. A 2 µL sample aliquot was injected to the inlet, set to 290 °C with a 1:10 split ratio. The oven temperature program started at 90 °C, which was held for two minutes before it was increased to a final temperature of 280 °C at a rate of 30 °C/min, without holding the final temperature. Selected Ion Monitoring (SIM) was used targeting the ions with m/z of 95, 130, and 60 for TCE and the ions with m/z of 91, 92 and 65 for toluene.

5.4 Results and Discussion

5.4.1 Evaluation of Mass Transfer into the Particles

The mass transfer coefficient into the sorbed state was assumed to be controlled by resistance to mass transfer inside the particles, as explained earlier. The evaluation of the model describing this process was conducted using parameters related to two analytes, TCE and toluene. Parameter values used in this evaluation are presented in Table 5-S2 (Appendix C). The bulk concentration was assumed to be equal to 5×10^{-4} mol/m^3. The total time of the evaluation was 20 days. The initial concentration in the pores of the particle was assumed to be equal to 5×10^{-6} mol/m^3 in the case of toluene sampling and 3×10^{-5} mol/m^3 in the case of TCE sampling. Zero initial concentrations were avoided as they resulted in extreme stiffness of the numerical integration. The effects of this assumption on the results of the model are presented in the sensitivity analysis section where the effects of the mass transfer coefficient on the results of the calculated sampler's uptake rate are examined.

The results for sampling both analytes were very similar. Figure 5-2 (a) shows the propagation of the normalized free concentration profile of TCE inside the particles, while Figure 5-2 (b) demonstrates the calculated k_c during the process. The results for sampling toluene are presented in Figure 5-S2 (Appendix C). It is clear that the value of k_c in both cases stabilizes shortly after the start of sampling, with a slow decrease over time (in the range of 0.0005 - 0.001 m/sec). An approximate value of 0.001 m/s was extracted from these results.

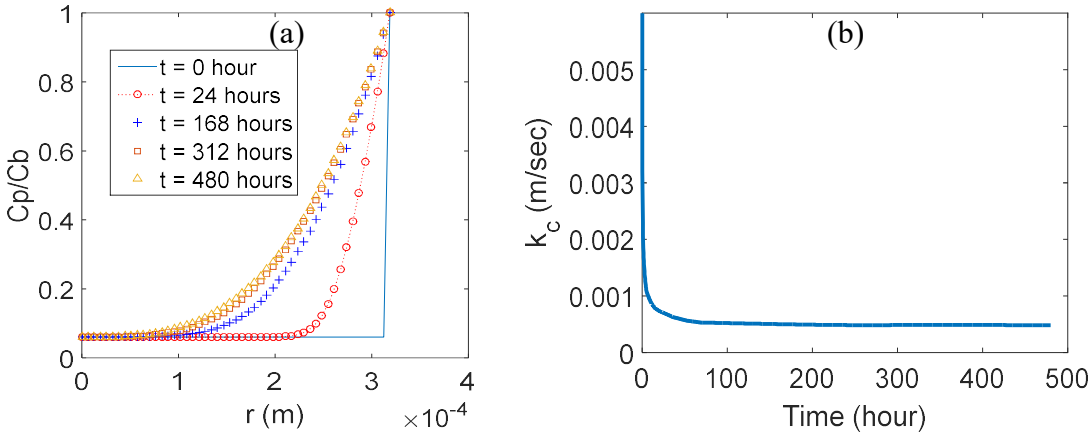

Figure 5-2: Propagation of the normalized free concentration profile of TCE inside the particle (a) and the calculated mass transfer coefficient (b) with time.

5.4.2 Model Evaluation

The uptake rate was calculated using the theoretical model described earlier with parameter values presented in Table 5-S2 (see Appendix C) for sampling of TCE and toluene using the WMS with Anasorb 747 (a highly porous adsorbent). All solutions were found using MATLAB software (R2015a, MathWorks, USA). The mesh sizes were as follows: $M = 50$, $N = 1000$. These sizes were chosen to be higher than those in the case of the previously evaluated adsorbent, Carbopack B, to produce smooth concentration profiles. Changing these sizes did not show significant effect on the uptake rate results. The model calculated the concentrations of the sampled analytes at all points of the sampler compartments. The total amount of sorbed analyte $M(t_n)$, at any sampling time, t_n, in the sorbent bed was calculated by integrating the moles of sorbed analyte over the entire sorbent bed. The uptake rate at time t_n was then calculated using the following equation:

$$U(t_n) = \frac{M(t_n)}{C_0 \cdot t_n} \tag{5.13}$$

The calculated uptake rate values were compared with the experimental ones. It was observed that the model results were sensitive to parameters related to mass transfer in the membrane, the diffusion coefficient in PDMS, D_m, and the partition coefficient between air and PDMS, K, as presented in Figures 5-S3 and 5-S4, respectively (see Appendix C). This sensitivity is further explored in the sensitivity analysis section. An excellent agreement between the experimental results for TCE sampling and the model results was achieved when the value of 1.3×10^{-10} cm^2/sec was used for the diffusion coefficient of TCE in PDMS (ref.[166]), whereas the value of 900 was used for the partition coefficient of TCE between air and PDMS (within the uncertainty range observed in the literature as presented in ref.[167]).

Figure 5-3 presents a comparison between the experimental and model results for three data sets of TCE sampling using the above values and the values listed in Table 5-S2 for the other parameters. Good agreement can be observed in all panels of this figure between the experimentally measured uptake rate values and the uptake rate profile calculated based on the model. Panels (a) and (b) show the uptake rate results obtained from an exposure of WMS to TCE vapor at a concentration of 8.96 mg/m^3. The samplers were of the regular 2 mL size, with the membrane thickness of 100 µm (a) and 200 µm (b). The Average Relative Error (*ARE*) calculated using eqn. (5.14) was 11 % and 8.8 % in (a) and (b), respectively. These *ARE* values are very reasonable as they are well below 20 %. The experimental data and the model results in both panels demonstrate stability of the uptake rate with slight, insignificant decrease over the evaluated sampling time (at a rate of approximately 8×10^{-12} m^3/s per hour in (a) and 1.5×10^{-12} m^3/s per hour in (b)). In panel (c) of Figure 5-3, the samplers with a 100 µm thick membrane were exposed to a higher concentration of TCE vapor of 27.56 mg/m^3. The calculated *ARE* for this set of experiments was 9.6 %. In this case, the model results predicted a more significant

decrease of the uptake rate with time (at a rate of approximately 1.6×10^{-11} m^3/s per hour). This observation is consistent with the previous results of the model when used with the adsorbent with non-porous particles, in which the decrease in the uptake rate with time became more significant as the concentration in the evaluated air increased.[140]

$$ARE = \frac{100}{N}\sum_{i=1}^{N}\left|\frac{U_{meas} - U_{calc}}{U_{meas}}\right|_i \quad (5.14)$$

In eqn. (5.14), *ARE* is the Average Relative Error, U_{meas} is the experimentally measured uptake rate, U_{cal} is the calculated uptake rate based on the model, and *N* is the number of data points.

In another set of experiments, the WMS containing Anasorb 747 and equipped with a 100 µm thick membrane was exposed to toluene vapor at a concentration of 6.8 mg/m^3. The uptake rate measured in these experiments and the uptake rate profile produced by the model simulations using parameters presented in Table 5-S2 are presented in Figure 5-4. The error band, shown in this figure, represents the uncertainty in the calculated uptake rate given the uncertainty in the model parameters. Since the results were sensitive to membrane parameters, the uncertainty was calculated based on the propagation of error using the relative standard deviation of the parameters related to the mass transfer in the membrane. These parameters are included in the uptake rate formula that assumes membrane control of the uptake rate expressed as follows:

$$U = \frac{D_m K A_m}{L_m} \quad (5.15)$$

In eqn. (5.15), A_m and L_m are the membrane sampling area and thickness, respectively. The relative standard deviations of these parameters were estimated, based on the variabilities of their values between different sources, to be 61 % for D_m and 3.6 % for *K*. The corresponding relative

standard deviations were estimated to be 10 % for both A_m and L_m based on the variabilities of the measured areas and membrane thickness, respectively. The resultant uncertainty in the uptake rate was $62._5$ %. Eqn. (5.15) was used here to estimate the overall uncertainty due to parameter uncertainties, but not in the calculation of the uptake rate. Both experimental and model results showed negligible change in the uptake rate with time. The experimental data points fell within the region of uncertainty related to the model-based uptake rate values.

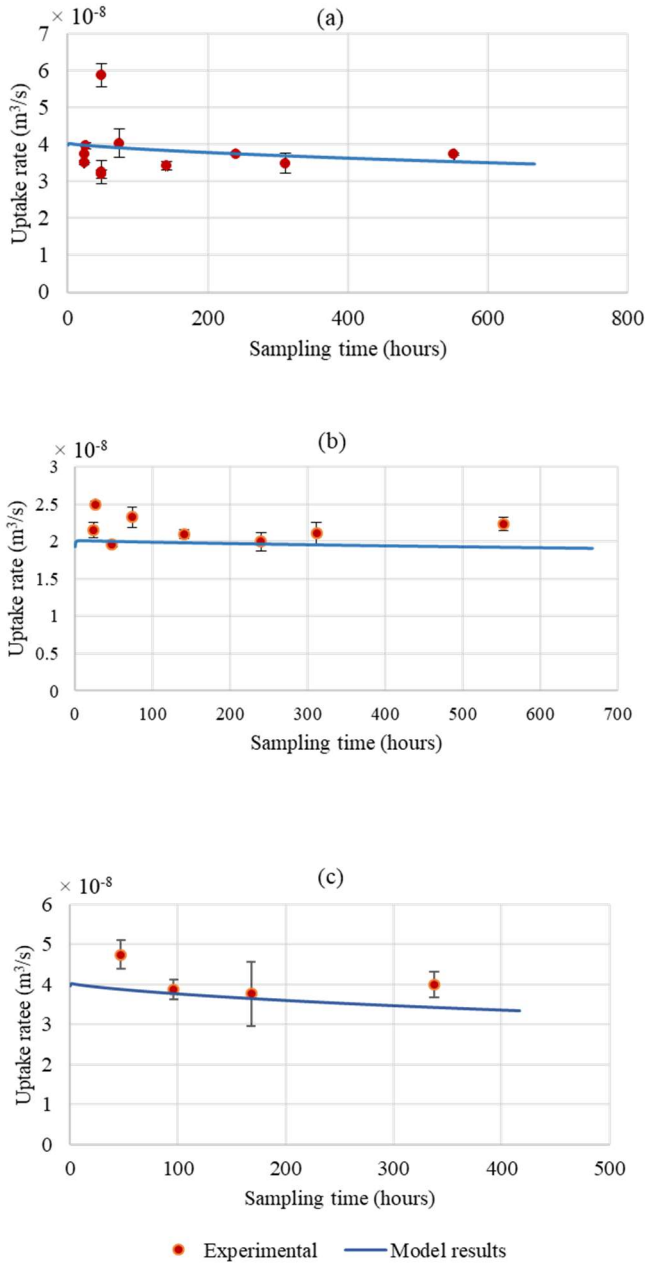

Figure 5-3: Uptake rate of the WMS towards TCE vs experimental data: (a) 100 µm (regular) thickness membrane, vapor concentration of 8.96 mg/m^3; (b) 200 µm thickness membrane, vapor concentration of 8.96 mg/m^3; and (c) 100 µm thickness membrane, vapor concentration of 27.56 mg/m^3.

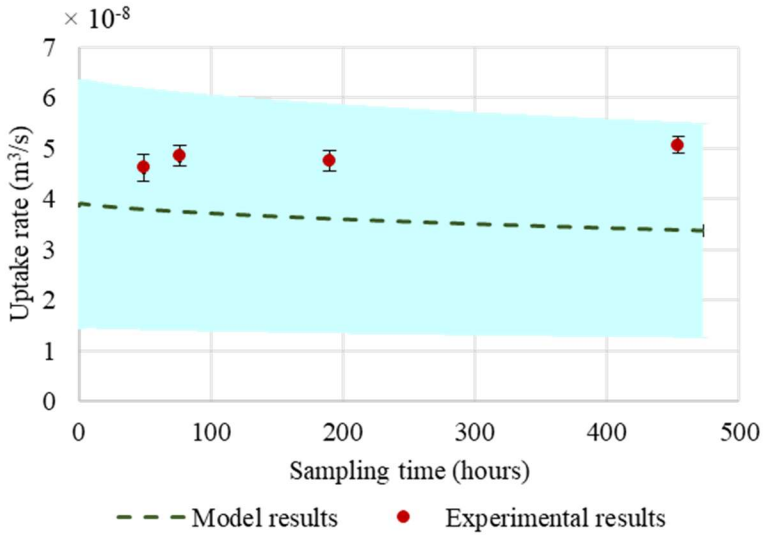

Figure 5-4: Comparison between the experimental values and the model results when sampling toluene at a concentration of 6.8 mg/m3 using the WMS (regular, 100 µm, membrane thickness). The band around the model results is the estimated uncertainty.

5.4.3 Sensitivity Analysis

Next, a comprehensive sensitivity analysis to investigate the parameters with the greatest influence on the uptake rate calculated by the model was performed. Not only does this analysis permit understanding of the contribution of uncertainties in different parameters to the variability in the model output, but it also allows optimization of the model parameters either to achieve a desirable output or to minimize output uncertainty.[168] Zhang and Wania presented a sensitivity analysis of a model that described the uptake of semivolatile organic compounds into a diffusive passive sampler.[103] The model was also applied to investigate the influence of chemical properties and temperature on the sampling rate.[103] Cao et al. developed an inverse problem optimization method for designing passive samplers.[102] They also relied on sensitivity analysis to investigate the influence of the model parameters on the relative error of the measured mass collected by the passive sampler, and presented an optimized design of a passive sampler.[102]

The uptake rate, U, calculated using eqn. (5.13), was chosen as the output of interest. The parameters evaluated included those related to mass transfer within the membrane and the sorbent bed, as presented in Figure 5-1. Those parameters included: the diffusion coefficient of the analyte in the membrane, D_m; the partition coefficient of the analyte between air and the membrane material, K; the effective diffusivity of the molecules within the void spaces of the sorbent bed, D_b; the mass transfer coefficient from the free phase to the sorbed phase, k_c; the porosity of the sorbent bed, ε; and the parameters, a and b, of the analyte-adsorbent isotherm given in the following equation:

$$C^* = aq^b \tag{5.16}$$

where C^*(mol/m^3) is the concentration in the gas phase that is in equilibrium with the adsorbed concentration, q. In order to explore the behavior of the chosen model's output (the uptake rate) when the input parameter values change, sensitivity analysis was initially performed by varying a single parameter at a time within the range of values predicted for VOCs, while using a given set of fixed values for the other parameters. The results of this evaluation are presented in the Supplementary Information section.

In a subsequent step, global sensitivity analysis was conducted, since the magnitude of a measured localized sensitivity is dependent on the selected base-case scenario, i.e. the output sensitivity behavior depends on the selected base values of the parameters.[169] For this analysis, the uptake rate sensitivity was evaluated within wide ranges of the isotherm parameter, a (see eqn.(5.16)), and the diffusivity in the sorbent bed, D_b, corresponding to a range of VOCs in a given sorbent. The range of the parameter a was estimated based on the knowledge of this parameter for several VOCs on the given sorbent (Table 5-S5, Appendix C). For Carbopack B,

this range was estimated to be 1×10^{-8} to 5×10^{-5}, while for Anasorb 747, it was estimated to be within 1×10^{-17} - 1×10^{-11}. Some VOCs could fall outside these boundaries due to lack of knowledge of the entire range of values for this parameter; nonetheless, the results provide very good insight into the uptake rate sensitivity that could be useful even for analytes that are outside the predicted ranges. The range of the effective diffusion coefficient in the sorbent bed, D_b, was assumed to be between 2.0×10^{-7} and 2.9×10^{-6} m^2/s for the non-porous particles of Carbopack B. This range was selected to include the range of diffusivities for most VOCs calculated using eqn. (5.1), considering that most VOCs have diffusivities in air within the range of $1 \times 10^{-6} – 1 \times 10^{-5}$ m^2/sec.[170] A wider range of effective diffusivity in the bed was used for the porous adsorbent, Anasorb 747, due to the complexity of the diffusion mechanism which results in higher uncertainty. The range selected in this case was 1.0×10^{-8} to 2.9×10^{-6} m^2/s.

Sensitivity was quantified using the gradient of the calculated uptake rate $\Delta U/\Delta x_i$, with respect to each parameter, x_i.[168] This gradient was obtained by perturbing the input parameter, x_i, between the upper bound and the lower bound defining its approximate uncertainty range, and recording the difference in the calculated response, U. To remove the effects of units, the gradient was divided by the ratio of the average uptake rate to the average parameter value between the upper bound and the lower bound scenarios.[169] As a result, the sensitivity coefficient (SC) becomes:

$$SC = \frac{\Delta U}{\Delta x_i} \cdot \frac{x_{i,ave}}{U_{ave}} \tag{5.17}$$

The base values in addition to the upper and lower bounds of the evaluated parameters are listed in Table 5-S4 for both types of adsorbents (see Appendix C). The upper and the lower bounds for the effective diffusion coefficient in the sorbent bed and for the isotherm parameter a

were calculated by varying each of them by 50 % of the parameter value. The evaluation was performed at two levels of *K,* the partition coefficient between air and PDMS: 800 and 10,000 in order to monitor the model behavior for a very wide range of VOCs. The model results were calculated for "sampling" an analyte vapor at a concentration of 1×10^{-5} mol/m^3 for 200 hours.

Figures 5-5 and 5-6 present the sensitivity analysis results for the non-porous adsorbent, Carbopack B, towards parameters of mass transfer in the membrane and mass transfer in the sorbent bed, respectively. Figures 5-7 and 5-8 summarize the sensitivity analysis towards parameters in the membrane and in the sorbent bed, respectively, in the case of the porous, strong adsorbent, Anasorb 747. It can be observed from Figures 5-5 and 5-7 that the uptake rate is more sensitive to parameters related to mass transfer in the membrane, D_m and K, especially in the case of the stronger adsorbent, Anasorb 747. In both cases, it is clear that the sensitivity decreases when moving diagonally from the top left corner to the bottom right corner. This direction corresponds to a decrease in the effective diffusivity in the bed and an increase in the isotherm parameter, a. It is useful here to point out that according to the isotherm expression used in the model (eqn. (5.16)), increasing a corresponds to a decrease in the sorption capacity. Therefore, moving in the direction identified above results in slower mass transfer in the sorbent bed, which, in turn, leads to a decrease in the sensitivity towards mass transfer parameters in the membrane. At the same time, the influence of parameters related to mass transfer in the sorbent bed increases in the same direction; therefore, the sensitivity increases towards the diffusivity in the sorbent bed and, to a lesser extent, towards the parameter a in this direction, as presented in Figures 5-6 and 5-8, panels A, B, C, and D.

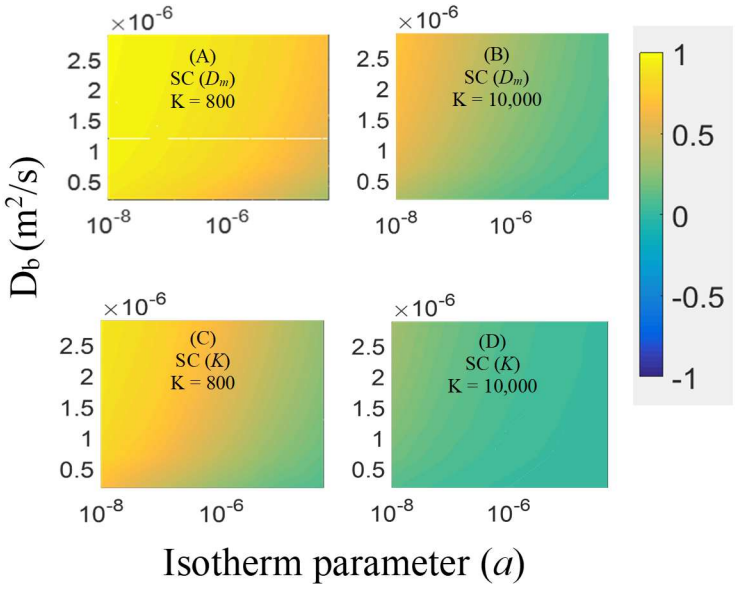

Figure 5-5: Sensitivity coefficients (SC) of the uptake rate of the WMS with Carbopack B for a range of VOCs with a range of isotherm parameter, a, values and a range of diffusivity in the sorbent bed, D_b, at two levels of partition coefficient between air and PDMS, K: 800 (A and C) and 10,000 (B and D), to variation in diffusivity in the membrane, D_m (A and B), and the partition coefficient, K (C and D).

Figures 5-5 and 5-7 also show that at the higher level of the partition coefficient, K, the sensitivity towards the parameters D_m and K, or the membrane's permeability ($P = D_m \times K$), decreases, whereas the sensitivity towards D_b and a increases, as presented in Figures 5-6 and 5-8. This can also be explained by the increase in the influence of the mass transfer process as it becomes slower. In the case of VOCs with higher permeability through the PDMS membrane, the sensitivity towards permeability parameters decreases while the sensitivity towards the mass transfer parameters in the sorbent bed increases. This also explains the higher sensitivity towards the membrane's parameters (Figures 5-5 and 5-7) and lower sensitivity towards the sorbent bed's parameters (Figures 5-6 and 5-8), in the case of the stronger adsorbent, Anasorb 747, compared to Carbopack B, except for the sensitivity towards the isotherm parameter, b, which exhibits a different behavior. It can also be observed that the sensitivity towards the diffusivity in the sorbent bed and towards the isotherm parameter, a, have similar magnitudes, but opposite

directions. The reason is that increasing the diffusivity in the bed facilitates mass transfer deeper in the bed, thus lowering the concentration in the gas phase of the bed and increasing the uptake rate of the sampler; on the other hand, increasing the parameter *a* leads to slower sorption rate, which increases the free concentration in the sorbent bed and, hence, reduces the uptake rate of the sampler.

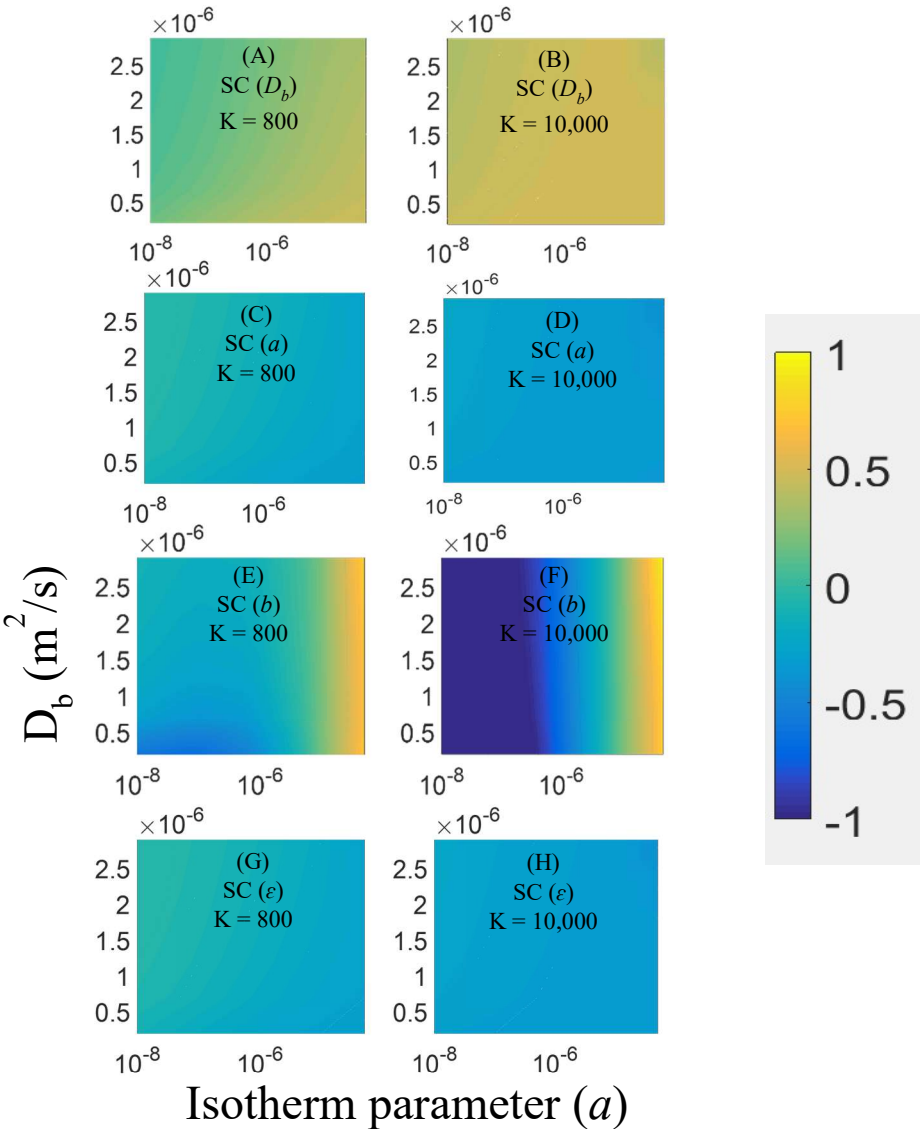

Figure 5-6: Sensitivity coefficients (SC) of the uptake rate of the WMS with Carbopack B for a range of VOCs with a range of isotherm parameter, *a*, values and a range of diffusivity in the sorbent bed, D_b, at two levels of partition coefficient between air and PDMS, *K*: 800 (A, C, E, and G) and 10,000 (B, D, F, and H), to variation in D_b (A and B), the parameter *a* (C and D), the isotherm parameter *b* (E and F), and the bed porosity, ε (G and H).

Increasing porosity of the sorbent bed has two influential but opposite effects. It facilitates diffusion inside the bed, which reduces the free concentration and increases the uptake rate; however, it reduces the fraction of the solid phase available for sorption, which has an opposite effect on the uptake rate. The extent of these two effects depends on the influence of the other parameters: partition coefficient between air and PDMS, diffusivity in the bed, and sorption rate. Based on that, one can explain the sensitivity towards the bed porosity presented in Figures 5-6 and 5-8 (panels G and H). The sensitivity towards the porosity is insignificant in the case of the strong adsorbent (although it seems to be slightly increasing in opposite directions when moving from top left to bottom right at the two different levels of K - Figure 5-8, panels G and H).

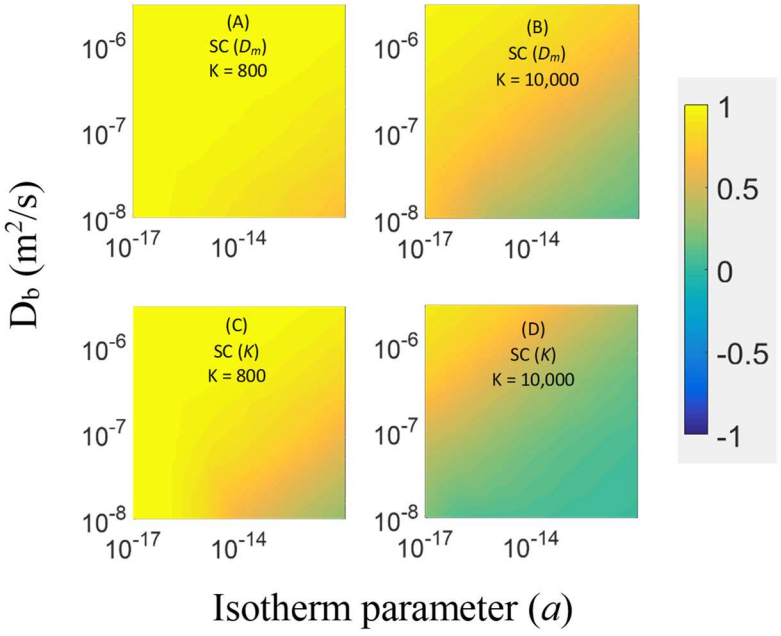

Figure 5-7: Sensitivity coefficients (SC) of the uptake rate of the WMS with Anasorb 747 for a range of VOCs with a range of isotherm parameter, a, values and a range of diffusivity in the sorbent bed, D_b, at two levels of partition coefficient between air and PDMS, K: 800 (A and C) and 10,000 (B and D), to variation in diffusivity in the membrane, D_m (A and B), and the partition coefficient, K (C and D).

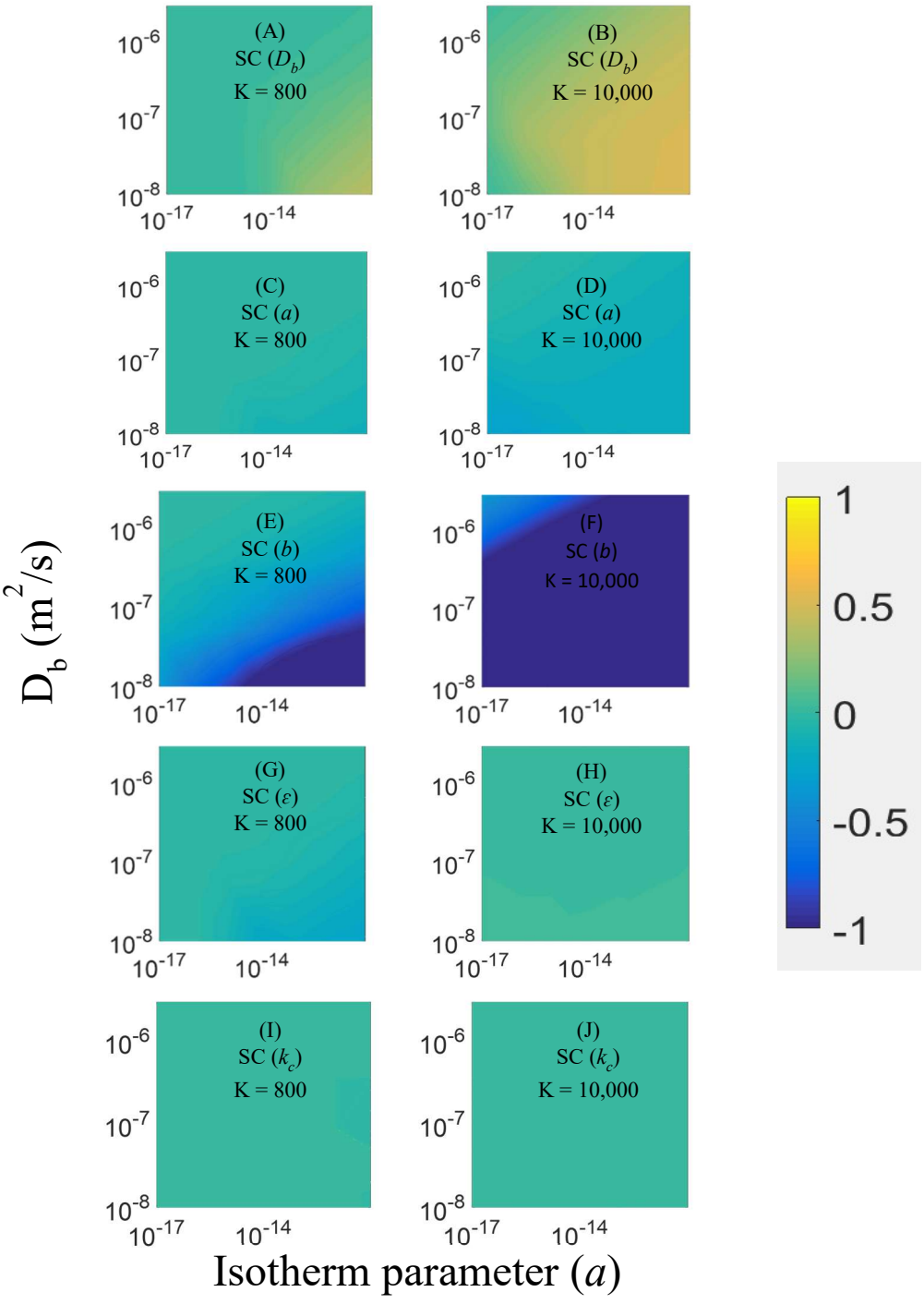

Figure 5-8: Sensitivity coefficients (SC) of the uptake rate of the WMS, with Anasorb 747 for a range of VOCs with a range of isotherm parameter, a, values and a range of diffusivity in the sorbent bed, D_b, at two levels of partition coefficient between air and PDMS, K: 800 (A, C, E, G and I) and 10,000 (B, D, F, H and J), to variation in D_b (A and B), the parameter a (C and D), the isotherm parameter b (E and F), the bed porosity, ε (G and H), and the mass transfer coefficient, k_c (I and J).

The sensitivity towards the porosity is more significant in the case of the weaker sorbent (Figure 5-6 – Panels G and H); however, the SC is below -0.5. The SC for the porosity changes in a very similar manner to the sensitivity towards the isotherm parameter *a* (Figure 5-6, panels C and D). This means that increasing the porosity value decreases the uptake rate of the sampler. Sensitivity towards the mass transfer coefficient, k_c, was not evaluated in the case of the non-porous adsorbent, since its value is correlated to the diffusion coefficient in the bed and the porosity (eqn. (5.1)). On the other hand, sensitivity of the uptake rate towards this parameter was evaluated in the case of the porous adsorbent, Anasorb 747, in which case the determination of this parameter involved a more complex calculation scheme and related approximations. Results from this evaluation are presented in Figure 5-8 I and J, in which the model results showed no sensitivity towards k_c, which means that the value obtained for one analyte can safely be used for other VOCs without the need for recalculation. These results also indicate that the approximations and assumptions made when estimating the value of k_c for porous particles had no consequences on the accuracy of the results.

The isotherm parameter, b, is the reciprocal of the exponent parameter in the common form of Freundlich isotherm ($q = kC^{\frac{1}{n}}$), which defines the shape of the isotherm. Sensitivity towards the parameter *b* showed behavior different from that of the other parameters. In the case of Carbopack B (Figure 5-6 E and F), colors are distributed as strips parallel to the D_b axis, which means that the SC changes only with *a* values. In this case, the uptake rate is insensitive to the *b* value around $a = 5 \times 10^{-6}$, while sensitivity increases to the left and right of this value in opposite directions. This explains the observation made in earlier evaluations of the sensitivity of the uptake rate to the parameter *b* when using toluene parameters as base values ($a = 7.67 \times 10^{-6}$). In both panels E and F of Figure 5-6 (K = 800 and 10,000 respectively), the results are highly

sensitive to the *b* value in the right-end of the *a* range, which corresponds to highly volatile compounds. The results also show high sensitivity to the *b* value in the left end of panel F of this figure (*K* = 10,000) but in the opposite direction. This end corresponds to the range of VOCs with low volatility. When using Anasorb 747, sensitivity towards parameter *b* shows a different trend (Figure 5-8). At the low level of *K* (*K* = 800, Panel E), the SC is insignificant except in the right-bottom corner, which corresponds to volatile components with low diffusivities. On the other hand, at the higher *K* level ((*K* = 10,000, Panel F), the model becomes highly sensitive to the value of *b*. This sensitivity is less significant at the upper-left corner of the figure, which corresponds to analytes with a high sorption rate (very small *a*) and high diffusivity in the bed.

The above observations help understand the influence of the uncertainty in different parameters on the model output, the uptake rate of the sampler, for a wide range of VOCs with different properties. Inevitably, some of the evaluated parameters are correlated and specific ranges of these parameters belong to specific regions of the space defined by the two dimensions, diffusivity in the bed and the parameter *a*. It is expected that the more volatile a compound is, the lower will be its partition coefficient between air and PDMS and its sorption rate into the adsorbent; therefore, for the low range of *K*, it is expected that the *a* values fall within the higher range; that is, at the *K* level of 800, the right-hand half of the space defined earlier should be taken into consideration. On the other hand, at the high level of *K* (*K* = 10,000), the left side of the parameter space should be considered. Diffusivity in the bed, D_b, is also correlated to *K*, since *K* tends to be higher for larger molecules, which usually have lower diffusivity in air.[170] These distributions can be seen in Figure 5-S7. This figure presents the distribution of a group of VOCs with measured or estimated parameters when Carbopack B adsorbent is used. The information given for these analytes can be used to explore trends useful for estimation of

parameters. Figure 5-S8 shows that a linear correlation between the natural logarithm of the isotherm parameter *a* and the natural logarithm of the partition coefficient *K* can be obtained using this information. The correlation becomes more significant when it is evaluated for a homologous group of VOCs (Figure 5-S8 B for linear hydrocarbons). The reader is reminded that this correlation is intended for demonstration only and requires further confirmation with more data from a larger set of VOCs.

5.4.4 Practical Implementation and Recommendations

5.4.4.1 Optimizing the membrane thickness

In order to compare the sensitivity coefficients (SCs) for different parameters used in this evaluation and monitor the magnitude and changes in SCs using actual values of these parameters for specific analyte/sorbent pairs, the SCs for the different parameters were plotted at parameter values specific for a given analyte and adsorbent versus the membrane thickness, L_m, as an independent variable. The "sampling" time was set to 200 hours at a concentration of 1×10^{-5} mol/m^3. Each parameter was varied by 10 % and the SC was calculated as described earlier. The results are presented in Figure 5-9 for two analytes: TCE and Toluene. In this figure, it can be seen that when a strong adsorbent such as Anasorb 747 is used (Figure 5-9 B and D), the SCs for parameters related to mass transfer within the sorbent bed become insignificant, while the model results are sensitive to membrane-related parameters, D_m and K. The most influential parameter inside the sorbent bed is the isotherm parameter *b*, which is mainly observed in the case of TCE with a membrane thickness of 0.1 mm (the regular thickness of the membrane). These observations support the conclusions that were based on Figure 5-8, which also predicts that the influence of the parameter *b* becomes more significant for analytes with higher *K* values. Nonetheless, based on Figure 5-9, the SC towards *b* is reduced as the thickness of the membrane

is increased without significantly changing the SCs for the other parameters. Sensitivity towards parameters of mass transfer within the sorbent bed is more significant in the case of the weaker adsorbent, Carbopack B (Figure 5-9 A and C and Figure 5-S9). In these Figures, it can be observed that increasing the membrane thickness decreases the sensitivity towards the sorbent bed's parameters while increasing sensitivity towards the membrane's parameters. It is clear also that the SCs for the isotherm parameter a and the porosity ε behave similarly and they are in the opposite direction to the SC for diffusivity in the sorbent bed, D_b. In the case of Carbopack B, sensitivity towards parameter b is negligible.

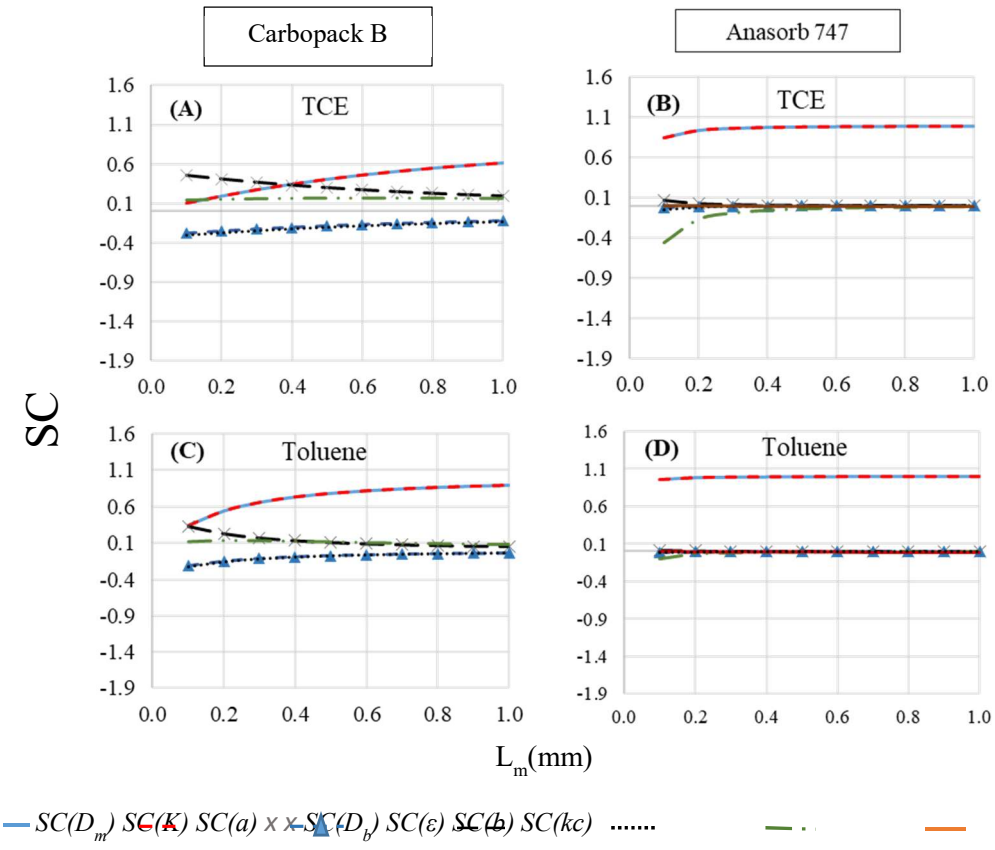

Figure 5-9: Comparison between the sensitivity coefficients (SCs) calculated when Carbopack B is used as a sorbent (A and C) and those calculated with Anasorb 747 (B and D) for two analytes: TCE (A and B) and toluene (C and D).

Based on the above observations, one can conclude that in the case of a strong adsorbent, the membrane is the main rate-determining barrier and the zero-sink assumption can be safely used, especially in the case of a thick membrane (1 mm). Using the zero-sink assumption allows the application of a simple formula, presented in eqn. (5.15), to predict the "ideal" uptake rate value. Nonetheless, using the model presented in this paper would still provide the advantage of predicting the significance of the uptake rate change with time, especially at high concentrations, as presented in Figure 5-3 (c); therefore, one can use this information to predict an appropriate exposure time without significant uptake rate change or apply a proper correction method when needed, as explained in our previous work.[171] Using a thicker membrane also reduces the sensitivity to the sorbent bed parameters in the case of the weaker sorbent. It is important, though, to identify the parameters D_m (diffusivity in the membrane) and K (partition coefficient between air and PDMS) accurately in both cases. Additionally, it is recommended to evaluate the isotherm parameter b for a wide range of VOCs to evaluate its ranges for different sorbents.

5.4.4.2 Influence of temperature on the uptake rate

To evaluate the effects of temperature on the uptake rate of the WMS, one needs to consider the influence of temperature on mass transfer in both the membrane and the sorbent bed, unless the membrane is the rate-determining barrier, as is the case with Anasorb 747. In this case, the temperature effect may be evaluated by determining the changes in D_m and K with temperature. Figure 5-10 shows the uptake rate values calculated for a range of D_m values between 5×10^{-11} and 1.5×10^{-10} m^2/s and a range of K values between 500 and 1,200 when Anasorb 747 (panel A) and Carbopack B (panel B) are used. These ranges for D_m and K were selected within the potential ranges of changes around the base values related to toluene permeating through PDMS. Other parameters were set at the base value set of the toluene-

Anasorb 747 pair presented in Table 5-S2 for panel A and at the base value set of toluene and Carbopack B, presented in Table 5-S3, for panel B.

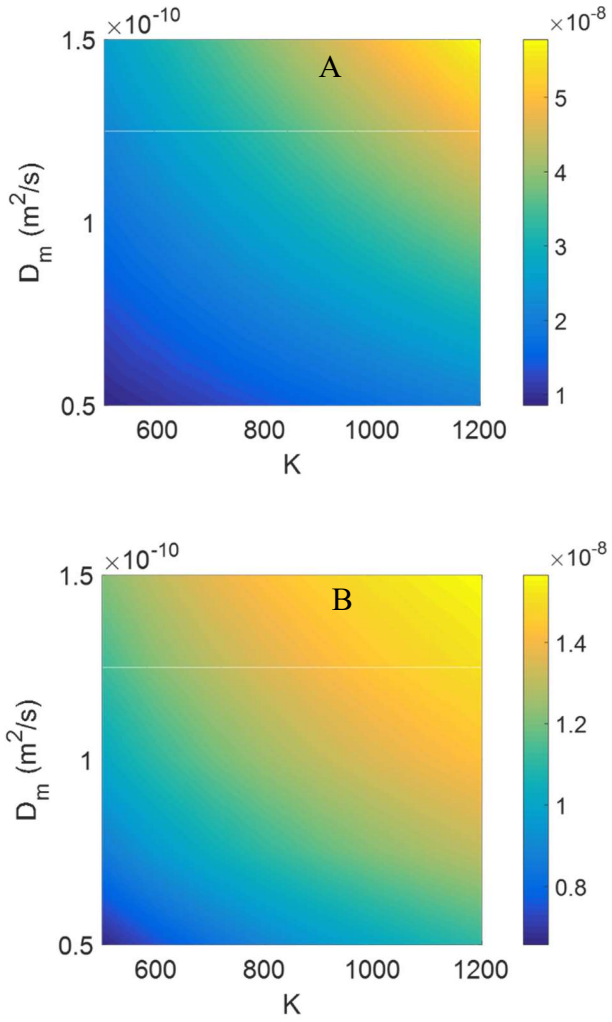

Figure 5-10: Calculated uptake rate levels for ranges of the diffusivity in the membrane, D_m, and the partition coefficient between air and PDMS, K, in the case of Anasorb 747 (A), and Carbopack B (B) adsorbents.

The colors in the contour plots of Figure 5-10 are distributed in strips spreading diagonally from the upper-left side to the bottom-right side of the plots. When temperature increases, the diffusivity in the membrane, D_m, increases, and the partition coefficient, K, decreases, and vice versa. This means that changing the temperature leads to a diagonal movement on the plots presented in Figure 5-10 similar to the direction of the color distribution;

therefore, the influence of temperature change is expected to be minimal on the uptake rate. However, the magnitude and the sign of the uptake rate change depend on the magnitude of the change in each of these two parameters with temperature. It was shown experimentally in a previous work using the WMS containing Anasorb 747 that the net effect of increasing temperature is a decrease in the uptake rate.[32] In this work, a linear relationship was observed between *ln(U)* and *1/T*, where T is the temperature.

In the case of the weaker adsorbent, Carbopack B, the effect of temperature on the mass transfer parameters inside the sorbent bed needs to be evaluated in addition to its influence on the permeability through the membrane. Figure 5-11 shows the changes in the uptake rate within the parameter space defined by the ranges used earlier for D_b and a. All other parameters were set to the base values for Carbopack B presented in Table 5-S4. As explained earlier, due to the correlation between the partition coefficient K and the isotherm parameter a (i.e. for the low range of K, the parameter, a, falls within the higher range of values, whereas at the high level of K, a falls within the lower range), at K = 800 (Figure 5-11 A), one is referred to the right half of the plot. On the other hand, at the value of 10,000 for the parameter K (Figure 5-11 B), one is referred to the left half of the plot. In both cases, it can be seen that the colors are distributed diagonally from the bottom left to the top right of the plots with more influence of the parameter, a, on the color distribution. Increasing the temperature is expected to increase the diffusivity in the bed and decrease the sorption rate. This means that increasing the temperature increases both D_b and a, which leads to a diagonal movement also from the bottom left to the top right. As a result, the net effect of increasing the temperature is expected to be minimal and not exceeding a factor of 0.5 decrease in the uptake rate for one order of magnitude increase in the value of a.

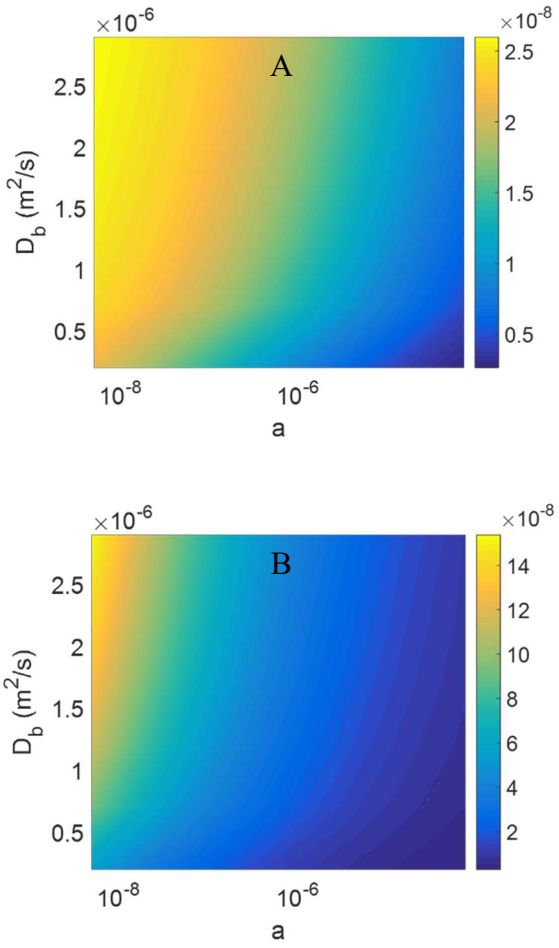

Figure 5-11: Calculated uptake rate levels for ranges of the diffusivity in the sorbent bed, D_b, and the isotherm parameter, a, at K=800 (A) and K=10,000 (B).

It was shown before that the exponents in Freundlich isotherms for ammonia and isobutene on activated carbons increase when temperature increases.[172] The exponent b in the isotherm form used in the current model, as presented in eqn. (5.16), is the inverse of the exponent parameter used in the original Freundlich form, as explained earlier in the sensitivity analysis. Consequently, assuming a similar behavior as presented in the previous work,[172] increasing the temperature is expected to reduce the value of the parameter b. As presented earlier in Figure 5-6 E and F, this parameter is influential for highly volatile compounds (Figure 5-6 E, the rightmost end of the plot) and for compounds with low volatility/high partition

coefficient values (Figure 5-6 F, the left half of the plot). The SC is positive in the former case (*U* decreases as *b* decreases), while SC is negative in the latter case (*U* increases as *b* decreases). Therefore, temperature affects the parameters *a* and *b* in opposite directions. In all cases, increasing *a* as a result of increasing temperature reduces the uptake rate; however, in the case of compounds in the high range of the partition coefficient *K* (i.e. at the 10,000 level and higher), reducing the parameter *b* as a result of increasing the temperature increases the uptake rate, which opposes the effect of changing the parameter *a* and, therefore, reduces the change in the uptake rate as a result of increasing the temperature. However, in the case of highly volatile compounds, changes in both *a* and *b* as a result of temperature variation affect the uptake rate in the same direction. In Figure 5-6 E, the *SC* becomes higher than 0.5 when *a* is around 5×10^{-5} and higher. This value is approximately equal to that corresponding to hexane as presented in Figure 5-S7. Therefore, it can be concluded that influence of the temperature change on the isotherm parameters becomes more influential for VOCs with a vapor pressure around and higher than 153 mm Hg at 25 °C (hexane vapor pressure[173]).

5.5 Conclusions

The mathematical model developed earlier to describe the sampling process in a permeation passive sampler with a non-porous adsorbent was successfully applied to the case of a porous adsorbent as a receiving phase in the passive sampler. Sensitivity analysis was performed to reveal influential parameters in both scenarios and to inform the optimization of passive sampler performance. Based on the results of this analysis, it can be concluded that using a stronger adsorbent limits the influential parameters to those related to the membrane; otherwise, increasing the membrane thickness would also lower the sensitivity towards the sorbent-related parameters relative to those that are membrane-related. Influential parameters in

the sorbent bed would also contribute to the total effect of temperature change on the uptake rate. It is expected, though, that the contribution of the sorbent bed parameters to the total temperature effect on the uptake rate is negligible within the small range of temperature changes usually encountered in environmental sampling except for the case of highly volatile compounds. This, however, requires further experimental confirmation.

CHAPTER 6.

MODELLING THE EFFECT OF LINEAR FLOW VELOCITY OF AIR

6.1 Introduction

Convection conditions around a passive sampler can affect the sampling/uptake rate of the sampler. Regardless of the convection conditions, a boundary layer exists at the interface between the evaluated medium and the sampling surface, as was presented in the Introduction of this thesis. While mass transport in the bulk of the matrix occurs as a result of both convection and diffusion, the contribution of the convective mass transport is decreased within the boundary layer as the distance towards the sampling surface becomes smaller until mass transport occurs purely by diffusion near the sampling surface.[90] The concentration of the sampled analyte within the boundary layer is also depleted in the same direction as a result of both the sampling process and the decrease in the convection rate. It is a common approach to simplify the boundary layer as a region of a defined length, through which only diffusive mass transfer takes place.[90] Although the diffusivity of an analyte does not change with the flow conditions, the thickness of the boundary layer, and hence the diffusion distance, increases as the flow rate in the evaluated medium decreases.[89] Therefore, resistance to mass transfer through the boundary layer becomes more significant and influential on the total resistance to mass transfer into the passive sampler as the flow velocity of the evaluated medium decreases. An opposite effect is observed in the case of a high face velocity at the inlet of the diffusive passive samplers due to disturbance of the static diffusion path.[174] This effect, however, does not occur in permeation passive samplers.

In the model presented earlier for the passive sampling process into the WMS, the calculated concentration in air reflected the concentration in the immediate vicinity of the sampling surface (the membrane), assuming negligible effect of the concentration gradient within the air boundary layer at the membrane surface. This assumption is true in many cases, especially considering that the diffusion coefficients of VOCs in PDMS are significantly smaller than they are in air (approximately four orders of magnitude); therefore, resistance to mass transfer in the membrane is expected to dominate the total resistance unless the boundary layer is very thick. When the air velocity across the membrane's surface is not sufficient to replenish the analyte at the sampling surface and to keep a negligible thickness of the air boundary layer, the effect of the boundary layer on the total uptake rate needs to be taken into consideration. The additional region of resistance to mass transfer into the surface of the sampler is demonstrated in

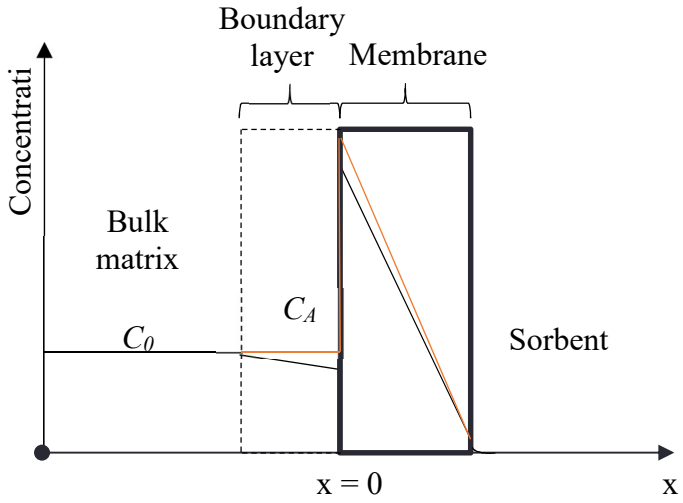

Figure 6-1: Concentration profile in the presence of resistance to mass transport in the air boundary layer at the sampling surface of the WMS (black line), compared with the ideal concentration profile with no resistance on the side of the evaluated air (orange line).

Figure 6-1. As a result of the decreased concentration at the air-membrane interface, the concentration gradient across the membrane decreases, and so does the uptake rate of the sampler. The aim of the work presented in this Chapter is to evaluate the effect of the resistance

to mass transfer within the boundary layer on the model results, and to predict the influence of the air face velocity on the uptake rate of the WMS. There is no assumption made here about a diffusion-limited mass transport within the boundary layer.

6.2 Theory

To account for the concentration gradient in the boundary layer, the following boundary condition was added at the interface of the membrane with the evaluated air:

$$h_m(C_{0-}C_A|_{x=0}) = -D_m \frac{\partial C_m}{\partial x}\Big|_{x=0} \tag{6.1}$$

where C_0 is the concentration of the analyte in the bulk air (mol/m^3), C_A is the concentration in the air boundary layer, D_m is the diffusion coefficient in the membrane (m^2/s), C_m is the analyte concentration in the membrane (mol/m^3), and h_m is the mass transfer coefficient (m/s) calculated using the following formula, based on equations of mass transfer into a flat plate:[175]

$$Sh = \frac{h_m d}{D_a} \tag{6.2}$$

In this equation, Sh is the Sherwood number, d is the diameter of the sampling surface (m), and D_a is the diffusion coefficient in air (m^2/s). The Sherwood number is calculated using the following relations:[175]

$$Sh = 0.664\, Re^{\frac{1}{2}}\, Sc^{\frac{1}{3}}\, when\ Re < 2 \times 10^5\ (laminar\ flow) \tag{6.3}$$

$$Sh = 0.0365\, Re^{0.8}\, Sc^{\frac{1}{2}}\, when\ Re \geq 2 \times 10^5\ (turbulent\ flow) \tag{6.4}$$

In eqns. (6.3) and (6.4), Re is the Reynolds number, $Re = \frac{\rho v_\infty d}{\mu}$; Sc is the Schmidt number, $Sc = \frac{\mu}{\rho D_a}$; ρ is the density of air (kg/m^3); v_∞ is the flow velocity of the bulk air (m/s); and μ is the viscosity of air [kg/(m·s)].

Another boundary condition at that interface is derived from a boundary condition in the original form of the model; that is, a local equilibrium is assumed at the air-membrane interface, as presented in eqn. (6.5).

$$C_m|_{x=0} = KC_A|_{x=0} \tag{6.5}$$

in which K is the partition coefficient of the analyte between the air and the PDMS membrane. The mass balance equation in the membrane is also applied in this extension of the model to the membrane's interface with the evaluated air as follows:

$$\left.\frac{\partial C_m}{\partial t}\right|_{x=0} = D_m \left.\frac{\partial^2 C_m}{\partial x^2}\right|_{x=0} \tag{6.6}$$

The finite difference approximation of eqn. (6.6) is expressed as follows:

$$\frac{dC_{m(j=1)}}{dt} = D_m \frac{C_{m(2)} - 2C_{m(1)} + C_{m(0)}}{(\Delta x_m)^2} \tag{6.7}$$

In this equation, j is the number of the node in the discretized membrane's thickness, j = 1,2,…, $M+1$; whereas Δx_m is the thickness of the slice resulting from discretizing the membrane of the thickness L_m, $\Delta x_m = L_m/M$. This approximation resulted in a fictitious point at j = 0. To remove the concentration at this fictitious point, $C_{m(0)}$, eqn. (6.1) can be approximated as follows:

$$h_m(C_{0-}C_A|_{x=0}) = D_m \frac{C_{m(0)} - C_{m(2)}}{2\Delta x_m} \tag{6.8}$$

By rearranging eqn. (6.8), the concentration $C_{m\,(0)}$ can be approximated as in the following equation:

$$C_{m(0)} = \frac{2\Delta x_m h_m(C_{0-}C_A|_{x=0})}{D_m} + C_{m(2)} \tag{6.9}$$

By substituting eqn. (6.9) into eqn. (6.7), one can write the following equation:

$$\frac{dC_{m(1)}}{dt} = 2D_m \frac{C_{m(2)} - C_{m(1)} + \left(\frac{\Delta x_m h_m(C_{0-}C_A|_{x=0})}{D_m}\right)}{(\Delta x_m)^2} \tag{6.10}$$

Equation (6.10) was added to the model equations along with the following equation that was derived from eqn. (6.5):

$$\left.\frac{\partial C_A}{\partial t}\right|_{x=0} = \frac{1}{K}\left.\frac{\partial C_m}{\partial t}\right|_{x=0} \tag{6.11}$$

Initially, the concentration in the air at the interface with the membrane is assumed to be equal to the bulk concentration, and the concentration in the membrane at the interface with the evaluated air is in equilibrium with that concentration, as follows:

$$C_A|_{x=0} = C_0 \; when \; t = 0 \tag{6.12}$$

$$C_m|_{x=0} = KC_0 \; when \; t = 0 \tag{6.13}$$

All other initial and boundary conditions remain the same as in the original model.

6.3 Results and Discussion

To evaluate the effects of the convection conditions on the uptake rate of the WMS, the scenario in which the membrane is the region of dominant resistance to mass transfer inside the

WMS was used. For this purpose, the case of a strong adsorbent inside the sampler and a short sampling time was considered. In this manner, and based on the results of the sensitivity analysis, the model results become insensitive to most parameters inside the sorbent bed. To minimize any effect of influential parameters, namely the isotherm parameter *b*, a short-term exposure of two days to analyte vapor of 2×10^{-7} mol/m^3 concentration in the evaluated air was evaluated. Biot modulus (*Bi*) is a dimensionless number that is used to describe the relative significance of the conductive (internal) and convection (external) resistances to heat transfer between a body and its surrounding.[175] Biot number was used in this work to investigate the relative importance of resistance to mass transfer in the air boundary layer and that in the membrane. In this case, Biot number, *Bi*, is defined as follows:

$$Bi = \frac{L_m/D_m}{1/h_m} = \frac{h_m L_m}{D_m} \tag{6.14}$$

Different parameters in the model were set at the values corresponding to sampling toluene using the standard, 2-mL WMS with Anasorb 747 at 21 °C, presented earlier in Table 5-S2 (Appendix C). Additional parameters used in the extension, presented in this chapter, are provided in Table 6-1.

Table 6-1: Values of parameter values used to estimate the mass transfer coefficient in the air boundary layer.

Parameter	Description	Value	Unit
d	Diameter of the sampling surface	5.5×10^{-3}	m
ρ	Air density	1.2047*	kg/m^3
μ	Air viscosity	1.8205×10^{-5}*	kg/(m·s)

* At T = 20° C (ref.[176])

With these parameters, the model results were obtained using a range of air velocities starting from an infinitely small value of 1×10^{-8} m/s up to 7 m/s. The results of the simulations, presented in Figure 6-2, demonstrated that the *Bi* number has very large (*Bi* >> 1) values for air

velocities within the common indoor air range, 0.1 – 3 m/s, for which the corresponding *Bi* values fall within the range of 6,800 – 37,000, respectively. This means that the membrane is the dominant rate limiting barrier in the process, and the contribution of the boundary layer to the total resistance to mass transfer is small. Resistance to mass transfer in the boundary layer becomes equally important as that in the membrane, meaning that the *Bi* number is around the value of one, when the velocity is infinitely small (1×10^{-8} m/s in this evaluation). As the value of the *Bi* number increases, the uptake rate increases, meaning that the resistance in the boundary layer becomes less significant, until it levels off around a value of 10,000 of the *Bi* number (for the specific values provided for all parameters). This value is the critical value after which the uptake rate is not affected by the face velocity in the evaluated air. For the specific case of toluene (with the provided parameters) and with the earlier-explained method of estimating the mass transfer coefficient from the evaluated air into the sampling surface, this value of the *Bi* number corresponds to air velocity of ~ 0.2 m/s. This value is close to the value of 0.35 m/s provided earlier by Seethapathy in his thesis, when he experimentally evaluated the effects of face velocity on the sampling rate of the WMS.[145]

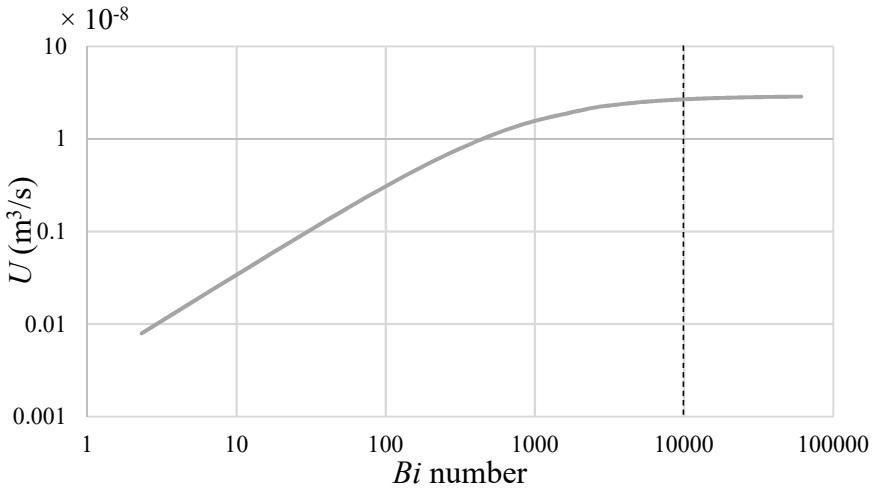

Figure 6-2: Variation of the uptake rate, U, with the value of the Bi number. The dashed line represents the approximate location of the critical value of Bi number, after which the uptake rate becomes independent of face velocity.

The simulations were repeated using values of the diffusivity in the membrane within the range expected for VOCs in PDMS, 1×10^{-11} to 1×10^{-9} m^2/s. The effect of changing the membrane thickness, within the range of 0.1 mm to 1 mm, was also evaluated. The results of these simulations are presented in Figure 6-3 and Figure 6-4, respectively. As predicted, varying the values of D_m or L_m did not change the critical Bi values. This becomes clearer when plotting the ratio of the concentration in the air at the interface with the membrane and the bulk concentration in air, $C_{A(\text{interface})}/C_0$ (Panels B of both figures). The value of the mass transfer coefficient, h_m, that corresponds to the critical Bi, however, is different in each scenario.

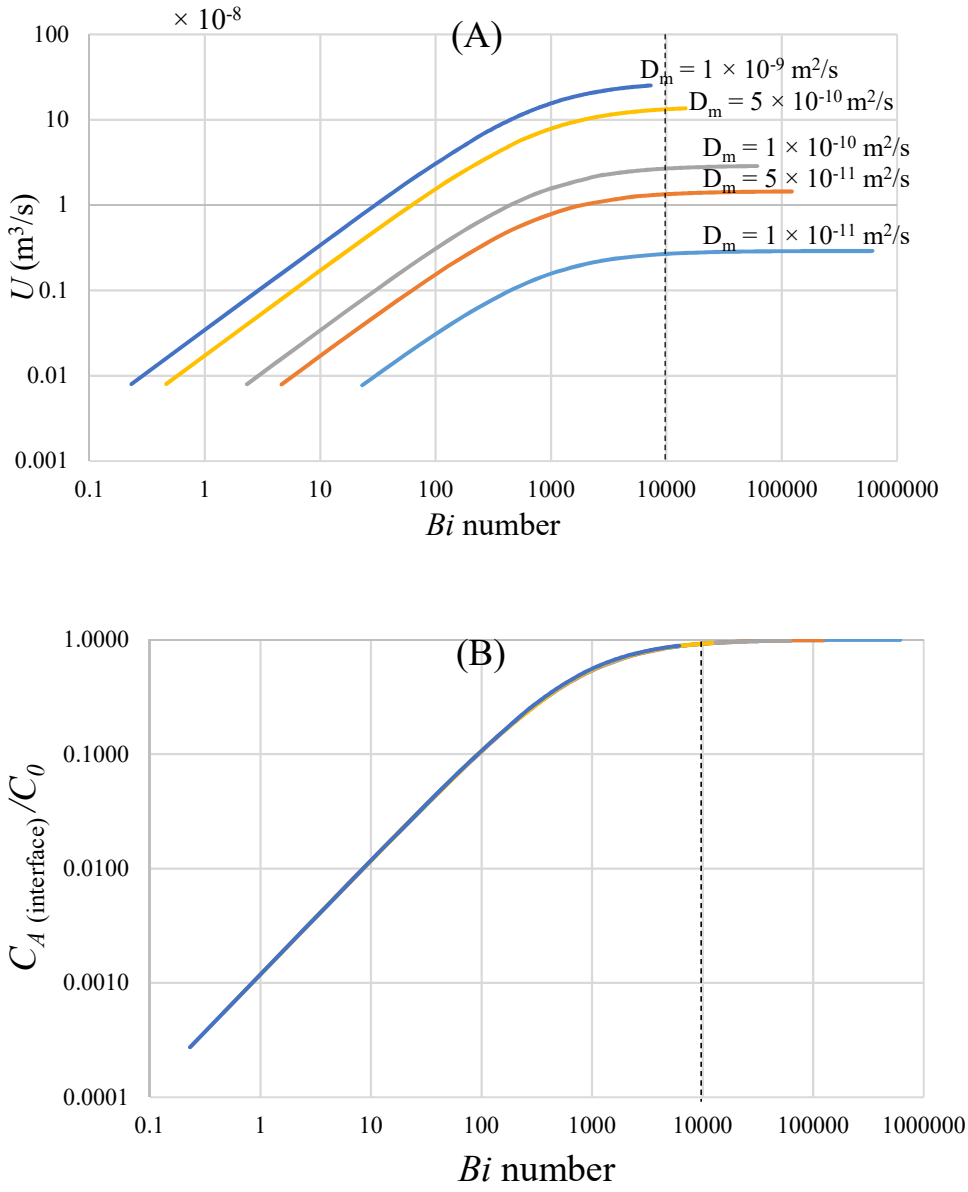

Figure 6-3: Demonstration of the independency of the critical *Bi* value (around 10,000 here) from diffusivity in the membrane.

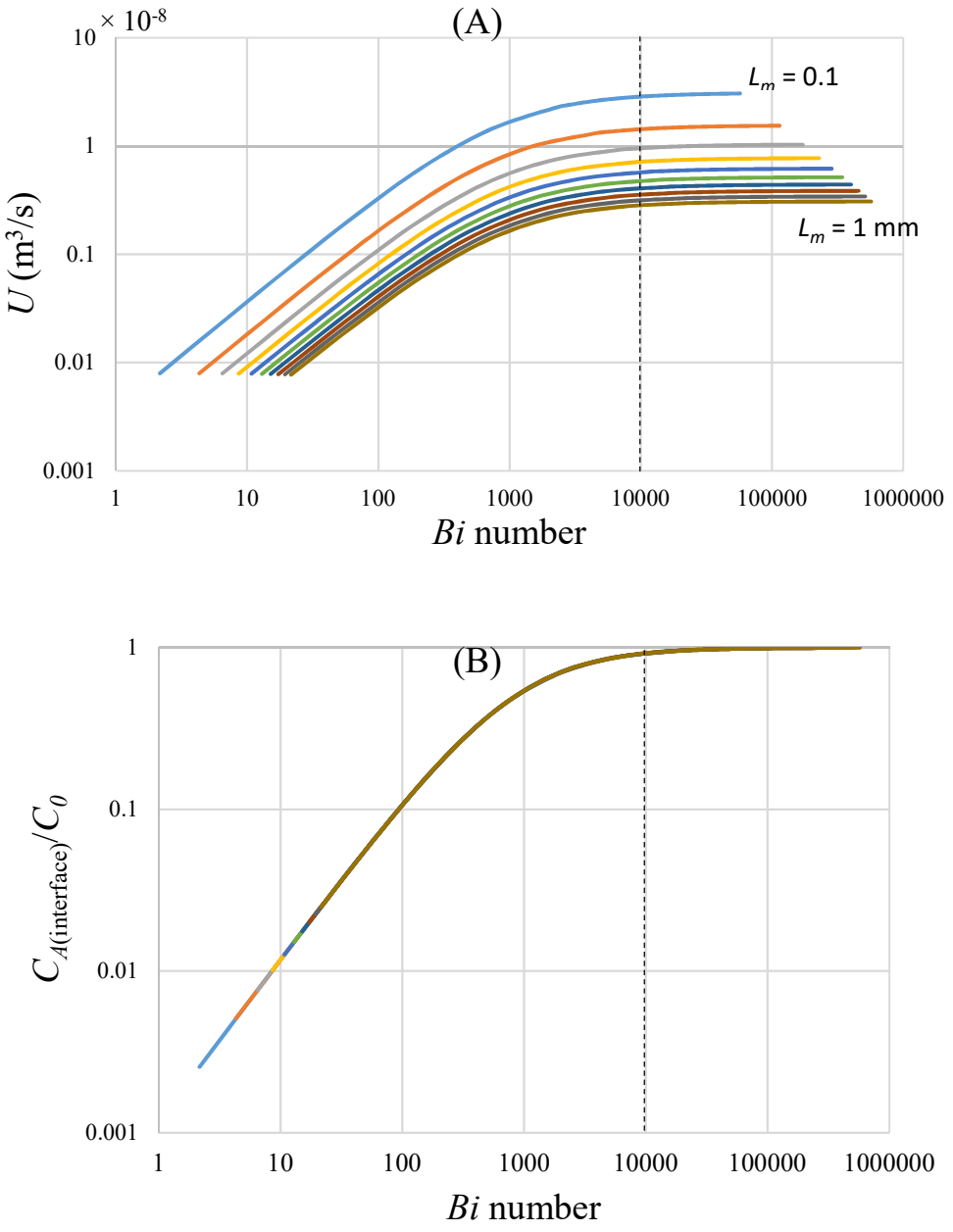

Figure 6-4: Demonstration of the independency of the critical *Bi* value (around 10,000 here) on the thickness of the membrane.

Based on the method presented earlier for estimating the mass transfer coefficient, one can relate the critical value of the *Bi* number to a critical face velocity (a minimum velocity above which the uptake rate is not affected by resistance in the air boundary layer) for the given

ranges of D_m and L_m. Figure 6-5 presents *log (Bi)* corresponding to a range of face velocities with a range of diffusivities in the membrane, Panel A; and with a range of membrane thicknesses, Panel B.

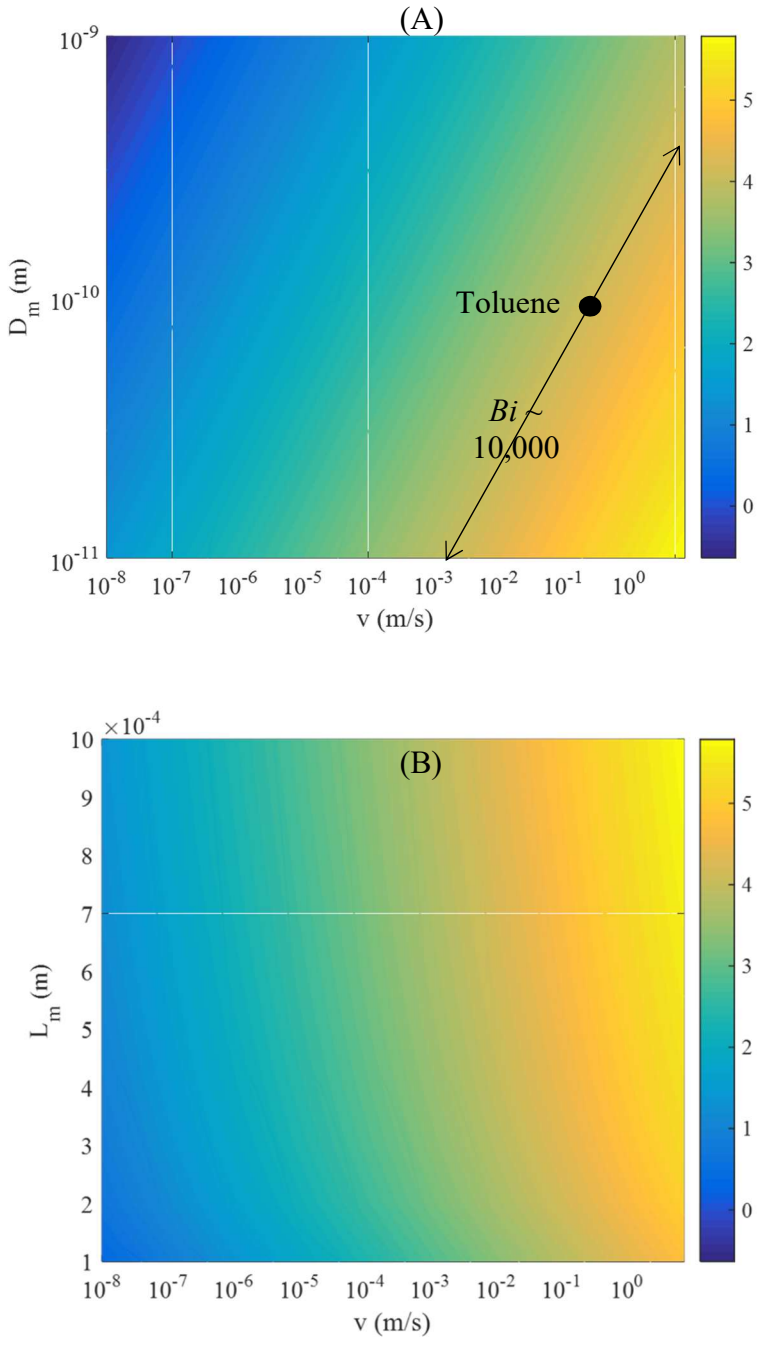

Figure 6-5: Variation of the *log (Bi)* with the air velocity and diffusivity in the membrane, (A), and with the air velcity and the thickness of the membrane, (B).

It can be seen in this figure that the critical value of the face velocity decreases as the diffusivity in the membrane decreases and/or as the thickness of the membrane increases. When evaluating the effect of changing the value of *K*, the partition coefficient between air and PDMS, the critical value of the *Bi* number increased with increasing *K*. These results are presented in Figure 6-6.

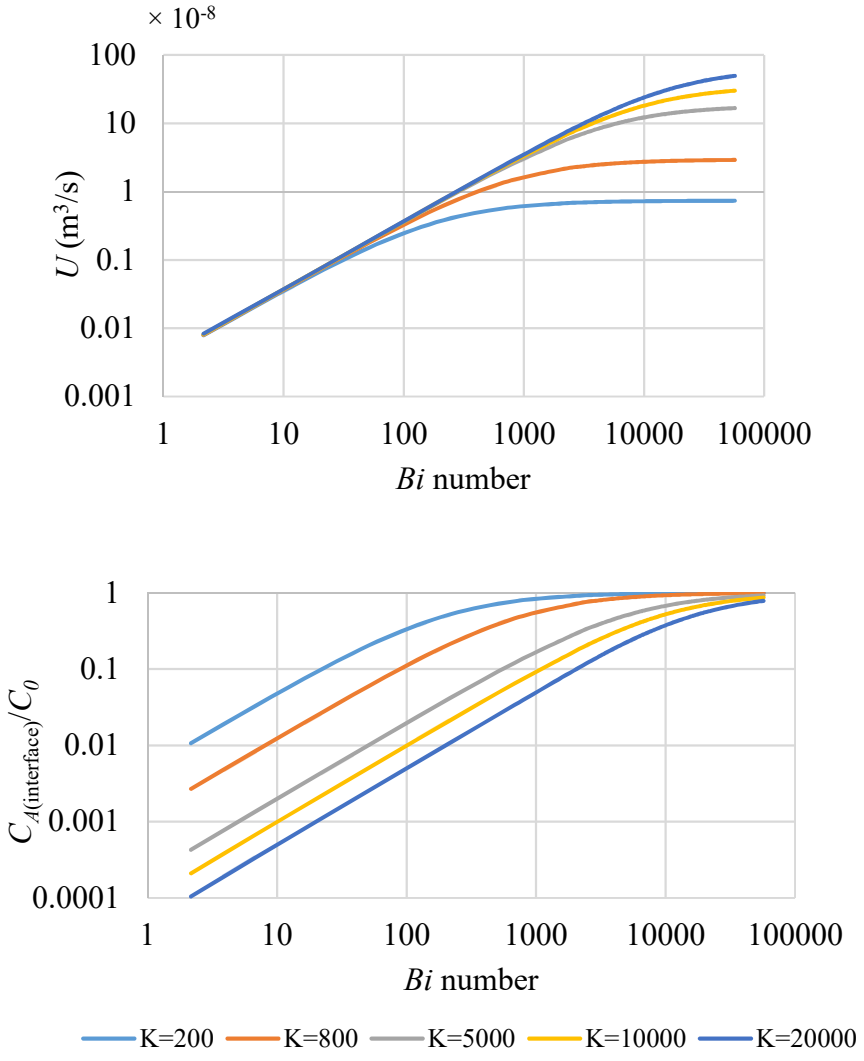

Figure 6-6: Demonstration of the dependency of the critical *Bi* value on the value of the partition coefficient between air and the PDMS material. .

In this figure, it can be seen that the uptake rate stabilizes at higher *Bi* value as *K* increases; nontheless, at *Bi* values below 100, the uptake rate values are very similar for all values of *K*. This can be explained by significant contribution of resistance to mass transfer in the air boundary layer within the low range of *Bi* number. When evaluating the critical *Bi* value for different alkanes, using the parameters listed in Table 6-2 , this observation was confirmed, as presented in Figure 6-7.

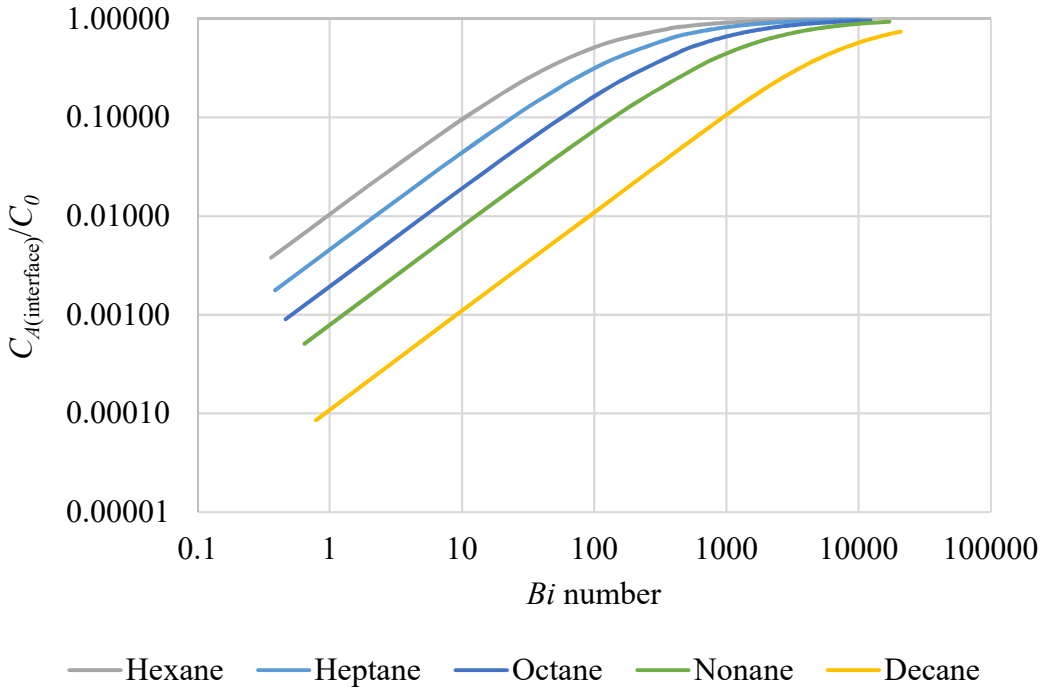

Figure 6-7: Variation of the critical value of the *Bi* number for different alkanes

The results of the simulation were obtained for a range of VOCs to estimate the suitability of the WMS with two membrane thicknesses, 0.1 mm (the regular thickness) and 1 mm (recently introduced to the design of the WMS) in indoor air monitoring. Generally, indoor air velocity is expected to be within the range of 0.1 – 3 m/s; therefore, a critical velocity of 0.1 m/s is desired for the sampler to be applicable in indoor air measurement with an acceptable error. The results of this evaluation are presented in Table 6-2.

Table 6-2: Estimated critical face velocities for sampling a group of VOCs with a range of *K* values using the WMS and the optimum membrane thickness recommended for indoor air sampling

Compound	*K*	$D_m \times 10^{10}$ (m^2/s)	$D_{air} \times 10^6$ (m^2/s)	Critical velocity for the 0.1-mm-thick PDMS membrane (m/s) (≤ 10 % error)	Critical velocity for the 0.1-mm-thick PDMS membrane (m/s) (≤ 20 % error)	Critical velocity for 1-mm-thick membrane (m/s) (≤ 20 % error)	Optimum membrane thickness (mm) for a critical velocity of 0.1 m/s (≤ 20 % error)
n-Hexane	95 (ref.[145])	6.00 (ref.[145])	7.47*	0.1	0.01	infinitely small	0.1
n-Heptane	218 (ref.[145])	5.30 (ref.[145])	6.88*	0.3	0.06	0.001	0.1
n-Octane	516 (ref.[145])	4.20 (ref.[145])	6.40*	1	0.2	infinitely small	0.2
Toluene	843£	1.07£	8.50£	0.1	0.03	0.001	0.1
TCE	900£	1.3£	8.75£	0.2	0.04	0.001	0.1
n-Nonane	1267 (ref.[145])	2.90 (ref.[145])	6.01*	3	0.6	0.01	0.3
m-Xylene	2140§	2.09 (ref.[115])	7.18*	4	0.8	0.01	0.3
Isopropylbenzene	3830§	1.35 (ref.[115])	6.65*	5	1	0.02	0.4
sec-Butylbenzene	8635§	1.23 (ref.[115])	6.22*	-	4	0.05	0.7
n-Decane	9166§	2.29 (ref.[115])	5.68*	-	-	0.2	1.5
1-Methyl-2-isopropylbenzene	11600§	1.51 (ref.[115])	6.22*	-	-	0.2	1.2
Undecane	23834§	1.86 (ref.[115])	5.40*	-	-	1	3.5

£ Value used in the previous chapters

* Estimated values using Fuller's equation (ref.[170])

§ Average value obtained from estimated and measured values reported in ref.[177]

It can be seen in this table that the WMS equipped with the regular 0.1-mm thick membrane can be used for sampling VOCs with *K* values smaller than 1,000 with an acceptable error caused by reduction of air concentration at the interface with the membrane (error ≤ 20 %). The critical face velocities for those compounds are smaller than or around the minimum indoor air velocity. When a maximum error of only 10 % is tolerated, the critical air velocity for those compounds falls within the range of 0.1- 1 m/s. Increasing the membrane thickness to 1 mm significantly reduces the critical air velocities for analytes within this group and expands the range of analytes that can be safely sampled, with an error less than 20 %, to include analytes with *K* at the 10,000 level. As *K* value reaches 20,000, the critical air velocity for this thickness of the membrane (1 mm) approaches the upper bound of velocities commonly encountered in indoor air and the error increases. In such situations, it is recommended to increase the membrane thickness, if possible, or use different membrane materials through which permeabilities of these analytes are smaller.

6.4 Conclusions

The effect of depletion of analyte concentration at the membrane interface with the evaluated air as a result of the formation of the boundary layer near this interface was evaluated. It was concluded that, under common indoor air velocities, the internal diffusive resistance to mass transfer is more significant than the external resistance in the boundary layer. Resistance to mass transfer in the air boundary layer was found to be equally important to that in the membrane only in cases of infinitely small air velocities (practically, in stagnant air). The critical value of the *Bi* number was observed to increase with increasing values of the partition coefficient between the air and the membrane. Based on that, the suitability of the WMS with the regular 0.1-mm-thick PDMS membrane for indoor air sampling was predicted to be limited to

VOCs with *K* values below 1,000. Increasing the membrane thickness was found to increase the applicability range in indoor air sampling. Recommendation regarding the membrane thickness and material was made accordingly.

CHAPTER 7.

SUMMARY AND FUTURE WORK

7.1 Summary

Passive sampling provides many advantages in environmental analysis compared to the conventional active sampling techniques. Understanding the theory behind the passive sampling method as well as factors influencing its accuracy is crucial for many purposes: for selecting a suitable passive sampling technique, for developing the sampling method, and for interpreting the results of the measurement and their accuracy. Several approaches have been presented to model the passive sampling process. The applicability of each of these models relies on the validity of the assumptions made in this model to the selected sampling technique for a given sampling scenario. In air passive samplers that rely on linear uptake of analytes into the passive sampler to measure the TWA concentrations, the receiving phase is assumed to behave as a zero sink, meaning that the sampled analyte is removed sufficiently from the gas phase of the receiving phase leaving negligible concentrations at the barrier-receiving phase interface. This ideal behavior maintains the concentration gradient across the barrier, and, hence, maintains a constant uptake rate.

In the work presented in this thesis, a dynamic model was presented to simulate the sampling process in permeation passive samplers. The model was applied to the WMS and validated experimentally. The model applies dynamic mass balance equations in all sampler compartments and all phases, assuming mass transfer in one dimension from the evaluated air into the sampler. The model assumes local equilibrium at both the air-membrane interface and

the membrane-sorbent bed interface. The rate of adsorption at each point of the sorbent bed is proportional to the difference between the concentration in the gas phase and that in equilibrium with the adsorbed concentration at that point. Initially, the model was applied to a WMS with a non-porous adsorbent, Carbopack B. In this case, the mass transfer coefficient from the free phase to the sorbed phase accounts for diffusion from the gas phase to the surface of the solid particle. Equilibrium adsorption isotherm of Freundlich type was used. Diffusivity of the analyte within the pores of the sorbent bed was estimated using the parallel-pore model, which accounts for mono-disperse pore-size distribution. The model equations were solved numerically using a MATLAB PDE solver. The model results were produced as concentrations in different compartments of the WMS. These concentrations were used to calculate the desired model output, the uptake rate during the sampling time. The calculated uptake rates were successfully compared to the experimental data. These results showed that the applicability of the zero-sink assumption is conditional and depends on the properties of the analyte-adsorbent pair, as well as the concentration level and the sampling time. The model predicted that resistance to mass transfer within the sorbent bed may develop during sampling and become significant to an extent that cannot be ignored. Therefore, the presented model provides the tool needed for predicting the significance of this effect in a given sampling scenario. This allows optimization of the sampling method, for example, by assigning an appropriate sampling time within which the deviation from linearity is not significant, or by optimizing the membrane thickness in a manner that reduces this effect.

Alternatively, a method of calculating the TWA concentration of the sampled analyte that accounts for this effect was demonstrated. In this method, the amount of analyte collected by the passive sampler is used initially to calculate the concentration using the ideal uptake rate value.

The calculated concentration is, afterwards, re-entered to predict the effective uptake rate at the end of the given exposure period, and the resulting uptake rate is used again to recalculate the concentration. The procedure is repeated in an iterative manner until the produced concentration values converge into the TWA concentration. This method can be applied regardless of the significance of the resistance to mass transfer inside the sorbent bed. Moreover, the model was extended to evaluate the post-sampling/storage period of analytes in the WMS. It was proven both theoretically and experimentally that analyzing the sorbent is sufficient, as the amounts of analytes retained in the PDMS membrane and in the storage vial are negligible after sampling. The experimental evaluation showed that the amounts of analytes detected in the sorbent were stable over up to three-weeks of storage at room temperature.

The model was also applied to the case of adsorbents with porous particles. The effects of the intraparticle resistance to mass transfer on both the diffusivity of an analyte inside the sorbent bed and its mass transfer coefficient from the free phase to the sorbed phase were taken into consideration. Diffusivity in the sorbent bed, in this case, was calculated using the random-pore model, which takes into account the bidisperse nature of the porous system with diffusion occurring through both the macro regions between the particles and the micro regions inside the particles. The mass transfer coefficient was predicted using a simplified case of a single porous particle. Mass transfer from the bulk fluid at the surface of this particle into the adsorption sites inside the particle was modelled separately, and used to predict a suitable value of the mass transfer coefficient. The applicability of the model was assessed experimentally using the WMS containing Anasorb 747, an adsorbent with highly porous particles, widely used in this sampler. This adsorbent was characterized to determine parameters needed for the model, including pore size distribution and porosity. Adsorption isotherm parameters were determined for the test

analytes by regression analysis of the maximum capacities of the adsorbent at different vapor concentrations. The modified Wheeler equation was used to calculate the maximum adsorbent capacity from the experimentally measured breakthrough time. Good agreement was obtained between the uptake rate profile produced based on the model results and the experimentally measured uptake rates.

A comprehensive sensitivity analysis was conducted to detect the influential parameters that have major control of the model output, the uptake rate, and identify those of negligible effect. This analysis included the two types of adsorbents used in the model evaluation: Carbopack B, which is a relatively week adsorbent with non-porous particles, and Anasorb 747, which is a strong adsorbent with microporous particles. An initial sensitivity analysis was conducted by varying one parameter at a time within a range of parameter values predicted for VOCs, while fixing the values of the other parameters at a selected set of base values. The aim of this step was to evaluate the behavior of the model when changing the values of different model parameters. The results of this initial analysis showed sensitivity of the produced uptake rate towards diffusivities in the membrane and in the sorbent bed. The results also showed sensitivity towards one of the isotherm parameters, namely the parameter a. Sensitivity towards the air-PDMS partition coefficient values was observed only during the initial stages of sampling.

This step was followed by a global sensitivity analysis that accounts for dependency of the model sensitivity towards a given parameter on the values of that parameter and the other parameters. Sensitivity, in this case, was evaluated using the sensitivity coefficient, representing the normalized uptake rate gradient between the upper bound and the lower bound of the range selected for the evaluated parameter. The results, for each parameter, were obtained for the entire ranges of values predicted for two of the parameters: the diffusivity of the free analyte within the

sorbent bed, and the isotherm parameter *a.* The evaluation was also conducted at two levels of the air-PDMS partition coefficient, *K*. In general, the results demonstrated sensitivity towards both the diffusivity in the membrane and the partition coefficient into the membrane, *K*, at the low level of *K.* This sensitivity is significantly decreased at the high level of *K.* The results also showed that sensitivity of the model results in the case of a strong adsorbent is limited to parameters related to mass transfer in the membrane, namely the diffusivity in the membrane and the air-PDMS partition coefficient; whereas sensitivity towards parameters related to mass transfer in the sorbent bed, including the bed porosity, the diffusivity in the bed, and the isotherm parameters, becomes more significant as the strength of the adsorbent decreases. Unlike the initial one-parameter-at-a-time analysis, the global sensitivity analysis uncovered and described the sensitivity towards the bed porosity and the exponential parameter in the isotherm. The sensitivity towards the latter parameter showed a behaviour that was different from the other parameters in the sorbent bed, and it was significant in the case of the high level of the air-PDMS partition coefficient for both adsorbents. Increasing the membrane thickness, nonetheless, decreased sensitivity towards parameters in the sorbent bed. The sensitivity analysis was also used to qualitatively demonstrate the effect of temperature change on the uptake rate of the sampler. The effect of temperature change is expected to be minimal on the permeability of an analyte through the membrane, as it affects both the air -PDMS partition coefficient and the diffusivity through the membrane, but in opposite directions. Changing temperature also affects influential parameters in the sorbent bed; however, this effect is expected to be negligible within the small range of temperature variations during a single environmental sampling event.

Finally, the application of the model was extended to estimate the effect of the air face velocity on the uptake rate of the WMS. Contribution of convective mass transfer declines as the

distance from the sampling surface decreases. This effect, along with the effect of the analyte flux into the sampler, reduces the concentration in the air layer right at the interface with the membrane. To account for the resulting resistance to mass transfer in the air boundary layer, an additional boundary condition was added to the previous model, describing the continuity in flux across the air-membrane interface. In this boundary condition, the flux from the bulk air to the sampling surface is proportional to the concentration gradient across the air boundary layer. The proportionality factor represents the mass transfer coefficient, which was estimated based on a model of mass transfer between a moving fluid and a flat plate. The results were presented using the *Biot* number, which describes the relative importance of an internal diffusive resistance to mass transfer and an external convective resistance. It was found that the *Bi* number had large values, which means that the resistance to mass transfer in the membrane is more significant than the external resistance in the boundary layer, except for cases of infinitely small air velocities in which both resistances become equally important. A critical value of the *Bi* number was observed above which the sampling process became independent of the external resistance in the air boundary layer. This critical value was observed to increase with increasing the value of the air-PDMS partition coefficient, *K*. The model results were used to determine the suitability of the WMS for sampling a variety of VOCs from indoor air and to provide recommendations regarding suitable membrane thicknesses for various ranges of *K* values and appropriate ranges of air face velocities.

The work presented in this thesis provides better understanding of the sampling process in permeation passive samplers similar to the WMS. This understanding is critical for the correct application of the sampler in environmental analysis. First, the model permits informed decision on the appropriate plan for a specific sampling purpose. That includes the choice of the sampling

time, the adsorbent material, and the membrane thickness, in addition to other parameters related to the sampler configuration (sampling surface or even the membrane material, for example). Furthermore, the model allows more accurate calculation of the TWA concentration rather than relying on a blind assumption of a zero-sink in the adsorbent bed. The model also provides insights into distribution and fate of the sampled analytes during and after sampling, which was used to predict the suitability of the current storage and analysis methods and to increase the confidence of the WMS users about the accuracy of the sampling method.

7.2 Future Work

To improve the applicability of the model, practical methods for parameter determination are needed. Because PDMS has been used as an extraction phase in many applications, values of parameters related to permeability through the membrane are mostly available or can be estimated. These parameters are the PDMS-air partition coefficient, which is available as an important parameter in solid-phase microextraction (SPME),[177,72] and the diffusion coefficient in the PDMS membrane, which has been also recognized as an important parameter in many passive sampling applications.[115] Diffusivity in air is also widely available and can also be estimated.[170] Adsorption parameters for various analyte/adsorbent pairs are not readily available and their measurement could be very time consuming. One simple method of measuring isotherm parameters uses chromatographic techniques.[178] Nowadays, the task of measuring the isotherm parameters has become easier with advanced instruments such as the Dynamic Vapor Sorption (DVS) Vacuum instrument, available from Surface Measurement Systems, Ltd., Allentown, PA, USA. Such an instrument is also capable of measuring the diffusivity through a membrane.

Predictions of the adsorption parameters might also be possible through modelling. That can be done by relating these parameters to other available parameters in a manner similar to that demonstrated in Chapter 5, when a correlation between the isotherm parameter, *a*, and the PDMS-air partition coefficient was observed. Alternatively, molecular parameters can be used to model the isotherm parameters in methods such as polyparameter linear free energy relationships (pp-LFER).[179]

Another issue that needs to be addressed is the effect of competitive adsorption when sampling a mixture of VOCs. The significance of this effect needs to be evaluated in order to be able to optimize the sampling method in a way that minimizes this effect or to correct for any significant resulting errors. This evaluation would include evaluation of the groups of analytes that would compete for adsorption sites and those the retention of which would be affected by the presence of others. Determination of the adsorption isotherms of analytes in the presence of other competing analytes would be necessary to achieve these goals. This study would be expected to describe situations in which additional precautions are required for accurate measurement and when additional corrections are needed.

The application of the WMS for sampling VOCs from water was evaluated previously in the author's master's thesis. This evaluation showed potential applicability of the sampler to water. Nonetheless, further optimization of the sampler's design is still needed. At the initial stages of the work on this Ph.D. thesis, several designs were proposed and tested. Although the microvial WMS is not yet tested in water, it is recommended to develop a design of the sampler that provides better sealing to prevent leakage of water into the sampler. The recommended design should also minimize permeation of water through the membrane. One suggested design is a silicon tube filled with an adsorbent material and sealed from both ends. Alternative

membrane materials with lower permeability towards water molecules may be tested. The model presented in this thesis can then be adapted to describe sampling from water.

REFERENCES

1. B. Vrana, I. J. Allan, R. Greenwood, G. A. Mills, E. Dominiak, K. Svensson, J. Knutsson and G. Morrison, Passive sampling techniques for monitoring pollutants in water, *TrAC Trends in Analytical Chemistry,* 2005, **24**, 845.

2. I. B. Roll and R. U. Halden, Critical review of factors governing data quality of integrative samplers employed in environmental water monitoring, *Water Res.,* 2016, **94**, 200.

3. T. Górecki and J. Namieśnik, Passive sampling, *TrAC Trends Anal. Chem.,* 2002, **21**, 276.

4. L. Tuduri, M. Millet, O. Briand and M. Montury, Passive air sampling of semi-volatile organic compounds, *TrAC Trends Anal. Chem.,* 2012, **31**, 38.

5. S. Seethapathy, T. Górecki and X. Li, Passive sampling in environmental analysis, *J. Chromatogr. A,* 2008, **1184**, 234.

6. M. Marć, M. Tobiszewski, B. Zabiegała, M. L. Guardia and J. Namieśnik, Current air quality analytics and monitoring: A review, *Anal. Chim. Acta,* 2015, **853**, 116.

7. S. V. Krupa and A. H. Legge, Passive sampling of ambient, gaseous air pollutants: An assessment from an ecological perspective, *Environ. Pollut.,* 2000, **107**, 31.

8. S. Król, B. Zabiegała and J. Namieśnik, Monitoring VOCs in atmospheric air II. sample collection and preparation, *TrAC Trends Anal. Chem.,* 2010, **29**, 1101.

9. C. S. Gordon and J. T. Lowe, Carbon-monoxide detectorUS Pat., 1,644,014A, 1927.

10. E D Palmes and A F Gunnison, Personal monitoring device for gaseous contaminants, *Am. Ind. Hyg. Assoc. J.,* 1973, **34**, 78.

11. K. D. Reiszner and P. W. West, Collection and determination of sulfur dioxide incorporating permeation and West-Gaeke procedure, *Environ. Sci. Technol.,* 1973, **7**, 526.

12. K. Booij, J. R. Hoedemaker and J. F. Bakker, Dissolved PCBs, PAHs, and HCB in pore waters and overlying waters of contaminated harbor sediments, *Environ. Sci. Technol.,* 2003, **37**, 4213.

13. L. A. Fernandez, W. Lao, K. A. Maruya, C. White and R. M. Burgess, Passive sampling to measure baseline dissolved persistent organic pollutant concentrations in the water column of the Palos Verdes shelf superfund site, *Environ. Sci. Technol.,* 2012, **46**, 11937.

14. G. Cornelissen, K. Wiberg, D. Broman, H. P. H. Arp, Y. Persson, K. Sundqvist and P. Jonsson, Freely dissolved concentrations and sediment-water activity ratios of PCDD/Fs and PCBs in the open Baltic Sea, *Environ. Sci. Technol.,* 2008, **42**, 8733.

15. L. Bragg, Z. Qin, M. Alaee and J. Pawliszyn, Field sampling with a polydimethylsiloxane thin-film, *J. Chromatogr. Sci.,* 2006, **44**, 317.

16. W. Zhao, G. Ouyang, M. Alaee and J. Pawliszyn, On-rod standardization technique for time-weighted average water sampling with a polydimethylsiloxane rod, *J. Chromatogr. A,* 2006, **1124**, 112.

17. J. O. Okeme, A. Saini, C. Yang, J. Zhu, F. Smedes, J. Klánová and M. L. Diamond, Calibration of polydimethylsiloxane and XAD-pocket passive air samplers (PAS) for measuring gas- and particle-phase SVOCs, *Atmos. Environ.,* 2016, **143**, 202.

18. J. N. Huckins, G. K. Manuweera, J. D. Petty, D. Mackay and J. A. Lebo, Lipid-containing semipermeable-membrane devices for monitoring organic contaminants in water, *Environ. Sci. Technol.,* 1993, **27**, 2489.

19. D. A. Alvarez, J. D. Petty, J. N. Huckins, T. L. Jones-Lepp, D. T. Getting, J. P. Goddard and S. E. Manahan, Development of a passive, in situ, integrative sampler for hydrophilic organic contaminants in aquatic environments, *Environmental Toxicology and Chemistry,* 2004, **23**, 1640.

20. A. Sunesson, in *Comprehensive Analytical Chemistry*, ed. R. Greenwood, G. Mills and B. Vrana, Elsevier, 2007, p. 57-83.

21. N. Yamamoto, T. Matsubasa, N. Kumagai, S. Mori and K. Suzuki, A diffusive badge sampler for volatile organic compounds in ambient air and determination using a thermal desorption-GC/MS system, *Anal. Chem.,* 2002, **74**, 484.

22. M. Vogel, Sampling of airborne pollutants: Strategies and developments, *Anal Bioanal Chem,* 2005, **381**, 84.

23. M. Shoeib and T. Harner, Characterization and comparison of three passive air samplers for persistent organic pollutants, *Environ. Sci. Technol.,* 2002, **36**, 4142.

24. R. Gioia, K. C. Jones and T. Harner, in *Comprehensive Analytical Chemistry*, ed. R. Greenwood, G. Mills and B. Vrana, Elsevier, 2007, p. 33-56.

25. L. Tuduri, T. Harner and H. Hung, Polyurethane foam (PUF) disks passive air samplers: Wind effect on sampling rates, *Environ. Pollut.,* 2006, **144**, 377.

26. K. Pozo, T. Harner, F. Wania, D. C. G. Muir, K. C. Jones and L. A. Barrie, Toward a global network for persistent organic pollutants in air: Results from the GAPS study, *Environ. Sci. Technol.,* 2006, **40**, 4867.

27. N. J. Herkert, S. N. Spak, A. Smith, J. K. Schuster, T. Harner, A. Martinez and K. C. Hornbuckle, Calibration and evaluation of PUF-PAS sampling rates across the global atmospheric passive sampling (GAPS) network, *Environ. Sci. Process. Impacts,* 2018, **20**, 210.

28. M. Shoeib, T. Harner, S. C. Lee, D. Lane and J. Zhu, Sorbent-impregnated polyurethane foam disk for passive air sampling of volatile fluorinated chemicals, *Anal. Chem.,* 2008, **80**, 675.

29. S. Genualdi, S. C. Lee, M. Shoeib, A. Gawor, L. Ahrens and T. Harner, Global pilot study of legacy and emerging persistent organic pollutants using sorbent-impregnated polyurethane foam disk passive air samplers, *Environ. Sci. Technol.,* 2010, **44**, 5534.

30. F. Wania, L. Shen, Y. D. Lei, C. Teixeira and D. C. Muir, Development and calibration of a resin-based passive sampling system for monitoring persistent organic pollutants in the atmosphere, *Environ. Sci. Technol.,* 2003, **37**, 1352.

31. S. Seethapathy and T. Górecki, Polydimethylsiloxane-based permeation passive air sampler. part I: Calibration constants and their relation to retention indices of the analytes, *J. Chromatogr. A,* 2011, **1218**, 143.

32. S. Seethapathy and T. Górecki, Polydimethylsiloxane-based permeation passive air sampler. part II: Effect of temperature and humidity on the calibration constants, *J. Chromatogr. A,* 2010, **1217**, 7907.

33. T. McAlary, X. Wang, A. Unger, H. Groenevelt and T. Górecki, Quantitative passive soil vapor sampling for VOCs- part 1: Theory, *Environ. Sci. Process. Impacts,* 2014, **16**, 482.

34. T. McAlary, H. Groenevelt, S. Seethapathy, P. Sacco, D. Crump, M. Tuday, B. Schumacher, H. Hayes, P. Johnson and T. Górecki, Quantitative passive soil vapor sampling for VOCs- part 2: Laboratory experiments, *Environ. Sci. Process. Impacts,* 2014, **16**, 491.

35. T. McAlary, H. Groenevelt, P. Nicholson, S. Seethapathy, P. Sacco, D. Crump, M. Tuday, H. Hayes, B. Schumacher, P. Johnson, T. Górecki and I. Rivera-Duarte, Quantitative passive soil vapor sampling for VOCs- part 3: Field experiments, *Environ. Sci. Process. Impacts,* 2014, **16**, 501.

36. T. McAlary, H. Groenevelt, S. Seethapathy, P. Sacco, D. Crump, M. Tuday, B. Schumacher, H. Hayes, P. Johnson, L. Parker and T. Górecki, Quantitative passive soil vapor sampling for VOCs - part 4: Flow-through cell, *Environ. Sci. Process. Impacts,* 2014, **16**, 1103.

37. O. Goli, T. Górecki, H. T. Mugammar, M. Marchesi and R. Aravena, Evaluation of the suitability of the Waterloo Membrane Sampler for sample preconcentration before compound-specific isotope analysis, *Environ. Sci. Technol.,* 2017, **7**, 141.

38. J. K. Kingston, R. Greenwood, G. A. Mills, G. M. Morrison and L. Björklund Persson, Development of a novel passive sampling system for the time-averaged measurement of a range of organic pollutants in aquatic environments, *J. Environ. Monit.,* 2000, **2**, 487.

39. R. Greenwood, G. A. Mills, B. Vrana, I. Allan, R. Aguilar-Martínez and G. Morrison, in *Comprehensive Analytical Chemistry*, ed. R. Greenwood, G. Mills and B. Vrana, Elsevier, 2007, p. 199-229.

40. D. A. Alvarez, J. N. Huckins, J. D. Petty, T. Jones-Lepp, F. Stuer-Lauridsen, D. T. Getting, J. P. Goddard and A. Gravell, in *Comprehensive Analytical Chemistry*, ed. R. Greenwood, G. Mills and B. Vrana, Elsevier Science & Technology, 2007, p. 171-197.

41. J. N. Huckins, M. W. Tubergen and G. K. Manuweera, Semipermeable membrane devices containing model lipid: A new approach to monitoring the bioavailability of lipophilic contaminants and estimating their bioconcentration potential, *Chemosphere,* 1990, **20**, 533.

42. J. C. Meadows, K. R. Echols, J. N. Huckins, F. A. Borsuk, R. F. Carline and D. E. Tillitt, Estimation of uptake rate constants for PCB congeners accumulated by semipermeable membrane devices and brown trout *(salmo trutta)*, *Environ. Sci. Technol.,* 1998, **32**, 1847.

43. J. N. Huckins, J. D. Petty, C. E. Orazio, J. A. Lebo, R. C. Clark, V. L. Gibson, W. R. Gala and K. R. Echols, Determination of uptake kinetics (sampling rates) by lipid-containing semipermeable membrane devices (SPMDs) for polycyclic aromatic hydrocarbons (PAHs) in water, *Environ. Sci. Technol.,* 1999, **33**, 3918.

44. P. Bergqvist and A. Zaliauskiene, in *Comprehensive Analytical Chemistry*, ed. R. Greenwood, G. Mills and B. Vrana, Elsevier, 2007, p. 311-328.

45. J. D. Petty, J. N. Huckins and J. L. Zajicek, Application of semipermeable membrane devices (SPMDs) as passive air samplers, *Chemosphere,* 1993, **27**, 1609.

46. W. A. Ockenden, H. F. Prest, G. O. Thomas, A. Sweetman and K. C. Jones, Passive air sampling of PCBs: Field calculation of atmospheric sampling rates by triolein-containing semipermeable membrane devices, *Environ. Sci. Technol.,* 1998, **32**, 1538.

47. H. F. Prest, L. A. Jacobson and J. N. Huckins, Passive sampling of water and coastal air via semipermeable membrane devices, *Chemosphere,* 1995, **30**, 1351.

48. W. A. Ockenden, A. J. Sweetman, H. F. Prest, E. Steinnes and K. C. Jones, Toward an understanding of the global atmospheric distribution of persistent organic pollutants: The use of semipermeable membrane devices as time-integrated passive samplers, *Environ. Sci. Technol.,* 1998, **32**, 2795.

49. S. Ly-Verdú, F. A. Esteve-Turrillas, A. Pastor and M. de la Guardia, Determination of volatile organic compounds in contaminated air using semipermeable membrane devices, *Talanta,* 2010, **80**, 2041.

50. G. Ouyang and J. Pawliszyn, Configurations and calibration methods for passive sampling techniques, *J. Chromatogr. A,* 2007, **1168**, 226.

51. M. Chai and J. Pawliszyn, Analysis of environmental air samples by solid-phase microextraction and gas chromatography/ion trap mass spectrometry, *Environ. Sci. Technol.,* 1995, **29**, 693.

52. L. Müller, T. Górecki and J. Pawliszyn, Optimization of the SPME device design for field applications, *Fresenius J Anal Chem,* 1999, **364**, 610.

53. P. A. Martos and J. Pawliszyn, Time-weighted average sampling with solid-phase microextraction device: Implications for enhanced personal exposure monitoring to airborne pollutants, *Anal. Chem.,* 1999, **71**, 1513.

54. Y. Chen and J. Pawliszyn, Time-weighted average passive sampling with a solid-phase microextraction device, *Anal. Chem.,* 2003, **75**, 2004.

55. J A Koziel, J Noah and J Pawliszyn, Field sampling and determination of formaldehyde in indoor air with solid-phase microextraction and on-fiber derivatization, *Environ. Sci. Technol.,* 2001, **35**, 1481.

56. S. Seethapathy and T. Górecki, Applications of polydimethylsiloxane in analytical chemistry: A review, *Anal. Chim. Acta,* 2012, **750**, 48.

57. M. van Pinxteren, A. Paschke and P. Popp, Silicone rod and silicone tube sorptive extraction, *J. Chromatogr. A,* 2010, **1217**, 2589.

58. J. O. Okeme, L. V. Nguyen, M. Lorenzo, S. Dhal, Y. Pico, V. H. Arrandale and M. L. Diamond, Polydimethylsiloxane (silicone rubber) brooch as a personal passive air sampler for semi-volatile organic compounds, *Chemosphere,* 2018, **208**, 1002.

59. S. G. O'Connell, L. D. Kincl and K. A. Anderson, Silicone wristbands as personal passive samplers, *Environ. Sci. Technol.,* 2014, **48**, 3327.

60. W. G. Whitman, The two-film theory of gas absorption, *Chem.Metall.Eng.,* 1923, **29**, 146.

61. G. D. Johnson, Hexane-filled dialysis bags for monitoring organic contaminants in water, *Environ. Sci. Technol.,* 1991, **25**, 1897.

62. T. Harner, N. J. Farrar, M. Shoeib, K. C. Jones and Gobas, Frank A P C, Characterization of polymer coated glass as a passive air sampler for persistent organic pollutants, *Environ. Sci. Technol.,* 2003, **37**, 2486.

63. J. F. Müller, D. W. Hawker, D. W. Connell, P. Kömp and M. S. McLachlan, Passive sampling of atmospheric SOCs using tristearin-coated fibreglass sheets, *Atmos. Environ.,* 2000, **34**, 3525.

64. S. Bayen, T. L. Ter Laak, J. Buffle and J. L. Hermens, Dynamic exposure of organisms and passive samplers to hydrophobic chemicals, *Environ. Sci. Technol.,* 2009, **43**, 2206.

65. J. N. Huckins, J. D. Petty, J. A. Lebo, F. V. Almeida, K. Booij, D. A. Alvarez, W. L. Cranor, R. C. Clark and B. B. Mogensen, Development of the permeability/performance reference compound approach for in situ calibration of semipermeable membrane devices, *Environ. Sci. Technol.,* 2002, **36**, 85.

66. M. E. Bartkow, K. Booij, K. E. Kennedy, J. F. Muller and D. W. Hawker, Passive air sampling theory for semivolatile organic compounds, *Chemosphere,* 2005, **60**, 170.

67. K. Booij, B. Vrana and J. N. Huckins, in *Comprehensive Analytical Chemistry*, ed. R. Greenwood, G. Mills and B. Vrana, Elsevier, 2007, p. 141-169.

68. B. S. Stephens, A. Kapernick, G. Eaglesham and J. Mueller, Aquatic passive sampling of herbicides on naked particle loaded membranes: Accelerated measurement and empirical estimation of kinetic parameters, *Environ. Sci. Technol.,* 2005, **39**, 8891.

69. B. Zabiegala, A. Kot-Wasik, M. Urbanowicz and J. Namieśnik, Passive sampling as a tool for obtaining reliable analytical information in environmental quality monitoring, *Anal. Bioanal. Chem.,* 2010, **396**, 273.

70. T. Harner, M. Shoeib, M. Diamond, G. Stern and B. Rosenberg, Using passive air samplers to assess urban− rural trends for persistent organic pollutants. 1. Polychlorinated biphenyls and organochlorine pesticides, *Environ. Sci. Technol.,* 2004, **38**, 4474.

71. K. Yates, I. Davies, L. Webster, P. Pollard, L. Lawton and C. Moffat, Passive sampling: Partition coefficients for a silicone rubber reference phase, *J. Environ. Monit.,* 2007, **9**, 1116.

72. P. A. Martos, A. Saraullo and J. Pawliszyn, Estimation of air/coating distribution coefficients for solid phase microextraction using retention indexes from linear temperature-programmed capillary gas chromatography. Application to the sampling and analysis of Total Petroleum Hydrocarbons in air, *Anal. Chem.,* 1997, **69**, 402.

73. J. O. Okeme, J. M. Parnis, J. Poole, M. L. Diamond and L. M. Jantunen, Polydimethylsiloxane-air partition ratios for semi-volatile organic compounds by GC-based measurement and COSMO-RS estimation: Rapid measurements and accurate modelling, *Chemosphere,* 2016, **156**, 204.

74. E. Reppas-Chrysovitsinos, A. Sobek and M. MacLeod, Screening-level models to estimate partition ratios of organic chemicals between polymeric materials, air and water, *Environ. Sci. Process. Impacts,* 2016, **18**, 667.

75. A. P. Francisco, T. Harner and A. Eng, Measurement of polyurethane foam – air partition coefficients for semivolatile organic compounds as a function of temperature: Application to passive air sampler monitoring, *Chemosphere,* 2017, **174**, 638.

76. J. O. Okeme, E. M. Webster, J. M. Parnis and M. L. Diamond, Approaches for estimating PUF-air partition coefficients for semi-volatile organic compounds: A critical comparison, *Chemosphere,* 2017, **168**, 199.

77. A. R. Restrepo, S. J. Hayward, J. M. Armitage and F. Wania, Evaluating the PAS-SIM model using a passive air sampler calibration study for pesticides, *Environ. Sci. Process. Impacts,* 2015, **17**, 1228.

78. N. Morin, C. Miège, M. Coquery and J. Randon, Chemical calibration, performance, validation and applications of the polar organic chemical integrative sampler (POCIS) in aquatic environments, *TrAC Trends Anal. Chem.,* 2012, **36**, 144.

79. K. Booij, H. M. Sleiderink and F. Smedes, Calibrating the uptake kinetics of semipermeable membrane devices using exposure standards, *Environ. Toxicol. Chem.,* 1998, **17**, 1236.

80. C. Moeckel, T. Harner, L. Nizzetto, B. Strandberg, A. Lindroth and K. C. Jones, Use of depuration compounds in passive air samplers: Results from active sampling-supported field deployment, potential uses, and recommendations, *Environ. Sci. Technol.,* 2009, **43**, 3227.

81. A. Belles, N. Tapie, P. Pardon and H. Budzinski, Development of the performance reference compound approach for the calibration of "Polar Organic Chemical Integrative Sampler" (POCIS), *Anal. Bioanal. Chem.,* 2014, **406**, 1131.

82. J. Ai, Solid phase microextraction for quantitative analysis in nonequilibrium situations, *Anal. Chem.,* 1997, **69**, 1230.

83. Y. Chen, J. O'Reilly, Y. Wang and J. Pawliszyn, Standards in the extraction phase, a new approach to calibration of microextraction processes, *Analyst,* 2004, **129**, 702.

84. Y. Chen and J. Pawliszyn, Kinetics and the on-site application of standards in a solid-phase microextration fiber, *Anal. Chem.,* 2004, **76**, 5807.

85. R. G. Adams, R. Lohmann, L. A. Fernandez, J. K. MacFarlane and P. M. Gschwend, Polyethylene devices: Passive samplers for measuring dissolved hydrophobic organic compounds in aquatic environments, *Environ. Sci. Technol.,* 2007, **41**, 1317.

86. L. A. Fernandez, C. F. Harvey and P. M. Gschwend, Using performance reference compounds in polyethylene passive samplers to deduce sediment porewater concentrations for numerous target chemicals, *Environ. Sci. Technol.,* 2009, **43**, 8888.

87. L. Melymuk, P. Bohlin, O. Sánka, K. Pozo and J. Klánová, Current challenges in air sampling of semivolatile organic contaminants: Sampling artifacts and their influence on data comparability, *Environ. Sci. Technol.,* 2014, **48**, 14077.

88. G. Ouyang, J. Cai, X. Zhang, H. Li and J. Pawliszyn, Standard-free kinetic calibration for rapid on-site analysis by solid-phase microextraction, *J. Sep. Sci.,* 2008, **31**, 1167.

89. W. K. Fowler, Fundamentals of passive vapor sampling, *Am. Lab.,* 1982, **14**.

90. J. Pawliszyn, in *Comprehensive Analytical Chemistry*, ed. D. Barceló, Elsevier, Amsterdam, 2002, p. 253.

91. R. W. Gale, Three-compartment model for contaminant accumulation by semipermeable membrane devices, *Environ. Sci. Technol.,* 1998, **32**, 2292.

92. F. Stuer-Lauridsen, Review of passive accumulation devices for monitoring organic micropollutants in the aquatic environment, *Environ. Pollut.,* 2005, **136**, 503.

93. N. Van Den Hoed and O. Van Asselen, A computer-model for calculating effective uptake rates of tube-type diffusive air samplers, *Ann. Occup. Hyg.,* 1991, **35**, 273.

94. C. Walgraeve, K. Demeestere, J. Dewulf, K. Van Huffel and H. Van Langenhove, Uptake rate behavior of tube-type passive samplers for volatile organic compounds under controlled atmospheric conditions, *Atmos. Environ.,* 2011, **45**, 5872.

95. X. Zhang, M. Tsurukawa, T. Nakano, Y. D. Lei and F. Wania, Sampling medium side resistance to uptake of semivolatile organic compounds in passive air samplers, *Environ. Sci. Technol.,* 2011, **45**, 10509.

96. J C Posner and G Moore, A thermodynamic treatment of passive monitors, *Am. Ind. Hyg. Assoc. J.,* 1985, **46**, 277.

97. E. Nordstrand and J. Kristensson, A computer program for simulating the performance of thick bed diffusive samplers, *Am. Ind. Hyg. Assoc. J.,* 1994, **55**, 935.

98. B. Tolnai, A. Gelencsér and J. Hlavay, Theoretical approach to non-constant uptake rates for tube-type diffusive samplers, *Talanta,* 2001, **54**, 703.

99. J. M. Armitage, S. J. Hayward and F. Wania, Modeling the uptake of neutral organic chemicals on XAD passive air samplers under variable temperatures, external wind speeds and ambient air concentrations (PAS-SIM), *Environ. Sci. Technol.,* 2013, **47**, 13546.

100. F J Hearl and M P Manning, Transient response of diffusion dosimeters, *Am. Ind. Hyg. Assoc. J.,* 1980, **41**, 778.

101. J. M. Thompson, C. Hsieh and R. G. Luthy, Modeling uptake of hydrophobic organic contaminants into polyethylene passive samplers, *Environ. Sci. Technol.,* 2015, **49**, 2270.

102. J. Cao, Z. Du, J. Mo, X. Li, Q. Xu and Y. Zhang, Inverse problem optimization method to design passive samplers for volatile organic compounds: Principle and application, *Environ.Sci.Technol.,* 2016, **50**, 13477.

103. X. Zhang and F. Wania, Modeling the uptake of semivolatile organic compounds by passive air samplers: Importance of mass transfer processes within the porous sampling media, *Environ. Sci. Technol.,* 2012, **46**, 9563.

104. R. W. Coutant, R. G. Lewis and J. Mulik, Passive sampling devices with reversible adsorption, *Anal. Chem.,* 1985, **57**, 219.

105. K. Patel, D. SIRL, W. J. THOMAS and U. Ullah, Dynamic characteristics of a toxic vapour monitor, *Chemical engineering research & design,* 1987, **65**, 326.

106. S. N. Semenov, J. A. Koziel and J. Pawliszyn, Kinetics of solid-phase extraction and solid-phase microextraction in thin adsorbent layer with saturation sorption isotherm, *Journal of Chromatography a,* 2000, **873**, 39.

107. N. W. Loney, *Applied Mathematical Methods for Chemical Engineers*, CRC Press, 2006.

108. J. Thomas, T. M. Holsen and S. Dhaniyala, Computational fluid dynamic modeling of two passive samplers, *Environ. Pollut.,* 2006, **144**, 384.

109. A. A. May, P. Ashman, J. Huang, S. Dhaniyala and T. M. Holsen, Evaluation of the polyurethane foam (PUF) disk passive air sampler: Computational modeling and experimental measurements, *Atmos. Environ.,* 2011, **45**, 4354.

110. N. T. Petrich, S. N. Spak, G. R. Carmichael, D. Hu, A. Martinez and K. C. Hornbuckle, Simulating and explaining passive air sampling rates for semivolatile compounds on polyurethane foam passive samplers, *Environ. Sci. Technol.,* 2013, **47**, 8591.

111. N. J. Herkert, A. Martinez and K. C. Hornbuckle, A model using local weather data to determine the effective sampling volume for PCB congeners collected on passive air samplers, *Environ. Sci. Technol.,* 2016, **50**, 6690.

112. X. Zhu, C. Zhou, B. Henkelmann, Z. Wang, X. Ma, G. Pfister, K. Schramm, J. Chen, Y. Ni, W. Wang and J. Mu, Monitoring of PAHs profiles in the urban air of Dalian, China with active high-volume sampler and semipermeable membrane devices, *Polycycl. Aromat. Compd.,* 2013, **33**, 265.

113. X. Zhu, G. Ding, W. Levy, G. Jakobi, I. Offenthaler, W. Moche, P. Weiss and K. Schramm, QSPR study about sampling rates of semipermeable membrane devices for monitoring of organochlorine pesticides in Alps air, *Chin. Sci. Bull.,* 2011, **56**, 1884.

114. T. H. Miller, J. A. Baz-Lomba, C. Harman, M. J. Reid, S. F. Owen, N. R. Bury, K. V. Thomas and L. P. Barron, The first attempt at non-linear in silico prediction of sampling rates for polar organic chemical integrative samplers (POCIS), *Environ. Sci. Technol.,* 2016, **50**, 7973.

115. A. Belles, C. Franke, C. Alary, Y. Aminot and J. W. Readman, Understanding and predicting the diffusivity of organic compounds in polydimethylsiloxane material for passive sampler applications using a simple quantitative structure–property relationship model, *Environ. Toxicol. Chem.,* 2018, **37**, 1291.

116. W. Lin, R. Jiang, Y. Shen, Y. Xiong, S. Hu, J. Xu and G. Ouyang, Effect of dissolved organic matter on pre-equilibrium passive sampling: A predictive QSAR modeling study, *Sci. Total Environ.,* 2018, **635**, 53.

117. J. N. Huckins, J. D. Petty and K. Booij, *Monitors of Organic Chemicals in the Environment : Semipermeable Membrane Devices*, Springer, New York, NY, 2006.

118. B. Vrana, G. A. Mills, M. Kotterman, P. Leonards, K. Booij and R. Greenwood, Modelling and field application of the Chemcatcher passive sampler calibration data for the monitoring of hydrophobic organic pollutants in water, *Environ. Pollut.,* 2007, **145**, 895.

119. K. Booij, H. E. Hofmans, C. V. Fischer and E. M. Van Weerlee, Temperature-dependent uptake rates of nonpolar organic compounds by semipermeable membrane devices and low-density polyethylene membranes, *Environ. Sci. Technol.,* 2003, **37**, 361.

120. W. Lao, K. A. Maruya and D. Tsukada, An exponential model based new approach for correcting aqueous concentrations of hydrophobic organic chemicals measured by polyethylene passive samplers, *Sci. Total Environ.,* 2019, **646**, 11.

121. C. Jia and X. Fu, Diffusive uptake rates of volatile organic compounds on standard ATD tubes for environmental and workplace applications, *Environments,* 2017, **4**, 87.

122. F. Salim, *Novel applications of the Waterloo Membrane Sampler (WMS) in volatile organic compound sampling from different environmental matrices*, MSc Thesis, University of Waterloo, 2013.

123. C. E. Chen, H. Zhang, G. G. Ying, K. C. Jones, Evidence and recommendations to support the use of a novel passive water sampler to quantify antibiotics in wastewaters, *Environ. Sci. Technol.*, 2013, 47, 13587.

124. J. Galceran, J. Puy, Interpretation of diffusion gradients in thin films (DGT) measurements: a systematic approach, *Environ. Chem.*, 2015, 12, 112.

125. T. McAlary, H. Groenevelt, S. Disher, J. Arnold, S. Seethapathy, P. Sacco, D. Crump, B. Schumacher, H. Hayes, P. Johnson, T. Górecki, Passive sampling for volatile organic compounds in indoor air-controlled laboratory comparison of four sampler types, *Environ. Sci. Process. Impacts*, 2015, 17, 896.

126. S. Batterman, T. Metts, P. Kalliokoski, Diffusive uptake in passive and active adsorbent sampling using thermal desorption tubes, *J. Environ. Monit*., 2002, 4, 870.

127. C. Jia, S. Batterman, C. Godwin, Continuous, intermittent and passive sampling of airborne VOCs, *J. Environ. Monit*., 2007, 9, 1220.

128. R. G. Rice, D. D. Do, *Applied mathematics and modeling for chemical engineers*, John Wiley & Sons, Hoboken, New Jersey, 2012.

129. O. T. Hanna, O. C. Sandall, *Computational methods in chemical engineering,* Prentice-Hall, Inc., Englewood Cliffs, N.J., 1995.

130. A. Kloskowski, W. Chrzanowski, M. Pilarczyk, J. Namieśnik, Partition coefficients of selected environmentally important volatile organic compounds determined by gas–liquid chromatography with polydimethylsiloxane stationary phase, *J. Chem. Thermodyn*. 2005, 37, 21.

131. ASTM International, Standard Guide for Risk-Based Corrective Action Applied at Petroleum Release Sites, E 1939-95 Reapproved 2015, West Conshohocken, PA, USA, 2015, www.astm.org/Standards/E1739.htm, (accessed July 2016).

132. Y. Sun, J. Chen, Sorption/desorption properties of ethanol, toluene, and xylene in poly (dimethylsiloxane) membranes, *J. Appl. Polym. Sci*., 1994, 51, 1797.

133. E. Boscaini, M. L. Alexander, P. Prazeller, T. D. Mark, Investigation of fundamental physical properties of a polydimethylsiloxane (PDMS) membrane using a proton transfer reaction mass spectrometer (PTRMS), *Int. J. Mass Spectrom*., 2004, 239, 179.

134. K. S. Oh, Y. M. Koo, K. W. Jung, Characterization of a sheet membrane interface for sample introduction into a time-of-flight mass spectrometer, *Int. J. Mass Spectrom*., 2006, 253, 65.

135. K. Chao, V. Wang, H. Yang, C. Wang, Estimation of effective diffusion coefficients for benzene and toluene in PDMS for direct solid phase microextraction, *Polym. Test*, 2011, 30, 501.

136. S. J. Lue, S. F. Wang, L. D. Wang, W. W. Chen, K. Du, S. Y. Wu, Diffusion of multicomponent vapors in a poly (dimethyl siloxane) membrane, *Desalination*, 2008, 233, 277.

137. G. Scott, D. Kilgour, The density of random close packing of spheres, *J. Phys. D: Appl. Phys.,*1969, 2, 863.

138. M. Mota, J. Teixeira, A. Yelshin, Image analysis of packed beds of spherical particles of different sizes, *Sep. Purif. Technol.,* 1999, 15, 59.

139. R. Bird, W. Stewart, E. Lightfoot, *Transport Phenomena*, Second Edition, John-Wiley & Sons, Inc., New York, c2007.

140. F. Salim, M. Ioannidis and T. Górecki, Experimentally validated mathematical model of analyte uptake by permeation passive samplers, *Environ. Sci.: Processes Impacts*, 2017, **19**, 1363.

141. K. Booij and F. Smedes, An improved method for estimating in situ sampling rates of nonpolar passive samplers, *Environ. Sci. Technol.*, 2010, **44**, 6789.

142. X. Zhang, C. Wong, Y. D. Lei and F. Wania, Influence of sampler configuration on the uptake kinetics of a passive air sampler, *Environ. Sci. Technol.*, 2012, **46**, 397.

143. X. Zhang, M. Hoang, Y. D. Lei and F. Wania, Exploring the role of the sampler housing in limiting uptake of semivolatile organic compounds in passive air samplers, *Environ. Sci.: Processes Impact,* 2015, **17**, 2006.

144. J. Klánová, P. Èupr, J. Kohoutek and T. Harner, Assessing the influence of meteorological parameters on the performance of polyurethane foam-based passive air samplers, *Environ. Sci. Technol.,* 2007, **42**, 550.

145. S. Seethapathy, *Uptake rate modeling and field applications of a new permeation passive sampler*, PhD Thesis, University of Waterloo, 2009.

146. A. L. Hines and R. N. Maddox, *Mass Transfer: Fundamentals and Applications*, Prentice-Hall Englewood Cliffs, NJ, 1985.

147. G. A. Turner, The flow-structure in packed beds: A theoretical investigation utilizing frequency response, *Chem. Eng. Sci.,* 1958, **7**, 156.

148. R. Tartarelli, S. Cioni and M. Capovani, On the second order reactions in heterogeneous catalysis, *J. Catal.,* 1970, **18**, 212.

149. E. E. Petersen, Adsorption in bidisperse-pore systems, *AIChE J.,* 1991, **37**, 671.

150. V. M. Silva and A. E. Rodrigues, Adsorption and diffusion in bidisperse pore structures, *Ind Eng Chem Res,* 1999, **38**, 4023.

151. E. Ruckenstein, A. S. Vaidyanathan and G. R. Youngquist, Sorption by solids with bidisperse pore structures, *Chem. Eng. Sci.,* 1971, **26**, 1305.

152. L. M. Sun and F. Meunier, Non-isothermal adsorption in a bidisperse adsorbent pellet, *Chem. Eng. Sci.,* 1987, **42**, 2899.

153. Y. H. Ma and T. Y. Lee, Transient diffusion in solids with a bipore distribution, *AIChE J.,* 1976, **22**, 147.

154. D. M. Ruthven, N. S. Raghavan and M. M. Hassan, Adsorption and diffusion of nitrogen and oxygen in a carbon molecular sieve, *Chem. Eng. Sci.,* 1986, **41**, 1325.

155. Y. H. Ma and S. Y. Ho, Diffusion in synthetic faujasite powder and pellets, *AIChE J.,* 1974, **20**, 279.

156. N. Hashimoto and J. M. Smith, Macropore diffusion in molecular sieve pellets by chromatography, *Ind. Eng. Chem. Fundam,* 1973, **12**, 353.

157. H. W. Haynes and P. N. Sarma, A model for the application of gas chromatography to measurements of diffusion in bidisperse structured catalysts, *AIChE J.,* 1973, **19**, 1043.

158. D. M. Smith, Sorption and diffusion in bidisperse porous cylinders, *Ind. Eng. Chem. Fundam,* 1984, **23**, 265.

159. S. K. Bhatia, Transport in bidisperse adsorbents: Significance of the macroscopic adsorbate flux, *Chem. Eng. Sci.,* 1997, **52**, 1377.

160. E. Sahin, T. Dogu and K. Mürtezaoğlu, Thermal effects on effectiveness of catalysts having bidisperse pore size distributions, *Chem. Eng. J.,* 2003, **93**, 143.

161. J. Solsvik and H. Jakobsen, A survey of multicomponent mass diffusion flux closures for porous pellets: Mass and molar forms, *Transp Porous Med,* 2012, **93**, 99.

162. J. M. Smith, *Chemical Engineering Kinetics*, McGraw Hill, Inc., New York, 1981.

163. T. Dogfu, Diffusion and reaction in catalyst pellets with bidisperse pore size distribution, *Ind Eng Chem Res,* 1998, **37**, 2158.

164. M. Sahimi, G. R. Gavalas and T. T. Tsotsis, Statistical and continuum models of fluid-solid reactions in porous media, *Chem. Eng. Sci.,* 1990, **45**, 1443.

165. Z. Horák and P. Schneider, Comparison of some models of porous media for gas diffusion, *The Chem. Eng. J.,* 1971, **2**, 26.

166. M. V. Chandak, Y. S. Lin, W. Ji and R. J. Higgins, Sorption and diffusion of volatile organic compounds in polydimethylsiloxane membranes, *J Appl Polym Sci,* 1998, **67**, 165.

167. M. K. Shetty, M. A. Limmer, K. Waltermire, G. C. Morrison and J. G. Burken, In planta passive sampling devices for assessing subsurface chlorinated solvents, *Chemosphere,* 2014, **104**, 149.

168. A. L. Polic, L. M. Lona, T. A. Duever and A. Penlidis, A protocol for the estimation of parameters in process models: Case studies with polymerization scenarios, *Macromol. Theory Simul.,* 2004, **13**, 115.

169. D. M. Hamby, A review of techniques for parameter sensitivity analysis of environmental models, *Environ. Monit. Assess.,* 1994, **32**, 135.

170. R. P. Schwarzenbach, P. M. Gschwend and D. M. Imboden, *Environmental Organic Chemistry*, John Wiley & Sons, 2016.

171. F. Salim, T. Górecki and M. Ioannidis, New applications of the mathematical model of a permeation passive sampler: Prediction of the effective uptake rate and storage stability, *Environ. Sci. Process. Impacts,* 2019, **21**, 113.

172. A. R. Khan, R. Ataullah and A. Al-Haddad, Equilibrium adsorption studies of some aromatic pollutants from dilute aqueous solutions on activated carbon at different temperatures, *J. Colloid Interface Sci.,* 1997, **194**, 154.

173. PubChem, https://pubchem.ncbi.nlm.nih.gov/compound/8058, (accessed Jan 20, 2019).

174. H. Hori and I. Tanaka, Effect of face velocity on performance of diffusive samplers, *Ann Occup Hyg,* 1996, **40**, 467.

175. J. R. Welty, C. E. Wicks, R. E. Wilson and G. L. Rorrer, *Fundamentals of Momentum, Heat, and Mass Transfer*, John Wiley & Sons, Inc, New York,US, 2001.

176. The Engineering Mindset, https://theengineeringmindset.com/properties-of-air-at-atmospheric-pressure/, (accessed Feb 22, 2019).

177. Ouyang, G., in *Handbook of Solid Phase Microextraction*, ed. J. Pawliszyn, Chemical Industry Press of China, China, 2009, p. 215.

178. K. Czech and P. M. Slomkiewicz, Determination of adsorption isotherms of chlorinated hydrocarbons on halloysite adsorbent by inverse gas chromatography, *J. Chromatogr. A*, 2013, 1288, 96.

179. Q. W. Chow, *Predicting adsorption isotherms in natural water using polyparameter linear free energy relationships*, PhD thesis, University of Illinois at Urbana-Champaign, 2010.

180. G. A. Lugg, *Anal. Chem*., Diffusion coefficients of some organic and other vapors in air, 1968, 40, 1072.

181. N. Vahdat, P. M. Swearengen, J. S. Johnson, S. Priante, K. Mathews and A. Neidhardt, Adsorption capacity and thermal-desorption efficiency of selected adsorbents, *Am. Ind. Hyg. Assoc. J.,* 1995, **56**, 32.

182. K. Y. Foo and B. H. Hameed, Insights into the modeling of adsorption isotherm systems, *Chem. Eng. J.*, 2010, **156**, 2.

APPENDIX

Appendix A

Chapter 3 Electronic Supplementary Material

Experimentally Validated Mathematical Model of Analyte Uptake by Permeation Passive Samplers

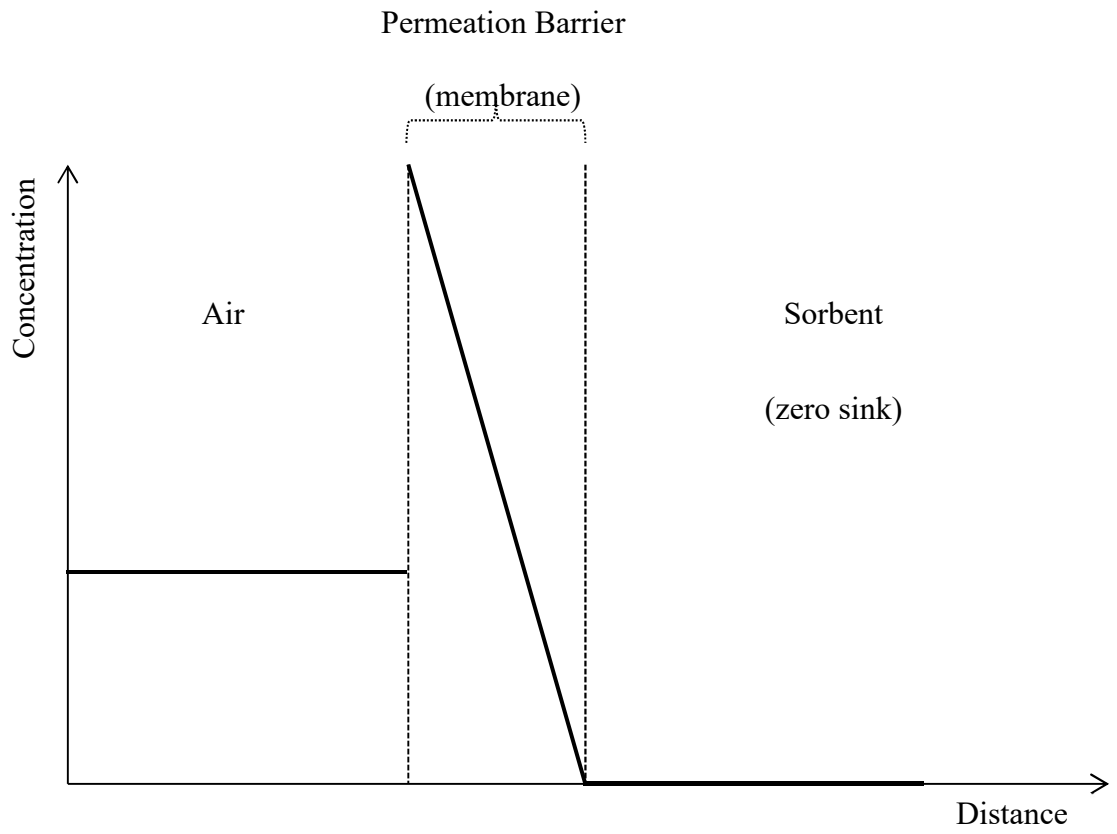

Figure 3-S 1: An ideal concentration profile in a permeation-based passive sampler.

Evaluation of Mass Transfer Efficiency Using the WMS

(Moved to Chapter 2)

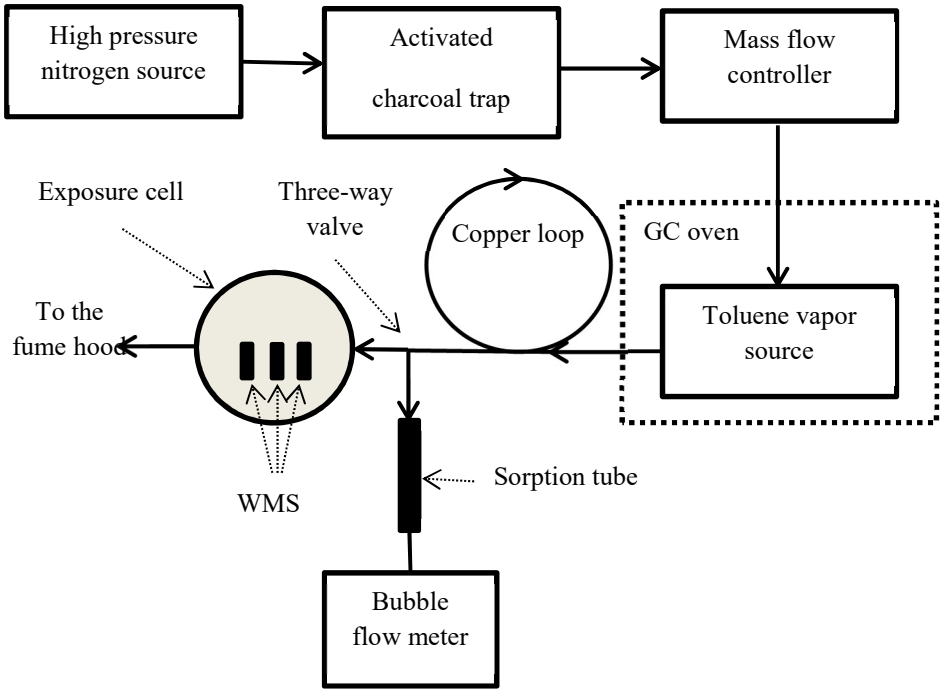

Figure 3-S 2: Experimental setup used for the experimental evaluation.

Table 3-S 1: Summary of Parameters used in the model.

Symbol	Description	Value	
		Regular 2-mL WMS	**Microvial WMS**
L_m	Membrane thickness (m)	1×10^{-4}	
L_b	Sorbent bed thickness (m)	1.4×10^{-2}	2.6×10^{-2}
A_m	Membrane sampling area (m^2)	34.476×10^{-6}	17.523×10^{-6}
D_m	Diffusion coefficient in the membrane (m^2/sec)	1.07×10^{-10}	
K	Partition coefficient between air and the membrane material (dimensionless)	843	
D_a	Diffusion coefficient in air (m^2/sec)	8.5×10^{-6}	
D_{eff}	Effective diffusion coefficient in the sorbent bed (m^2/sec)	2.11×10^{-6}	
ε	Sorbent bed porosity (dimensionless)	0.4	
τ	Tortuosity (dimensionless)	1.61	
α	Specific surface area (m^2/m^3)	$11226 \times 10^{+4}$	
k_c	Mass transfer coefficient (m/sec)	0.0198	
d	Sorbent particle diameter (m)	2.135×10^{-4}	
a	Parameter for the isotherm $C^* = a \times q^b$	7.66647×10^{-6}	
b	Parameter for the isotherm $C^* = a \times q^b$	1.566	

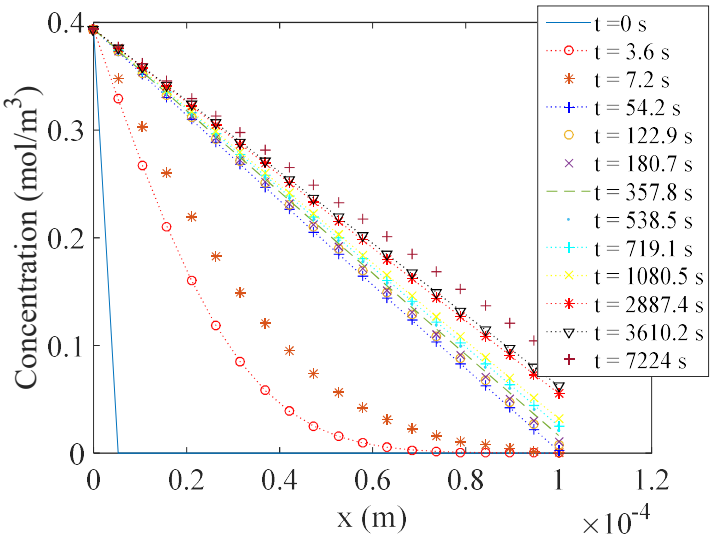

Figure 3-S 3: Concentration profiles, produced by the model, in the membrane at selected time points within total exposure time of 2 hour at a toluene concentration of 0.01 ppmv in the air.

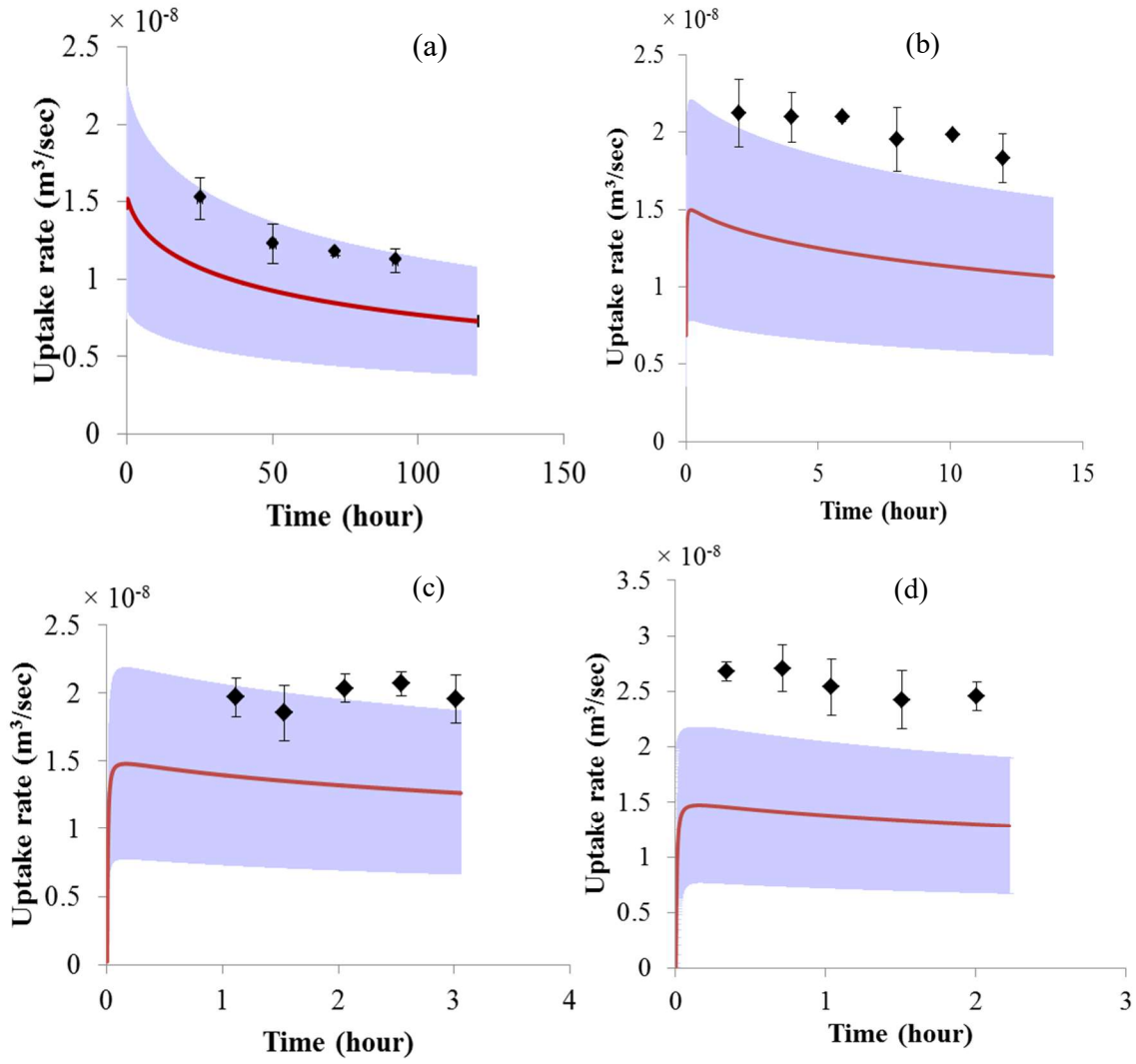

Figure 3-S 4: Experimental data of the microvial WMS uptake rate at the concentrations: 1.6 mg/m3 (a), 9.2 mg/m3 (b) , 26.8 mg/m3 (c), and 43.0 mg/m3 (d) compared to the model results. (⋅ Experimental data, - Model results)

Appendix B

Chapter 4 Electronic Supplementary Material

New Applications of the Mathematical Model of a Permeation Passive Sampler: Prediction of the Effective Uptake Rate and Storage Stability

Experimental

Waterloo Membrane Sampler (WMS)

The WMS (Figure 4-S1a) was prepared by filling a glass chromatographic vial with a certain amount of the adsorbent material. The PDMS membrane, cut into the size of the vial opening, was then fixed in place at the vial's mouth using a polytetrafluoroethylene (PTFE) washer and an aluminium crimp cap. Two sizes of chromatographic vials, with different sampling areas, were used in this evaluation: a regular 2-ml vial (C223682C, Chromatographic Specialties Inc., Brockville, ON, Canada) filled with approximately 250 mg of the adsorbent, and a 300-µL microvial (round bottom microvial, C2211051, Chromatographic Specialties Inc.) filled with approximately 93 mg of the adsorbent. The sorbent used was Carbopack B^{TM}, which is a non-porous adsorbent made of graphitized carbon black obtained from Supelco, Sigma-Aldrich (Oakville, Ontario, Canada). The process of fabrication of the PDMS membrane is described elsewhere.[122] The thickness of the membrane was controlled through weight. The membranes were always cut using the same die for a given sampler geometry, hence their surface areas were constant and reproducible. The target weight of the membrane for the 2-mL WMS was 8.0 ± 0.5 mg to obtain a 100-µm thick membrane, and 16.0 ± 0.5 mg to obtain a 200-

μm thick membrane. The PTFE washers for this size of the sampler were of the dimensions 0.040" × 0.440" × 0.216" (thickness × OD × ID) (virgin PTFE, purchased from Penn Fibre Plastics, Bensalem, PA, US). The target weight of the PDMS membrane for the microvial WMS was 3.7 ± 0.2 mg to obtain a 100-μm thick membrane, and the PTFE washers used for this version were of the dimensions 0.040" × 0.281" × 0.188" (thickness × OD × ID), purchased from the same vendor.

Experimental procedure

Uptake rate prediction method

In the setup used for the experimental evaluation, purified nitrogen gas flowed at a rate of 896 mL/min controlled by a mass flow controller. The nitrogen flow was passed through an analyte vapor generator, which consisted of a flow-through vessel containing a custom-made permeation vapor source. To control the vapor concentration, the vessel was placed inside a GC oven used as a tool for controlling the temperature and, therefore, controlling the vapor concentration. The standard gas was then passed through a thermostated chamber consisting of a 10-liter cylindrical glass jar with a circulation fan inserted through the center of the top cover. Holes were drilled in the top cover to insert the samplers. They were kept closed before and during the exposure. The temperature was controlled by wrapping the glass jar with Tygon tubing connected to a water circulation thermostat and insulating it with an insulating jacket. The concentration was measured actively either by direct injection of a 1 ml sample of the standard gas, drawn using a gas-tight syringe, into the GC in splitless mode, or by passing 10 ml of the standard gas through a sorption tube packed with Carbopack B using a gas-tight syringe. In the latter method, the sorption tube was analyzed in the same manner as the sorbent of the passive sampler (WMS). In all the experiments, the sorbent from the WMS was transferred after the

exposure into a pre-cleaned thermal desorption tube and was sandwiched between two layers of thermally cleaned glass wool. The packed tube was transferred afterwards to a thermal desorption unit connected to a GC-MS system for analysis.

Additional experiments were conducted by exposing the WMS to an atmosphere containing trichloroethylene (TCE) vapour using the experimental setup described above. TCE vapour was obtained by passing nitrogen gas through a vessel containing a TCE permeation source (the chemical purchased from Sigma-Aldrich, Canada Co. Oakville, Ontario). Active samples of the TCE vapour were collected by drawing the vapour through a sorption tube packed with 200 mg of Anasorb 747 (SKC Inc., USA) using AirCheck® sampling pump (XR5000, from SKC Inc.). Anasorb 747 was transferred for analysis to a 4 mL glass vial with an open-top screw cap and a PTFE/Silicone septum (purchased from Fisher Scientific, Ottawa, Ontario). The vial was placed in an ice bath while adding 1 ml of carbon disulfide (purchased from Sigma-Aldrich) for desorption. Keeping the vial sealed, it was subsequently left for 40 min at ambient temperature with intermittent shaking. An aliquot of the extract was then transferred to a 2 mL crimp top chromatographic vial with a 100 μL glass insert (purchased from Chromatographic Specialties Inc.). Analysis was performed using an Agilent 6890 GC- 5973 MS system in all experiments in this paper. Direct solvent injection was used to inject the carbon disulfide extract aliquots using a 7683 Agilent autosampler with a tray of 100-sample capacity and a Hewlett Packard 3683 injector. The inlet was set to 290 °C with a 1:10 split ratio. The oven temperature program started at 90 °C, which was held for two minutes before it was increased to a final temperature of 280 °C at a rate of 30 °C/min (no hold). Selected Ion Monitoring (SIM) was used targeting the ions with m/z of 95, 130, and 60.

Evaluation of the post-sampling period

Calibration

A 1-µl aliquot of each standard was spiked into a bed of approximately 250 mg of Carbopack B packed in between two layers of glass wool in a sorption tube. The tubes with the standards were analysed using the same method used to analyse the sorbent from the WMS. Standards of 29 VOCs in methanol, in one set of the experiments, were spiked into a flow of helium through the sorbent bed at a flow rate of 78 ml/min for one minute.

Chemicals

All standards were prepared in methanol, HPLC grade (≥99.9%), purchased from Sigma-Aldrich (Oakville, Ontario, Canada). All chemicals used in this evaluation were of a ≥ 99 % purity and were also purchased from Sigma-Aldrich. These chemicals included benzene, anhydrous toluene, trichloroethylene, tetrachloroethylene, 11-dichloroethane, *cis*-1,2-dichloroethylene, chloroform, 1,1,1-trichloroethane, 1,2-dichloropropane, 1,1,2-trichloroethane, dibromochloromethane, 1,2-dibromomethane, chlorobenzene, ethylbenzene, *p*-xylene (anhydrous), *o*-xylene, 1,1,2,2-tetrachloroethane, 1,2,3-trichloropropane, propylbenzene, *tert*-butylbenzene, *sec*-butylbenzene, 1,2-dichlorobenzene, 1,3-dichlorbenzene, 1,4-dichlorobenzene, 1,2,3-trichlorobenzene, isopropylbenzene (cumene), 1,2,4-trimethylbenzene (pseudocumene), 1,2,4-trichlorobenzene, and naphthalene. Two pressurized cylinders containing mixtures of VOCs were used. The first cylinder was obtained from Air Liquide (Plumsteadville, PA, USA), while the second cylinder contained a mixture of 29 VOCs custom-made in pressurized nitrogen.

Experimental setup

The experimental setup used to expose the samplers to an atmosphere with a single analyte was similar to that presented in Ref. 140 and is illustrated in Figure 4-S3. In this setup,

nitrogen gas was purified by passing it through an activated charcoal bed before it reached a mass flow controller (MKS, Andover, MA, 0-100 mL/min, model # 1179A12CR1BV--S). This controller was connected to an MKS 4-channel readout system (Andover, MA, Type 247) to set and monitor the flow rate. The nitrogen gas was then directed through an analyte vapor generator at a rate of 100 mL/min. The vapor generator consisted of a flow-through vessel containing a vapor source, which was either a custom-made PTFE permeation tube filled with the pure analyte, or a diffusion source prepared by filling a chromatographic vial with a neat analyte and sealing it with an open-top cap equipped with a Teflon/Silicon septum penetrated by a deactivated fused silica capillary acting as a diffusion barrier. The length and the diameter of the capillary varied depending on the desired concentration and the volatility of the analyte. The flow-through vessel was placed inside a GC oven as a method of controlling the vapor concentration via controlling the temperature. The standard gas was then passed through an approximately 4-m long copper tube of a 1/8" OD before it entered the exposure cell. A 1 L, 3-neck, round-bottom flask was used as the exposure cell, with the standard gas entering the cell through one side neck and flowing to the other side neck. The standard gas was then directed to the fume hood using a flexible tube. The WMS were inserted through the top neck into the exposure cell and hanged using thin fishing lines. The top cap was kept closed at all times and only opened shortly during sampler insertion and removal. To evaluate the concentration of the standard gas, active samples were collected by switching a three-way valve, connected before the exposure cell, to allow the standard gas to flow through a sorption tube packed with Carbopack B for a controlled time. The other end of the sorption tubes was connected to a bubble flow meter to measure the flow.

For the experiments in which the samplers were exposed to an atmosphere of a mixture of VOCs, a similar setup was used except that a cylinder containing a pressurized standard gas mixture of VOCs in nitrogen was used as a vapour source. The flow of this standard gas was controlled using a mass flow controller (MKS, range 50 SCCM) connected to the 4-channel readout system. The standard gas mixture flowed through a stainless steel three-way connector to be diluted with nitrogen gas flowing at a controlled flow rate, as explained earlier. The diluted standard gas entered the exposure cell in the manner explained above. In one set of experiments, the standard gas mixture, containing seven VOCs, flowed at a rate of 9.8 ml/min. This standard gas was diluted with nitrogen gas flowing at a rate of 82 ml/min. In the other set of experiments, the standard gas mixture, containing a mixture of 29 VOCs, flowed at a rate of 20.8 ml/min to be diluted with the nitrogen gas flowing at a rate of 81 ml/min.

Instruments

Initial experiments were conducted by exposing the microvial-based WMS to a vapor of a single VOC in nitrogen. In these experiments, a manual Dynatherm thermal desorption (TD) unit (model 9300 ACEM, CDS Analytical, Oxford, PA, USA) was used for sorbent analysis. This TD unit was equipped with a single glass sorbent tube, 8 mm OD × 6 mm ID × 114 mm length, with a glass frit. In later experiments, in which the regular 2 ml vial WMS were exposed to mixtures of VOCs, an automated Perkin Elmer thermal desorption unit (ATD 400) was used for desorption. The TD unit was equipped with stainless steel desorption tubes, 6.35 mm OD and 90 mm long. The TD unit in both cases was connected to an Agilent 6890 GC-5973 MS system. The Dynatherm TD unit was connected to the GC-MS system through a heated transfer line inserted into the GC injector, whereas the heated transfer line of the Perkin Elmer TD unit was connected to the column of the GC using a press-tight universal connector (Restek, Bellefonte,

PA, USA). An Rxi®-624Sil MS capillary column was used in the GC (60 m × 0.32 mm ID × 1.8 μm film thickness) purchased from Restek (Bellefonte, PA). Helium was used as the carrier gas. Data acquisition and processing were achieved using ChemStation software (Enhanced ChemStation G1701CA, Version C.00.00 21-Dec-1999, Agilent Technologies). This software was also employed for calibration and quantification using multi-point calibration curve.

TD-GC-MS methods

In all the experiments using the Dynatherm TD unit, the sorption tube was thermally desorbed at 330 °C for 7 min with the focusing trap held at ambient temperature. Tube cooling for 1 min followed desorption before heating the focusing trap to 300 °C for 5 min. Tubes with the standards were desorbed after a solvent drying step lasting 1 min. The GC inlet was set to 250 °C with a split ratio of 1:10 and a 1 mL/min carrier gas flow through the column. The parameters in the Perkin Elmer TD unit were set as follows: the tube was first purged with helium for one minute. The desorption temperature was 330 °C, which was held for five minutes, and the trapping temperature was -16 °C, which was held for 5 min. No split was applied and the desorption flow was set to 22.7 ml/min. The carrier gas pressure was set to 120 kPA. Table 4-S2 details the GC-MS methods in the three sets of experiments, in which toluene, p-xylene, and 1,2,4-trichlorobenzene were sampled and analyzed separately.

In the following sets of experiments, the WMS was used to sample a mixture of VOCs starting with a mixture of seven VOCs followed by a more complex mixture containing 29 VOCs. Pekin Elmer TD unit, used in these experiments, was operated using the method explained above. For the first mixture (seven VOCs), the composition, GC oven temperature

program and MS SIM method are described in Table 4-S3, while data for the latter mixture (29 VOCs) are presented in Table 4-S4.

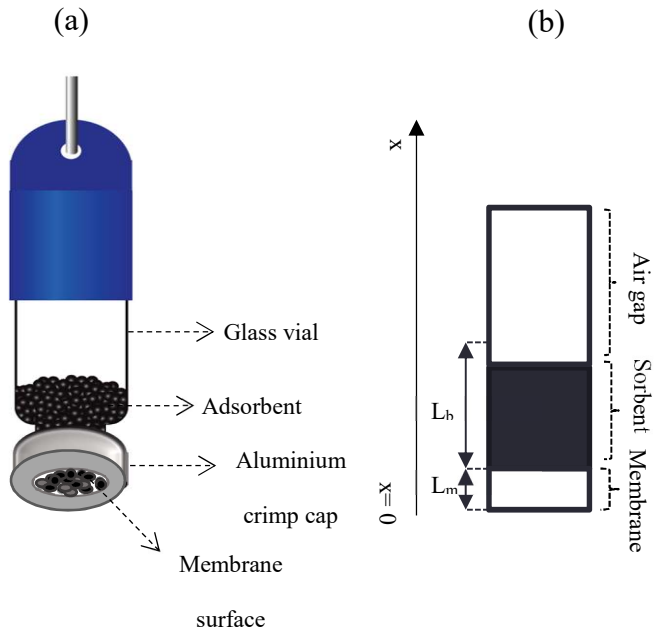

Figure 4-S 1: The Waterloo Membrane Sampler (WMS) (a), and the conceptual representation of the WMS used in the model (b) (based on ref.[140]).

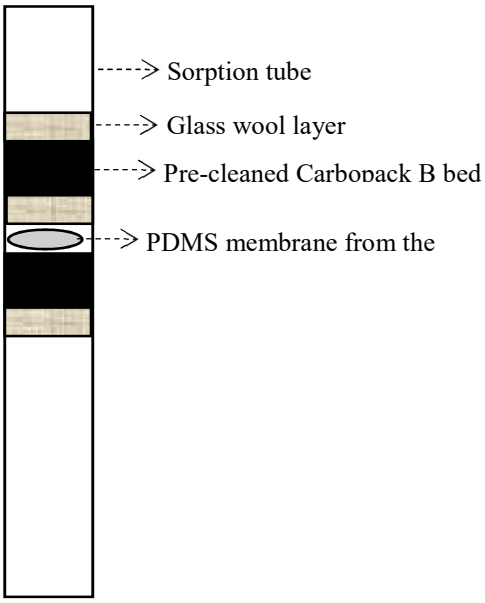

Figure 4-S 2: Schematic diagram of the WMS membrane prepared for analysis in a thermal desorption tube

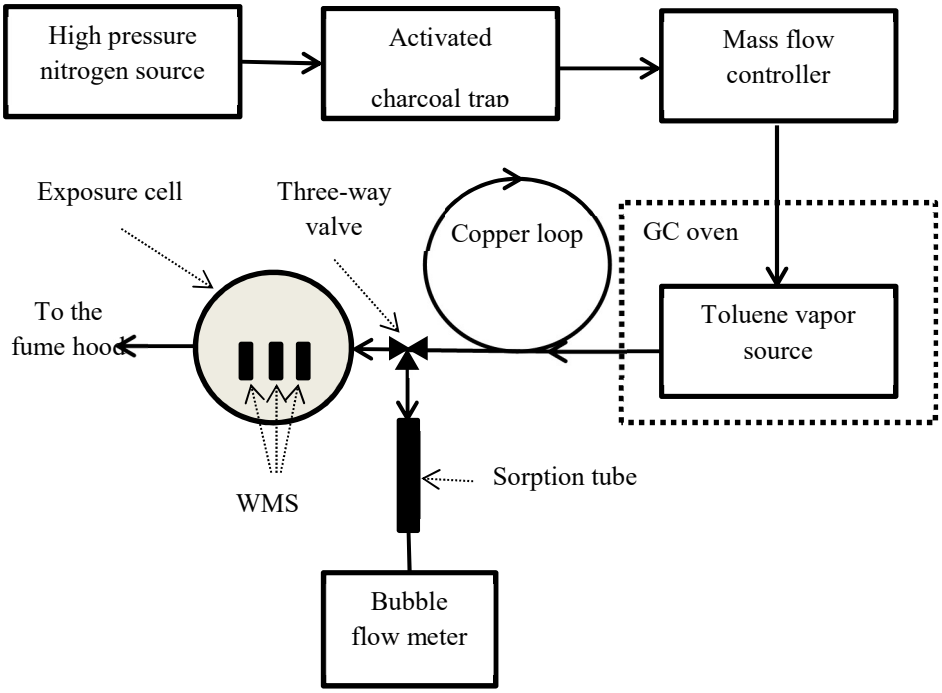

Figure 4-S 3: Apparatus used in experimental evaluation[140]

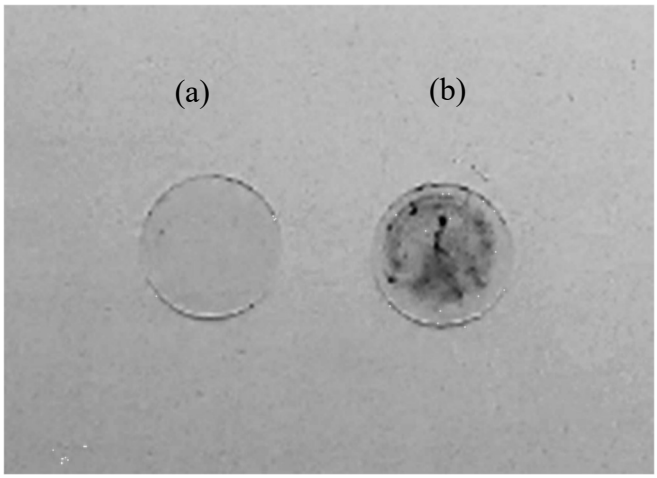

Figure 4-S 4: An image of the PDMS membrane before sampling (a) and after sampling (b) when Carbopack B was used as the adsorbent

Table 4-S 1: Values of parameters used in the uptake rate prediction method

Symbol	Description	Value	
	Compound	Toluene	TCE
L_m	Membrane thickness (m)	1×10^{-4}	1×10^{-4} & 2×10^{-4}
L_b	Sorbent bed thickness (m)	1.4×10^{-2}	
A_m	Membrane sampling area (m^2)	34.5×10^{-6}	
D_m	Diffusion coefficient in the membrane (m^2/sec)	1.07×10^{-10} (ref.[132-136])*	4.81×10^{-10} (ref.[115,166])*
K	Partition coefficient between air and the membrane material (dimensionless)	843 (ref.[72,130])*	621 (ref.[167])
D_a	Diffusion coefficient in air (m^2/sec)	8.5×10^{-6}(ref.[131])	8.75×10^{-6}(ref.[180])
D_{eff}	Effective diffusion coefficient in the sorbent bed (m^2/sec)	2.11×10^{-6}	2.17×10^{-6}
ε	Sorbent bed porosity (dimensionless)	0.40	
τ	Tortuosity (dimensionless)	1.61	
α	Specific surface area (m^2/m^3)	$11226 \times 10^{+4}$	
k_c	Mass transfer coefficient (m/sec)	0.0198	0.0204
d	Sorbent particle diameter (m)	2.135×10^{-4}	
a	Parameter for the isotherm $C^* = a \times q^b$	7.67×10^{-6}(ref.[93])	9.78×10^{-6}
b	Parameter for the isotherm $C^* = a \times q^b$	1.566 (ref.[93])	1.60

**An average value from the references listed*

Table 4-S 2: GC-MS method used in the initial experiments with a single analyte sampled from a nitrogen atmosphere

Experiment number	Analyte	GC oven Program		MS mode	Ions/Scan range (m/z)
1	Toluene	Initial temperature	90 °C	SIM	65, 91
		Hold	5 min		
		Next ramp	50 °C/min		
		Next temperature	300 °C		
		Hold	1 min		
2	*p*-xylene	Initial temperature	90 °C	Scan	50-550
		Hold	2 min		
		Next ramp	30 °C/min		
		Next temperature	300 °C		
		Hold	7 min		
3	1,2,4-trichlorobenzene	Initial temperature	90 °C	Scan	50-550
		Hold	2 min		
		Next ramp	30 °C/min		
		Next temperature	300 °C		
		Hold	7 min		

Table 4-S 3: GC-MS method used in the analysis of the samples containing a mixture of seven analytes

GC oven Program		Compound	Ions (m/z)
Initial temperature	35 °C	Trichloroethylene	95, 130, 60
Hold	2 min	Tetrachloroethylene	166, 131, 194
Next ramp	30 °C/min	1,2,4-Trimethylbenzene	105, 120
Next temperature	300 °C	1,4-dichlorobenzene	146, 111, 75
Hold	3.5 min	1,2-Dichlorobenzene	146, 111, 75
		1,2,4-Trichlorobenzene	180, 145, 109

Table 4-S 4: GC-MS method used in the analysis of the samples containing a mixture of 29 analytes

GC oven Program		Compound	Ions (m/z)
Initial temperature	35 °C	1,1-Dichloroethane	63, 83
Hold	5 min	cis-1,2-Dichloroethylene	61, 96
Next ramp	4 °C/min	Chloroform	83
Next temperature	280 °C	1,1,1-Trichloroethane	97, 61
Hold	10 min	Benzene	78, 77
		1,2-Dichloroethane	62, 64
		Trichloroethylene	95, 130
		1,2-Dichloropropane	63, 76
		Toluene	91, 92
		1,1,2-Trichloroethane	97, 83
		Tetrachloroethylene	166, 131
		Dibromochloromethane	129
		1,2-Dibromoethane	107
		Chlorobenzene	112, 77
		Ethylbenzene	91, 106
		p-Xylene	91, 106
		o-Xylene	91, 106
		Isopropylbenzene	105, 120
		1,1,2,2-Tetrachloroethane	83
		1,2,3-Trichloropropane	75, 110
		Propylbenzene	91
		tert-Butylbenzene	119, 91, 134
		1,2,4-Trimethylbenzene	105, 120
		sec-Butylbenzene	105, 134
		1,2-Dichlorobenzene	146, 111, 75
		1,4-Dichlorobenzene	146, 111, 75
		1,3-Dichlorobenzene	146, 111, 75
		1,2,4-Trichlorobenzene	182, 180, 145
		1,2,3-Trichlorobenzene	182, 180, 145

Table 4-S 5: Amounts of analytes detected in the adsorbent and percent amounts detected in the membrane after different storage times (uncertainties represent 95 % confidence intervals).

Analyte	Exposure concentration (mg/m^3)	Exposure time (hour)	Storage time (hour)	0.08		2		4		24		48		72	
				Amount (µg)	*Fraction (%)*	Amount (µg)	*Fraction (%)*	Amount (µg)	*Fraction (%)*	Amount (µg)	*Fraction (%)*	Amount (µg)	*Fraction (%)*	Amount (µg)	*Fraction (%)*
Toluene	9.07	2	**Amount detected in the sorbent (µg)/ *Fraction detected in the membrane (%)***	1.3 ± 0.3	*0.35 ± 0.20*	1.3 ± 0.3	*0.04 ± 0.15*	1.3 ± 0.2	*0.07 ± 0.0.19*	1.3 ± 0.2	*0.01 ± 0.18*	1.37 ± 0.06	*0.11 ± 0.28*	1.4 ± 0.3	*0.03 ± 0.06*
	77.6	1		6.8 ± 0.4	*0.26 ± 0.18*	7.0 ± 0.7	*0.22 ± 0.26*	7 ± 5	*0.02 ± 0.00*	6.5 ± 0.3	*0.27 ± 0.13*	7.3 ± 0.9	*0.09 ± 0.14*	7.0 ± 1.0	*0.10 ± 0.19*
1,2,4-Trichlorobenzene	20.7	1		4 ± 1	*1.8 ± 3.3*	4.35 ± 0.40	*0.29 ± 0.80*	4 ± 1	*0.01 ± 0.04*	4.2 ± 0.3	*0.0 ± 0.0*	4.9 ± 0.4	*0.0 ± 0.0*	4.2 ± 0.5	*0.21 ± 0.89*
	7.6	1		1.2 ± 0.6	*2.5 ± 6.2*	1.6 ± 0.6	*0.84 ± 0.33*	1.5 ± 0.6	*0.24 ± 0.53*	2 ± 1	*0.6 ± 1.5*	1.6 ± 0.9	*0.04 ± 0.12*	2 ± 1	*1.0 ± 3.7*
***p*-Xylene**	33.5	1		4 ± 1	*0.30 ± 0.16*	4.2 ± 0.5	*0.18 ± 0.06*	4.3 ± 0.8	*0.18 ± 0.04*	4.0 ± 0.3	*0.17 ± 0.06*	4.0 ± 0.4	*0.16 ± 0.03*	4 ± 1	*0.15 ± 0.02*
			Storage time (hours)	**0.08**		**2**		**4**		**27**		**49**		**94**	
				Amount (µg)	***Fraction (%)***	**Amount (µg)**	***Fraction (%)***	**Amount (µg)**	***Fraction (%)***	**Amount (µg)**	***Fraction (%)***	**Amount (µg)**	***Fraction (%)***	**Amount (µg)**	***Fraction (%)***
	88.6	1	**Amount detected in the sorbent (µg)/ *Fraction detected in the membrane (%)***	12 ± 8	*0.45 ± 0.27*	15 ± 9	*0.09 ± 0.40*	13 ± 2	*0.03 ± 0.05*	15 ± 1	*0.025 ± 0.009*	14 ± 6	*0.04 ± 0.09*	11 ± 5	*0.05 ± 0.07*

Appendix C

Chapter 5 Electronic Supplementary Material

Modelling Permeation Passive Sampling: Intra-Particle Resistance to Mass Transfer and Comprehensive Sensitivity Analysis

Numerical Method to Solve PDEs of Mass Transfer Inside the Particle

The radial distance along the particle radius is discretized into $z + 1$ points with the thickness of the resultant finite sections equal to $\Delta r = R/z$, as shown in Figure 5-S1; therefore, the distance r_k at each point k from the center of the sphere, where $k = 1, 2, \ldots, z+1$, can be expressed as follows:

$$r_k = [(z+1) - k]\Delta r \tag{5.S1}$$

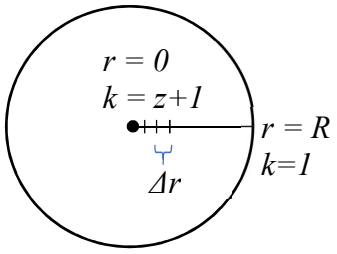

Figure 5-S 1: Cross section of the discretized particle

At each point k one can write:

$$\left.\frac{1}{r_k^2}\frac{\partial}{\partial r}\left(r^2\frac{\partial C_p}{\partial r}\right)\right|_{r=r_k} = \left.\frac{\partial^2 C_p}{\partial r^2}\right|_{r=r_k} + \left.\frac{2}{r_k}\frac{\partial C_p}{\partial r}\right|_{r=r_k} \approx \frac{C_{p(k+1)} - 2C_{p(k)} + C_{p(k-1)}}{(\Delta r)^2} + \left(\frac{2}{[(z+1)-k]\Delta r}\right)\left(\frac{C_{p(k+1)} - C_{p(k-1)}}{2\Delta r}\right) \tag{5.S2}$$

The above means that Equation (5.5) for points $1 < k < z+1$ becomes:

$$\varepsilon_\mu \frac{dC_{p(k)}}{dt} = D_p \left[\frac{C_{p(k+1)} - 2C_{p(k)} + C_{p(k-1)}}{(\Delta r)^2} + \left(\frac{2}{[(z+1)-k]\Delta r}\right)\left(\frac{C_{p(k+1)} - C_{p(k-1)}}{2\Delta r}\right)\right] - (1 - \varepsilon_\mu)\left(\frac{dq_{p(k)}}{dt}\right) \quad (5.S3)$$

Based on eqn. (5.7), one can write:

$$\frac{dq_{p(k)}}{dt} = \text{k}(1/n) C_p^{(\frac{1}{n}-1)} \frac{dC_{p(k)}}{dt} \quad (5.S4)$$

Therefore, eqn. (5.S3) can be re-written as follows:

$$\varepsilon_\mu \frac{dC_{p(k)}}{dt} + (1-\varepsilon_\mu)\text{k}(1/n) C_p^{(\frac{1}{n}-1)} \frac{dC_{p(k)}}{dt} = D_p \left[\frac{C_{p(k+1)} - 2C_{p(k)} + C_{p(k-1)}}{(\Delta r)^2} + \left(\frac{2}{[(z+1)-k]\Delta r}\right)\left(\frac{C_{p(k+1)} - C_{p(k-1)}}{2\Delta r}\right)\right] \quad (5.S5)$$

The first term in the left-hand side of eqn. (5.S5) is negligible compared to the second term (*k* is a large number); thus, this equation can be restated as follows:

$$\frac{dC_{p(k)}}{dt} = \left(\frac{D_p C_p^{(1-\frac{1}{n})}}{(1-\varepsilon_\mu)\text{k}(\frac{1}{n})}\right)\left[\frac{C_{p(k+1)} - 2C_{p(k)} + C_{p(k-1)}}{(\Delta r)^2} + \left(\frac{2}{[(z+1)-k]\Delta r}\right)\left(\frac{C_{p(k+1)} - C_{p(k-1)}}{2\Delta r}\right)\right] \quad (5.S6)$$

At the center of the particle, using Taylor approximation about r = 0, one can write:

$$\frac{1}{r}\frac{\partial C_p}{\partial r} \approx \frac{\partial^2 C_p}{\partial r^2} \Longrightarrow \frac{\partial^2 C_p}{\partial r^2} + \frac{2}{r}\frac{\partial C_p}{\partial r} = 3\frac{\partial^2 C_p}{\partial r^2} \quad (5.S7)$$

Also, from the boundary condition in eqn. (5.9),

$$\left.\frac{\partial C_p}{\partial r}\right|_{r=0\ (k=z+1)} \approx \frac{C_{p(z+2)} - C_{p(z)}}{2\Delta r} = 0 \Longrightarrow C_{p(z+2)} \approx C_{p(z)} \quad (5.S8)$$

From eqn. (5.5) and eqn. (5.S7), it can be concluded that at the center of the particle where *r = 0* and *k = z+1*, the differential equation becomes:

$$\varepsilon_\mu \frac{dC_{p(z+1)}}{dt} = 3D_p \left[\frac{C_{p(z+2)} - 2C_{p(z+1)} + C_{p(z)}}{(\Delta r)^2}\right] - (1-\varepsilon_\mu)\left(\frac{dq_{p(z+1)}}{dt}\right) \quad (5.S9)$$

From Equations (5.S9), (5.S8), and (5.S4) the equation at the center of the particle becomes:

$$\varepsilon_\mu \frac{dC_{p(z+1)}}{dt} + (1-\varepsilon_\mu)\text{k}\frac{1}{n} C_p^{\frac{1}{n}-1} \frac{dC_{p(z+1)}}{dt} = 6D_p \frac{C_{p(z)} - C_{p(z+1)}}{\Delta r^2} \quad (5.S10)$$

The first term on the left-hand side of this equation is negligible compared to the second term; therefore, this equation can be re-written as follows:

$$\frac{dC_{p(z+1)}}{dt} = \left(\frac{6D_p C_p^{1-\frac{1}{n}}}{(1-\varepsilon_\mu)\text{k}\frac{1}{n}}\right)\left(\frac{C_{p(z)} - C_{p(z+1)}}{\Delta r^2}\right) \quad (5.S11)$$

The solutions for the resultant ordinary differential equations (ODEs) were found using a MATLAB code (R2015a, MathWorks, USA), using ODE15s solver.

Calculating the Average Concentration Inside the Particle

After calculating the concentration at each node of the discretized particle, the number of free moles, M_{free}, in the finite volume (ΔV) defined by two nodes (k and $k+1$) is calculated as follows:

$$M_{free,\Delta V} = \frac{C_{p(k)} + C_{p(k+1)}}{2} \cdot \Delta V = \frac{C_{p(k)} + C_{p(k+1)}}{2} \cdot 4\pi \left(\frac{r_k + r_{k+1}}{2}\right)^2 \cdot \Delta r \quad (5.S12)$$

The total number of moles in the particle, $M_{free,V}$, was then calculated by summing the number of moles in the discrete volumes of the particle. Average concentration inside the particle, $C_{p(ave)}$, was calculated by dividing the total number of moles, $M_{free,V}$, by the average particle volume.

The free concentration gradient inside the particle at its surface, $\frac{dC_p}{dr}\Big|_{r=R}$ was approximated as follows:

$$\left.\frac{dC_p}{dr}\right|_{r=R} \approx \frac{C_{p(2)} - C_{p(1)}}{\Delta r} \quad (5.S13)$$

Table 5-S 1: Details of vapor concentrations and their measurement.

Experiment	Target analyte	Temperature of the vapor source (°C)	Adsorbent used in the sorption tube	Pumping tool	Volume sampled	Average measured concentration (mg/m^3)
1	TCE	40	Carbopack B	10-ml-gas-tight syringe	10 ml	8.96
			Anasorb 747	Sampling pump	1500 - 3040 ml	
2	Toluene	60	Anasorb 747	10-ml-gas-tight syringe	50 ml	6.81
3	TCE	60	Anasorb 747	10-ml-gas-tight syringe	50 ml	27.56

Table 5-S 2: Values of parameters used in the evaluation of the model results with Anasorb 747.[§]

Symbol	Description	Values corresponds to the sampled analyte	
		Toluene	**TCE**
L_m	Membrane thickness (m)	1.0×10^{-4}	2.0×10^{-4}
L_b	Sorbent bed thickness (m)	1.4×10^{-2}	
A_m	Membrane sampling area (m^2)	34.5×10^{-6}	
D_m	Diffusion coefficient in the membrane (m^2/sec)	1.35×10^{-10}(ref.[132-136,115])*	1.3×10^{-10} (ref. [166])
K	Partition coefficient between air and the membrane material (dimensionless)	843 (ref.[72,130])*	900 (based on ref.[167])
D_a	Diffusion coefficient in air (m^2/sec)	8.50×10^{-6} (ref.[131])	8.75×10^{-6}(ref.[180])
ε_μ	Particle porosity	0.45	
D_b	Effective diffusion coefficient in the sorbent bed (m^2/sec)	1.44×10^{-6}	1.46×10^{-6}
ε or ε_M	Sorbent bed porosity (dimensionless)	0.40	
τ	Tortuosity (dimensionless)	$\varepsilon^{(-1/2)}$	
a	Specific surface area (m^2/m^3)	629899050	
k_c	Mass transfer coefficient (m/sec)	0.001	0.001
d	Sorbent particle diameter (m)	6.375×10^{-4}	
a	Parameter for the isotherm $C^* = a \times q^b$	2.52×10^{-12}	4.77×10^{-16}
b	Parameter for the isotherm $C^* = a \times q^b$	2.44	3.59
r_p	Average pore radius (m)	5.84×10^{-10}	
D_k	Knudsen diffusivity (m^2/sec)	1.01×10^{-7}	8.47×10^{-8}
$D_{p,eff}$	Effective pore diffusion coefficient (m^2/sec)	3.05×10^{-8}	2.56×10^{-8}
k	Parameter for the isotherm $q_p = \mathrm{k} C_p^{\frac{1}{n}}$	57204	18335
$1/n$	Parameter for the isotherm $q_p = \mathrm{k} C_p^{\frac{1}{n}}$	0.41	0.28

**An average value from the references listed*

[§] Measurement and calculations of parameter values are presented in the sections "Measurement of the isotherm parameters" and "Characterization of Anasorb 747" of this supplementary information.

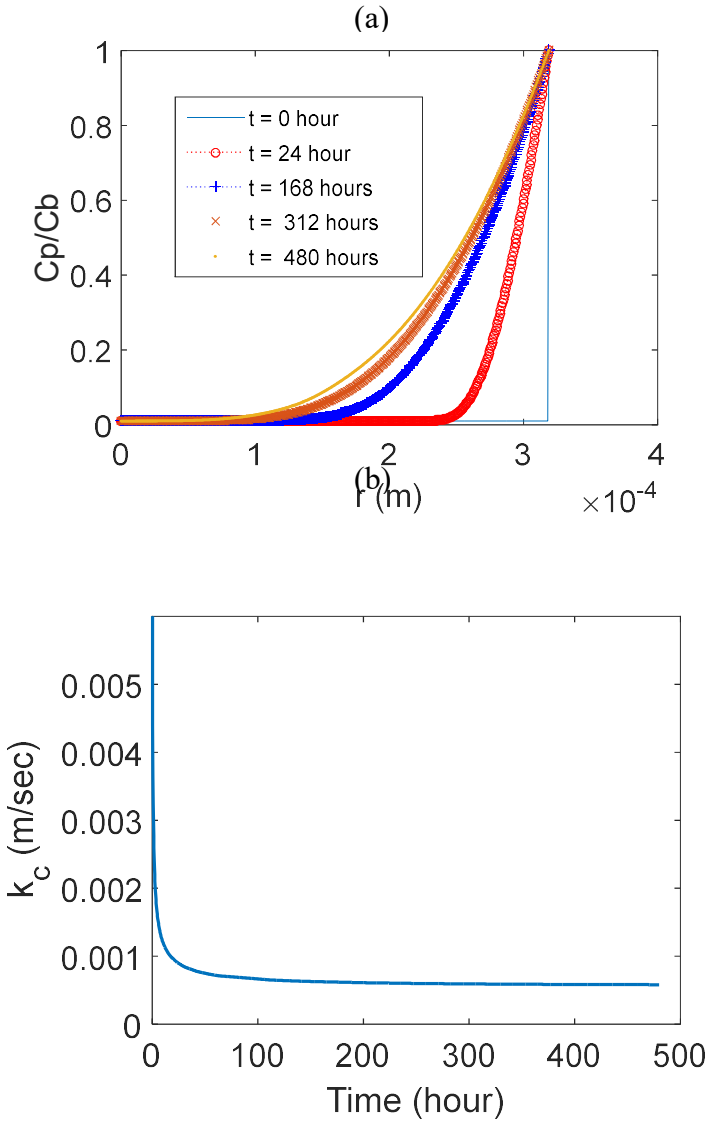

Figure 5-S 2: Propagation of the normalized free concentration profile of toluene inside the particle (a) and the calculated mass transfer coefficient, kc, (b) with time.

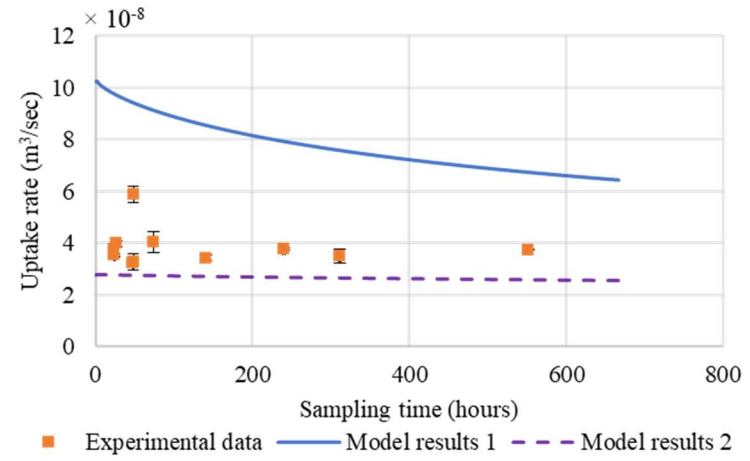

Figure 5-S 3: Comparison between the experimental uptake rate values for TCE with those obtained using the model when K = 621, while $D_m = 4.8 \times 10^{-10}$ m^2/s (Model results 1) and $D_m = 1.3 \times 10^{-10}$ m^2/s (Model results 2).

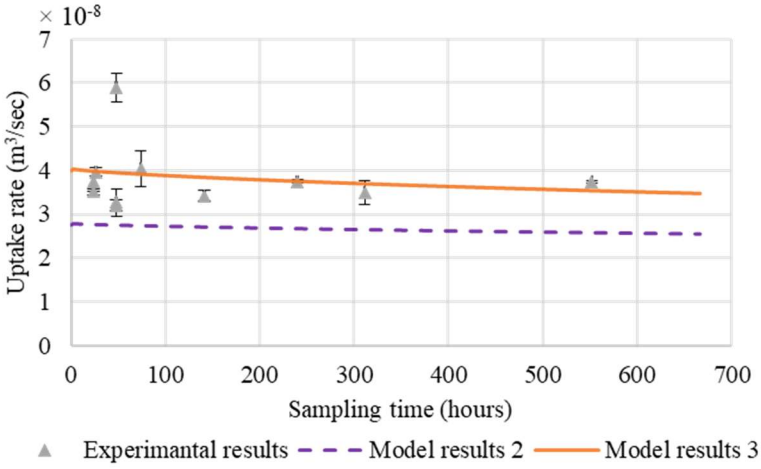

Figure 5-S 4: Comparison between the experimental uptake rate values for TCE with those obtained using the model when $D_m = 1.3 \times 10^{-10}$ m^2/s, while K = 621 (Model results 2) and K = 900 (Model results 3).

Initial Sensitivity Analysis (one-parameter-at-a-time)

This evaluation was conducted over a sampling time of up to 500 hours at a concentration of 0.00001 mol/m^3. The base set of parameters corresponded to "sampling" toluene vapor using WMS (with the PDMS membrane) containing Carbopack B adsorbent. These values and the ranges used for selected parameters are presented in Table 5-S3.

Table 5-S 3: Parameters involved in the initial sensitivity analysis and the ranges/values used for these parameters.

Symbol	Description	Sensitivity analysis	
		Base value	Range/Values
L_m	Membrane thickness (m)	1×10^{-4}	
L_b	Sorbent bed thickness (m)	1.4×10^{-2}	
A_m	Membrane sampling area (m^2)	34.5×10^{-6}	
D_m	Diffusion coefficient in the membrane (m^2/sec)	1.07×10^{-10}(ref.[132-136])*	1×10^{-11} - 2×10^{-10}
K	Partition coefficient between air and the membrane material (dimensionless)	843 (ref.[72,130])*	150 - 10000
D_a	Diffusion coefficient in air (m^2/sec)	8.5×10^{-6}(ref.[131])	$1.0 \times 10^{-6} – 1.0 \times 10^{-5}$
ε_μ	Particle porosity		
D_b	Effective diffusion coefficient in the sorbent bed (m^2/sec)	2.11×10^{-6}	2.48×10^{-7} - 1×10^{-6}
$\varepsilon/\varepsilon_M$	Sorbent bed porosity (dimensionless)	0.40	0.30, 0.40, 0.50
τ	Tortuosity (dimensionless)	1.61	
α	Specific surface area (m^2/m^3)	$11226 \times 10^{+4}$	
k_c	Mass transfer coefficient (m/sec)	0.0198	
d	Sorbent particle diameter (m)	2.135×10^{-4}	
a	Parameter for the isotherm $C^* = a \times q^b$	7.67×10^{-6}(ref.[181])	7.67×10^{-7}, 7.67×10^{-6}, 7.67×10^{-7}
b	Parameter for the isotherm $C^* = a \times q^b$	1.566 (ref.[181])	1.466, 1.566, 1.866, 2.400

An average value from the references listed

The results of this analysis are presented in Figure 5-S5 and Figure 5-S6. In Figure 5-S5A, changes in the uptake rate for a range of values of diffusivity in the membrane, D_m, are evaluated with sampling time. The results show high sensitivity to this parameter, which is mainly influential on the initial value of the uptake rate and the rate of its decrease with sampling time. Higher value of the diffusion coefficient in the membrane produces higher initial value of the uptake rate and higher rate of decrease over time. This can be explained by the fact that higher diffusivity in the membrane increases the flux of analyte molecules into the sorbent bed. If mass transfer parameters inside the sorbent bed do not change, increasing the flux into the bed increases the concentration in the gas phase at the interface between the membrane and the sorbent bed. Although this also increases the sorption rate, which initially increases the uptake rate, the free concentration at the bed interface with the membrane will increase more rapidly, leading to more rapid reduction in the uptake rate.

Figure 5-S5B presents the sensitivity of the uptake rate to the partition coefficient value between air and PDMS, K. The uptake rate is only sensitive to this parameter at the beginning of

the sampling time. Shortly after, the uptake rate stabilizes, with no significant change as the partition coefficient value changes. This partition coefficient appears in the boundary conditions of the model; therefore, its effect is mainly on the concentration in the membrane at its interface with the outside air and on the free concentration in the sorbent bed at its interface with the membrane. The increase in the latter concentration as a result of the increase in K is expected to be the cause of the initial effect on the uptake rate. The influence of the diffusion coefficient in the sorbent bed, D_b, on the uptake rate over time is demonstrated in Figure 5-S5C. It can be observed in this figure that increasing the diffusivity in the sorbent bed decreases the rate at which the uptake rate changes over the sampling time. This effect can be explained by the fact that higher diffusivity in the sorbent bed facilitates more efficient mass transfer within the bed, which reduces the concentration of the free analyte molecules at the interface of the sorbent bed with the membrane.

Figure 5-S6 shows the results of the initial sensitivity analysis for the sorption isotherm parameters, a and b, and for the bed porosity, ε. From these three parameters, only the isotherm parameter, a, seems to be influential on the uptake rate value. It can be seen in Panel (A) of this figure that higher uptake rate values and smaller rate of decrease over time are obtained as a becomes smaller. This can be explained when evaluating the effect of the parameter, a, on the free concentration of the analyte, as presented in the isotherm in Table 5-S2. Decreasing the isotherm parameter, a, increases the sorption rate and decreases the free concentration of the analyte in the sorbent bed, which maintains the concentration gradient between both sides of the membrane.

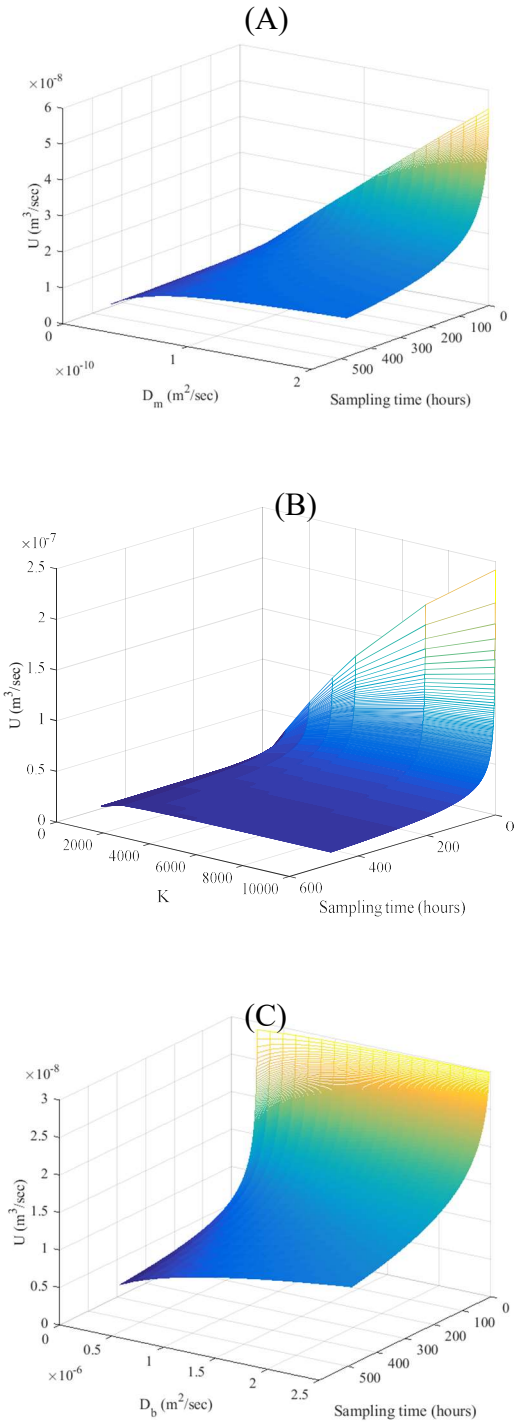

Figure 5-S 5: Results of the initial sensitivity analysis of the uptake rate towards the diffusivity in the membrane (A), the partition coefficient between air and PDMS (B), and the diffusivity in the sorbent bed (C).

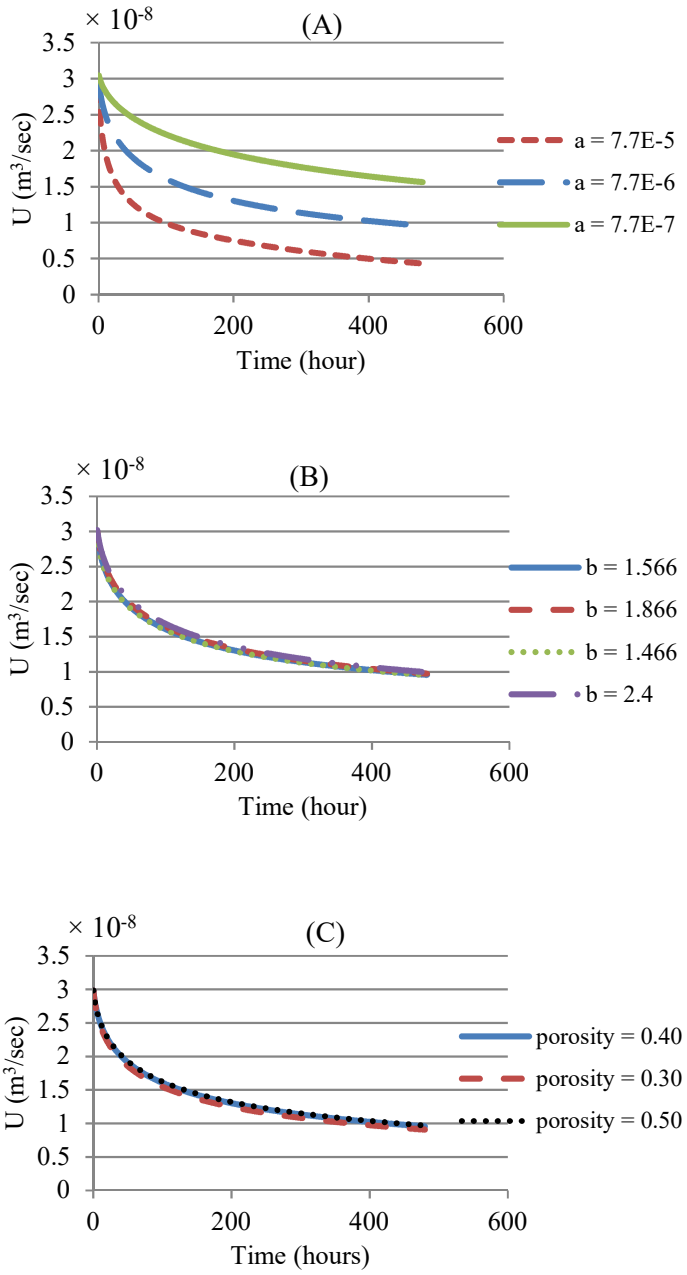

Figure 5-S 6: Results of the initial sensitivity analysis of the uptake rate towards the isotherm parameters a (A) and b (B), and the bed porosity (C).

Table 5-S 4: Values of input parameters used in the sensitivity analysis.

Parameter	Sorbent					
	Carbopack B			Anasorb 747		
	Base value	Lower bound	Upper bound	Base value	Lower bound	Upper bound
D_m (m^2/sec)	1×10^{-10}	1×10^{-11}	1×10^{-9}	1×10^{-10}	1×10^{-11}	1×10^{-9}
K	800	600	1000	800	600	1000
	10000	7500	12500	10000	7500	12500
ε	0.40	0.36	0.44	0.40	0.36	0.44
k_c (m/sec)	0.02	-	-	0.001	0.0001	0.05
b	1.566	1	2	3	2	4

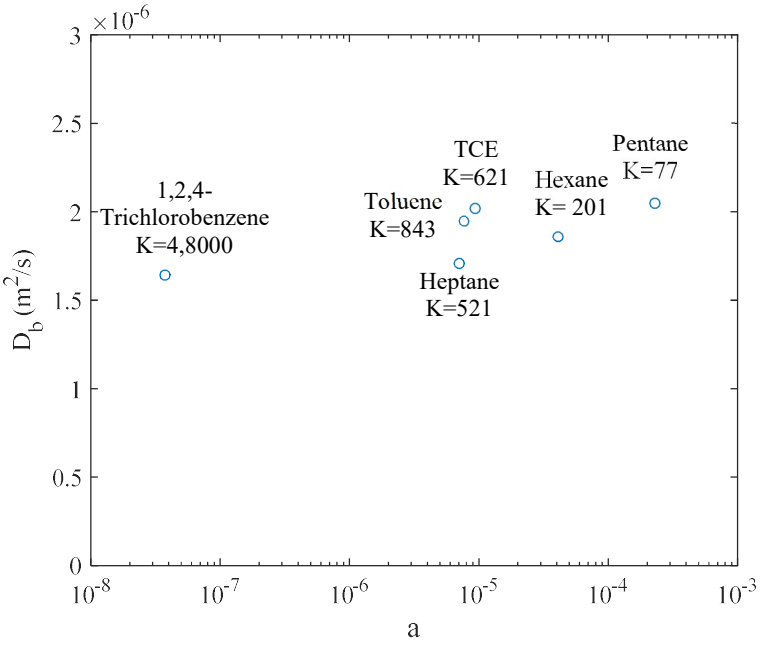

Figure 5-S 7: Distribution of a group of VOCs with different values of the partition coefficient, K, values within the parameter space of (D_b , a).

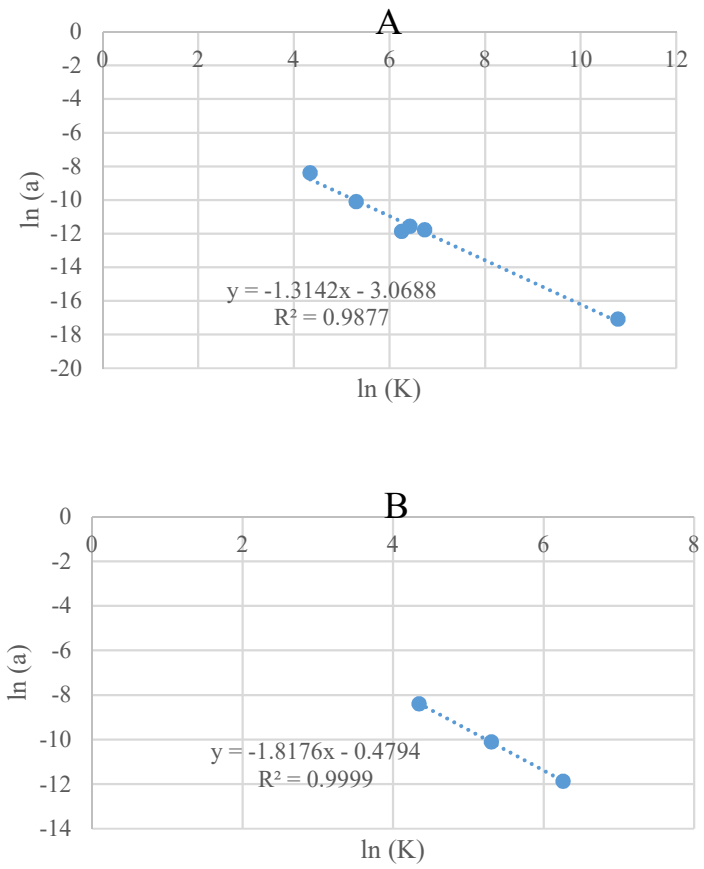

Figure 5-S 8: Observed correlations between the isotherm parameter, a, and the partition coefficient, K, for a group of VOCs (A) and for linear hydrocarbons (B).

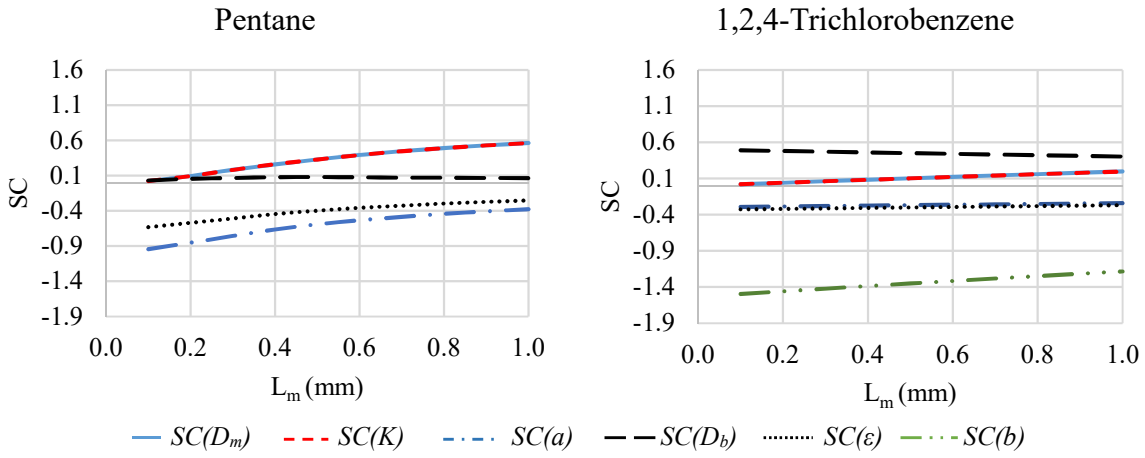

Figure 5-S 9: Sensitivity coefficients (SCs) as a function of the membrane thickness, L_m, for two analytes: pentane and 1,2,4-trichlorobenzene, when Carbopack B is used as a sorbent.

Determination of the Isotherm Parameters

Method

To determine the isotherm parameters, *a* and *b*, as presented in Table 5-1, the maximum capacities of the adsorbent at different gas concentrations were determined using the modified Wheeler equation:[1]

$$t_b = \left(\frac{W_e}{C_o Q}\right)\left[W - \left(\frac{\rho_B Q}{k_v}\right) ln\left(\frac{C_0 - C_x}{C_x}\right)\right] \quad (5.S14)$$

In this equation, t_b is the breakthrough time (min), which is defined as the time needed for the standard gas to pass through the adsorbent bed before the analyte starts to elute from the bed, C_o is the inlet concentration (g/cm^3), W_e is the adsorption capacity (g/g), Q is the volumetric flow rate (cm^3/min), W is the weight of adsorbent (g), ρ_B is the bulk density of the bed (g/cm^3), k_v is the rate coefficient (min^{-1}), and C_x is the exit concentration (g/cm^3), which is a time-dependent concentration. The plot of t_b versus the adsorbent weight, W, at a given vapor concentration, C_0, when all other parameters are constant, produces a straight line with an equation of the form: $t_b = mW + B$. In this equation, m and B are the slope and intercept, respectively. The slope, m, can be expressed as follows:

$$m = \frac{W_e}{C_o Q} \quad (5.S15)$$

Eqn. (5.S15) allows the calculation of the maximum capacity of the adsorbent, W_e, at a given concentration, C_o, if the flow rate, Q, is known.

In order to measure the breakthrough time at a given analyte concentration, the standard gas of that concentration was passed through a bed of the adsorbent with an accurately measured

mass and at a controlled temperature. The flow rate of the standard gas through the bed was monitored during the experiment. The effluent was directed towards a detector to monitor the analyte at the outlet of the packed tube. The experiment continued until a breakthrough curve, similar to that presented in Figure 5-S10, was obtained. The time at the intercept between the tangent of the curve at the inflection point with the abscissa was considered the breakthrough time.

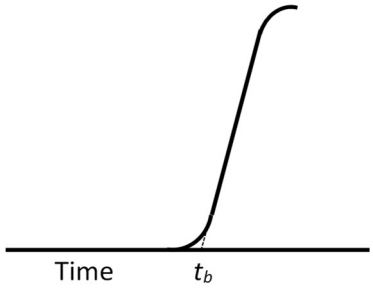

Figure 5-S 10: Breakthrough curve

The experiment was repeated at the same concentration level with different masses of the adsorbent in order to plot the changes in the breakthrough time with the adsorbent mass and obtain the slope described in eqn. (5.S15). After determining the maximum adsorbent capacity at a given concentration, the procedure was repeated with different concentrations until enough points were collected to establish the isotherm equation.

Experimental setup

The setup illustrated in Figure 5-S11 was used to measure the breakthrough time at a given concentration. In this setup, nitrogen gas, from a high-pressure source, was passed through an activated charcoal purifier. It was passed, afterwards, through a mass flow controller (MKS, Andover, MA, USA, 0-100 mL/min), the flow rate through which was set and monitored using an MKS 4-channel readout system (Andover, MA, Type 247). The nitrogen gas was passed through a vapor generator, which consisted of a flow-through vessel, containing an analyte vapor

source, placed inside a GC oven to control the temperature. The analyte vapor source consisted of a diffusion source or a PTFE permeation source depending on the desired concentration level. The diffusion source consisted of a glass vial containing the analyte neat liquid. The vial was sealed with an open top cap and Teflon/Silicon septum or by a silicon stopper. A fused silica capillary (Restek guard column) was inserted through the cap septum or the stopper as a diffusion path. The length and the ID of the capillary varied within the ranges of 40 – 55 mm and 0.25 – 0.53 mm, respectively, depending on the volatility of the analyte and the desired concentration. For details about the PTFE permeation source, the reader is referred to Ref. [3]. Changing the temperature of the vapor source was used as a method of adjusting the concentration. The oven temperature ranged between 40 ^{o}C and 90 ^{o}C. The standard gas was passed, afterwards, through an approximately 4 m long copper tube of a 1/8" OD to equilibrate the gas temperature with the ambient temperature before the gas was passed through the sorptive tube packed with a certain amount of the adsorbent. The tube used for this purpose was a stainless steel tube, 6.35 mm OD × 90 mm long, originally used in Perkin Elmer thermal desorption unit (ATD 400). The adsorbent, inside the tube, was packed in between two layers of glass wool (Fisher Scientific, Ottawa, ON, Canada) of approximately 1.5 cm thickness for each layer. The packed tube was kept at a constant temperature of 21 ^{o}C by placing it inside a thermostated chamber. This chamber consisted of a ten-liter, double-layer glass jar. The inner layer was wrapped with a copper tube connected to a circulating bath equipped with a programmable temperature controller (Model 1147P, VWR International, LLC, PA, USA). The chamber was also wrapped with an insulating layer and covered with a top plate consisting of two layers with holes that allowed passing the tubes into and out of the chamber, and a thermometer to monitor the temperature inside. The inner layer of the top plate was a PTFE plate

with an O-ring to provide good sealing with the edge of the glass jar, while the top layer consisted of a stainless steel plate. The flow through the packed tube was monitored using a rotameter (150 mm Flow Tube, Direct-Reading for 100 mL/min Nitrogen, Cole-Parmer Instrument Co., Montreal, Canada). The rotameter, seated on top of the chamber, was connected from one end to the packed tube, while the other end was connected to a ¼" PTFE tube. This tube was used to direct the effluent gas to a split point before entering the detector. A stainless steel tee connected to the PTFE tube was used for this purpose. One end of the Tee was connected to the FID detector using a 0.53-ID deactivated fused silica tube, while the other end was directed to the fume hood after passing through a needle valve to maintain enough pressure to force the flow into the detector. The flow through the packed tube was measured to be 103 ml/min, while the flow into the detector was 31 ml/min. The detector used in these experiments was an FID detector installed in a GC-FID instrument (FINNIGAN Focus GC, Thermo Scientific, USA).

A three-way stainless steel valve was connected before the packed tube to direct the flow through the tube (Line 1) or to the fume hood during concentration equilibration time (Line 2). The flow through Line 2 was passed through a needle valve to control the pressure, so that the pressure and, therefore, the flow rate were maintained when switching the flow between the two lines. Active sampling was conducted as a method for determining the standard gas concentration. Active samples were collected by switching the flow through Line 2 to pass through a sorption tube connected to a bubble flow meter on the opposite end, used to accurately determine the flow rate. Sorption tubes used for active sampling were packed with either Carbopack B or Anasorb 747. Details about analysing both adsorbents can be found in the experimental section.

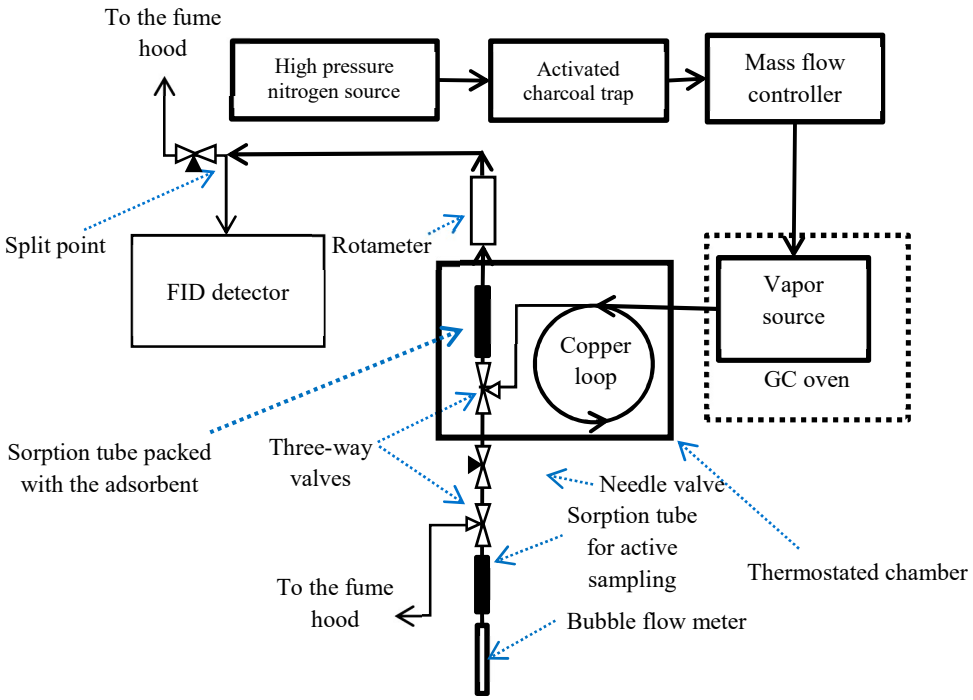

Figure 5-S 11: Experimental setup used in the breakthrough experiments

Results

The concentration of the sorbed analyte was determined by fitting the data points to the linearized Freundlich isotherm form presented in eqn. (5.S16).

$$\log(q) = \log(K) + \frac{1}{n}\log(C) \tag{5.S16}$$

In this equation, q and C are the concentrations of the sorbed analyte (mole per m^3 of the solid phase) and the concentration in the gas phase (mol/m^3), respectively. K and n are empirical constants.

The measurement included two types of adsorbents: Carbopack B and Anasorb 747. Carbopack B is a non-porous adsorbent with specific surface area of 100 m^2/g (as provided by the manufacturer). The density of the solid particles was measured using a pycnometer: ρ_s =

1.87 ± 0.19 g/cm^3. Anasorb 747 is a highly porous adsorbent with a specific surface area 1145 m^2/g (see details in the next section). The solid density was calculated to be ρ_s = 1.47 g/cm^3 (calculations are presented in the following section). The results of the isotherm determination are presented in Table 5-S5. The Average Relative Error (*ARE*) of each measurement was also calculated using eq. (5.S17)[182] and is presented in Table 5-S5.

$$ARE = \frac{100}{N}\sum_{i=1}^{N}\left|\frac{q_{meas} - q_{calc}}{q_{meas}}\right|_i \qquad (5.S17)$$

In this equation, N is the number of data points, q_{meas} is the measured sorbed concentration at equilibrium, and q_{calc} is the calculated sorbed concentration based on the fitted parameters. The residual plots, presented in Figure 5-S12 and Figure 5-S13, show no discernible pattern, which means that the models are adequate.

Table 5-S 5: Results of the isotherm measurement

							Isotherm parameters ($q = K C^{1/n}$)			Isotherm parameters ($C = a q^b$)	
Adsorbent	**Compound**	**Standard gas concentration, C (mol/m^3)**	**Slope of the curve, t_b vs. W (min/g)**	**R^2**	**W_e (g/g)**	**Sorbed concentration, q (mol/m^3)**	**K**	**1/n**	**ARE (%)**	**a**	**b**
Carbopack B	TCE	9.72×10^{-3}	80.92	1.00	1.55×10^{-3}	22.11	1355.06	0.62	3.44	9.48×10^{-6}	1.60
		4.29×10^{-3}	114.11	0.99	1.04×10^{-3}	14.75					
		7.17×10^{-5}	151.58	0.95	6.64×10^{-4}	9.46					
		2.00×10^{-3}	124.86	1.00	7.46×10^{-4}	10.63					
		4.75×10^{-4}	167.32	1.00	4.54×10^{-4}	6.46					
Carbopack B	1,2,4-Trichloro benzene	4.56×10^{-4}	3809.15	0.97	3.26×10^{-2}	336.29	19995.09	0.56	7.81	1.87×10^{-8}	1.80
		2.38×10^{-4}	3870.50	0.99	1.73×10^{-2}	178.03					
		6.38×10^{-4}	2430.47	0.99	2.91×10^{-2}	299.99					
		5.38×10^{-4}	2765.70	1.00	2.79×10^{-2}	288.12					
		4.24×10^{-4}	3380.24	1.00	2.69×10^{-2}	277.03					
		9.72×10^{-4}	2229.56	0.98	4.06×10^{-2}	419.09					
Anasorb 747	Toluene	1.09×10^{-4}	79675.00	1.00	8.24×10^{-2}	1314.73	57204.45	0.41	3.47	2.52×10^{-12}	2.44
		7.11×10^{-4}	29112.00	0.99	1.97×10^{-1}	3137.71					
		1.70×10^{-3}	16198.00	0.99	2.61×10^{-1}	4161.48					
		3.07×10^{-3}	11053.00	0.99	3.22×10^{-1}	5138.16					
Anasorb 747	TCE	1.02×10^{-2}	3220.92	0.99	4.45×10^{-1}	4982.89	18335.37	0.28	8.66	4.77×10^{-16}	3.59
		1.41×10^{-3}	15716.24	1.00	3.02×10^{-1}	3373.79					
		6.68×10^{-4}	20407.18	1.00	1.85×10^{-1}	2072.26					
		3.23×10^{-4}	41501.64	0.98	1.82×10^{-1}	2035.30					

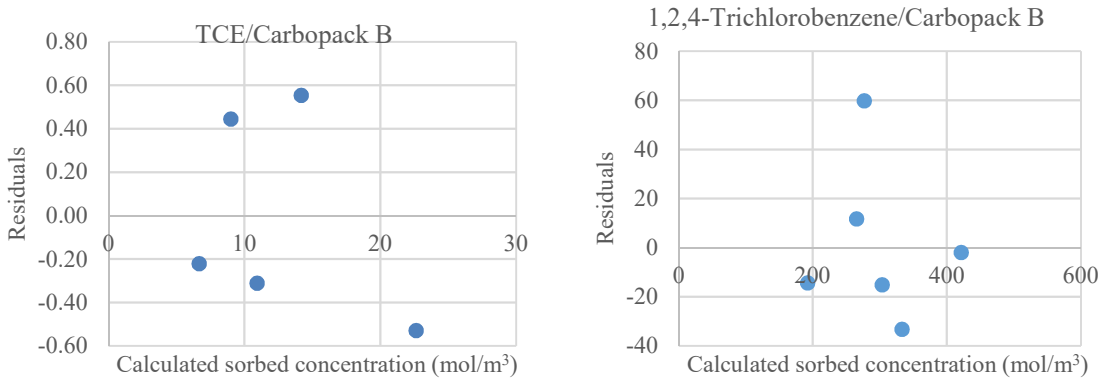

Figure 5-S 12: Plots of residuals for the fitted isotherm models for Carbopack B

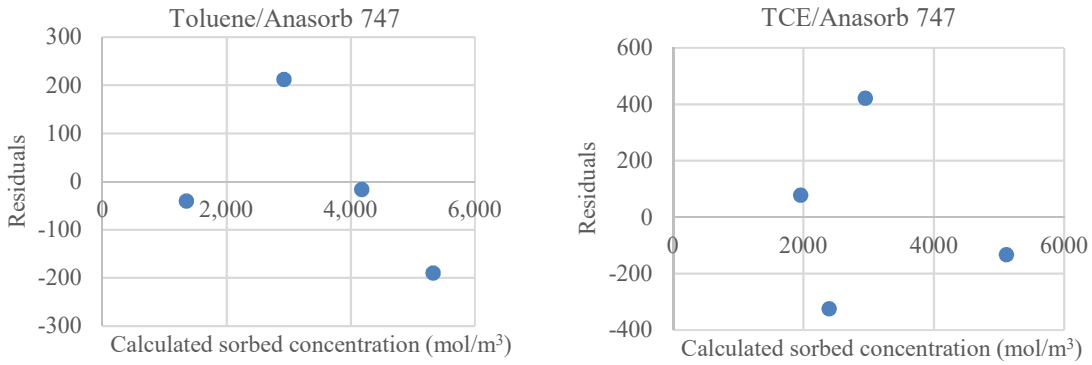

Figure 5-S 13: Plots of residuals for the fitted isotherm models for Anasorb 747

Characterization of Anasorb 747

Anasorb 747 was characterized using an Automated Gas Sorption Analyzer (Autosorb *iQ*) to determine the specific surface area, the pore size and the pore volume. The *BET* determination yielded a surface area of 1145.271 m²/g. The pore size distribution is presented in Figure 5-S14. The results show major pore distribution below 2 nm of half pore width. An average value of the pore radius, using the Trapezoid rule, was calculated as follows:

$$< r > = \frac{\int_{r_1}^{r_2} r dV_p dr}{\int_{r_1}^{r_2} dV_p dr} \quad (5.S18)$$

r is the pore half width (pore radius assuming cylindrical pores), r_1 and r_2 are the smallest and largest values in the range of pore size distribution, and dV_p is the pore volume corresponding to the pore size per unit of mass ($cm^3/Å/g$). This integration produced an average value of <r> = 0.5839 nm for the half pore width.

The measured pore volume was 0.547 cm^3/g. To estimate the particle porosity and the solid density, calculations were done using the following steps: first, the average particle weight was measured to be 0.26 ± 0.06 mg (avg. ± STD). The average particle volume was calculated to be 0.319 mm^3; therefore, the particle density, ρ_p, was found to be approximately 0.81 g/cm^3. By multiplying the pore volume value listed above by the particle density, the particle porosity, ε_μ, was found to be approximately 0.45, which is within the range of expected values. The solid density of the particles (ρ_s) was calculated using eqn.(5.S19), which yielded a value of 1.47 g/cm^3.

$$\rho_s = \frac{\rho_p}{(1 - \varepsilon_\mu)} \quad (5.S19)$$

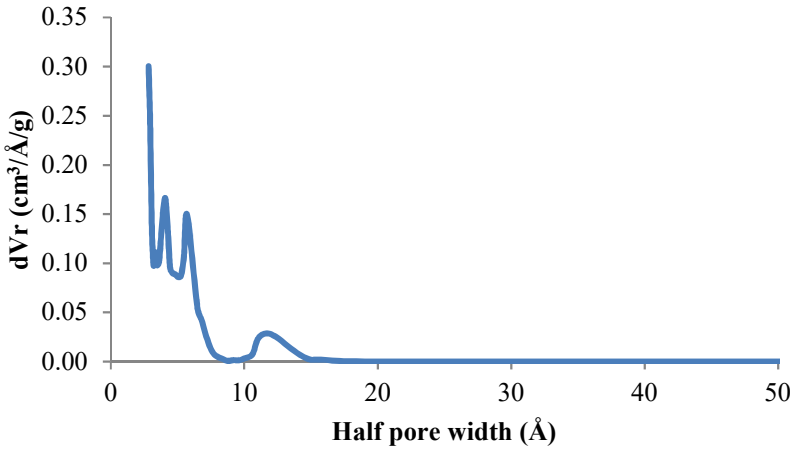

Figure 5-S 14: Pore size distribution for Anasorb 747

Appendix D

Matlab Codes

Sampling Using a Regular 2-mL WMS with Carbopack B

```
clear all
clc
global Lm M Dm x1 x2 x3 dxm2 Lb Db N e kca A Va a b K dxm dxb Da kc
Lm=1E-4; % membrane thickness (m)
Lb=1.4E-2;  % sorbent bed thickness (m)
A=6.79E-5;  % cross section area of the air gap (m2)
Va=1.3586E-6;  % volume of the air gap (m3)
d=(425e-6+850e-6)/2;%(177e-6+250e-6)/2; % Particle diameter
e=0.40;   % porosity
tor=1.61; % tortuosity
s=1145.271;%specific surface area (m2/g)
den=0.55e+6;; % Bulk density (g/m3)
as=den*s;%specific surface area (m2/m3)
a =4.77e-16;%7.67e-6; Isotherm parameter
b= 3.59; %1.566; Isotherm parameter
Am=3.4476e-5; % Area of the membrane (m2)
Ca=0.000068212;% Air concentration (mol/m3)
K=900;
Dm=1.3E-10;%1.07E-10% Diffusion coefficient in the membrane (m2/s)
Da=8.75e-6;%8.5e-6;%8.5e-6 % diffusivity in air
Db=e*Da/tor;
kc=(2*Db/d);
kca=kc*as;  % mass transfer rate coefficient (1/s)
M=19;  % number of sections in the membrane
N=200;  % number of sections in the sorbent bed
% Initial conditions
co=zeros(M+2*N+4,1);
t0=0;
tf=2400000;  % exposure time (s)
n=2000;
tspan=linspace(t0,tf,n);
co(1)=K*Ca; % Concentration at the membrane air interface
reltol=1.0e-04; abstol=1.0e-04;
options=odeset('reltol',reltol,'abstol',abstol);
[t,c]= ode15s('ms4',tspan,co,options); % Apply ODE solver
format long
MnTot=zeros(n,1); % Total moles in the membrane at different times
for i=1:M
  Mmi=((c(:,i+1)+c(:,i))/2).*(Am*dxm); % moles in each section of the
membrane
  MnTot=MnTot+Mmi;
end
MbTot=zeros(n,1); % Total free moles in the sorbent bed at different times
for i=M+2:M+N+1
 Mbi=((c(:,i+1)+c(:,i))/2).*(Am*dxb*e);% free moles in each section of the
sorbent bed
  MbTot=MbTot+Mbi;
```

```
end
MsTot=zeros(n,1); % Total sorbed moles in the sorbent bed at different times

for i=M+2+N+2:M+N+1+N+2
Msi=(c(:,i+1)+c(:,i))/2.*(Am*dxb*(1-e));% sorbed moles in each section of the
sorbent bed
  MsTot=MsTot+Msi;
end
MTot=MsTot+MbTot+MnTot;
U=MsTot./(Ca.*tspan'); % Uptake rates at different times

% Plots
figure
 plot(t,c(:,1))
 hold on
 plot(t,c(:,3))
 plot(t,c(:,5))
 plot(t,c(:,7))
 plot(t,c(:,9))
 plot(t,c(:,11))
 plot(t,c(:,13))
 plot(t,c(:,15))
 plot(t,c(:,17))
 plot(t,c(:,19))
 plot(t,c(:,20),'--')
 title('Concentration profiles at different nodes (0.01 mm apart) in the
membrane')
 xlabel('Time (s)')
 ylabel('Concentration (mol/m3)')

legend('j=1','j=3','j=5','j=7','j=9','j=11','j=13','j=15','j=17','j=19','j=M+
1')
 hold off

  % Plot of concentration of free molecules in the sorbent bed
 figure
 plot(t,c(:,M+2))
 hold on
 plot(t,c(:,M+22))
 plot(t,c(:,M+42))
 plot(t,c(:,M+62))
 plot(t,c(:,M+82))
 plot(t,c(:,M+102))
 plot(t,c(:,M+122),'b--')
 plot(t,c(:,M+142),'y--')
 plot(t,c(:,M+162),'r--')
 plot(t,c(:,M+182),'g--')
 plot(t,c(:,M+202),'c--')
 plot(t,c(:,M+N+2),'.')
 plot(t,c(:,M+N+3),'k--') % concentration in the air gap
 title('Concentration profiles of the free molecules at different nodes (1 mm
apart)in the sorbent bed')
 xlabel('Time (s)')
 ylabel('Concentration (mol/m3)')
```

```
legend('cb1','cb21','cb41','cb61','cb81','cb101','cb121','cb141','cb161','cb1
81','cb201','cb(M+N+2','cag')
 hold off


 % Plot of concentration of sorbed molecules in the sorbent bed
figure
 plot(t,c(:,M+2+N+2))
 hold on
 plot(t,c(:,M+22+N+2))
 plot(t,c(:,M+42+N+2))
 plot(t,c(:,M+62+N+2))
 plot(t,c(:,M+82+N+2))
 plot(t,c(:,M+102+N+2))
 plot(t,c(:,M+122+N+2),'b--')
 plot(t,c(:,M+142+N+2),'y--')
 plot(t,c(:,M+162+N+2),'r--')
 plot(t,c(:,M+182+N+2),'g--')
 plot(t,c(:,M+202+N+2),'m--')
 plot(t,c(:,M+N+2+N+2),'c--')
 plot(t,c(:,M+N+3),'k--') % concentration in the air gap
 title('Concentration profiles of the sorbed molecules at different nodes (1
mm apart) in the sorbent bed')
 xlabel('Time (s)')
 ylabel('Concentration (mol/m3)')
legend('q1','q21','q41','q61','q81','q101','q121','q141','q161','q181','q201'
,'q(M+N+2)','cag')
 hold off

 % Plot of the uptake rate profile
%Texp=xlsread('Model test for Toluene.xlsx',6,'B13:B17');
%Uexp=xlsread('Model test for Toluene.xlsx',6,'D13:D17');
%std=xlsread('Model test for Toluene.xlsx',6,'E13:E17');
%figure
plot(tspan',U)
%hold on
%plot(Texp',Uexp','*')
%legend('MATLAB data','Experimental data')
%errorbar(Texp',Uexp',std')
title('Uptake Rate Profile')
xlabel('Time (s)')
ylabel('Uptake rate (m3/s)')
%hold off


% Plot of the concentration profile in the membrane
figure
j=1:M+1;
xj=(j-1)*dxm;
plot(xj,c(1,j))
hold on
plot(xj,c(2,j),'r:o')
plot(xj,c(3,j),'*')
plot(xj,c(16,j),'b:+')
plot(xj,c(35,j),'o')
```

```
plot(xj,c(51,j),'x')
plot(xj,c(100,j),'--')
plot(xj,c(150,j),'.')
plot(xj,c(200,j),'c:+')
plot(xj,c(300,j),'y:x')
plot(xj,c(800,j),'r:*')
plot(xj,c(1000,j),'k:v')
plot(xj,c(2000,j),'+')
legend('1','2','3','16','35','51','100','150','200','300','800','1000','2000'
)
title('Concentration profile in the membrane')
xlabel('x (m)')
ylabel('Concentration (mol/m3)')
hold off

figure
j=1:M+1;
i=M+2:M+N+2;
xj=(j-1)*dxm;
xi=Lm+((i-(M+2))*dxb);
[AX,H1,H2]=plotyy(xj,c(n,j),xi,c(n,i))
set(AX(1),'yLim',[0 +inf])%0.1
set(AX(2),'ylim',[0 0.5e-5])%20e-5])
legend('Membrane','Free in the sorbent bed')
title('Concentration profile')
xlabel('x (m)')
ylabel('Concentration (mol/m3)')

figure
plot(xj,c(n,j))
hold on
plot(xi,c(n,i+N+2))
legend('membrane','sorbed')
title('Concentration profile')
xlabel('x (m)')
ylabel('Concentration (mol/m3)')
hold off


%xlswrite('Factors affecting U-March',Am,1,'K3')
%xlswrite('Factors affecting U-March',tspan',1,'A4:A2003')
%xlswrite('Factors affecting U-March',U,1,'K4:K2003')
%xlswrite('testing Db',Ca,1,'D1')
%xlswrite('testing Db',Db,1,'D2')
%xlswrite('testing Db',tspan',1,'A4:A2003')
%xlswrite('testing Db',U,1,'D4:D2003')
%xlswrite('sorbent test after entering e to mass
collected',tspan',2,'A4:A2003')
%xlswrite('sorbent test after entering e to mass collected',U,2,'F4:F2003')

% concentration profile of the sorbed analyte and in the membrane
% seperately
figure
plot(xj,c(68,j),'r:*')
%hold on
plot(xj,c(468,j))
```

```
plot(xj,c(n,j),'--')
xlabel('x (m)')
ylabel('Concentration (mol/m3)')
%legend('after 1 day','after 1 week','after 1 month')
title('Concentration profile in the membrane')
%hold off

figure
plot(xi,c(68,i+N+2),'r:*')
hold on
plot(xi,c(468,i+N+2))
plot(xi,c(n,i+N+2),'--')
legend('after 1 day','after 1 week','after 1 month')
title('Concentration profile of the sorbed analyte in the sorbent bed')
xlabel('x (m)')
ylabel('Concentration (mol/m3)')
hold off

% concentration profile of the free analyte
figure
plot(xi,c(68,i),'r:*')
hold on
plot(xi,c(468,i))
plot(xi,c(n,i),'--')
legend('after 1 day','after 1 week','after 1 month')
title('Concentration profile of the free analyte in the sorbent bed')
xlabel('x (m)')
ylabel('Concentration (mol/m3)')
hold off
```

```
function dcdt = ms4(t,c)
global Lm x1 x2 x3 dxm2 Lb dxm dxb dxb2
global M Dm N Db e kca A Va a b K Am
x1=0;
x2=Lm;
x3=Lm+Lb;
dxm=(x2-x1)/M;
dxm2=dxm^2;
dxb=((x3-x2)/N);
dxb2=dxb^2;
    % Boundary conditions in the sorbent bed
        dcdt(M+2+N+2)=(kca/(1-e))*(c(M+2)-a*c(M+2+N+2)^b); % The adsorbed
portion
        dcdt(M+2)=(Db/e)*((c(M+3)-2*c(M+2)+(c(M+3)+2*(Dm/Db)*(dxb/dxm)*(c(M)-
c(M+1))))/dxb2)-((1-e)/e)*dcdt(M+2+N+2);

    if Va~=0
        dcdt(M+N+2+N+2)=(kca/(1-e))*(c(M+N+2)-a*c(M+N+2+N+2)^b); % The
adsorbed portion
        dcdt(M+N+2)=((Db/e)*(c(M+N+3)-2*c(M+N+2)+c(M+N+1))/dxb2)-(((1-
e)/e)*dcdt(M+N+2+N+2));
```

```
        dcdt(M+N+3)=(-A/Va)*Db*(c(M+N+3)-c(M+N+1))/(2*dxb); % in the air gap
    else
        dcdt(M+N+2+N+2)=(kca/(1-e))*(c(M+N+2)-a*c(M+N+2+N+2)^b);
        dcdt(M+N+2)=((Db/e)*(2*c(M+N+1)-2*c(M+N+2))/dxb2)-((1-
e)/e)*dcdt(M+N+2+N+2);
        dcdt(M+N+3)=0;
    end
    % The internal points in the sorbent bed
    for j=M+3:M+N+1
        dcdt(j+N+2)=(kca/(1-e))*(c(j)-a*c(j+N+2)^b); % The adsorbed portion
        dcdt(j)=(Db/e)*((c(j+1)-2*c(j)+c(j-1))/dxb2)-((1-e)/e)*dcdt(j+N+2);
    end
    % Boundary conditions in the membrane
    dcdt(1)=0;
    dcdt(M+1)=K*dcdt(M+2);
    % Internal points in the membrane
    for j=2:M
        dcdt(j)= Dm*((c(j+1)-2*c(j)+c(j-1))/dxm2);
    end

    dcdt=dcdt';


end
```

Sampling Using a Regular 2-mL WMS with Anasorb 747

```
clear all
clc
global Lm M Dm x1 x2 x3 dxm2 Lb Db N e kca A Va K dxm dxb a b
Lm=1E-4; % membrane thickness (m)
Lb=1.4E-2;  % sorbent bed thickness (m)
A=6.79E-5;  % cross section area of the air gap (m2)
Va=1.3586E-6;  % volume of the air gap (m3)
d=(425e-6+850e-6)/2; % Particle diameter
%eb=0.40;   % porosity
e=0.40; %=eb+(1-eb)*0.45;
tor=1.61; % tor=e^(-0.5); % tortuosity
s=1145.271;%specific surface area (m2/g)
den=0.55e+6; % Bulk density (g/m3)
as=den*s;%specific surface area (m2/m3)
K=900; %621;% Partition coefficient
Dm=1.07E-10; %1e-10;% Diffusion coefficient in the membrane (m2/s)
Db= 1.43514E-06; Diffusion coefficient in the sorbent bed (m2/s)
kc=0.001;% mass transfer rate coefficient (1/s)

a=2.52088e-12;%4.77434E-16; % Isotherm parameter
b=2.437965; %3.59372413;%2.437965; %3.59372413; % Isotherm parameter
Am=3.4476e-5; % Area of the membrane (m2)
Ca=0.000068212;%7.38692E-05;% Air concentration (mol/m3)
kca=kc*as;%(1e-3)*as;
M=50;  % number of sections in the membrane
N=1000;  % number of sections in the sorbent bed
```

```
% Initial conditions
co=zeros(M+2*N+4,1);
t0=0;
tf=2400000;%1700000;%20*24*60*60;  % exposure time (s)
n=2000;
co(1)=K*Ca; % Concentration at the membrane air interface
tspan=linspace(t0,tf,n);
reltol=1.0e-04; abstol=1.0e-04;
options=odeset('reltol',reltol,'abstol',abstol);
[t,c]= ode15s('ms4',tspan,co,options); % Apply ODE solver
format long
MnTot=zeros(n,1); % Total moles in the membrane at different times
for i=1:M
  Mmi=((c(:,i+1)+c(:,i))/2).*(Am*dxm); % moles in each section of the
membrane
  MnTot=MnTot+Mmi;
end
MbTot=zeros(n,1); % Total free moles in the sorbent bed at different times
for i=M+2:M+N+1
 Mbi=((c(:,i+1)+c(:,i))/2).*(Am*dxb*e);% free moles in each section of the
sorbent bed
  MbTot=MbTot+Mbi;
end
MsTot=zeros(n,1); % Total sorbed moles in the sorbent bed at different times

for i=M+2+N+2:M+N+1+N+2
Msi=(c(:,i+1)+c(:,i))/2.*(Am*dxb*(1-e));% sorbed moles in each section of the
sorbent bed
  MsTot=MsTot+Msi;
end
%MTot=MsTot+MbTot;
U=MsTot./(Ca.*tspan'); % Uptake rates at different times
```

Mass Transfer into the Particle

```
clear all
clc
global dr dr2 Z cb  Db
global Dp ep a b d

d=(425e-6+850e-6)/2; % Particle diameter
Db=2.035e-6;
ep= 0.45;
s=1145.271;%specific surface area (m2/g)
den=0.55e+6; % Bulk density (g/m3)
as=den*s;%specific surface area (m2/m3)
dp=1.299e-9; %pore diameter
Dp=2.55809E-08;
%a=7.66647E-6; % Isotherm parameter
%b=1.566; % Isotherm parameter
a=18335.37138;
b=0.278262873;
```

```
cb=5e-4;% bulk concentration (mol/m3)
Z=500;% Initial conditions
co=zeros(Z+1,1);
t0=0;
tf=20*24*60*60;  % exposure time (s)
n=2000;
tspan=linspace(t0,tf,n);
co(:,:)=3e-5;
co(1)=cb; % Concentration at the surface of the particle
%co(1+Z+1)=a*cb^b;
dbstop if error
reltol=1.0e-04; abstol=1.0e-04;
options=odeset('reltol',reltol,'abstol',abstol);
[t,c]= ode15s('particle',tspan,co,options); % Apply ODE solver
format long
c'

time=t./(60*60); %time in hour
% Plot of the concentration profile in the membrane
figure
j=1:Z+1;
rj=((Z+1)-j)*dr;
Cn=c(:,:)./cb;
plot(rj,c(1,j))
hold on
plot(rj,c(100,j),'r:o')
plot(rj,c(300,j),'*')
plot(rj,c(700,j),'b:+')
plot(rj,c(1000,j),'o')
plot(rj,c(1300,j),'x')
plot(rj,c(1700,j),'--')
plot(rj,c(2000,j),'.')
%plot(rj,c(200,j),'c:+')
%plot(rj,c(300,j),'y:x')
%plot(rj,c(800,j),'r:*')
%plot(xj,c(1000,j),'k:v')
%plot(xj,c(2000,j),'+')
%legend('1','2','3','16','35','51','100','150','200','300','800','1000','2000
')
title('Concentration profile in the particle')
xlabel('r (m)')
ylabel('Concentration (mol/m3)')
hold off

figure
plot(rj,Cn(1,j))
hold on
plot(rj,Cn(100,j),'r:o')
%plot(rj,Cn(300,j),'*')
plot(rj,Cn(700,j),'b:+')
%plot(rj,Cn(1000,j),'o')
plot(rj,Cn(1300,j),'x')
%plot(rj,Cn(1700,j),'--')
plot(rj,Cn(2000,j),'.')
title('Normalized concentration profile in the particle')
xlabel('r (m)')
ylabel('Cp/Cb')
```

```
legend('t = 0 hour','t = 2.4 hours','t = 16.8 hours','t = 31.2 hours','t = 48
hours');
hold off



Mtot=zeros(n,1); % Total moles at different times
for i=1:Z;
  Mi=((c(:,i+1)+c(:,i))/2)*4*pi*((((Z+1)-i)*dr+((Z+1)-(i+1))*dr)/2)^2*dr; %
moles in each section of the membrane
  Mtot=Mtot+Mi;
end
Cave=Mtot/((4/3)*pi*(d/2)^3);

figure
plot(time,Cave)
title('Accumulation of analyte inside the particle')
xlabel('Time (hour)')
ylabel('Average concentration in the particle (mol/m^3)')

% at time point l

Slope=(c(:,2)-c(:,1))/(dr); % slope near the surface
kc= -Dp.*Slope./((c(:,1)-Cave(:)));
%xlswrite('Anasorb test after entering e to mass collected-
Reg',kc,'Sheet12','Bv')

%xlswrite('Anasorb test after entering e to mass collected-
Reg',U,'Sheet12','H4:H2003')
(c(500,1)-c(500,2))/dr;
kc

figure
plot(time,kc)
title('Mass transfer coefficient')
xlabel('Time (hour)')
ylabel('k_c (m/sec)')
```

```
function dcdt = particle(t,c)
global dr dr2 Z
global Dp ep a b d

dr=d/(2*Z);
dr2=dr^2;
    % Boundary conditions in the sorbent
     % instantaneous equilibration at the surface,
        dcdt(1)= 0;  % in the gas phase at the surface (first point)

       dcdt(Z+1)=6*Dp*c(Z+1)^(1-b)/((1-ep)*a*b)*(c(Z)-c(Z+1))/dr2;%Free
```

```
    % The internal points in the sorbent bed
    for k=2:Z
       dcdt(k)=Dp*c(k)^(1-b)/((1-ep)*a*b)*(((c(k+1)-2*c(k)+c(k-
1))/dr2)+(2/(((Z+1)-k)*dr))*((c(k+1)-c(k-1))/(2*dr)));

    end

    dcdt=dcdt';


end
```

Evaluation of the Post-Sampling Period

```
clear all
clc
global Lm M Dm x1 x2 x3 dxm2 Lb Db N e kca A Va a b K dxm dxb Am Vb
Lm=1E-4; % membrane thickness (m)
Lb=2.6E-2;  % sorbent bed thickness (m)
A=12.566e-6;  % cross section area of the air gap (m2)
Va=A*4E-3;  % volume of the air gap (m3)
d=(177e-6+250e-6)/2;
e=0.40;   % porosity
tor=1.61;
s=100;%specific surface area (m2/g)
den=(1-e)*1.871e+6; % Bulk density (g/m3)
as=den*s;%specific surface area (m2/m3)
K= 621;%843;% Partition coefficient
Dm=1.3e-10;%1.07E-10;% Diffusion coefficient in the membrane (m2/s)
Db=(8.75e-6)*e/tor;%(8.5e-6)*e/tor;% Diffusion coefficient in the sorbent bed
(Da*e/?) (m2/s)
kca=(2*Db/d)*as;  % mass transfer rate coefficient (1/s)
a=9.48e-6;%7.66647E-6; % Isotherm parameter
b=1.60;%1.566; % Isotherm parameter
Am=1.75e-5; % Area of the membrane (m2)
Vb=19e-6;% volume of the air in the outside vial
Ca=0.0001;% Air concentration (mol/m3)
M=19;  % number of sections in the membrane
N=200;  % number of sections in the sorbent bed
n=2000;
% Initial conditions
co=zeros(M+2*N+4,1);
t0=0;
tf=24*60*60;  % exposure time (s)
co(1)=K*Ca; % Concentration at the membrane air interface
tspan=linspace(t0,tf,n);
reltol=1.0e-04; abstol=1.0e-04;
options=odeset('reltol',reltol,'abstol',abstol);
[t,c]= ode15s('ms4',tspan,co,options); % Apply ODE solver
format long
MnTot=zeros(n,1); % Total moles in the membrane at different times
for i=1:M
```

```
   Mmi=((c(:,i+1)+c(:,i))/2).*(Am*dxm); % moles in each section of the
membrane
  MnTot=MnTot+Mmi;
end
MbTot=zeros(n,1); % Total free moles in the sorbent bed at different times
for i=M+2:M+N+1
 Mbi=((c(:,i+1)+c(:,i))/2).*(Am*dxb*e);% free moles in each section of the
sorbent bed
  MbTot=MbTot+Mbi;
end

MsTot=zeros(n,1); % Total sorbed moles in the sorbent bed at different times
for i=M+2+N+2:M+N+1+N+2
Msi=((c(:,i+1)+c(:,i)))/2.*(Am*dxb*(1-e));
  MsTot=MsTot+Msi;
end
U=MsTot./(Ca.*tspan'); % Uptake rates at different times
%%
co=c(n,1:M+2*N+4)';
c(n,M+2*N+5)=0;
co=c(n,1:M+2*N+5)';
co(1)=K*c(n,M+2*N+5);
tf=7*24*60*60;
tspan=linspace(t0,tf,n);
[t,c]= ode15s('ms4b',tspan,co,options); % Apply ODE solver
format long
MnTot=zeros(n,1); % Total moles in the membrane at different times
for i=1:M
   Mmi=((c(:,i+1)+c(:,i))/2).*(Am*dxm); % moles in each section of the
membrane
  MnTot=MnTot+Mmi;
end
MbTot=zeros(n,1); % Total free moles in the sorbent bed at different times
for i=M+2:M+N+1
 Mbi=((c(:,i+1)+c(:,i))/2).*(Am*dxb*e);% free moles in each section of the
sorbent bed
  MbTot=MbTot+Mbi;
end

MsTot=zeros(n,1); % Total sorbed moles in the sorbent bed at different times
for i=M+2+N+2:M+N+1+N+2
Msi=((c(:,i+1)+c(:,i)))/2.*(Am*dxb*(1-e));
  MsTot=MsTot+Msi;
end
% Display data
disp('Number of moles of sorbed, free molecules in the sorbent bed and number
of moles in the membrane: ')
disp([MsTot MbTot MnTot])
```

```
function dcdt = ms4b(t,c)
global Lm x1 x2 x3 dxm2 Lb dxm dxb dxb2 Vb
global M Dm N Db e kca A Va a b K Am
x1=0;
x2=Lm;
x3=Lm+Lb;
```

```
dxm=(x2-x1)/M;
dxm2=dxm^2;
dxb=((x3-x2)/N);
dxb2=dxb^2;
    % Boundary conditions in the sorbent bed
        dcdt(M+2+N+2)=(kca/(1-e))*(c(M+2)-a*c(M+2+N+2)^b); % The adsorbed
portion
        dcdt(M+2)=(Db/e)*((c(M+3)-2*c(M+2)+(c(M+3)+2*(Dm/Db)*(dxb/dxm)*(c(M)-
c(M+1))))/dxb2)-((1-e)/e)*dcdt(M+2+N+2);

    if Va~=0
        dcdt(M+N+2+N+2)=(kca/(1-e))*(c(M+N+2)-a*c(M+N+2+N+2)^b); % The
adsorbed portion
        dcdt(M+N+2)=((Db/e)*(c(M+N+3)-2*c(M+N+2)+c(M+N+1))/dxb2)-(((1-
e)/e)*dcdt(M+N+2+N+2));
        dcdt(M+N+3)=(-A/Va)*Db*(c(M+N+3)-c(M+N+1))/(2*dxb); % in the air gap
    else
        dcdt(M+N+2+N+2)=(kca/(1-e))*(c(M+N+2)-a*c(M+N+2+N+2)^b);
        dcdt(M+N+2)=((Db/e)*(2*c(M+N+1)-2*c(M+N+2))/dxb2)-((1-
e)/e)*dcdt(M+N+2+N+2);
        dcdt(M+N+3)=0;
    end
    % The internal points in the sorbent bed
    for j=M+3:M+N+1
        dcdt(j+N+2)=(kca/(1-e))*(c(j)-a*c(j+N+2)^b); % The adsorbed portion
        dcdt(j)=(Db/e)*((c(j+1)-2*c(j)+c(j-1))/dxb2)-((1-e)/e)*dcdt(j+N+2);
    end
    % Boundary conditions in the membrane
    dcdt(M+2*N+5)=-Am/Vb*Dm*(c(1)-c(2))/(dxm);
    dcdt(1)=K*dcdt(M+2*N+5);
    dcdt(M+1)=K*dcdt(M+2);
    % Internal points in the membrane
    for j=2:M
        dcdt(j)= Dm*((c(j+1)-2*c(j)+c(j-1))/dxm2);
    end

    dcdt=dcdt';


end
```

Calculation of the Effective Uptake Rate and the TWA Concentration

```
 clear all
clc
global Lm M Dm x1 x2 x3 dxm2 Lb Db N e kca A Va a b K dxm dxb
Lm=1E-4; % membrane thickness (m)
Lb=1.4E-2;  % sorbent bed thickness (m)
A=6.79E-5;  % cross section area of the air gap (m2)
Va=1.3586E-6;  % volume of the air gap (m3)
d=(177e-6+250e-6)/2; % Particle radius
e=0.40;   % porosity
tor=1.61; % tortuosity
s=100;%specific surface area (m2/g)
```

```
den=(1-e)*1.871e+6; % Bulk density (g/m3)
as=den*s;%specific surface area (m2/m3)
K=621;%843;% Partition coefficient
Dm=4.8088e-10;%1.07E-10;% Diffusion coefficient in the membrane (m2/s)
Db=(8.75e-6)*e/tor;%(8.5e-6)*e/tor;% Diffusion coefficient in the sorbent bed
(m2/s)
kca=(2*Db/d)*as;  % mass transfer rate coefficient (1/s)
a=9.48e-6; %7.66647E-6; % Isotherm parameter
b=1.60;%1.566; % Isotherm parameter
Am=3.4476e-5; % Area of the membrane (m2)
Ui=K*Dm*Am/Lm; % Ideal Uptake Rate (m3/s))
Mol=131.4; % molar mass (g/mol)
%mass=2.43e-5; % mass collected (g)
Amount=1.26639E-06;% Amount of analyte (ug)
M=19;  % number of sections in the membrane
N=200;  % number of sections in the sorbent bed
% Initial conditions
co=zeros(M+2*N+4,1);
t0=0;
tf=953220;  % exposure time (s)
z=1;
C(z)=Amount/(Ui*tf);
Ca=C(z);
n=2000;
tspan=linspace(t0,tf,n);
co(1)=K*Ca; % Concentration at the membrane air interface
reltol=1.0e-04; abstol=1.0e-04;
options=odeset('reltol',reltol,'abstol',abstol);
[t,c]= ode15s('ms4',tspan,co,options); % Apply ODE solver
format long
MnTot=zeros(n,1); % Total moles in the membrane at different times
for i=1:M
  Mmi=((c(:,i+1)+c(:,i))/2).*(Am*dxm); % moles in each section of the
membrane
  MnTot=MnTot+Mmi;
end
MbTot=zeros(n,1); % Total free moles in the sorbent bed at different times
for i=M+2:M+N+1
 Mbi=((c(:,i+1)+c(:,i))/2).*(Am*dxb*e);% free moles in each section of the
sorbent bed
  MbTot=MbTot+Mbi;
end
MsTot=zeros(n,1); % Total sorbed moles in the sorbent bed at different times

for i=M+2+N+2:M+N+1+N+2
Msi=(c(:,i+1)+c(:,i))/2.*(Am*dxb*(1-e));% sorbed moles in each section of the
sorbent bed
  MsTot=MsTot+Msi;
end
MTot=MsTot+MbTot+MnTot;
U=MsTot./(Ca.*tspan'); % Uptake rates at different times
z=z+1;
C(z)=Amount/(U(n)*tf);
while C(z)/C(z-1)>1
    Ca=C(z);
    co=zeros(M+2*N+4,1);
n=2000;
```

```
tspan=linspace(t0,tf,n);
co(1)=K*Ca; % Concentration at the membrane air interface
reltol=1.0e-04; abstol=1.0e-04;
options=odeset('reltol',reltol,'abstol',abstol);
[t,c]= ode15s('ms4',tspan,co,options); % Apply ODE solver
format long
MnTot=zeros(n,1); % Total moles in the membrane at different times
for i=1:M
  Mmi=((c(:,i+1)+c(:,i))/2).*(Am*dxm); % moles in each section of the
membrane
  MnTot=MnTot+Mmi;
end
MbTot=zeros(n,1); % Total free moles in the sorbent bed at different times
for i=M+2:M+N+1
 Mbi=((c(:,i+1)+c(:,i))/2).*(Am*dxb*e);% free moles in each section of the
sorbent bed
  MbTot=MbTot+Mbi;
end
MsTot=zeros(n,1); % Total sorbed moles in the sorbent bed at different times
for i=M+2+N+2:M+N+1+N+2
Msi=(c(:,i+1)+c(:,i))/2.*(Am*dxb*(1-e));% sorbed moles in each section of the
sorbent bed
  MsTot=MsTot+Msi;
end
MTot=MsTot+MbTot+MnTot;
U=MsTot./(Ca.*tspan'); % Uptake rates at different times
z=z+1;
C(z)=Amount/(U(n)*tf);
U(n)
end
C'
```

Evaluation of the Effect of the Air Face Velocity

```
clear all
clc
global Lm M Dm x1 x2 x3 dxm2 Lb Db N e kca A Va a b K dxm dxb Da kc Q hm Ca
W=1;
for Lm=[1e-4:1e-4:2e-3]; % membrane thickness (m)
Lb=1.4E-2;  % sorbent bed thickness (m)
x1=0;
x2=Lm;
x3=Lm+Lb;

A=6.79E-5;  % cross section area of the air gap (m2)
Va=1.3586E-6;  % volume of the air gap (m3)
d=(425e-6+850e-6)/2; % Particle diameter
%eb=0.40;   % porosity
e=0.40; %=eb+(1-eb)*0.45;
tor=1.61; % tor=e^(-0.5); % tortuosity
s=1145.271;%specific surface area (m2/g)
den=0.55e+6; % Bulk density (g/m3)
as=den*s;%specific surface area (m2/m3)
```

```
K=8635; %621;% Partition coefficient
Dm=1.23E-10; %1e-10;% Diffusion coefficient in the membrane (m2/s)
Db=1.43514E-06;%1.32954E-06;%9.1e-7;%9.9047e-08; %(8.5e-6)*e/tor;% Diffusion
coefficient in the sorbent bed (m2/s)
kc=0.001;% mass transfer rate coefficient (1/s)
Da=6.22E-06;%
a=2.52088e-12;%4.77434E-16; % Isotherm parameter
b=2.437965; %3.59372413;%2.437965; %3.59372413; % Isotherm parameter
Am=3.4476e-5; % Area of the membrane (m2)
Ca=2E-7; %1e-05;% Air concentration (mol/m3)
kca=kc*as;  % mass transfer rate coefficient (1/s)
M=50;  % number of sections in the membrane
N=1000;  % number of sections in the sorbent bed
dxm=(x2-x1)/M;
di= 5.5*10^(-3);  % sampling surface diameter
p=1.2047;%1.1769; % air density (Kg/m3)
vis=1.8205e-5;%1.8464*10^(-5); % air viscosity (Pa.sec)

for v=[1e-8 1e-7 1e-6 1e-5 1e-4 1e-3 0.01 0.02 0.03 0.04 0.05 0.06 0.07 0.08
0.09 0.1 0.12 0.18 0.23 0.29 0.35 0.41 0.47 0.53 0.6 0.8 1 2 3 4 5 6 7] %
linear air velocity m/sec)

Re=p*v*di/vis;
Sc=vis/(p*Da); %
if Re<=2e+5
    Sh=0.664*Re^(1/2)*Sc^(1/3);
else
    Sh=0.0365*Re^(0.8)*Sc^(1/3);
end
hm=Sh*Da/di;
Q=Dm/hm/dxm;
% Initial conditions
co=zeros(M+2*N+4+1,1);
t0=0;
tf=2*24*60*60;%200*60*60;%20*24*60*60;  % exposure time (s)
n=2000;
tspan=linspace(t0,tf,n);
co(1)=K*Ca; % Concentration at the membrane air interface
co(M+2*N+5)=Ca;
%dbstop if error
reltol=1.0e-04; abstol=1.0e-04;
options=odeset('reltol',reltol,'abstol',abstol);
[t,c]= ode15s('msB',tspan,co,options); % Apply ODE solver
format long
MnTot=zeros(n,1); % Total moles in the membrane at different times
for i=1:M
  Mmi=((c(:,i+1)+c(:,i))/2).*(Am*dxm); % moles in each section of the
membrane
  MnTot=MnTot+Mmi;
end
MbTot=zeros(n,1); % Total free moles in the sorbent bed at different times
for i=M+2:M+N+1
 Mbi=((c(:,i+1)+c(:,i))/2).*(Am*dxb*e);% free moles in each section of the
sorbent bed
  MbTot=MbTot+Mbi;
end
```

```
MsTot=zeros(n,1); % Total sorbed moles in the sorbent bed at different times

for i=M+2+N+2:M+N+1+N+2
Msi=(c(:,i+1)+c(:,i))/2.*(Am*dxb*(1-e));% sorbed moles in each section of the
sorbent bed
  MsTot=MsTot+Msi;
end
MTot=MsTot+MbTot+MnTot;
U=MsTot./(Ca.*tspan'); % Uptake rates at different times
UR(W)=U(n);
Bi(W)=hm*Lm/Dm;
MTC(W)=hm;
Conc(W)=c(n,M+2*N+5);
display('v')
display(v)
display('U')
display(U(n))
W=W+1;
end
end
Urate=UR';
Biot=Bi'
```

```
function dcdt = msB(t,c)
global Lm x1 x2 x3 dxm2 Lb dxm dxb dxb2
global M Dm N Db e kca A Va a b K Am hm Q Ca
x1=0;
x2=Lm;
x3=Lm+Lb;
dxm=(x2-x1)/M;
dxm2=dxm^2;
dxb=((x3-x2)/N);
dxb2=dxb^2;

    % Boundary conditions in the sorbent bed
        dcdt(M+2+N+2)=(kca/(1-e))*(c(M+2)-a*c(M+2+N+2)^b); % The adsorbed
portion
        dcdt(M+2)=(Db/e)*((c(M+3)-2*c(M+2)+(c(M+3)+2*(Dm/Db)*(dxb/dxm)*(c(M)-
c(M+1))))/dxb2)-((1-e)/e)*dcdt(M+2+N+2);

    if Va~=0
        dcdt(M+N+2+N+2)=(kca/(1-e))*(c(M+N+2)-a*c(M+N+2+N+2)^b); % The
adsorbed portion
        dcdt(M+N+2)=((Db/e)*(c(M+N+3)-2*c(M+N+2)+c(M+N+1))/dxb2)-(((1-
e)/e)*dcdt(M+N+2+N+2));
        dcdt(M+N+3)=(-A/Va)*Db*(c(M+N+3)-c(M+N+1))/(2*dxb); % in the air gap
    else
        dcdt(M+N+2+N+2)=(kca/(1-e))*(c(M+N+2)-a*c(M+N+2+N+2)^b);
        dcdt(M+N+2)=((Db/e)*(2*c(M+N+1)-2*c(M+N+2))/dxb2)-((1-
e)/e)*dcdt(M+N+2+N+2);
        dcdt(M+N+3)=0;
    end
    % The internal points in the sorbent bed
    for j=M+3:M+N+1
        dcdt(j+N+2)=(kca/(1-e))*(c(j)-a*c(j+N+2)^b); % The adsorbed portion
```

```
        dcdt(j)=(Db/e)*((c(j+1)-2*c(j)+c(j-1))/dxb2)-((1-e)/e)*dcdt(j+N+2);
    end
    % Boundary conditions in the membrane
    dcdt(1)=2*Dm/dxm2*(c(2)-c(1)+(1/Q)*(Ca-c(M+2*N+4+1)));
    dcdt(M+2*N+4+1)=(1/K)*dcdt(1);
    dcdt(M+1)=K*dcdt(M+2);
    % Internal points in the membrane
    for j=2:M
        dcdt(j)= Dm*((c(j+1)-2*c(j)+c(j-1))/dxm2);
    end

    dcdt=dcdt';


end
```